COMPUTATIONAL MODELS FOR FRP-CONFINED CONCRETE AND FRP-CONFINED RC COLUMNS

XIAO QIONGGUAN

Ph.D

The Hong Kong Polytechnic University

2013

THE HONG KONG POLYTECHNIC UNIVERSITY

DEPARTMENT OF CIVIL AND ENVIRONMENTAL ENGINEERING

COMPUTATIONAL MODELS FOR FRP-CONFINED CONCRETE AND FRP-CONFINED RC COLUMNS

XIAO Qiongguan

A Thesis Submitted in Partial Fulfillment of the Requirements for the Degree of Doctor of Philosophy

July 2013

CERTIFICATE OF ORIGINALITY

I hereby declare that this thesis is my own work and that, to the best of my knowledge and belief, it reproduces no material previously published or written, nor material that has been accepted for the award of any other degree or diploma, except where due acknowledgement has been made in the text.

_____(Signed)

Xiao Qiongguan_____(Name of Student)

ABSTRACT

The use of FRP jackets to strengthen RC columns has become popular in recent years due to the well-known phenomenon that lateral confinement can significantly enhance the strength and the deformation capacity of concrete. However, the related confinement mechanism of concrete, particularly when under non-uniform confinement, is still inadequately understood. This thesis is thus concerned with the development of a deeper understanding of the confinement mechanism of concrete in FRP-confined RC columns.

This thesis first presents a series of axial compression tests on FRP-confined high strength concrete cylinders. These tests are an important supplement of the existing test data. Based on these tests, a stress-strain model applicable to both normal strength concrete and high strength concrete under active confinement is proposed. Moreover, an existing analysis-oriented stress-strain model for FRP-confined concrete is shown to be applicable to concretes of different strength grades. This analysis-oriented stress-strain model served as a basis of the subsequent studies on the numerical modelling of FRP-confined concrete and FRP-confined RC columns presented in the thesis.

Attention is then shifted to the performance of plasticity models and plastic-damage models in predicting the stress-strain behaviour of confined concrete. In the plasticity models or the plasticity part of the plastic-damage

models, two techniques have been utilized to define the plastic deformation process: the scaling technique in which the hardening law is defined as a function of the confining pressure and the plastic volume strain technique in which the plastic volume strain serves as the hardening variable. While both techniques are shown to lead to accurate predictions for actively-confined concrete, they are shown to be incapable of providing accurate predictions for FRP-confined concrete. This is because both approaches cannot accurately simulate the lateral deformation process of FRP-confined concrete. In addition, the thesis also presents a study of the use of Bazant's micro-plane model in predicting the behaviour of confined concrete; an improved version of the M4 model, referred to as the $M4^+$ model, is presented for the numerical modelling of FRP-confined concrete. Several important parameters of the $M4^+$ model were set to be confinement-dependent. The improved model provides accurate predictions for FRP-confined concrete.

The next part of the thesis is on the development and application of advanced finite element models for FRP-confined non-circular columns. Two constitutive models, that is, Yu et al.'s plastic-damage model and the $M4^+$ model, were employed in the finite element models to predict the behaviour of FRP-confined square and elliptical columns. Numerical results from the finite element model show favourable agreement with the experimental results.

The final part of the thesis presents a three-dimensional finite element

model for FRP-confined RC columns based on Yu et al.'s plastic-damage model. For this finite element model, a local analysis-oriented stress-strain model is proposed for adoption to avoid the double counting of end restraint effects. This finite element model is shown to produce accurate predictions of the stress-strain behaviour of transverse steel-confined concrete columns and FRP-confined RC columns.

LIST OF PUBLICATIONS

Refereed Journal Paper

Xiao, Q.G., Teng J.G., and Yu, T. (2010). "Behaviour and Modelling of Confined High-Strength Concrete", *Journal of Composites for Construction,* ASCE,14(3): 249-259.

Conference Papers

Xiao, Q.G., Teng, J.G. and Yu, T. (2009). "Behaviour of FRP-confined High Strength Concrete", *Proceedings, Fourth International Conference on Adv -anced Composites in Construction*, Edinburgh, Scotland, UK, pp. 169-177.

Xiao, Q.G., Teng, J.G., Yu, T., and Lam, L. (2010). "Three-Dimensional Finite Element Model for FRP-confined Circular Concrete Cylinders under Axial Compression", *5th International Conference on FRP Composites in Civil Engineering*, 27-29 September, 654-657, Beijing, China.

ACKNOWLEDGEMENT

First and most importantly I would like to express my heartfelt gratitude to my supervisor, Professor Jin-Guang Teng for his enlightening guidance, rigorous training and enthusiastic support throughout the course of my PhD study. Professor Teng's rigorous approach to academic research, breadth and depth of knowledge in structural engineering, and creative and unique insight into many academic problems have demonstrated the essential qualities that a good researcher should possess and all of these qualities have given me great benefit. I would also like to express my warmest thanks to my co-supervisors, Dr. Lik Lam and Dr. Tao Yu, for their generous support and valuable suggestions and advice. I also wish to express my sincere thanks to Prof. Jian-Fei Chen who was formerly at the University of Edinburgh and now at Queen's University Belfast for the help he provided to me, both concerning my personal life and my study, during my stay at the University of Edinburgh as a visiting PhD student.

I am grateful to both the Research Grants Council of the Hong Kong Special Administrative Region and The Hong Kong Polytechnic University for their financial support. I am also grateful to The Hong Kong Polytechnic University for making the research facilities available to me.

Thanks are due to the technical support team from the Heavy Structures Laboratory of the Department of Civil and Structural Engineering, in particular, Messrs. K.H. Wong, W.C. Chan, K. Tam, M.C. Ng, C.F. Cheung and T.T. Wai for their valuable advice and assistance during the experimental part of this PhD project.

Special thanks go to my friends and colleagues in the Department of Civil and Enviromental Engineering of The Hong Kong Polytechnic University, in particular, Drs. Tao Jiang, Guang-Ming Chen, Shi-Shun Zhang, Yue-Ming Hu, Dilum Fernando, and Yu-Ru Wang, as well as Messrs. Bing Zhang, Jun-Liang Zhao, Bing Fu, Guan Lin, Xue-Fei Nie, Pang Xie, Jun-Jie Zeng, Qin-Kai Wang, Yi-Nan Yang, Jing-Yun Wu, Jie-Kai Zhu, Jiong-Yi Zhu, Yi-Xin Peng, and Jing-Hua Lin, not only for their constructive discussions but also for their encouragement at times of difficulty during the course of study.

Last but certainly not the least, I wish to express my profound gratitude to my parents, to whom this thesis is dedicated. Without their everlasting love, support and encouragement, I would never have embarked on my doctoral study and would not have had the opportunity to write this thesis. I am indebted to them for so many things which cannot be described in words.

My heartfelt thanks also go to my sister Qing-Ying Xiao for her spiritual support.

LIST OF TABLES

LIST OF FIGURES

CONTENTS

CHAPTER 1

INTRODUCTION

1.1 BACKGROUND

Fibre-reinforced polymer (FRP) composites are composite materials which comprise fibres of high tensile strength (e.g. carbon, glass and aramid fibres) embedded in a resin matrix (e.g. vinylester or epoxy resin). These composite materials, compared to steel which is a widely used modern construction material, have many benefits including their high strength, light weight, corrosion resistance and tailorability of mechanical properties. For instance, CFRP composites can be ten times as strong as conventional structural steel but only a quarter as heavy as steel; in addition, unlike steel, they are non-corrosive. The high strength-to-weight ratio of FRP composites means that FRP composites are easy to handle on site, reducing labour costs and minimizing interruptions to existing services while their corrosion-resistant property leads to durable performance. Due to these advantages, FRP composites have a tremendous potential for engineering applications, especially as their prices fall down with the expansion of the production volume.

FRP composites have been used in the aerospace industry for many years. They have become increasingly accepted over the past two decades by civil engineers as a new class of structural material as their superior material properties become increasingly noticed by civil engineers. Nowadays, various forms of FRP products are commercially available for civil

engineering applications, including bars, sheets, plates and shapes/profiles. These FRP products may be used in the retrofit of existing structures or to replace steel in the construction of new structures. In strengthening applications, FRP composites are commonly used as externally bonded reinforcement, but they may also be used as embedded reinforcement near the surface of structural members.

When used in construction, FRP composites also have some disadvantages. First, FRP composites show poor performance in fire. Therefore, if they are required to be the main load-resisting material in indoor applications where fire resistance is an important issue, special care (e.g. appropriate fire insulation) needs to be exercised. Second, FRP composites are linear-elastic-brittle materials (i.e. they exhibit linear-elastic behaviour in tension up to brittle rupture failure), creating the issue of lack of ductility compared to steel. Third, FRP composites have low elastic modulus-to-strength ratios, so it is less than desirable to use them to bear compressive stresses directly or to offer the stiffness needed. For instance, when a GFRP plate is used to stiffen a reinforced concrete (RC) beam to reduce its deformation, a very thick GFRP plate may be required due to the small elastic modulus of the GFRP composite.

One application of FRP composites where their advantages are fully utilized but their disadvantages are avoided or minimized involves the use of FRP composites to provide lateral confinement to concrete so that both the strength and ductility of the concrete under compression can be

substantially enhanced. This mechanism has been exploited in both the retrofit of existing structures and in the construction of new structures, but the former application has been much more common in practice so far. In this type of applications, all four advantages of FRP composites mentioned above (i.e. high strength, light weight, corrosion resistance and tailorability of properties) are utilized, and the last two disadvantages of FRP composites can be naturally overcome. In such FRP-confined RC columns, the fibres are oriented in the hoop or a near-hoop direction, so the FRP material is not used as the main component to carry axial loading; instead, the FRP is used for providing lateral confinement to the core concrete to increase its strength and ductility. The brittleness of the FRP composite failing in axial tension is thus not a significant issue. In addition, due to the substantial lateral deformation capacity of the concrete, the high strength of the FRP composite can be fully utilized despite its relatively small elastic modulus. For this type of structures, the poor fire performance of FRP is also not a serious problem as long as a proper design procedure is followed to ensure that the load-carrying capacity contributed by the FRP strengthening system is not required during a fire. Indeed, when FRP confinement is used to enhance seismic resistance, the coupled action of fire and earthquake generally does not need to be considered.

1.2 STRENGTHENING OF RC COLUMNS WITH FRP COMPOSITES

As discussed in the above section, FRP composites in the form of jackets or wraps have been extensively used to strengthen RC columns by providing lateral confinement. In such jackets/wraps, the fibres are typically oriented

entirely in the hoop direction, so the axial stiffness of the jacket can be ignored. FRP jackets for column strengthening can be categorized into wet-layup jackets and prefabricated (or preformed) jackets. Wet-layup jackets are jackets which are formed in-situ from fibre sheets or fabrics that are impregnated with a resin and wrapped continuously or discretely on the surface of existing concrete columns. These wet-layup jackets can easily follow the actual shape of the concrete column and are particularly suitable for the retrofit of existing columns. However, the process involves considerable site work and requires due attention to site quality control. By contrast, prefabricated jackets are made in factory using machines, so the product quality can be better controlled; however, the need to pre-order jackets of specific sizes creates difficulties and delays. Wet-layup jackets have been the dominant form of FRP jackets used to confine RC columns due to their flexibility in shape and ease for transportation.

In the 1980s, FRP jackets were first applied to RC columns to provide additional confinement in Japan (Katsumata et al. 1987). Since then, various experimental and analytical studies have been conducted in this area. The fundamental mechanism underlying this strengthening technique is that the axial compressive strength and ultimate axial compressive strain of the concrete can be significantly increased through lateral confinement. This fundamental mechanism was first exploited for concrete under uniform confinement as is the case with circular columns. For FRP-confined circular RC columns, for which uniform confinement from the FRP jacket can be assumed, many stress-strain models for FRP-confined concrete have been

developed. These models have commonly been classified into two classes (Teng and Lam 2004): design-oriented stress-strain models and analysis-oriented stress-strain models. The best of these models can provide quite accurate quantitative predictions for the stress-strain behaviour of FRP-confined concrete in circular columns.

The confinement mechanism for concrete in FRP-confined non-circular columns is much less understood as the concrete is under non-uniform confinement in such columns. A large amount of experimental and analytical work has been conducted on the behaviour of FRP-confined concrete in rectangular RC columns over the past decade, leading to various stress-strain models. No consensus on the reliability of these models, however, has been achieved, particularly with regard to their capability of predicting the behaviour of FRP-confined concrete in large/full-scale rectangular RC columns. There is therefore still a strong need for more work on the stress-strain response and the failure mechanism of this type of FRP-confined RC columns. Even less is known about FRP-confined concrete in other non-circular columns such as elliptical columns which may result from the shape modification of existing rectangular columns.

Two approaches have been commonly used for developing analytical models for FRP-confined non-circular RC columns. These two approaches focus on modelling the behaviour of confined concrete, as it is the key and the most complex part in modelling the behaviour of the entire RC column.

In the first approach, the concept of "effective confinement" is utilized to estimate the amount of effective confining pressure acting on the concrete. This estimation is typically done by evaluating the stress in the confining material (e.g. the FRP jacket), the effectiveness of confinement over the cross-section, and other cross-sectional properties. The improvement in concrete strength is then explicitly determined by referring to experimental results for concrete at an equivalent uniform confining pressure. This approach, however, fails to capture the stress variation over the cross-section.

In the second approach, a constitutive model for concrete is used in a finite element analysis to implicitly model the effect of confinement of concrete. The confinement mechanism is explicitly modelled in this approach with the confinement material (e.g. the FRP jacket) being explicitly represented in the finite element model. Interaction between the concrete and the confining material is properly accounted for and the effect of confinement variation over a non-circular section can be taken into account. Due to these reasons, the second approach (i.e. the finite element method) was the main approach adopted in the present research project to model the behaviour of FRP-confined concrete/RC columns.

1.3 OBJECTIVES AND SCOPE

The ability of the finite element method to predict the behaviour of FRP-confined RC columns depends mainly on the concrete constitutive model employed in the analysis. The primary aim of this thesis is thus to develop generic constitutive models which are capable of predicting the

behaviour of concrete when it is confined.

Extensive constitutive models already exist for describing the mechanical behaviour of concrete. Depending on the theoretical frameworks employed, these models are referred to as nonlinear elasticity models (e.g. Elwi and Murray 1979), plasticity models (e.g. Imran and Pantazopoulou 2001), plastic-damage models (e.g. Lee and Fenves 1998), endochronic models (e.g. Bazant and Bhat 1976), and microplane models (e.g. Bazant et al. 2000). These models have been used in finite element analyses to predict the complex behaviour of concrete under general states of stresses. Each constitutive model has its advantages and drawbacks, and is likely to work well only in particular types of applications. A more in-depth discussion of concrete constitutive models can be found in Chen and Han (2007).

The primary aim of this research is to develop constitutive models capable of predicting the behaviour of concrete under varying levels of confinement. To achieve this aim, existing constitutive models which have an adequate potential in producing close predictions for the behaviour of actively-confined concrete are focused on in this thesis. Accurate predictions of the behaviour of confined concrete require accurate predictions of the peak stress, the axial strain at peak stress, as well as the slope of the descending branch for actively-confined concrete or the slope of the ascending branch for FRP-confined concrete. Three types of constitutive models are examined in this thesis, including plasticity models, plastic-damage models and

microplane models. More detailed descriptions of these models can be found in the subsequent chapters of the thesis.

Apart from a reliable constitutive model for the concrete, the determination of appropriate values for the parameters in the model is also crucially important. Two approaches of parameter identification are examined in this thesis. The first approach is based on the test results of confined concrete. This method is used to explain how the experimental results can be predicted using a given concrete constitutive model. The second approach is based on empirical models developed for confined concrete. This method can be used as a predictive method; that is, the values of some of the material parameters for a concrete constitutive model are derived from an empirical model which is capable of providing accurate predictions for confined concrete (mainly uniformly-confined concrete). Previous attempts of using the second approach can be found in Oh (2002), Yu et al. (2010a) and Yu et al.(2010b).

What should also be mentioned is that concrete is a brittle material with distinctively different responses in tension and compression. The constitutive models used for description of the behaviour of these two parts, therefore, may be significantly different from each other. In this thesis, only constitutive models for concrete under compression are examined. Constitutive models for concrete under tension are mentioned only when the possibility of tension-softening of concrete arises. The thesis consists of 10 chapters as detailed below.

In Chapter 2, a literature review of issues related to the work presented in this PhD thesis is presented. It starts with a brief review of existing stress-strain models for actively-confined concrete and FRP-confined concrete based on tests on small-scale specimens under concentric compression. Constitutive models developed for modelling confined concrete are then reviewed with reference to the theoretical frameworks adopted. Existing finite element studies on FRP-confined concrete/RC columns are also reviewed. Needs for the work presented in the subsequent chapters are identified.

Chapter 3 presents an experimental study on the behaviour of FRP-confined high strength concrete (HSC). Experimental results for FRP-confined HSC were obtained to expand the existing test database. A unified stress-strain model for actively-confined concrete, applicable to both normal strength concrete and HSC, is proposed; a similarly unified FRP-confined concrete model (an analysis-oriented stress-strain model) is next presented. By comparing these two stress-strain models, it is shown that the path independence assumption commonly utilized in analysis-oriented stress-strain models is only partially justified.

Chapters 4 and 5 examine plasticity-based concrete models, which can be categorized into two groups: plasticity models using the so-called scaling technique and plasticity models using the plastic volume strain as the hardening variable. The advantage and disadvantages of these models are

investigated by comparing their results with selected experimental results.

Chapter 6 is concerned with the capability of plastic-damage models in modelling the behaviour of confined concrete. Those two techniques (i.e. the scaling technique and the novel hardening variable approach) used in the plasticity part of the plastic-damage models for improving their performance in prediction for confined concrete are also examined.

Chapter 7 presents a so-called $M4^+$ model based on the original M4 model (a microplane model) developed by Bazant et al.(2000). The drawbacks of the original M4 model reported in existing literature are remedied first and then some confinement sensitive features are incorporated into this model leading to so-called $M4^+$ model. This $M4^+$ model is capable of providing accurate predictions for confined concrete, including both actively-confined concrete and FRP-confined concrete.

In Chapter 8, the ability of two constitutive models to predict the behaviour of FRP-confined square and elliptical columns subjected to monotonic axial loading is studied. These two constitutive models are the $M4^+$ model presented in Chapter 7 and a refined version of the plastic-damage model proposed by Yu et al (2010b). The performance of these two models is assessed by comparing their predictions with experimental results. The confinement mechanism is investigated using results from finite element models based on these constitutive models.

In Chapter 9, a three-dimensional finite element model for FRP-confined circular concrete cylinders and RC columns based on Yu et al.'s (2010b) modified Concrete Damage Plasticity Model (CDPM) is presented. The finite element model is capable of modelling specimens with deformation non-uniformity in the axial direction. The effect of end restraint on the lateral-to-axial strain relationship of FRP-confined concrete is discussed, and a local analysis-oriented stress-strain model is proposed to eliminate this effect. This finite element model can also provide accurate predictions for FRP-confined RC columns.

Finally, Chapter 10 presents a summary of the research results presented in the thesis and outlines future research needs on various aspects of FRP-confined concrete and RC columns.

1.4 REFERENCES

Bazant, Z. P., and Bhat, P. D. (1976). "Endochronic theory of inelasticity and failure of concrete." *Journal of the Engineering Mechanics Division*, ASCE, 102(4), 701-722.

Bazant, Z. P., Caner, F. C., Carol, I., Adley, M. D., and Akers, S. A. (2000). "Microplane model M4 for concrete. I: Formulation with work-conjugate deviatoric stress." *Journal of Engineering Mechanics,* ASCE, 126(9), 944-953.

Chen, W. F., and Han, D. J. (2007). *Plasticity for structural engineers*, J Ross Pub.

Elwi, A. A., and Murray, D. W. (1979). "A 3D hypoelastic concrete constitutive relationship." *Journal of the Engineering Mechanics Division*, ASCE, 105(4), 623-641.

Imran, I., and Pantazopoulou, S. J. (2001). "Plasticity model for concrete under triaxial compression." *Journal of Engineering Mechanics*, ASCE, 127(3), 127- 281.

Jiang, T., and Teng, J. G. (2007). "Analysis-oriented stress-strain models for FRP-confined concrete." *Engineering Structures*, 29(11), 2968-2986.

Katsumata, H., Kobatake, Y., and Takeda, T. (1987). "A study on the strengthening with carbon fiber for earthquake-resistant capacity of existing concrete columns." *Proceedings from the Workshop on Repair and Retrofit of Existing Structures*, U.S.-Japan Panel on Wind and Seismic Effects, U.S.-Japan Cooperative Program in Natural Resources,Tsukuba, Japan, 1816-1823.

Lee, J. H., and Fenves, G. L. (1998). "Plastic-damage model for cyclic loading of concrete structures." *Journal of Engineering Mechanics,* ASCE, 124(8), 892-900.

Oh, B. (2002). *A plasticity model for confined concrete under uniaxial loading*, Lehigh University. 84.

Teng, J.G., and Lam, L. (2004). “Behaviour and modelling of fiber reinforced polymer-confined concrete”, *Journal of Structural*

Engineering, ASCE, 130(11), 1713-1723.

Yu, T., Teng, J. G., Wong, Y. L., and Dong, S. L. (2010a). "Finite element modelling of confined concrete-I: Drucker-Prager type plasticity model." *Engineering Structures*, 32(3), 665-679.

Yu, T., Teng, J. G., Wong, Y. L., and Dong, S. L. (2010b). "Finite element modelling of confined concrete-II: Plastic-damage model." *Engineering Structures*, 32(3), 680-691.

CHAPTER 2

LITERATURE REVIEW

2.1 INTRODUCTION

This chapter presents a review of existing knowledge related to confined concrete, with a special focus on studies that are related to FRP-confined concrete. As pointed out in Chapter 1, failure of reinforced concrete (RC) columns under axial loading involves cracking and substantial lateral dilatation. If this lateral deformation can be restrained through lateral confinement by hydraulic pressure, steel stirrups/spirals or FRP jackets, both the strength and ductility of the concrete/column can be substantially increased.

Of the different methods of providing lateral confinement, the direct use of hydraulic pressure provides a lateral confining pressure which is independent of the lateral deformation of the RC column, and this type of confinement is referred to as active confinement. By contrast, the use of steel stirrups/spirals or FRP jackets provides a lateral confining pressure which is dependent on the lateral deformation of the RC column, and this type of confinement is referred to as passive confinement. Various theoretical formulations have been developed for predicting the behaviour of concrete (and/or RC columns) with different types of lateral confining devices, including active, passive or both. These formulations range from simple empirical models based on regression analysis of experimental

results (e.g. Mander et al. 1988; Lam and Teng 2003) to finite element procedures (e.g. Mirmiran et al. 2000; Ghazi et al. 2002) that implement advanced techniques and theories.

Many of the existing theoretical formulations for confined concrete are capable of predicting complete axial stress-strain curves (e.g. Xie et al. 1995; Attard and Setunge 1996; Xiao and Wu 2000; Candappa et al. 2001; Lam and Teng 2003; Jiang and Teng 2007). Besides the axial stress-strain curves, the dilation behaviour of confined concrete, especially when passively-confined concrete is concerned, plays a very important role in the development of a confinement model; additionally, a number of attempts have been made to capture this aspect accurately. Experimental results for confined concrete, which contain information regarding the lateral dilation, have been collected to establish databases (e.g. Imran and Pantazopoulou 1996; Candappa et al. 2001; Teng et al. 2007; Cui and Sheikh 2010) although the data of lateral dilation shows a relatively large scatter compared to those of concrete strength (Teng et al. 2007). Consequently, recent theoretical models (including empirical models and constitutive models) have placed more emphasis on the dilation properties of confined concrete (Candappa et al. 2001; Oh 2002; Teng et al. 2007; Yu et al. 2010a).

The review of existing work in this chapter is divided into three parts. The first part describes experimental investigations into various parameters of confined concrete behaviour with particular attention to actively-confined concrete and FRP-confined concrete. In this part, experimental results for

actively-confined concrete and FRP-confined concrete are emphasized because they are used in the subsequent chapters to assess the capability of selected computational models. The second part covers empirical models proposed on the basis of experimental observations. The last part discusses computational models (primarily finite element models) based on various constitutive models.

2.2 EXPERIMENTAL WORK

Confined concrete has been an active research topic. A large amount of experimental work has been conducted by many researchers during the past few decades. Early research dates back to 1920's. The pioneering work on confined concrete was conducted by Richart et al. (1928). In their research, concrete cylinders were confined by either uniform hydrostatic pressure or spiral steel reinforcement. This study created a fundamental framework for confined concrete research. Afterwards, Balmer and McHenry (1947) performed a number of tri-axial loading tests at high confining pressure levels. Different researchers, such as Gardner (1969), Mills and Zimmerman (1970), Cedolin et al. (1977), Gerstle (1981), Setunge et al. (1993), Xie et al. (1995), Attard and Setunge (1996), Imran and Pantazopoulou (1996), Rutland and Wang (1997), Ansari and Li (1998), Candappa et al. (2001), Sfer et al. (2002), Lu and Hsu (2006) and Tan and Sun (2006) have conducted numerous tests on actively-confined concrete. These studies have shown that insignificant difference exists between concrete with active confinement and that with passive confinement from closely-spaced circular steel spirals in terms of concrete strength gains due to lateral confinement.

Moreover, different researchers, such as Ahmad and Shah (1982), Sheikh and Uzumeri (1980), Scott et al. (1982), and Mander et al. (1988) have conducted numerous tests on stirrups/spirals-confined concrete. Extensive studies have also been conducted on FRP-confined concrete (e.g. Demers and Neale 1994; Watanabe et al. 1997; Matthys et al. 1999; Rochette and Labossiere 2000; Parvin and Wang 2001; Lam and Teng 2003; Lam and Teng 2004; Berthet et al. 2005; Lam et al. 2006; Li 2006; Jiang and Teng 2007; Teng et al. 2007; Rousakis et al. 2007; Lee et al. 2008; Eid et al. 2009; Lee et al. 2010; and Silva 2011), with the emergence of FRP composites as a new class of confining materials. Generally speaking, for actively-confined and steel-confined concrete, there are sufficient experimental data for both normal strength concrete (NSC) and high strength concrete (HSC); however, test data for FRP-confined HSC are still limited despite the large number of tests on FRP-confined NSC.

2.3 EMPIRICAL MODELS FOR CONCRETE IN CIRCULAR COLUMNS

Various empirical models have been developed for predicting the behaviour of confined concrete. Empirical models for actively-confined concrete have commonly been derived from the regression of experimental results. The confinement behaviour provided by steel stirrups/spirals is similar to that of active confinement although it is a kind of passive confinement. A major difference between actively-confined concrete and steel-bar-confined concrete is that in the former case the concrete is under uniform confinement while in the latter case concrete is under non-uniform confinement in the axial direction. Therefore, an equivalent confining

pressure is widely used in the latter case to represent the effect of axial non-uniformity of confinement. Empirical models developed for actively-confined concrete can be used for predicting the behaviour of steel-bar-confined concrete, once an equivalent uniform confining pressure is defined. This is because steel (particularly mild steel) yields at small strains and the confining pressure provided by steel remains constant after yielding; this confinement condition is thus very similar to that of active confinement from hydraulic pressure.

The behaviour of FRP-confined concrete, however, is significantly different from that of actively-confined concrete. In FRP-confined concrete, the confining pressure increases continuously as the axial deformation (and hence lateral dilation) increases. FRP-confined concrete with an adequate level of confinement (i.e. the FRP jacket is sufficiently strong) has a stress-strain curve that is monotonically ascending with a typical bilinear shape while the stress-strain curve of actively-confined concrete always has a softening branch. In the early stage of research, most of the empirical models developed for FRP-confined concrete were extensions of models previously developed for steel-confined concrete. These models fail to predict the behaviour of FRP-confined concrete accurately due to the difference in performance characteristics between steel-confined and FRP-confined concrete as mentioned above.

Realizing the difference between steel-confined concrete and FRP-confined concrete, empirical models specific to FRP-confined concrete were later

developed. These empirical models can be divided into two types (Teng and Lam 2004). One type is referred to as design-oriented stress-strain models. Empirical models of the first type are directly derived from experimental results of FRP-confined concrete. The second type of empirical models for FRP-confined concrete is referred to as analysis-oriented stress-strain models. This type of models is based on empirical models for actively-confined concrete. Using the so-called path-independence assumption, the behaviour of FRP-confined concrete in a given stress state is taken to be the same as that of actively-confined concrete in the same stress state. The interaction between the FRP jacket and the concrete core is taken into account through an incremental process based on radial displacement compatibility and equilibrium. Analysis-oriented stress-strain models are thus more versatile than design-oriented stress-strain models and can be easily extended to concrete confined by materials other than FRP or steel; they are however generally limited to uniformly confined concrete. More detailed descriptions of analysis-oriented stress-strain models are given later in the chapter.

Among various empirical models for confined concrete as mentioned above, only some typical empirical models are briefly reviewed in this section to keep the review reasonably concise; indeed, a more exhaustive review is not warranted given that the present thesis is primarily concerned with computational models for FRP-confined concrete.

2.3.1 Ahmed and Shah's (1982) Model

An empirical model was proposed by Ahmed and Shah (1982) for

predicting the ascending and descending parts of the stress-strain curve for concrete confined by steel spirals and subjected to tri-axial stresses. This empirical model is based on the properties of the confining reinforcement and the constitutive relationship for plain concrete, and is applicable only to concrete in circular columns.

In their study, the effectiveness of confinement was defined by the following equations:

$$f'^{*}_{cc} = f'_{co} + K_1(\sigma_l)_{eq} \quad (2.1)$$

$$\varepsilon^{*}_{cc} = \varepsilon_{co} + K_2(\sigma_l)_{eq} \quad (2.2)$$

where f'_{co} and f'^{*}_{cc} are the strengths of unconfined concrete and confined concrete, respectively; $(\sigma_l)_{eq}$ is the equivalent confining pressure (i.e. the average confining pressure) at the strength of concrete due to the spirals; ε_{co} and ε^{*}_{cc} are axial strains corresponding to peak stresses of unconfined and confined concrete, respectively. Here, compressive stresses and strains in the concrete are considered to be positive. K_1 and K_2 are functions of the unconfined concrete strength f'_{co} and the equivalent confining pressure $(\sigma_l)_{eq}$.

It was observed by these authors from experimental results that the effectiveness of confinement becomes negligible as the spacing of spirals becomes large. A pitch equal to 1.25 times the diameter of the confined concrete core was thus suggested by these authors as the upper boundary of the spacing of spirals to ensure a significant level of confinement. Based on this observation, and along with the equilibrium conditions between the

concrete core and the steel spirals, the following expression was derived to calculate $(\sigma_l)_{eq}$

$$(\sigma_l)_{eq} = \frac{\rho_s f_y}{2}\left(1 - \sqrt{\frac{S_{sp}}{1.25 d_{cc}}}\right) \tag{2.3}$$

$$\rho_s = \frac{\pi d_{sp}^2}{d_{cc} S_{sp}} \tag{2.4}$$

Here, d_{sp} is the diameter of the steel spiral; d_{cc} is the diameter of the confined concrete core; S_{sp} is the pitch of the steel spirals and f_y is the yield strength of the steel spirals.

The two constants, K_1 and K_2, are calculated as follows:

$$K_1 = \frac{6.61(\sigma_l)_{eq}^{0.04}}{f'_{co}} \text{ (in ksi)} \tag{2.5}$$

$$K_2 = \frac{0.047(\sigma_l)_{eq}^{0.12}}{f'^{1.2}_{co}} \text{ (in ksi)} \tag{2.6}$$

$$\varepsilon_{co} = 0.001648 + 0.000114 f'_{co} \text{ (in ksi)} \tag{2.7}$$

$$\theta_s = 6.6128 + 2.9137 f'_{co} - 44.2315(\sigma_l)_{eq} \text{ (in ksi)} \tag{2.8}$$

Here, θ_s represents the average value of the slope of the descending branch between the axial strain at peak stress and twice the axial strain at peak stress. Eq. (2.8) indicates that with an increase in the unconfined concrete strength, the slope of the descending region of the stress-strain curve becomes steeper. By contrast, with an increase in the equivalent confining pressure $(\sigma_l)_{eq}$, the slope of the descending region of the stress-strain curve becomes flatter.

The stress-strain curves predicted by this empirical model were compared

with their own experimental results as well as those of Iyengar et al. (1970) and Burdette et al. (1971). Adequate agreement was shown between the analytical results and the experimental results. The comparison indicated that complete stress-strain curves of confined concrete can be predicted from the tri-axial stress-strain curves of plain concrete and tensile stress-strain curves of the confining material. However, the validity of the equation for a much larger experimental database is uncertain, as its axial strain at peak stress is not a dimensionless equation.

2.3.2 Mander et al.'s (1988) Model

In Mander et al.'s (1988) study, thirty-one nearly full-size RC columns with different arrangements of longitudinal and transverse steel reinforcements were tested under axial compression. These specimens had different shapes of cross section including, circular, square, and rectangular shapes. All circular columns were of 500 mm in diameter with a 25 mm cover to spirals and were 1500 mm in length. These columns were divided into two groups based on the arrangement of reinforcement. The first group had an identical amount of longitudinal steel reinforcement but different amounts and sizes of transverse steel reinforcement. By contrast, the second group had different amounts and sizes of longitudinal steel reinforcement but identical transverse steel reinforcement. Square columns with square and octagonal ties tested by Scott et al.(1982) were also included in the test database. Moreover, sixteen rectangular walls containing rectangular hoops with additional crossties were cast and tested. Each wall had a cross section of 150 mm×700mm with an overall height of 1200 mm. In these tests, the amount and configuration of the transverse reinforcement were taken as the

principal variables.

Based on these experimental results, an empirical model was developed to describe the stress-strain response of concrete under uni-axial compression and confined by transverse reinforcement. This model works for both circular and rectangular shaped transverse reinforcement. It considers the interaction between the concrete core and the steel spirals through arching action. The angle of arching action is assumed to be 45 degrees and the area of the confined zone is calculated from the areas enclosed by parabolic curves. For the concrete compressive strength, a five parameter failure surface defined by William and Warnke (1975) was adopted. The concrete peak stress under an equivalent confining pressure $(\sigma_l)_{eq}$ is determined by the following equation:

$$f'^{*}_{cc} = f'_{co}\left(-1.254 + 2.254\sqrt{1 + \frac{7.94(\sigma_l)_{eq}}{f'_{co}}} - 2\frac{(\sigma_l)_{eq}}{f'_{co}}\right) \tag{2.9}$$

The axial strain at peak stress ε^{*}_{cc} of the confined concrete is empirically related to the peak stress increment factor through the following equation originally suggested by Richart et al.(1928):

$$\varepsilon^{*}_{cc} = \varepsilon_{co}\left(1 + 5\left(\frac{f'^{*}_{cc}}{f'_{co}} - 1\right)\right) \tag{2.10}$$

In this strain model, the stress-strain relationship suggested by Popovics (1973) is employed to describe the axial stress-strain response of confined concrete. At an axial strain ε_c, the axial compressive stress f_c, is given by following equation:

$$f_c = \frac{f'^{*}_{cc} x r}{r - 1 - x^r} \quad (2.11)$$

where,

$$x = \varepsilon_c / \varepsilon^{*}_{cc} \quad (2.12)$$

$$r = \frac{E_c}{E_c - E_{sec}} \quad (2.13)$$

$$E_{sec} = f'^{*}_{cc} / \varepsilon^{*}_{cc} \quad (2.14)$$

Here, E_c is the tangent modulus of the concrete.

An energy method was utilized in this model so as to calculate the ultimate strain of the confined concrete. This approach assumes that the ultimate strain of the confined concrete core is reached when first hoop fracture occurs. The additional strain energy in the core concrete is assumed in this approach of being provided by the energy stored in the transverse reinforcement. When the energy accumulated in the concrete core exceeds the available energy of the transverse reinforcement, hoop fracture occurs and the section is taken to have reached its ultimate deformation. Mander et al.'s (1988) model achieved a large degree of success in predicting the stress-strain behaviour of steel-confined concrete and was thus modified by subsequent researchers for predicting the stress-strain behaviour of FRP-confined concrete. However, the direct application of this model to FRP-confined concrete is inappropriate and leads to inaccurate predictions as it is a model specific to steel-confined concrete.

2.3.3 Attard and Setunge's (1996) Model

An empirical model was proposed in Attard and Setunge's (1996) study for predicting the complete stress-strain curve of actively-confined and

uni-axially loaded circular concrete cylinders. This model is applicable to a wide range of concrete strengths ranging from 20 to 130 MPa in circular columns. The following nonlinear equation was developed for the peak stress of actively-confined concrete:

$$\frac{f'^{*}_{cc}}{f'_{co}} = \left(1 + \frac{\sigma_l}{f_t}\right)^{k_{AS}} \tag{2.15}$$

Here, f_t is the tensile strength of concrete which is approximately 0.9 times the split cylinder tensile strength f_{sp}, and the parameter k_{AS} is related to f'_{co} as follows:

$$k_{AS} = 1.25\left(1 + 0.062\frac{\sigma_l}{f'_{co}}\right) f'^{\,0.21}_{co} \tag{2.16}$$

From the experimental observations, silica fume was found to have a significant effect on the split cylinder tensile strength f_{sp}. Therefore, two equations were suggested for the determination of the split cylinder tensile strength f_{sp}

$$f_{sp} = \begin{cases} 0.32(f'_{co})^{0.67}\ \text{MPa}, & \text{no silica fume} \\ 0.62\sqrt{f'_{co}}\ \text{MPa}, & \text{silica fume} \end{cases} \tag{2.17}$$

Eqs. (2.15) and (2.17) indicate that silica fume can influence the confinement effectiveness of actively-confined concrete.

The following equation was developed to describe the relationship between the axial strain at peak stress and the confining pressure σ_l:

$$\frac{\varepsilon^{*}_{cc}}{\varepsilon_{co}} = 1 + (17 - 0.06f'_{co})\left(\frac{\sigma_l}{f'_{co}}\right) \tag{2.18}$$

Beyond the point of peak stress, a point of inflexion on the descending branch of the stress-strain curve is defined in this model to control the slope

of the descending branch.

For concrete under uni-axial compression, the inflexion point on the descending branch is defined by the following approximate expressions:

$$\frac{\varepsilon_{ic}}{\varepsilon_{co}} = 2.5 - 0.3\ln(f'_{co})\ \text{MPa} \tag{2.19}$$

$$\frac{f_{ic}}{f'_{co}} = 1.47 - 0.17\ln(f'_{co})\ \text{MPa} \tag{2.20}$$

Here, f_{ic} and ε_{ic} are the axial stress and the axial strain at the inflexion point, respectively.

For confined concrete, the inflexion point of the descending branch is defined by the following approximate expressions:

$$\frac{f_i}{f'^{*}_{cc}} = \frac{\frac{f_{ic}}{f'_{co}} - 1}{5.06\left(\frac{\sigma_l}{f'_{co}}\right)^{0.57} + 1} + 1 \tag{2.21}$$

$$\frac{\varepsilon_i}{\varepsilon^{*}_{cc}} = \frac{\frac{\varepsilon_{ic}}{\varepsilon_{co}} - 2}{1.12\left(\frac{\sigma_l}{f'_{co}}\right)^{0.26} + 1} + 2 \tag{2.22}$$

Furthermore, the axial stress f_{2i} at $\varepsilon_{2i} = 2\varepsilon_i$ is defined by the following equation which is similar to Eq. (2.21):

$$\frac{f_{2i}}{f'^{*}_{cc}} = \frac{\frac{f_{2ic}}{f'_{co}} - 1}{6.35\left(\frac{\sigma_l}{f'_{co}}\right)^{0.62} + 1} \tag{2.23}$$

where f_{2ic}, being for the uni-axial case, can be estimated from

$$\frac{f_{2ic}}{f'_{co}} = 1.45 - 0.25\ln(f'_{co})\ \text{MPa} \tag{2.24}$$

The following non-dimensional mathematical expression suggested by

Sargin (1971) was employed for the stress-strain curve of confined concrete:

$$y = \frac{A_{AS}x + B_{AS}x^2}{1 + C_{AS}x + D_{AS}x^2} \tag{2.25}$$

where $y = \frac{f_c}{f'^*_{cc}}$.

For the ascending branch, the four constants in Eq. (2.25) are given by

$$A_{AS} = \frac{E_{ti}\varepsilon^*_{cc}}{f'^*_{cc}} \tag{2.26}$$

$$B_{AS} = \frac{(A_{AS}-1)^2}{\alpha_a\left(1-\frac{f_{pl}}{f'^*_{cc}}\right)} + \frac{A_{AS}^2(1-\alpha_a)}{\alpha_a^2\frac{f_{pl}}{f'^*_{cc}}\left(1-\frac{f_{pl}}{f'^*_{cc}}\right)} - 1 \tag{2.27}$$

$$C_{AS} = A_{AS} - 2 \quad D_{AS} = B_{AS} + 1 \tag{2.28}$$

where $f_{pl} = 0.45f'_{co}$, E_{cc} is the secant modulus measured at a stress of f_{pl}, E_{ti} is the initial tangent modulus for confined concrete, and $\alpha_a = E_{ti}/E_{cc}$.

For the descending, these four constant are given by

$$A_{AS} = \left(\frac{\varepsilon_{2i}-\varepsilon_i}{\varepsilon^*_{cc}}\right)\left[\frac{\varepsilon_{2i}E_i}{f'^*_{cc}-f_i} - \frac{4\varepsilon_i E_{2i}}{f'^*_{cc}-f_{2i}}\right] \tag{2.29}$$

$$B_{AS} = (\varepsilon_i - \varepsilon_{2i})\left[E_i - \frac{4E_{2i}}{f'^*_{cc}-f_{2i}}\right] \tag{2.30}$$

$$C_{AS} = A_{AS} - 2 \quad D_{AS} = B_{AS} + 1 \tag{2.31}$$

where

$$E_i = \frac{f_i}{\varepsilon_i} \text{ and } E_{2i} = \frac{f_{2i}}{\varepsilon_{2i}} \tag{2.32}$$

The authors compared the predictions of this model with the their own experimental results and those of Richart et al. (1928). Adequate agreement was found in most cases except their experimental results for the specimens with no silica fume in the concrete mix and at a higher level of confinement.

This model has been employed in some subsequent analysis-oriented stress-strain models for FRP-confined concrete (e.g. Cui and Sheikh 2010) as the active confinement base model because of its high accuracy for actively-confined concrete.

2.3.4 Candappa et al.'s (2001) Model

A series of tests were conducted in Candappa et al.'s (2001) study to investigate the stress-strain behaviour and dilation characteristics of circular concrete cylinders subjected to tri-axial stresses. The cylinders were 98 mm in diameter and 200 mm in height. The concrete strength ranged from 41.1 MPa to 103 MPa. Three lateral pressure values of 4 MPa, 8 MPa, and 12 MPa were applied on the surface of these specimens using oil pressure in a tri-axial cell. Based on the experimental results, the concrete peak stress under a low lateral confining pressure σ_l (i.e., $\sigma_l < 0.2f'_{co}$) was found to be well represented by the following equation:

$$f'^{*}_{cc} = f'_{co} + 5.3\sigma_l \tag{2.33}$$

The axial strain at peak stress of concrete, ε^{*}_{cc}, was found to have a linear relationship with the confinement ratio, as described by the equation below:

$$\frac{\varepsilon^{*}_{cc}}{\varepsilon_{co}} = 1 + 20\left(\frac{\sigma_l}{f'_{co}}\right) \tag{2.34}$$

This equation indicates that the axial strain at a peak stress does not depend on the unconfined concrete strength.

The secant Poisson's ratio model implemented in Ottosen's (1979) model was modified based on the experimental observations of concrete dilation characteristics. A so-called non-linearity index, which is defined by the axial stress ratio $\beta^{I} = f_c/f'^{*}_{cc}$, was related to the secant Poisson's ratio μ^{α} as

follows:

$$\mu^{\alpha} = \begin{cases} \mu_i^{\alpha}, \ \beta^I \leq \beta_1^I \\ \mu_f^{\alpha} - (\mu_f^{\alpha} - \mu_i^{\alpha}) \sqrt{1 - \left(\frac{\beta^I - \beta_1^I}{1 - \beta_1^I}\right)^2}, \ \beta^I > \beta_1^I \end{cases} \quad (2.35)$$

where μ_i^{α} and μ_f^{α} are the initial and final values of the Poisson's ratio. β_1^I is the value taken by β^I when the Poisson's ratio begins to increase. In Ottosen's (1979) model, β_1^I is taken as 0.8, and it shows adequate agreement with experimental results.

With regard to μ_i^{α}, the following equation was suggested based on the curve fitting of the experimental results.

$$\mu_i^{\alpha} = 8 \times 10^{-6}(f'_{co})^2 + 0.0002 f'_{co} + 0.138 \quad (2.36)$$

Based on their experimental observations, the descending curves of $\mu^{\alpha} \sim \beta^I$ were approximately the same, regardless of the uniaxial strength of concrete and the level of lateral confinement. Hence, the following equation was developed for the non-linearity index for the descending portion:

$$\beta_D^I = -0.5(\mu^{\alpha})^2 + 0.45\mu^{\alpha} + 0.9 \quad (2.37)$$

The results of this empirical model were compared with the authors' experimental results and adequate agreement was obtained. The test data of concrete dilation characteristics were also employed in developing the lateral-to-axial strain relationship of the analysis-oriented stress-strain model proposed by Teng et al. (2007)

2.3.5 Lam and Teng's (2002) Model

Lam and Teng (2002) reviewed an extensive database of FRP-confined circular concrete cylinders of about 200 test results. The parameters

examined include the unconfined concrete strength, specimen size, length-to-diameter ratio, and the tensile strength of FRP. Based on the large database, available equations for the compressive strength of FRP-confined concrete were assessed. A simple compressive strength model for design purposes was then proposed.

In this model, the lateral confining pressure acting on the concrete core σ_l is given by

$$\sigma_l = \frac{2f_{frp}t_{frp}}{D_{cor}} \tag{2.38}$$

Here, f_{frp} is the tensile strength of the FRP jacket determined from either flat coupon tests or ring splitting tests; t_{frp} is the thickness of the FRP jacket; and D_{cor} is the diameter of the concrete cylinder.

A linear equation was proposed by Lam and Teng (2002) for the ultimate axial stress of FRP-confined concrete f_{cu} as follows:

$$f_{cu} = f'_{co} + 2\sigma_l \tag{2.39}$$

This simple equation can be used in the design process for the estimation of the compressive strength of FRP-confined concrete. These authors found from Eq. (2.39) that the enhancement of concrete strength due to confinement does not depend on f'_{co}, the specimen size, or the specimen length-to-diameter ratio.

Although this model was simpler and more accurate than the previous compressive strength models for FRP-confined concrete at that time, it does suffer from the limitation that it can only predict the experimental results

accurately when $\frac{\sigma_l}{f'_{co}} < 1$.

2.3.6 Lam and Teng's (2003a) Model

Lam and Teng (2003a) presented a design-oriented stress-strain model for FRP-confined concrete in circular cylinders/columns with the fibers in the FRP jacket being oriented only or predominantly in the hoop direction. This stress-strain model captures all the major features of the stress-strain behaviour of concrete confined with different types of FRP. This model included an FRP efficiency factor K_{frp} to consider the reduced tensile rupture strain of the FRP jacket in FRP-confined concrete cylinders; this was based on the experimental observation that the tensile strength of the FRP material obtained from flat coupon tests is generally not reached when the FRP jacket ruptures in an FRP-confined circular concrete cylinder. The FRP efficiency factor is defined as the ratio of the actual FRP hoop rupture strain $\varepsilon_{h,rup}$ determined from the tests of FRP-confined concrete cylinders to the FRP rupture strain obtained from flat coupon tests ε_{frp}. That is

$$K_{frp} = \varepsilon_{h,rup}/\varepsilon_{frp} \tag{2.40}$$

In this model, the FRP efficiency factor K_{frp} is employed for calculating the so-called actual hoop rupture strain and the actual maximum confining pressure $f_{l,a}$ in the FRP-confined concrete. That is,

$$f_{l,a} = \frac{2f_{h,frp}t_{frp}}{D_{cor}} = \frac{2E_{frp}\varepsilon_{h,frp}t_{frp}}{D_{cor}} \tag{2.41}$$

Using the actual maximum confining pressure, the following linear equation was proposed for the ultimate axial stress of FRP-confined concrete f_{cu}:

$$f_{cu} = f'_{co} + 3.3f_{l,a} \tag{2.42}$$

For the ultimate axial strain, the following expression was proposed:

$$\frac{\varepsilon_{cu}}{\varepsilon_{co}} = 1.75 + 12\frac{f_{l,a}}{f'_{co}}\left(\frac{\varepsilon_{h,rup}}{\varepsilon_{co}}\right)^{0.45} \quad (2.43)$$

Based on the experimental results of 52 CFRP-wrapped specimens, an average value 0.582 was suggested for the FRP efficiency factor K_{frp}. As a result, Eq. (2.43) can be rewritten as

$$\frac{\varepsilon_{cu}}{\varepsilon_{co}} = 1.75 + 5.53\frac{f_{l,a}}{f'_{co}}\left(\frac{\varepsilon_{frp}}{\varepsilon_{co}}\right)^{0.45} \quad (2.44)$$

With this equation and the FRP efficiency factor, the user only needs to know the tensile strain ε_{frp} which is commonly provided by the manufacturer.

The following stress-strain model was proposed for FRP-confined concrete:

$$\sigma_c = \begin{cases} E_c\varepsilon_c - \frac{(E_c-E_2)^2}{4f'_{co}}\varepsilon_c^2, & 0 \le \varepsilon_c \le \varepsilon_t \\ f'_{co} + E_2\varepsilon_c, & \varepsilon_t \le \varepsilon_c \le \varepsilon_{cu} \end{cases} \quad (2.45)$$

where

$$\varepsilon_t = \frac{2f'_{co}}{(E_c-E_2)} \quad (2.46)$$

and

$$E_2 = \frac{f_{cu}-f'_{co}}{\varepsilon_{cu}} \quad (2.47)$$

This model can only provide stress-strain curves for well-confined concrete with an ascending second branch. It was found by these authors that to obtain an ascending second branch for FRP-confined concrete cylinders, the actual confinement ratio $\frac{f_{l,a}}{f'_{co}}$ should be not smaller than 0.07.

This empirical model is a typical design-oriented stress-strain model for

FRP-confined concrete. This model was later extended to predict the stress-strain behaviour of FRP-confined concrete in rectangular columns as explained later in this chapter.

2.3.7 Teng et al.'s (2007) Model

Teng et al. (2007) presented an analysis-oriented stress-strain model for FRP-confined concrete in circular columns with the fibers in the FRP jacket being oriented only or predominantly in the hoop direction. An analysis-oriented stress-strain model is more versatile when compared to a design-oriented stress-strain model (e.g. Lam and Teng 2003a). It can predict either a typical bi-linear stress-strain curve for well-confined concrete or an ascending-descending stress-strain curve for weakly-confined concrete.

As mentioned previously, an analysis-oriented stress-strain model is based on an active confinement model. The active confinement model describes the axial stress-strain relationship for concrete under a constant confining pressure. The so-called path independency assumption is adopted to relate the axial stress under active confinement to that under passive confinement. This assumption supposes that the axial stress and axial strain of concrete confined by an FRP jacket at a given lateral strain should be the same as those of the same concrete confined by a constant confining pressure equal to that supplied by the FRP jacket. To obtain the axial strain at a given lateral strain, a lateral-to-axial strain equation is adopted in the analysis-oriented stress-strain model. Teng et al. (2007) found that the relationship between the lateral strain and axial stain in concrete under

varying levels of lateral confinement can be represented by the following expression:

$$\emptyset\left(\frac{-\varepsilon_l}{\varepsilon_{co}}\right)=\frac{\frac{\varepsilon_c}{\varepsilon_{co}}}{\left(1+8\frac{f_l}{f'_{co}}\right)}=A_t\left\{\left[1+B_t\left(\frac{-\varepsilon_l}{\varepsilon_{co}}\right)\right]^{C_t}-\exp\left[-D_t\left(\frac{-\varepsilon_l}{\varepsilon_{co}}\right)\right]\right\} \quad (2.48)$$

In this equation, the constants A_t, B_t, C_t, and D_t are 0.85, 0.75, 0.7 and 7, respectively. They were calibrated against test data for unconfined, actively confined and FRP confined concrete through a trial-and-error procedure. Eq. (2.48) indicates that the confining pressure has a significant effect on the lateral-to-axial strain relationship.

With the lateral-to-axial strain equation clarified, Eq. (2.11) proposed by Popovic (1973) was adopted in the active confinement model for the description of axial stress-strain relationship. The concrete peak stress under a lateral confining pressure σ_l is given by the following equation:

$$f'^{*}_{cc}=f'_{co}+3.5\sigma_l \quad (2.49)$$

The equation for the axial strain at peak stress of concrete ε^{*}_{cc} is given by

$$\frac{\varepsilon^{*}_{cc}}{\varepsilon_{co}}=1+17.5\left(\frac{\sigma_l}{f'_{co}}\right) \quad (2.50)$$

In a subsequent study by the same research group (Jiang and Teng 2007), Eq. (2.50) was revised to

$$\frac{\varepsilon^{*}_{cc}}{\varepsilon_{co}}=1+17.5\left(\frac{\sigma_l}{f'_{co}}\right)^{1.2} \quad (2.51)$$

This modification aimed to achieve more accurate predictions for FRP-confined concrete with relatively weak confinement.

This analysis-oriented stress-strain model can provide accurate predictions for FRP-confined concrete at different confinement levels. It also has the

capability to provide accurate predictions for actively-confined concrete and steel-confined concrete. As the two analysis-oriented stress-strain models (Teng et al. 2007; Jiang and Teng 2007) were only verified using test data for FRP-confined normal strength concrete, their accuracy for FRP-confined high strength concrete is still uncertain.

2.3.8 Cui and Sheikh's (2010) Model

Cui and Sheikh (2010) presented an analysis-oriented stress-strain model for FRP-confined concrete in circular columns with the aim of modelling concrete with a wide range of strength from 25 MPa to 112 MPa. This model was developed based on material properties, force equilibrium, and strain compatibility. A new active confinement model which is a modified version of Attard and Setunge (1996), was proposed in this analysis-oriented stress-strain model, in which the following equations defining the point of peak stress were developed to replace those in Attard and Setunge (1996):

$$\frac{f'^{*}_{cc}}{f'_{co}} = \begin{cases} \left(1 + 10\frac{\sigma_l}{f'_{co}}\right)^{0.6}, & f'_{co} < 60\ MPa \\ \left(1 + 14\frac{\sigma_l}{f'_{co}}\right)^{0.5}, & f'_{co} \geq 60\text{MPa} \end{cases} \tag{2.52}$$

and

$$\frac{\varepsilon^{*}_{cc}}{\varepsilon_{co}} = 1 + \left(70 - 13\ln(f'_{co})\right)\left(\frac{\sigma_l}{f'_{co}}\right) \tag{2.53}$$

Using a general formulation proposed by Imran and Pantazopoulou (1996), the following dilation model was proposed to determine the relationship between the volumetric strain ε_v and the axial strain ε_c:

$$\varepsilon_v = (1 - 2\mu_o)\left[\frac{2\sigma_l}{E_c} + \varepsilon_c^{vo}\left(\frac{\varepsilon_c}{\varepsilon_c^{vo}} - b_{CS}\left[\frac{\langle\varepsilon_c - \varepsilon_c^{lim}\rangle}{\varepsilon_c^{vo} - \varepsilon_c^{lim}}\right]^{c_{CS}}\right)\right] \tag{2.54}$$

Here, μ_o is the Poisson's ratio of concrete and $\varepsilon_c^{vo} = a_{CS}\varepsilon^{*}_{cc}$ is the

reference strain. Parameters a_{CS}, b_{CS}, and c_{CS} are material parameters calibrated from experimental results. In addition, b_{CS} and c_{CS} are found to be the main parameters controlling the effect of the confinement ratio on the shape of the axial-volumetric strain curve while a_{CS} depends mainly on the unconfined concrete strength f'_{co}. The McCauley bracket $\langle\cdot\rangle$ is defined as $\langle x\rangle = 0.5[x + abs(x)]$. ε_c^{lim} is the axial strain corresponding to concrete cracking in the lateral direction. It can be determined as

$$\varepsilon_c^{lim} = \frac{1-\mu_o}{\mu_o E_c}\sigma_l - \frac{\varepsilon_{cr}}{\mu_o} \tag{2.55}$$

Here, ε_{cr} can be determined from the splitting tensile strength f_{cr} as proposed by Aroglu et al.(2006):

$$\varepsilon_{cr} = \frac{f_{cr}}{E_c} = 0.387 f_{co}'^{0.63}/E_c \tag{2.56}$$

The following equations were suggested for parameters a_{CS}, b_{CS}, and c_{CS}:

$$0.65 \le a_{CS} = \frac{f'_{co}}{\langle f'_{co}-50\rangle+40} - 0.1 \le 1.1 \tag{2.57}$$

$$b_{CS} = 1 - \sigma_l/f'_{co} \ge 0.7 \tag{2.58}$$

$$c_{CS} = (f'_{co} - \sigma_l)/30 \ge 2.0 \tag{2.59}$$

Eq. (2.58) indicates that for concrete with different strengths but similar confinement ratios, a similar b_{CS} can be expected; whereas Eq. (2.59) indicates that parameter c_{CS} increases with the unconfined concrete strength but decreases with the lateral pressure.

Although this model was developed for FRP-confined concrete, it can be also applied to steel hoops/spirals-confined concrete columns as long as the assumption of effectively-confined concrete area A_e is adopted. The same assumption as suggested by Sheikh and Uzumeri (1982) and adopted in

Mander et al.(1988) was used to determine the effectively-confined concrete area A_e:

$$A_e = \begin{cases} \left(1 - \frac{s}{2D_{cor}}\right)^2 A_c, & \text{(for circular hoops)} \\ \left(1 - \frac{s}{2D_{cor}}\right) A_c, & \text{(for circular spirals)} \end{cases} \quad (2.60)$$

where A_c is the total area surrounded by the concrete hoops/spirals, s is the clear spacing between steel hoops/spirals.

This model was employed to predict the behaviour of actively-confined concrete and FRP-confined concrete. For actively-confined concrete, the model was capable of providing accurate predications; for FRP-confined normal strength concrete, the model was also capable of providing accurate predictions for the axial stress at a given axial strain but incapable of providing accurate predictions for the ultimate axial strain; for FRP-confined very high strength concrete (e.g. with a concrete strength up to 110.6 MPa), the model significantly underestimated the axial stress at an axial strain near the transition zone between the parabolic first portion and the linear second portion of the stress-strain curve. The model can be applied in predicting the stress-strain behaviour of FRP-confined concrete with discontinuous FRP jackets, when Eq. (5.60) is used to calculate the effectively-confined concrete area A_e.

2.3.9 Lam and Teng's (2003b) Model

Lam and Teng (2003b) presented a simple design-oriented stress-strain model for FRP-confined concrete in rectangular columns. This model was

an extension of their design-oriented stress-strain model for concrete uniformly-confined by FRP jackets (Lam and Teng 2003a), and was verified with a database of experimental results collected by the authors. Compared to their design-oriented stress-strain model developed for concrete uniformly confined with FRP, the major difference lies in the equations used for the prediction of the ultimate axial stress and the ultimate axial strain. Experimental results have shown that the confinement of FRP jackets in rectangular columns is not as effective as that in circular columns. Therefore, two shape factors, k_{s1} and k_{s2}, were introduced by the authors to consider the effect of section shape on the ultimate axial stress and the ultimate axial strain, respectively. That is, the ultimate axial stress is given by

$$f_{cu} = f'_{co} + k_1 k_{s1} f_{l,a} \tag{2.61}$$

while the ultimate axial strain is given by

$$\frac{\varepsilon_{cu}}{\varepsilon_{co}} = 1.75 + k_2 k_{s2} \frac{f_{l,a}}{f'_{co}} \left(\frac{\varepsilon_{h,rup}}{\varepsilon_{co}}\right)^{0.45} \tag{2.62}$$

Here, $k_1 = 3.3$ and $k_2 = 12$ as was proposed by Lam and Teng (2003a).

For FRP-confined concrete in rectangular columns, the hoop stress and the hoop strain in the FRP jacket vary considerably around the periphery. Therefore, Eq. (2.38), which was proposed to calculate the confining pressure under uniform confinement, is not applicable to FRP-confined concrete in rectangular columns. To address this critical issue in developing the particular design-oriented stress-strain model, an equivalent circular column was defined, which has an assumed diameter D_{eq}. Using this assumed diameter D_{eq}, Eq. (2.38) can thus be used for the calculation of

the equivalent confining pressure. The equivalent diameter D_{eq} is defined in this model as the diagonal length of the section (see Fig. 2.1). That is

$$D_{eq} = \sqrt{h^2 + b^2} \tag{2.63}$$

where h is the length of the long side of the rectangle, and b is the length of the short side of the rectangle.

The two shapes factors, k_{s1} and k_{s2}, are defined as follows:

$$k_{s1} = \left(\frac{b}{h}\right)^2 \frac{A_e}{A_c} \tag{2.64}$$

and

$$k_{s2} = \left(\frac{h}{b}\right)^{0.5} \frac{A_e}{A_c} \tag{2.65}$$

The effective confinement area ratio A_e/A_c is given by:

$$\frac{A_e}{A_c} = 1 - \frac{\frac{b}{h}(h-2R_c)^2 + \frac{h}{b}(b-2R_c)^2}{3A_g} \tag{2.66}$$

Here, R_c is the radius of the rounded corners, and A_g is the gross area of the column section with rounded corners, which is given by

$$A_g = bh - (4-\pi)R_c^2 \tag{2.67}$$

This model is simple and can provide accurate predictions for the experimental results available at the time. The limitation of the model is that it can only be used to predict the stress-strain behaviour of FRP-confined concrete in rectangular columns. Moreover, this empirical model is not based on a rigorous understanding of the confinement mechanism in the rectangular section. Lack of rigorous understanding of the confinement mechanism is the common and fundamental drawback of empirical

stress-strain models of this type.

2.3.10 Youssef et al.'s (2007) Model

Youssef et al. (2007) presented a design-oriented stress-strain model for FRP-confined concrete in circular or rectangular columns. This model is also based on experimental results covering a wide range of confinement ratios. Experimental observations showed that the following factors have a significant effect on the stress-strain behaviour of FRP-confined concrete: unconfined concrete strength f'_{co}, volume ratio of the FRP jacket ρ_j, ultimate lateral strength of the FRP jacket f_{ju}, and cross-sectional geometry. Such parameters were analyzed statistically based on experimental results, and equations were proposed to predict the effects of these parameters.

In this model, the ultimate confining pressure f_{lu} for both circular and rectangular sections is defined by the confinement ratio ρ_j (i.e. the jacket volume divided by the concrete volume). That is

$$f_{lu} = \frac{1}{2}\rho_j f_{ju} \tag{2.68}$$

The following ultimate effective lateral confining pressure f'_{lu} is used to replace f_{lu} so as to obtain a unified model for FRP-confined concrete in both circular and rectangular sections. In this model, the ultimate effective lateral confining pressure is defined as:

$$f'_{lu} = k_e f_{lu} \tag{2.69}$$

Here, k_e is the confinement effectiveness coefficient, which is defined as

$$k_e = \begin{cases} 1, \text{ for circular section} \\ 1 - \frac{\frac{b}{h}(h-2R_c)^2 + \frac{h}{b}(b-2R_c)^2}{3A_g}, \text{ for rectangular section} \end{cases} \tag{2.70}$$

The definition of parameters b, h, R_c and A_g are the same as those in Lam and Teng's (2003b) model.

The stress-strain curve of FRP-confined concrete in this model is controlled by two characteristic points: the transition point and the ultimate point. To define the ultimate point, the compressive strength of FRP-confined concrete is given as

$$\frac{f_{cu}}{f'_{co}} = \begin{cases} 1 + 2.25\left(\frac{f'_{lu}}{f'_{co}}\right)^{5/4}, & \text{for circular section} \\ 0.5 + 1.225\left(\frac{f'_{lu}}{f'_{co}}\right)^{3/5}, & \text{for rectangular section} \end{cases} \tag{2.71}$$

The ultimate axial strain of FRP-confined concrete is given as

$$\varepsilon_{cu} = \begin{cases} 0.003368 + 0.2950\left(\frac{f'_{lu}}{f'_{co}}\right)\left(\frac{f_{ju}}{E_{frp}}\right)^{\frac{1}{2}}, \\ \text{for circular section} \\ 0.004325 + 0.2625\left(\frac{f'_{lu}}{f'_{co}}\right)\left(\frac{f_{ju}}{E_{frp}}\right)^{\frac{1}{2}}, \\ \text{for rectangular section} \end{cases} \tag{2.72}$$

For the transition point, the axial stress f_{tran} is defined as

$$\frac{f_{tran}}{f'_{co}} = \begin{cases} 1 + 3.0\left(\frac{\rho_j E_{frp}\varepsilon_{frp,t}}{f'_{co}}\right)^{5/4}, & \text{for circular section} \\ 1 + 1.1350\left(\frac{\rho_j E_{frp}\varepsilon_{frp,t}}{f'_{co}}\right)^{5/4}, & \text{for rectangular section} \end{cases} \tag{2.73}$$

where $\varepsilon_{frp,t}$ is the strain of FRP at the transition point. Similarly, the axial strain ε_{tran} at the transition point is defined as

$$\varepsilon_{tran} = \begin{cases} 0.002748 + 0.1169\left(\frac{\rho_j E_{frp}\varepsilon_{frp,t}}{f'_{co}}\right)^{\frac{6}{7}}\left(\frac{f_{ju}}{E_{frp}}\right)^{\frac{1}{2}}, \\ \text{for circular section} \\ 0.002 + 0.0775\left(\frac{\rho_j E_{frp}\varepsilon_{frp,t}}{f'_{co}}\right)^{\frac{6}{7}}\left(\frac{f_{ju}}{E_{frp}}\right)^{\frac{1}{2}}, \\ \text{for rectangular section} \end{cases} \tag{2.74}$$

Once the transition point and the ultimate point are determined, the slope of the second branch E_2 can be calculated by

$$E_2 = \frac{f_{cu} - f_{tran}}{\varepsilon_{cu} - \varepsilon_{tran}} \tag{2.75}$$

The stress-strain relationship for FRP-confined concrete is defined by a two-region model to form a unified model. For FRP-confined concrete with an ascending second branch (i.e. $E_2 > 0$), the expression for the stress-strain relationship is

$$f_c = \begin{cases} E_c\varepsilon_c \left[1 - \frac{1}{n}\left(1 - \frac{E_2}{E_c}\right)\left(\frac{\varepsilon_c}{\varepsilon_{tran}}\right)^{n-1}\right], & 0 \le \varepsilon_c < \varepsilon_u \\ f_{tran} + E_2\varepsilon_c, & \varepsilon_{tran} \le \varepsilon_c < \varepsilon_u \end{cases} \tag{2.76}$$

Here, $n = \frac{(E_c - E_2)\varepsilon_{tran}}{E_c\varepsilon_{tran} - f_{tran}}$.

For FRP-confined concrete with a descending second branch (i.e. $E_2 < 0$), the expression for the stress-strain relationship is

$$f_c = \begin{cases} E_c\varepsilon_c \left[1 - \frac{1}{n}\left(\frac{\varepsilon_c}{\varepsilon_{tran}}\right)^{n-1}\right], & 0 \le \varepsilon_c < \varepsilon_u \\ f_{tran} + E_2\varepsilon_c, & \varepsilon_{tran} \le \varepsilon_c < \varepsilon_u \end{cases} \tag{2.77}$$

Here, $n = \frac{E_c\varepsilon_{tran}}{E_c\varepsilon_{tran} - f_{tran}}$.

This model still falls into the category of design-oriented stress-strain models, although a more complex formulation was adopted. The common and fundamental drawback of empirical stress-strain models of this type still exists in this model. The lateral confining pressure is obtained using the confinement ratio ρ_j and a reduced factor k_e. However, this k_e is still not

based on a rigorous understanding of the confinement mechanism.

2.4 COMPUTATIONAL MODELS

The finite element method has frequently been employed for predicting the experimental results of concrete columns/sections under complex stress states. This method is capable of capturing stress variations within the entire test specimen and predicting interactions between components (e.g. between the FRP jacket and the concrete core in an FRP-confined concrete column). Therefore, the finite element method provides a powerful tool to investigate the confinement mechanism of FRP-confined concrete. However, the success of a finite element computational model to a large extent depends on the use of an appropriate constitutive model for each component material. Various constitutive models for concrete under tri-axial stress states have been developed. Some of these models have been applied in predicting the response of confined concrete columns with some degree of success. The more significant of these constitutive models are reviewed below to reflect the development of constitutive models for confined concrete.

2.4.1 Constitutive models in ABAQUS

In general, constitutive models coded into commercially available software packages, such as ABAQUS, are most widely accessible to researchers. These models are also well maintained and possibly extendable. However, as commercially available software packages are for general-purpose finite element modelling, they may not have all the features required for a particular application of interest.

In ABAQUS, two commonly used constitutive models for concrete in tri-axial compression are available. One is the Extended Drucker-Prager (D-P) Model which employs a modified D-P type yield criterion (Drucker and Prager 1952). In order to describe the different confinement responses of biaxial compression and tri-axial compression (e.g. a cylindrical core sample is loaded axially to failure at constant confining pressure), the effect of the third deviatoric stress invariant is included in this model. This model also allows the user definition of strain hardening/softening and the adoption of a non-associated flow rule. The other model available in ABAQUS is the Concrete Damaged Plasticity Model (CDPM). It is a plastic-damage model combining isotropic damaged elasticity with isotropic tensile and compressive plasticity to describe the inelastic behaviour of concrete. This model adopts the yield criterion proposed by Lee and Fenves (1998) which reduces to the D-P type yield criterion for the special case of concrete under equal tri-axial compression. It also includes the effect of the third deviatoric stress invariant, with a large range of allowed shear strength ratio which covers normal experimental results of concrete. A scalar damage variable, which varies with the plastic deformation, is used in this model to reflect the degradation of elastic stiffness under loading. Moreover, strain hardening/softening can be defined by the user and a non-associated flow rule is utilized to describe the dilation characteristics of concrete.

An equivalent plastic strain is taken as the only variable in the strain hardening/softening function in these two constitutive models. Due to the limitation of this type of hardening/softening rule, which is carefully

discussed in Chapters 4 and 5 of this thesis, these two constitutive models fail to capture the increased deformation capacity of concrete under tri-axial compression even for actively-confined concrete.

2.4.2 Barros' (2001) Model

A constitutive model based on the theory of elasto-plasticity was presented by Barros (2001) for concrete under tri-axial compression. This model was developed for both the D-P type yield criterion and the Ottosen yield criterion (Ottosen 1977). The hardening/softening behaviour of concrete is modelled using the MC90 (CEB-FIP MC 1990) equation developed for uni-axial compression. The confinement effect is depicted through multiplying the hardening/softening modulus by a function of the intermediate principal stress. The numerical results obtained for the concrete cylinders tested by Iyengar et al.(1970) showed reasonable agreement with the experimental results.

In Barros' (2001) elasto-plastic model, the stress increment vector $d\boldsymbol{\sigma}$ and the strain increment vector $d\boldsymbol{\varepsilon}$ are related by the elasto-plastic material matrix $\mathbf{D}_{ep}$. That is

$$d\boldsymbol{\sigma} = \mathbf{D}_{ep}\, d\boldsymbol{\varepsilon} \tag{2.78}$$

where $\mathbf{D}_{ep}$ is defined as follows:

$$\mathbf{D}_{ep} = \mathbf{D} - \frac{\mathbf{D}\mathbf{b}_m\mathbf{a}_m^T\mathbf{D}}{\mathbf{a}_m^T\mathbf{D}\mathbf{b}_m + \mathbf{H}} \tag{2.79}$$

Here, $\mathbf{D}$ is the elastic material matrix, $\mathbf{a}_m$ and $\mathbf{b}_m$ are the gradients of the yield and potential functions F and G respectively, $\mathbf{H}$ is the hardening parameter, and the superscript T indicates the transpose of vector and

matrix.

$$\mathbf{a_m} = \frac{dF}{d\boldsymbol{\sigma}} \tag{2.80}$$

$$\mathbf{b_m} = \frac{dG}{d\boldsymbol{\sigma}} \tag{2.81}$$

If a non-associative flow rule is used, the yield and the potential functions F and G are different. The hardening parameter **H** is a function of the yield function.

The following MC90 (CEB-FIP MC 1990) equation for uni-axial compression was used by Barros (2001) to model the hardening and softening behaviour:

$$\sigma_C = -\frac{\left(\frac{E_c\varepsilon_c}{E_{c1}\varepsilon_{c1}} - \left(\frac{\varepsilon_c}{\varepsilon_{c1}}\right)^2\right)}{1+\left(\frac{E_c}{E_{c1}}-2\right)\frac{\varepsilon_c}{\varepsilon_{c1}}} f'_{co} \tag{2.82}$$

where $\varepsilon_{c1} = -0.0022$ is the strain at peak-stress f'_{co}, $E_{c1} = f'_{co}/0.0022$ is the secant modulus of elasticity at peak stress, and ε_c is the total strain.

The confinement effect is modeled by a change in the stress-strain curve in the softening zone. The slope E_T in this zone is multiplied by a factor R that is a function of the intermediate principal stress σ_2:

$$R = e^{\chi\sigma_2} \tag{2.83}$$

where χ was taken as 0.867. This type of approach is referred to as the scaling technique in the follow-up studies, and the approach adopted in this model can be seen as an earlier version of this technique.

The model was applied by Barros (2001) for the analysis of the circular concrete cylinders tested by Iyengar et al. (1970). These cylinders had the

standard dimensions of 150 mm × 300 mm with concrete strengths ranging from 25MPa to 34MPa, and were reinforced with spirals. The finite element computational model based on the proposed constitutive model predicted the strengths of the test cylinders with reasonable accuracy (Barros 2001). However, its predictions for the pre- and post peak behaviour deviated substantially from the experimental results. Barros (2001) suggested that using a non-associated flow rule could eliminate this discrepancy. However, this author only used an associated flow rule as using a non-associative flow rule causes convergence problems in their numerical analyses.

In summary, Barros (2001) introduced a scaling technique in the hardening/softening rule of an elasto-plastic constitutive model for concrete. The proposed constitutive model is capable of providing accurate predictions for the peak stress of confined concrete and can also depict the change in slope of the softening branch of axial stress-strain curves due to the effect of confinement. However, an associated flow rule was adopted in the model due to the requirement of the numerical convergence; as a result, the stress-strain behaviour of steel spirals-confined concrete could not be accurately predicted.

2.4.3 Johansson and Akesson's (2002) Model

Johansson and Akesson (2002) also proposed a concrete constitutive model based on the theory of elasto-plasticity to consider the effect of confinement on the compressive response of concrete. This model was developed based

on the D-P type yield criterion which was used with an associated flow rule for the description of the three-dimensional state of stresses and strains in concrete. A confinement-sensitive hardening/softening rule was introduced into the constitutive model, and this introduction was achieved by applying two adjustment functions to the strength and the plastic modulus. More accurate predictions can be expected from this constitutive model when compared to the constitutive model developed by Barros (2001), which only involves the scaling technique on the plastic modulus. A series of experiments on circular concrete cylinders subjected to active confinement were analyzed using this constitutive model. In addition, the model was used in predicting the response of concrete-filled steel tubes. The model was shown to be capable of providing accurate predictions for both actively-confined concrete and concrete-filled steel tubes.

This model employs the D-P type yield surface, which is a linear function, as detailed below:

$$F(\sigma, K) = q + p\tan\alpha_{JA} - K_{JA} \tag{2.84}$$

$$q = \sqrt{\frac{2}{3}(\mathbf{S}:\mathbf{S})} \tag{2.85}$$

$$p = -\frac{1}{3}\boldsymbol{\sigma}:\mathbf{I} \tag{2.86}$$

$$\mathbf{S} = \boldsymbol{\sigma} + p\mathbf{I} \tag{2.87}$$

where α_{JA} is the frictional angle adopted in this model, K_{JA} is the cohesion strength, $\boldsymbol{\sigma}$ is the stress tensor, and $\mathbf{I}$ is the unit tensor.

As an associated flow rule is used, the expression for the plastic strain increments $d\boldsymbol{\varepsilon}_p$ can be written as

$$d\boldsymbol{\varepsilon}_p = d\lambda \frac{\partial F}{\partial \boldsymbol{\sigma}} \tag{2.88}$$

The last component of the model is the hardening rule. It consists of two parts and can be written as

$$d\kappa = d\lambda \frac{\partial F}{\partial K_{JA}} = d\lambda \text{ and } K_{JA} = -\mathbf{H} d\lambda \tag{2.89}$$

where **H** is the same as that in Barros (2001).

A confinement-sensitive hardening rule was employed to achieve accurate predictions for the confinement effect. Two adjustment functions f_{JA} and g_{JA} were adopted to scale the hardening rule. These two functions are defined as polynomials of arbitrary power, i.e.

$$f_{JA}(\sigma_{lat}) = \sum_{i=0}^{n} a_i \sigma_{lat}^i \tag{2.90}$$

$$g_{JA}(\sigma_{lat}) = \sum_{i=0}^{n} b_i \sigma_{lat}^i \tag{2.91}$$

where σ_{lat} is the equivalent confining pressure which is taken as the mean value of the two smallest principal stresses if the mean value is positive (compressive); otherwise it is set to zero.

$$\sigma_{lat} = \frac{\sigma_1 + \sigma_2}{2} \geq 0 \tag{2.92}$$

The constants a_i and b_i in Eqs. (2.89) and (2.90) require to be calibrated from the corresponding test data. This requirement means that the effect of confinement varies with the characteristics of concrete. That is, the values of a_i and b_i vary from one set of experimental data to another. The function f_{JA} is used to scale the strength K_{JA} (concrete strength) according to the current confinement level while the function g_{JA} is used to scale the

hardening parameter κ (concrete deformation). With these two adjustment functions, an appropriate $K_{JA} - \kappa$ relationship can be achieved. Fig. 2.2 illustrates the procedure of scaling.

In summary, Johansson and Akesson (2002) introduced a scaling technique for the hardening rule of an elasto-plastic model for confined concrete. Two adjustment functions, f_{JA} and g_{JA} , were employed to scale the strength K_{JA} and the hardening parameter κ respectively to achieve an accurate hardening rule under lateral confinement. In addition, an equivalent confining pressure σ_{lat} was adopted to consider effect of non-uniform confinement. This equivalent confining pressure σ_{lat} was taken as the mean value of the two smallest principal compressive stresses. This constitutive model employs a complete scaling technique (scaling both the strength and the slope) as compared with the constitutive model developed by Barros (2001). Therefore, a finite element computational model based on this constitutive model can provide accurate predictions for actively-confined concrete and concrete-filled steel tubes. However, the applicability of this constitutive model to FRP-confined concrete is questionable as the scaling technique was not verified using experimental results of FRP-confined concrete.

2.4.4 Grassl et al.'s (2002) Model

Grassl et al. (2002) proposed a constitutive model based on the theory of elasto-plasticity for the modelling of plain concrete in tri-axial compression. This model was based on the Menetrey and William yield criterion and a non-associated flow rule. A novel hardening law with the volumetric plastic

strain, ε_v^p , employed as the hardening/softening parameter was employed. The novel hardening/softening rule is different from the classical strain hardening rule in which the length of the plastic strain (i.e. the equivalent plastic strain) is used as the hardening/softening parameter (e.g. the CDPM model provided in ABAQUS).

As explained in the reviews of other models above, the classical elasto-plasticity theory uses the length of the plastic strain as the hardening/softening parameter but this approach fails to describe the increase of plastic deformation in the tri-axial compression stress state. Therefore, the scaling technique is required in such models to achieve a close representation of the deformation behaviour of confined concrete, which leads to undesirable complexity and empiricism (e.g. Barros 2001).

In Grassl et al.'s (2002) model, the effect of confinement on deformation behaviour is depicted using a modified strain-hardening/softening parameter, the volumetric plastic strain ε_v^p. In combination with a flow rule in which a non-linear plastic potential is employed, the deformation capacity of concrete under tri-axial compression can be properly predicted with a simple hardening/softening rule.

Three hypotheses were adopted in formulating this model to simplify the procedure of parameter calibration. The first hypothesis is that the peak stress in uni-axial compression, f'_{co}, is reached when the volumetric strain, ε_v, is equal to zero. The second hypothesis is that the volumetric plastic

strain ε_v^p at peak stress in a uni-axial stress state and that in a equal tri-axial stress state are identical, which means that ε_v at peak stresses in equal tri-axial stresses is also always 0. The third hypothesis is that the inclination of the total plastic strain is identical to the gradient of the plastic potential within the same state of loading. These hypotheses have been used in subsequent studies on this type of constitutive models.

The three-parameter yield surface proposed by Menetrey and William (1995) is used in this model. It can be expressed in the Haigh-Westergaard space as

$$F = \left(\sqrt{1.5}\rho\right)^2 + q_h(\kappa)m\left[\frac{\rho}{6}r(\theta, e) + \frac{\xi}{3}\right] - q_h(\kappa)q_s(\kappa) \tag{2.93}$$

where m is defined as

$$m = 3\frac{f_{co}'^2 + f_t^2}{f_{co}' f_t}\frac{e}{e+1} \tag{2.94}$$

and r is defined as

$$r(\theta, e) = \frac{4\left(1-e^2\right)\cos^2\theta + (2e-1)^2}{2(1-e^2)\cos\theta + (2e-1)[4(1-e^2)\cos^2\theta + 5e^2 - 4e]^{1/2}} \tag{2.95}$$

Here, r controls the out-of-roundness of the deviatoric section and is determined by the eccentricity parameter e.

In addition, ξ, ρ, θ are three components of the Haigh-Westergaard coordinates; they are defined as

$$\xi = \frac{I_1}{\sqrt{3}f_{co}'} \tag{2.96}$$

$$\rho = \frac{\sqrt{2J_2}}{f_{co}'} \tag{2.97}$$

$$\cos 3\theta = \frac{3\sqrt{3}}{2}\frac{1/3J_3}{(J_2)^{3/2}} \tag{2.98}$$

where I_1 is the first stress invariant, while J_2 and J_3 are the second and

third stress invariants of deviatoric stresses.

Equations for $q_h(\kappa)$ and $q_s(\kappa)$ were not directly proposed by Grassl et al. (2002). They are the ascending and the descending parts of the parameter $q(\kappa)$, respectively. That is

$$q(\kappa) = q_h(\kappa)q_s(\kappa) \quad = (\sigma_c / f'_{co})^2 \tag{2.99}$$

A non-associated flow rule is employed in this model, which means that the form of the plastic potential differs from the form of the yield surface. The plastic potential G in this model is defined in the Haigh-Westergaard space as

$$G = -A_{Gr}\left(\frac{\rho}{\sqrt{q(\kappa)}}\right)^2 - B_{Gr}\frac{\rho}{\sqrt{q(\kappa)}} + \frac{\xi}{\sqrt{q(\kappa)}} \tag{2.100}$$

Here, A_{Gr} and B_{Gr} are parameters determined from the axial strain stated in uni-axial and equal tri-axial compression.

Numerical results obtained using this constitutive model were shown to compare well with experimental results for concrete under uni-axial and equal tri-axial compression (Grassl et al. 2002). In a subsequent paper (Grassl 2004), this constitutive model was employed to model the dilation characteristics of concrete in compression. The influence of the dilation characteristics of concrete on the behaviour of steel-confined and FRP-confined circular concrete cylinders was studied. The numerical results indicated that the constitutive model can generally capture the trend of both steel-confined concrete and CFRP-confined concrete. The limitation of the numerical results is that, for FRP-confined concrete cylinders, only results for one selected value of confinement stiffness was compared. Therefore, it is unsure whether this constitutive model can describe the true dilation

characteristics of FRP-confined concrete at different levels of confinement stiffness.

2.4.5 Mirmiran et al.'s (2000) Model

Mirmiran et al. (2000) utilized an elasto-plastic D-P type model in the nonlinear finite element modelling of FRP-confined concrete. The numerical results were compared with experimental results for circular and square specimens wrapped with 6, 10, and 12 plies of E-glass fibers. The predicted stress-strain curves compared favorably with the test results although the dilation of FRP-confined columns was not captured well.

In this D-P type formulation, an equivalent stress σ_e is defined as

$$\sigma_e = 3\beta_{Mi}\sigma_m + \left[\frac{1}{2}\mathbf{S}^T\mathbf{M}\mathbf{S}\right]^{1/2} \tag{2.101}$$

where σ_m is the hydrostatic stress, **S** is the deviatoric stress vector and **M** is a 3×3 matrix, β_{Mi} is a material constant and it can be related to the internal angle of friction $\emptyset_M$. That is

$$\beta_{Mi} = \frac{2\sin\emptyset_M}{\sqrt{3}(3-\sin\emptyset_M)} \tag{2.102}$$

Based on the definition of the equivalent stress, the yield function F can be expressed as:

$$F = \sigma_e - \sigma_y \tag{2.103}$$

where the yield parameter σ_y is given by

$$\sigma_y = \frac{6c_M\sin\emptyset_M}{\sqrt{3}(3-\sin\emptyset_M)} \tag{2.104}$$

In this study, a non-associated flow rule was employed and a zero dilation angle was suggested by the authors based on numerical results obtained from their sensitivity analysis.

The two remaining parameters, $\emptyset_M$ and c_M, for the constitutive model were determined as functions of the unconfined concrete strength f'_{co} and the confinement effectiveness factor k_{1M}, respectively. The value of k_{1M} can be calculated from the formulae proposed by one of the following models: Richart et al. (1928), Mander et al. (1988), Samaan et al. (1998), or Rochette and Labossiere (2000).

From the numerical results (Mirmiran et al. 2000), this D-P type model was found to predict linearly increasing volumetric compaction, which does not reflect the true volumetric behaviour of FRP-confined concrete. Moreover, the dilation ratio predicted by the computational model remained at a constant value close to 0.5 which is the incompressibility limit. This value also differs from the corresponding value obtained from experimental results. Generally speaking, the finite element computational model succeeded in predicting the overall axial stress-strain curve of FRP-confined concrete but failed to predict the experimental dilation characteristics. This contradiction has been discussed in detail by Yu et al.(2010a). Yu et al. (2010a) showed that in Mirmiran et al.'s (2000) finite element analysis, the lateral dilation of concrete at the beginning of the loading process was underestimated but the stress of confined concrete was overestimated due to the perfect elastio-plasticity assumption adopted in the constitutive model. These two factors counteract each other. Another point worth noting is that the post-peak region and the ultimate axial strain of FRP-confined square columns were significantly overestimated by the finite element model. This

overestimation further indicates that a simple D-P type plasticity model cannot provide accurate predictions for FRP-confined concrete.

2.4.6 Liu and Foster's (2000) Model

A three-dimensional finite element computational model was presented by Liu and Foster (2000) for the analysis of concrete under uni-axial as well as tri-axial compression. An explicit microplane model proposed by Carol et al. (1992) was employed in the study. The parameter values of this constitutive model were obtained from a back analysis of circular concrete cylinders under various confining pressures.

The concept of the microplane model was first put forward by Bazant (1983). Since its first appearance, the microplane approach has become progressively more popular for the description of the constitutive behaviour of concrete. The main idea behind the microplane model is relatively simple: it predicts the constitutive behaviour for a two- or three-dimensional continuum by relying on modelling the behaviour of a plane of generic orientation, which is then integrated over all possible directions in space. Based on this microplane concept, the constitutive model is formulated through the following three steps. First, the micro-level strains can be obtained from the macro-level strain tensor ε_{ij} using the assumption of kinematic constraints. Second, the volumetric, deviatoric and tangential micro-level stresses can be calculated from the corresponding micro-level strains by applying the constitutive equations defined at the micro-level. Third, the macro-level stress tensor can be calculated from micro-level stresses by applying the principal of virtual work. A more detailed

description of this type of model is given in Chapter 7.

In the second step, it is assumed that the direction of a micro-level stress is the same as that of the corresponding micro-level strain. The corresponding micro-level material law used in Carol et al. (1992) is as follows:

For the volumetric stress σ_v,

$$\sigma_v = \begin{cases} E_v^o \varepsilon_v [(1 + |\varepsilon_v|/a)^{-p} + (|\varepsilon_v|/b)^q], & \text{in compression} \\ E_v^o \varepsilon_v e^{-(|\varepsilon_v|/b)^{p_1}}, & \text{in tension} \end{cases} \tag{2.105}$$

For the deviatoric stress σ_D,

$$\sigma_D = \begin{cases} E_D^o \varepsilon_D e^{-(|\varepsilon_D|/a_2)^{p_2}}, & \text{in compression} \\ E_D^o \varepsilon_D e^{-(|\varepsilon_D|/a_1)^{p_1}}, & \text{in tension} \end{cases} \tag{2.106}$$

For the shear stress σ_T,

$$\sigma_T = \tau \varepsilon_T / \gamma \tag{2.107}$$

$$\tau = E_T^o \gamma e^{-(\gamma/a_3)^{p_3}} \tag{2.108}$$

Here, E_v^o is the initial modulus of elasticity; ε_v, ε_D and ε_T refer to the volumetric, deviatoric, and tangential micro-level strains, respectively; and γ is the length of the tangential strain vector ε_T.

Following the three steps as mentioned above, the formulation of the incremental stress tensor $d\sigma_{ij}$ is given by

$$d\boldsymbol{\sigma}_{ij} = \mathbf{E}_{ijkl}^{tan} d\boldsymbol{\varepsilon}_{kl} \tag{2.109}$$

where $\mathbf{E}_{ijkl}^{tan}$ is the tangential stiffness tensor and $d\boldsymbol{\varepsilon}_{kl}$ is the incremental strain tensor.

To calibrate these 10 empirical parameters [shown in Eqs. (2.105)-(2.108)],

five of them were fixed for all concrete strengths, while the other five parameters were calibrated for different concrete strengths and different values of the σ_3/σ_1 ratio. Here, σ_3 is the maximum principal stress while σ_1 is the minimum principal stress; they correspond to the confinement pressure and the stress in the compressive loading direction for concrete under uniform confinement.

Two square columns tested by Razvi and Saatcioglu (1996) were analyzed under axial compression. The columns were modeled using brick elements for the concrete and truss elements for the steel. The material model for concrete was the microplane model and that for steel was the elastic-perfectly plastic model. The effect of cover spalling was also taken into account. The numerical model considering the effect of cover spalling was found to be capable of reproducing the experimental results. Experimental results from a column tested by Sheikh and Uzumeri (1980) were also used for comparison with the numerical results. The analysis also simulated the phenomenon of cover spalling and steel yielding. The numerical results showed adequate agreement with the experimental results for the overall stress-strain behaviour, with only the initial stiffness of the column being slightly overestimated.

As the predictions of the computational model were only compared with experimental results for steel-confined concrete columns and actively-confined concrete columns, the capability of the model in providing accurate predictions for concrete under other types of

confinement is still uncertain. Another drawback of the constitutive model (microplane model M2) is the spurious volumetric strain when dealing with elements under tensile loading, which was first noted by Jirasek (1993).

2.4.7 Ghazi et al.'s (2002) Model

In a study by Ghazi et al. (2002), the microplane model M4 (or referred to as M4 model) proposed by Bazant et al. (2000) was applied in modelling the behaviour of concrete under uni-axial and tri-axial compression. In this model, the finite-strain microplane model M4 was adopted in a total Lagrangian finite element formulation. Compared to the microplane model M2 used in Liu and Foster (2000), the spurious volumetric strain under tensile loading is generally eliminated in the M4 model. The M4 model was adjusted in this study for the particular case of concrete columns under low confinement. This modification focused on aspects of the post-peak regime and the increase of the peak stress of confined concrete.

As discussed in Section 2.4.6, the microplane model relates the micro-level strains and stresses to the macro-level strain and stress tensors. Constitutive equations defined at the micro-level are used to calculate micro–level stresses from the corresponding micro-level strains. The macro-level stress tensor is then calculated by integrating the micro-level stresses over a unit semi-sphere. The formulation of the M4 model, and the corresponding formulation to calculate the stress tensor, will be discussed in detail in Chapter 7.

The M4 model has a total of 21 parameters. Among them, c_1 to c_{17} are

fixed parameters whose values can remain unchanged for different concrete mixes. The other four parameters, K_1 to K_4, are adjustable parameters whose values should vary with the concrete mix. These four parameters control the values for the uni-axial concrete strength and the strain at peak stress etc. In other words, the concrete strength in M4 model is not an input parameter but an output result.

To investigate the uni-axial compressive behaviour of concrete, the M4 model was used by Ghazi et al. (2002) for the analysis of a circular concrete cylinder with a diameter of 100 mm and a height of 200 mm. The numerical results were compared with the empirical stress-strain curves obtained from the formulae of Attard and Setunge (1996). It was found that the results of the computational model differed significantly from those of the empirical model in the post-peak regime.

For confined concrete, the results of M4 model were also compared with those of the empirical model by Attard and Setunge (1996). The peak stress obtained from M4 model was found to be smaller than that obtained from the empirical model. In addition, the post-peak response predicted by the computational model decays faster than the empirical curve obtained from the model of Attard and Setunge (1996).

To address the discrepancies mentioned above, the following modifications were implemented into the M4 model. Parameter c_{10} was modified to be a function of the volumetric strain and the confinement ratio; whereas

parameters c_7 and K_1 were made a function of the concrete strength. The computational model based on the modified constitutive model showed adequate agreement with the empirical model for actively-confined concrete. The modified model was also employed in the analysis of steel-confined concrete and provided accurate predictions.

Similar to the model adopted in Liu and Foster (2000), the modified constitutive model proposed by Ghazi et al. (2002) was only compared with test data for steel-confined concrete and actively-confined concrete. Therefore, the capability of the model in providing accurate predictions for concrete under other types of confinement is uncertain. Moreover, other researchers (e.g. Tue et al. 2008) had found that the original M4 model has some drawbacks in terms of numerical computation. Therefore, it is necessary to eliminate these drawbacks before the M4 model can be further modified to provide accurate predictions for confined concrete.

2.4.8 Montoya et al.'s (2006) Model

Montoya et al. (2006) presented a constitutive model based on the Modified Compression Field Theory (MCFT) for modelling the behaviour of plain concrete in multi-axial compression. The MCFT was initially developed to analyze the behaviour of concrete under two-dimensional loading (Vecchio and Collins 1986). Later, this approach was extended to address three-dimensional problems (Selby and Vecchio 1993). This model can consider the effect of tensile stress, strength increment due to confinement, and a varying Poisson's ratio.

The MCFT uses a special nonlinear elasticity methodology. Orthotropic elasticity is defined on the basis of the secant modulus. The concept of pre-strains is introduced to account for non-stress related strains. This concept is also used in calculating the dilation strain ε_{co}^{i} in the following form:

$$\varepsilon_{co}^{i} = -v_{ij}\frac{f_{cj}}{E_{cj}} - v_{ik}\frac{f_{ck}}{E_{ck}} \tag{2.110}$$

where i, j, and k are the principal directions, v_{ij} is the Poisson's ratio in direction i when subjected to a stress f_{cj} in direction j, and E_{cj} is the secant modulus of concrete in direction j.

The varying Poisson's ratio in this model is obtained from the lateral-to-axial relationship which is given as follows:

$$\varepsilon_{cl} = \left(1.9 + 24.2\frac{f_{cl}}{f'_{co}}\right)\left(\frac{\varepsilon_c}{\varepsilon_{cc}}\right)^2 \tag{2.111}$$

where ε_c is the current axial strain, ε_{cc} is the axial strain at peak stress, ε_{cl} is the current lateral strain, and f_{cl} is the current lateral pressure. Figs. 2.3 show that this equation significantly overestimates the lateral strain at a given axial strain for both actively-confined and FRP-confined concrete. What should also be noted is that in Figs. 2.3 the lateral strain is taken to be positive.

The secant Poisson's ratio v can be related to the initial Poisson's ratio v_o through

$$v = \left(1.9 + 24.2\frac{f_{cl}}{f'_{co}}\right)\left(\frac{\varepsilon_c}{\varepsilon_{cc}^2}\right) + v_o \tag{2.112}$$

Eq. (2.112) is similar to Eq. (2.111). The lateral-to-axial relationships in

these two equations are both related to the current confining pressure.

A four-parameter Ottosen-type failure criterion in the principal stress space is employed for considering the strength enhancement of confined concrete. The expression of this failure criterion is given by

$$a_{O1}\frac{J_2}{f_{co}'^2}+\lambda_o\frac{\sqrt{J_2}}{f_{co}'}+b_{O1}\frac{I_1}{f_{co}'}-1=0 \tag{2.113}$$

$$\lambda_o=k_{O1}+k_{O2}\cos 3\theta \tag{2.114}$$

The parameters, a_{O1}, b_{O1}, k_{O1} and k_{O2}, need to be defined for the failure criterion.

To consider the enhancement of strain at peak stress for confined concrete, the following equation is employed:

$$\frac{\varepsilon_{cc}}{\varepsilon_{co}}=1.0+k_{cc}\frac{f_{cl}}{f_{co}'} \tag{2.115}$$

where

$$k_{cc}=24.4-0.116f_{co}' \tag{2.116}$$

Based on the peak stress and the axial strain at peak stress as defined above, an active confinement model becomes available for the description of the axial stress-strain relationship of concrete at a given lateral confining pressure, f_{cl}.

A comparison of this model with an analysis-oriented stress-strain model such as Teng et al.'s (2007) model indicates that these two models have many things in common. Both of them employ an active-confinement base model and an equation to describe the lateral-to-axial relationship.

Therefore, the empirical model employed in the MCFT can also be used as an analysis-oriented stress-strain model. For concrete under uniform confinement, the MCFT can be seen as the numerical implementation of an analysis-oriented stress-strain model within the framework of nonlinear elasticity. The effect of non-uniform confinement on concrete can be properly considered by implementing the MCFT in a finite element model. The only limitation is that Eq. (2.112) needs to be used for the determination of the value of Poisson ratio corresponding to the current confining pressure, so the stress increment cannot be directly calculated from the strain increment. As a result, this method is not very convenient for implementation in a finite element model driven by strain or displacement increments. Moreover, as this model overestimates the lateral strain of FRP-confined concrete as Eq. (2.111) is regressed from a small database (Montoya 2003), its capability in providing accurate predictions for FRP-confined concrete is thus questionable.

2.4.9 Yu et al.'s (2010b) Model

In a recent study by Yu et al. (2010b), a modified plastic-damage model was proposed to model the behaviour of FRP-confined concrete in compression. The main characteristics of FRP-confined concrete are properly captured by this model in which concrete responds as an elastic-plastic material following a modified D-P type model. This constitutive model is defined within the theoretical framework of the Concrete Damaged Plasticity Model (CDPM) in the ABAQUS software. The modifications to the CDPM model were realized through the SDFV option provided by ABAQUS. The proposed modifications include three main aspects based on detailed

observations of concrete behaviour in laboratory tests. First, the third deviatoric stress invariant was included into the yield criterion as suggested for the original CDPM model. Second, a confinement-dependent hardening/softening rule was introduced to reflect the difference in stress-strain behaviour between unconfined concrete and actively-confined concrete. Third, a confinement-dependent non-associated flow rule was employed to consider the dilation behaviour of confined concrete, especially FRP-confined concrete. The analysis-oriented stress-strain model proposed by Teng et al. (2007) was employed to generate input data for the confinement-dependent hardening/softening rule and the confinement-stiffness-dependent flow rule. For uniform confinement, the constitutive model in this study can be seen as the numerical implementation of an analysis-oriented stress-strain model (Teng et al. 2007) within the framework of plastic-damage theory.

The model proposed by Yu et al. (2010b) has been successfully implemented only as a finite element slice model containing a single layer of elements so that the axial non-uniformity in stress and strain was not taken into account. In this thesis, the implementation of Yu et al.'s (2010b) constitutive model in a three-dimensional computational model for FRP-confined concrete columns will be presented. Moreover, as the analysis-oriented stress-strain model itself was only verified for FRP-confined normal strength concrete, its accuracy for FRP-confined high strength concrete is uncertain. More details of Yu et al.'s (2012b) model can be found in Chapters 8 and 9.

2.5 CONCLUSIONS

Many notable experimental and analytical studies on confined concrete have been reviewed in this chapter. This review indicates that the confinement mechanism of concrete columns under compressive loading has been under investigation for near a century; a large amount of experimental work has contributed to the current understanding of the behaviour of confined concrete and led to a large experimental database. It is now universally accepted that confinement of concrete in compression leads to significant increases in both strength and ductility.

Using FRP composites to provide lateral confinement to concrete columns is a comparatively new technique. The behaviour of FRP-confined concrete is different from that of steel-confined concrete due to the following reasons. Steel has a yield plateau which is reached significantly before the failure point of concrete is attained. The steel provides a constant lateral pressure independent of the additional deformation of the concrete once it has yielded. By contrast, FRP is a linear elastic material. Therefore, it provides a monotonically increasing lateral pressure as the compressive load on the concrete increases until the FRP jacket ruptures. At high axial compressive strains, the axial stress-strain curve of steel-confined concrete exhibits a descending branch while the stress of FRP-confined concrete always increases with strain until rupture of the FRP jacket occurs, provided the stiffness of the FRP jacket is above a threshold value.

A large number of attempts have been made to predict the behaviour of

actively-confined concrete, steel-confined concrete, and FRP-confined concrete. Extensive empirical models have been proposed to represent the experimental results. These empirical models were developed for actively-confined concrete and steel-confined model (e.g. Ahmad and Shah 1982; Attard and Setunge 1996; Candappa et al. 2001; Mander et al. 1988) in the earlier stage. Empirical models developed for steel-confined concrete are also applicable to actively-confined concrete as they show similar performance after the yielding of steel.

It is now well established that empirical models developed for steel-confined concrete cannot accurately predict the behaviour of FRP-confined concrete. As a result, many empirical models have recently been proposed specifically for FRP-confined concrete in circular columns where the FRP confinement is uniform (e.g. Lam and Teng 2002; Lam and Teng 2003a; Lam and Teng 2003b; Youssef et al. 2007). The majority of these empirical models have been developed by the curve-fitting of experimental results of FRP-confined concrete for design use (i.e. design-oriented stress-strain models); these models are in closed-form expressions. In contrast, a smaller number of empirical models have adopted a more complex incremental form to explicitly account for interactions between the confining material and the confined concrete core; these models are referred to as analysis-oriented stress-strain models (Cui and Sheikh 2010; Jiang and Teng 2007; Teng et al. 2007). Analysis-oriented stress-strain models are more versatile and powerful as they are applicable to concrete confined by different materials (e.g. steel and FRP) and to both

active confinement and passive confinement.

In FRP-confined square, rectangular or other non-circular RC columns, the concrete around the perimeter is non-uniformly confined by the FRP jacket. That is, the degree of confinement of the concrete varies over the section, and the axial stress also varies over the section. This non-uniform confinement condition leads to a much more complicated problem than that of uniform FRP confinement. As a result, an analysis-oriented stress-strain model with explicit consideration of the jacket-concrete core interaction becomes much less desirable as both the axial stress and the confining pressure need to be empirically treated in an average sense. Therefore, there has been little effort so far on the development of analysis-oriented stress-strain models for FRP-confined concrete in non-circular sections. Instead, existing work on the stress-strain behaviour of FRP-confined concrete in rectangular (including square) columns has been focused on the development of empirical design-oriented stress-strain models (e.g. Lam and Teng 2003b; Youssef et al. 2007). These models have been extended from stress-strain models for FRP-confined concrete in circular columns. Such extensions involve modifications of the original ultimate condition equations to account for the effect of non-uniform confinement. The revised ultimate condition equations are generally formulated using the concepts of effective-confinement area and equivalent circular section. These concepts transform a rectangular section into an equivalent circular section explicitly (e.g. Lam and Teng 2003b) or implicitly (e.g. Youssef et al. 2007). With the modified ultimate condition equations, the stress-strain equations for

FRP-confined concrete in circular columns can be applied to predict the stress-strain behaviour of FRP-confined concrete in rectangular columns.

The concepts of effective-confinement area and equivalent circular section, however, have a fundamental drawback that they cannot describe the stress/strain distribution within a rectangular section. Stress-strain models for FRP-confined concrete in rectangular columns are thus purely empirical models; that is, they are not based on a rigorous understanding of the confinement mechanism in a rectangular section. Instead, they have been based on empirical parameters to estimate the confinement effect and to provide a good fit to the available test data. Due to these reasons, the accuracy of a particular empirical stress-strain model based on one set of test data in predicting another set of test data can be highly uncertain.

The finite element method has the potential in providing accurate predictions for non-uniformly confined concrete such as concrete in rectangular columns. In particular, finite element modelling offers a powerful tool to study the confinement mechanism of concrete under non-uniform confinement. The pre-requisite for an accurate finite element model for confined concrete columns is the availability of an accurate constitutive model for confined concrete. A number of constitutive models for confined concrete have been developed over the past three decades. The theory of plasticity has been used as the basis for most of these models. Other theories that have been explored include the MCFT and the microplane theory. For actively-confined concrete and steel-confined

concrete, several existing constitutive models (e.g. Ghazi et al. 2002; Grassl et al. 2002; Johansson and Akesson 2002; Liu and Foster 2000; Barros 2001) can already provide predictions of experimental results with acceptable accuracy. However, the accuracy of these models in predicting the stress-strain behaviour of FRP-confined concrete is still uncertain. The research work presented in Chapters 4 to 6 was thus conducted to address this issue.

The constitutive models proposed by Montoya et al. (2006) and Yu et al. (2010b) can capture the major characteristic of the stress-strain behaviour of FRP-confined circular concrete columns. Both of these two models have their roots in their corresponding analysis-oriented stress-strain models, although the accuracy of the former model for FRP-confined circular concrete columns is still questionable. Another limitation of Montoya et al.'s (2006) constitutive model is that this model is not a true material constitutive model because its numerical implementation in a finite element model requires some modifications also at the element level. Yu et al.'s (2010b) model does not suffer from this limitation, but its numerical implementation has not considered the non-uniformity of confinement perpendicular to the slice plane. Moreover, their base analysis-oriented stress-strain model (i.e. Teng et al. 2007) has not been verified for FRP-confined high strength concrete, so its accuracy for FRP-confined high-strength concrete is uncertain. An experimental study on FRP-confined high strength concrete was conducted and is presented in Chapter 3 to address this particular issue. Furthermore, for FRP-confined rectangular

columns, the reliability of both models is still uncertain; the finite element modelling of FRP-confined concrete in non-circular columns is the main issue examined in Chapter 8 using finite element slice models. Finally, the effect of non-uniformity of confinement perpendicular to the slice plane is investigated in Chapter 9.

2.6 REFERENCES

Ahmad, S. H., and Shah, S. P. (1982). "Stress-strain curves of concrete confined by spiral reinforcement." *ACI Journal Proceedings*, 79(6), 484-490.

Ansari, F., and Li, Q. B. (1998). "High-strength concrete subjected to triaxial compression." *ACI Materials Journal*, 95(6), 747-755.

Aroglu, N., Girgin, Z. C., and Aroglu, E. (2006). "Evaluation of ratio between splitting tensile strength and compressive strength for concretes up to 120 MPa and its application in strength criterion." *ACI Materials Journal*, 103(1), 18-24.

Attard, M. M., and Setunge, S. (1996). "Stress-strain relationship of confined and unconfined concrete." *ACI Materials Journal*, 93(5), 432-442.

Balmer, G. G., and McHenry, D. (1947). "Determination of boundary porosity by triaxial compression tests of concrete." *Laboratory Report SP-15, Aug*, 8.

Barros, M. H. F. (2001). "Elasto-plastic modelling of confined concrete

elements following MC90 equations." *Engineering Structures*, 23(4), 311-318.

Bazant, Z. P. (1983). "Microplane model for fracture analysis of concrete structures." *Proc. Symp. Interact. Non-Nucl. Munitions Struct*, US Air Force Academy, Springs, Co, 49-55.

Bazant, Z. P., Caner, F. C., Carol, I., Adley, M. D., and Akers, S. A. (2000). "Microplane model M4 for concrete. I: formulation with work-conjugate deviatoric stress." *Journal of Engineering Mechanics*-ASCE, 126(9), 944-953.

Berthet, J. F., Ferrier, E., and Hamelin, P. (2005). "Compressive behaviour of concrete externally confined by composite jackets. Part A: experimental study." *Construction and Building Materials*, 19(3), 223-232.

Candappa, D. C., Sanjayan, J. G., and Setunge, S. (2001). "Complete triaxial stress-strain curves of high-strength concrete." *Journal of Materials in Civil Engineering*, 13(3), 209-215.

Carol, I., Prat, P. C., and Bazant, Z. P. (1992). "New explicit microplane model for concrete: theoretical aspects and numerical implementation." *International Journal of Solids and Structures*, 29(9), 1173-1191.

CEB–FIP. Model Code 1990 Committee Euro-International du Beton. London: Thomas Telford, 1990.

Cedolin, L., Dei Poli, S., and Crutzen, Y. R. J. (1977). "Triaxial stress-strain relationship for concrete." *Journal of the Engineering Mechanics Division*, 103(3), 423-439.

Cui, C., and Sheikh, S. A. (2010). "Analytical model for circular normal- and high-strength concrete columns confined with FRP." *Journal of Composites for Construction*, 14(5), 562-572.

Demers, M., and Neale, K. W. (1994). "Strengthening of concrete columns with unidirectional composite sheets." *Developments in Short and Medium Span Bridge Engineering*, 94, 895-905.

Drucker, D.C., and Prager, W. (1952). "Soil mechanics and plastic analysis or limit design." *Quarterly of Applied Mathematics,* 10, 157-165.

Eid, R., Roy, N., and Paultre, P. (2009). "Normal- and high-strength concrete circular elements wrapped with FRP composites." *Journal of Composites for Construction*, 13(2), 113-124.

Gardner, N. J. (1969). "Triaxial behaviour of concrete." *ACI Journal Proceedings*, 66(2), 136-146.

Gerstle, K. H. (1981). "Simple formulation of triaxial concrete behaviour." *ACI Journal Proceedings*, 78, 382-387.

Ghazi, M., Attard, M. M., and Foster, S. J. (2002). "Modelling triaxial compression using the microplane formulation for low confinement." *Computers & Structures*, 80(11), 919-934.

Grassl, P. (2004). "Modelling of dilation of concrete and its effect in triaxial

compression." *Finite Elements in Analysis and Design*, 40(9-10), 1021-1033.

Grassl, P., Lundgren, K., and Gylltoft, K. (2002). "Concrete in compression: a plasticity theory with a novel hardening law." *International Journal of Solids and Structures*, 39(20), 5205-5223.

Imran, I., and Pantazopoulou, S. J. (1996). "Experimental study of plain concrete under triaxial stress." *ACI Materials Journal*, 93(6), 589-601.

Iyengar, K.T.S.R, Desaiy, P., and Reddy, K.N. (1970) "Stress–strain characteristics of concrete confined in steel binders." *Magazine of Concrete Research*, 22(72), 173–184.

Jiang, T., and Teng, J. G. (2007). "Analysis-oriented stress-strain models for FRP-confined concrete." *Engineering Structures*, 29(11), 2968-2986.

Jirasek, M. (1993). *Modelling of fracture and damage in quasibrittle materials*, Northwestern Univ., Chicago, IL (United States).

Johansson, M., and Akesson, M. (2002). "Finite element study of concrete-filled steel tubes using a new confinement-sensitive concrete compression model." *Nordic Concrete Research -Publications*, 27, 43-62.

Lam, L., and Teng, J. G. (2003a). "Design-oriented stress-strain model for FRP-confined concrete." *Construction and Building Materials*,

17(6-7), 471-489.

Lam, L., and Teng, J. G. (2003b). "Design-oriented stress-strain model for FRP-confined concrete in rectangular columns." *Journal of Reinforced Plastics and Composites*, 22(13), 1149-1186.

Lam, L., and Teng, J. G. (2004). "Ultimate condition of fiber reinforced polymer-confined concrete." *Journal of Composites for Construction*, 8(6), 539-548.

Lam, L., Teng, J. G., Cheung, C. H., and Xiao, Y. (2006). "FRP-confined concrete under axial cyclic compression." *Cement & Concrete Composites*, 28(10), 949-958.

Lee, J., Yi, C., and Oh, Y. J. (2008). "Strengthening of concrete with mixed confinement materials-steel hoops and FRP composites." *Science and Engineering of Composite Materials*, 15(1), 1-20.

Lee, J. H., and Fenves, G. L. (1998). "Plastic-damage model for cyclic loading of concrete structures." *Journal of Engineering Mechanics*-ASCE, 124(8), 892-900.

Lee, J. Y., Yi, C. K., Jeong, H. S., Kim, S. W., and Kim, J. K. (2010). "Compressive response of concrete confined with dteel dpirals and FRP composites." *Journal of Composite Materials*, 44(4), 481-504.

Li, G. Q. (2006). "Experimental study of FRP confined concrete cylinders." *Engineering Structures*, 28(7), 1001-1008.

Liu, J., and Foster, S. J. (2000). "A three-dimensional finite element model

for confined concrete structures." *Computers & Structures*, 77(5), 441-451.

Lu, X. B., and Hsu, C. T. T. (2006). "Behaviour of high strength concrete with and without steel fiber reinforcement in triaxial compression." *Cement and Concrete Research*, 36(9), 1679-1685.

Mander, J. B., Priestley, M. J. N., and Park, R. (1988). "Theoretical stress-strain model for confined concrete." *Journal of Structural Engineering*-ASCE, 114(8), 1804-1826.

Matthys, S., Taerwe, L., and Audenaert, K. (1999). "Tests on axially loaded concrete columns confined by fiber reinforced polymer sheet wrapping." *ACI Special Publications*, 188, 217-228.

Menetrey, P., and Willam, K. J. (1995). "Triaxial failure criterion for concrete and its generalization." *ACI Structural Journal*, 92(3), 311-318.

Mills, L. L., and Zimmerman, R. M. (1970). "Compressive strength of plain concrete under multiaxial loading conditions." *ACI Journal Proceedings*, 67, 802-807.

Mirmiran, A., Zagers, K., and Yuan, W. Q. (2000). "Nonlinear finite element modelling of concrete confined by fiber composites." *Finite Elements in Analysis and Design*, 35(1), 79-96.

Montoya, E. (2003). *Behavior and analysis of confined concrete*, PhD Thesis, Department of Civil Engineering, University of Toronto,

Toronto, Canada.

Montoya, E., Vecchio, F. J., and Sheikh, S. A. (2006). "Compression field modelling of confined concrete: constitutive models." *Journal of Materials in Civil Engineering*, 18(4), 510.

Ottosen, N. (1977). "A failure-criterion for concrete." *Journal of Engineering Mechanics Division*, ASCE, 103(4), 527-535.

Ottosen, N. S. (1979). "Constitutive model for short-time loading of concrete." *Journal of Engineering Mechanics Division*, ASCE, 105(2), 127–141.

Parvin, A., and Wang, W. (2001). "Behaviour of FRP jacketed concrete columns under eccentric loading." *Journal of Composites for Construction*, 5(3), 146-152.

Popovics, S. (1973). "A numerical approach to the complete stress-strain curve of concrete." *Cement and Concrete Research*, 3(5), 583-599.

Razvi, S., and Saatcioglu, M. (1996). "Tests of high strength concrete columns under concentric loading." *Report OCEERC 96-03, 147 pp,* Department of Civil Engineering, University of Ottawa.

Richart, F. E., Brandtzaeg, A., and Brown, R. L. (1928). "A Study of the failure of concrete under combined compressive stresses." *Bulletin No. 185, Engineering Experiment Station*, University of Illinois, Urbana, U.S.A.

Rochette, P., and Labossiere, P. (2000). "Axial testing of rectangular column

models confined with composites." *Journal of Composites for Construction*-ASCE, 4(3), 129-136.

Rousakis, T. C., Karabinis, A. I., and Kiousis, P. D. (2007). "FRP-confined concrete members: axial compression experiments and plasticity modelling." *Engineering Structures*, 29(7), 1343-1353.

Rutland, C. A., and Wang, M. L. (1997). "The effects of confinement on the failure orientation in cementitious materials experimental observations." *Cement and Concrete Composites*, 19(2), 149-160.

Samaan, M., Mirmiran, A., and Shahawy, M. (1998). "Model of concrete confined by fiber composites." *Journal of Structural Engineering*-ASCE, 124(9), 1025-1031.

Sargin, M. (1971). *Stress-strain relationships for concrete and the analysis of structural concrete sections*, Solid Mechanics Division, University of Waterloo.

Scott, B. D., Park, R., and Priestley, M. J. N. (1982). "Stress-strain behaviour of concrete confined by overlapping hoops at low and high strain rates." *ACI Journal Proceedings*, 79(1), 13-27.

Selby, R.G., and Vecchio, F.J. (1993). *Three-dimensional analysis of reinforced concrete solids*, Civil Engineering Report, University of Toronto, Toronto, Canada.

Setunge, S., Attard, M. M., and Darvall, P. L. (1993). "Ultimate strength of confined very high-strength concretes." *ACI Structural Journal*,

90(6), 632-641.

Sfer, D., Carol, I., Gettu, R., and Etse, G. (2002). "Study of the behaviour of concrete under triaxial compression." *Journal of Engineering Mechanics*-ASCE, 128(2), 156-163.

Sheikh, S. A., and Uzumeri, S. M. (1980). "Strength and ductility of tied concrete columns." *Journal of the Structural Division*-ASCE, 106(5), 1079-1102.

Sheikh, S. A., and Uzumeri, S. M. (1982). "Analytical model for concrete confinement in tied columns." *Journal of the Structural Division*, 108(12), 2703-2722.

Silva, M. A. G. (2011). "Behaviour of square and circular columns strengthened with aramidic or carbon fibers." *Construction and Building Materials*, 25(8), 3222-3228.

Sundara Raja Iyengar, K. T., Desayi, P., and Reddy, K. N. (1970). "Stress-strain characteristics of concrete confined in steel binders." *Magazine of Concrete Research*, 22(72), 173-184.

Tan, T. H., and Sun, X. (2006). "Failure criteria of concrete under triaxial compression." *ACI Special Publications*, 238, 235.

Teng, J. G., Huang, Y. L., Lam, L., and Ye, L. P. (2007). "Theoretical model for fiber-reinforced polymer-confined concrete." *Journal of Composites for Construction*, 11(2), 201-210.

Tue, N. V., Li, J. B., Schenk, G., Mucha, S., and Puschel, T. (2008).

"Computational aspects of microplane model M4 for concrete: deficiencies and improvements." Proceedings of the 3rd International Conference on the Concrete Future, X. G. Zhou, C. T. Tam, L. H. Han, and Y. B. Shao, eds., Ci-Premier Pte Ltd, Singapore, 411-418.

Vecchio, F.J., and Collins, M.P. (1986). "The modified compression field theory for reinforced concrete solids subjected to shear. " *Journal of the American Concrete Institute,* 83(2), 219–31.

Watanabe, K., Nakamura, H., Honda, Y., Toyoshima, M., Iso, M., Fujimaki, T., Kaneto, M., and Shirai, N. (1997). "Confinement effect of FRP sheet on strength and ductility of concrete cylinders under uniaxial compression." *Non-Metallic (FRP) Reinforcement for Concrete Structures*, 1, 233-240.

William, K., and Warnke, E. (1975). "Constitutive model for the triaxial behaviour of concrete." *Procedings International Association for Bridge and Structural Engineering*, 174.

Xie, J., Elwi, A. E., and Macgregor, J. G. (1995). "Mechanical-properties of 3 high-strength concretes containing silica fume." *ACI Materials Journal*, 92(2), 135-145.

Youssef, M. N., Feng, M. Q., and Mosallam, A. S. (2007). "Stress-strain model for concrete confined by FRP composites." *Composites Part B: Engineering*, 38(5-6), 614-628.

Yu, T., Teng, J. G., Wong, Y. L., and Dong, S. L. (2010a). "Finite element modelling of confined concrete-I: Drucker-Prager type plasticity model." *Engineering Structures*, 32(3), 665-679.

Yu, T., Teng, J. G., Wong, Y. L., and Dong, S. L. (2010b). "Finite element modelling of confined concrete-II: Plastic-damage model." *Engineering Structures*, 32(3), 680-691.

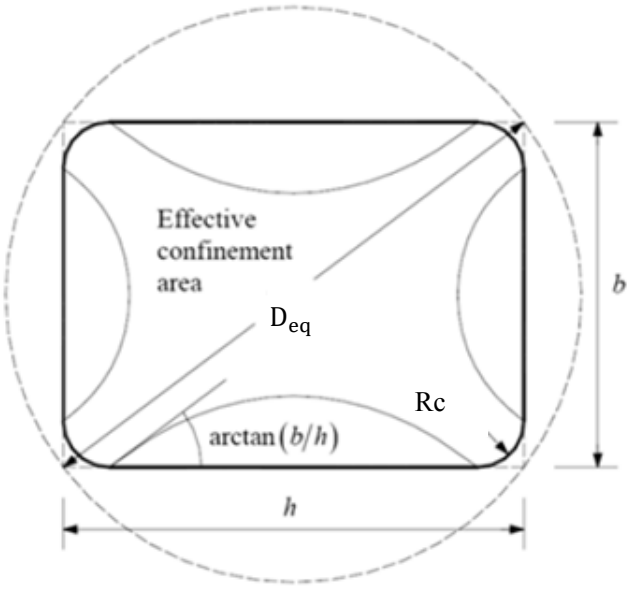

Figure 2.1 Lam and Teng's model for FRP-confined concrete in rectangular columns

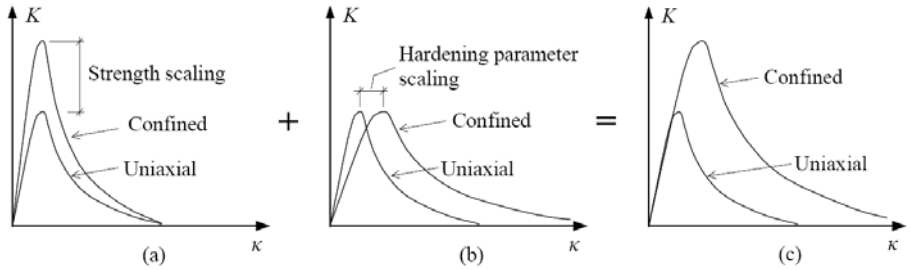

(a) Strength scaling; (b) hardening parameter scaling; (c) resulting scaling

[after Johansson and Akesson (2002)]

Figure 2.2 Illustration of the scaling technique

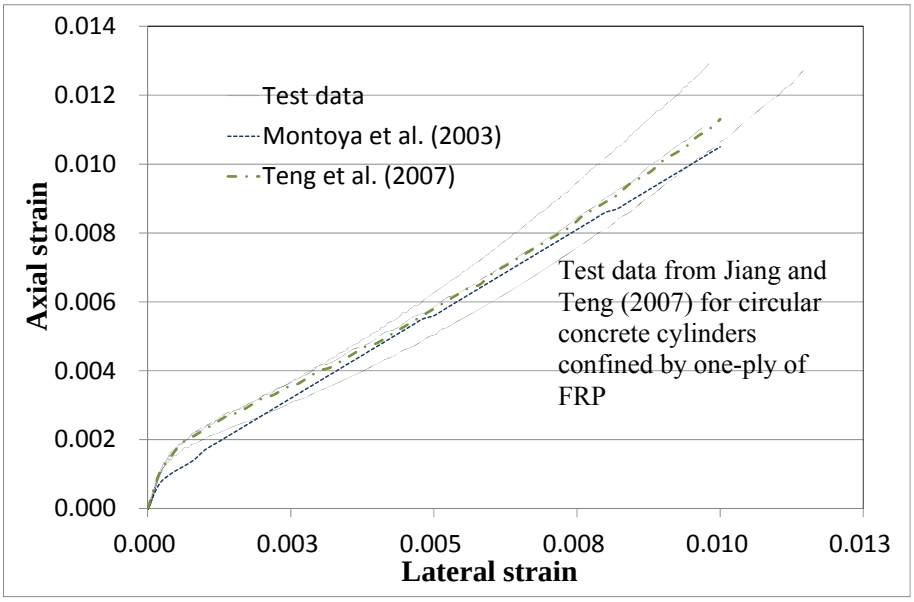

(a) Specimens confined by one-ply FRP

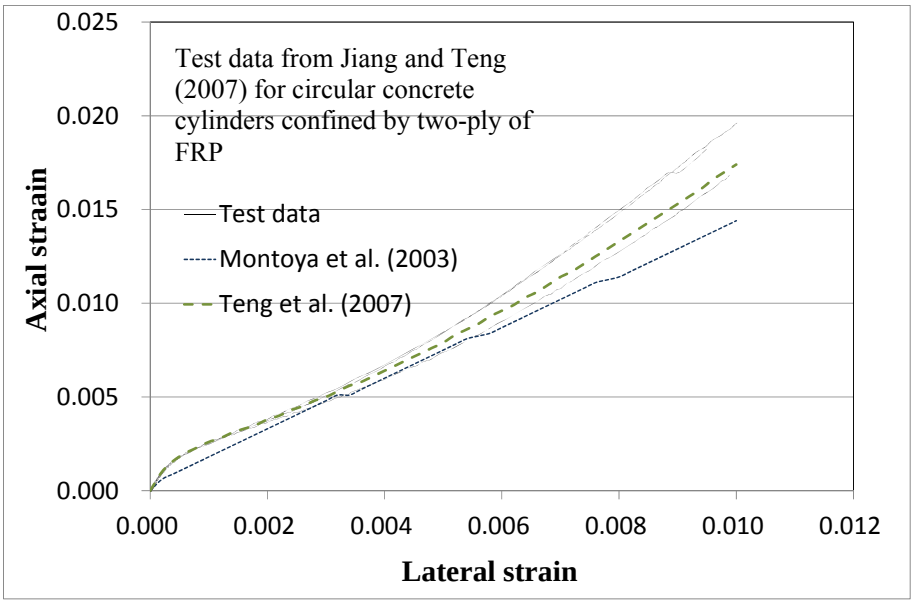

(b) Specimens confined by two-ply FRP

Figure 2.3 Lateral-to-axial strain curves of FRP-confined concrete

CHAPTER 3

BEHAVIOUR AND MODELLING OF CONFINED HIGH STRENGTH CONCRETE

3.1 INTRODUCTION

From the literature review presented in Chapter 2, it is clear that although test results of FRP-confined normal strength concrete (NSC) can now be closely predicted by some of the existing empirical stress-strain models (e.g. Jiang and Teng 2007; Teng *et al.* 2007), much less is known about the behaviour of high strength concrete (HSC) confined with an FRP jacket due to the limited existing research (Berthet *et al*. 2005; Mandal *et al*. 2005; Almusallam 2006; Li 2006). Therefore, further work on FRP-confined HSC is needed. In particular, Yu et al.'s (2010) constitutive model for confined concrete relies on an accurate analysis-oriented stress-strain model as its input. The applicability of this constitutive model to HSC requires the development of an accurate analysis-oriented stress-strain model for HSC.

HSC has found increasingly wide applications in structural engineering especially where reductions in structural self-weight and/or size are important (Holland 2005). The definition of HSC has evolved with time but in many recent studies (e.g. Attard and Setunge 1996; Wee *et al.* 1996; Candappa *et al.* 2001;), HSC has been defined as concrete with a cylinder compressive strength exceeding 50 MPa. This is also the definition adopted in the present chapter. It is widely accepted that HSC structural members generally behave differently from those of NSC (e.g. more brittle failure

processes), so direct application of theoretical models developed for NSC to HSC may lead to unsafe designs (Attard and Setunge 1996; Wee *et al.* 1996).

HSC can be further divided into two types according to whether mineral admixtures are used. Incorporating mineral admixtures is a widely accepted practice in making HSC and affects significantly its behaviour (Lam *et al.* 1998). The most commonly used mineral admixture is silica fume. Setunge *et al.* (1993) found from tri-axial tests that silica fume had a significant effect on the behaviour of confined HSC. To address this difference, separate models are needed for these two types of confined HSC. For HSC with silica fume, the effect of this additional mineral admixture on confinement effectiveness is still difficult to quantify due to the limited and controversial nature of the existing test results (Xie *et al.* 1995; Attard and Setunge 1996; Ansari and Li 1998). This chapter is therefore primarily concerned with the behaviour and modelling of confined HSC without silica fume although the effect of silica fume is noted where appropriate. Hereafter in this chapter, "HSC" refers only to HSC without silica fume unless otherwise specified. The behaviour of HSC confined with a constant external pressure (active confinement) is first examined, followed by a study of the behaviour of HSC confined with FRP; the former is expected to serve as a basis for understanding and modelling the latter.

3.2 ACTIVELY-CONFINED HSC

3.2.1 General

Many experimental studies have been conducted on actively-confined HSC (Xie *et al.* 1995; Attard and Setunge 1996; Imram and Pantazopoulou 1996; Ansari and Li 1998; Candappa *et al.* 2001; Tan and Sun 2004; Lu and Hsu 2006). Xie *et al.* (1995), Attard and Setunge (1996), Ansari and Li (1998) and Lu and Hsu (2006) have also proposed models specifically for actively-confined HSC (referred to as "active-confinement models for HSC" hereafter). Each of these models was, however, based on the originators' own test data, so their wide applicability is uncertain. In addition, most of these models do not differentiate between HSC with and without silica fume. In this section, an accurate active-confinement model for HSC is presented on the basis of a large test database of actively-confined HSC assembled in the present study.

The present database for actively-confined HSC contains all the test data from existing studies that meet the following criteria: (1) the concrete had an unconfined (cylinder compressive) strength higher than 50 MPa and did not include silica fume; (2) the concrete cylinder specimens had not been submerged in water to achieve a saturated condition prior to testing. Saturated specimens have been excluded as they are known to show obviously inferior performance (Imram and Pantazopoulou 1996) and are not commonly found in practice. The database includes the results of 51 actively-confined concrete cylinder specimens from Attard and Setunge (1996), Imram and Pantazopoulou (1996), Candappa *et al.* (2001), and Tan

and Sun (2004), Lu and Hsu (2006). The unconfined concrete strength of the database ranges from 51.8 to 126 MPa, while the confinement ratio, which is defined as the ratio of the confining pressure to the unconfined concrete strength, ranges from 0.01 to 0.84. Further details of the database are given in Table 3.1. It should be noted that the test data of Tan and Sun (2004) were also used by Jiang and Teng (2007) as the unconfined concrete strength is very close to the lower bound of the strength range of HSC defined herein.

It is well known that the performance of an active-confinement model depends on its accuracy in predicting: (a) the peak axial stress; (b) the axial strain at peak stress; and (c) the axial stress-strain equation. These three key components are examined in the following sub-sections based on the test database presented in Table 3.1.

3.2.2 Peak Axial Stress

The peak axial stress on the axial stress–strain curve of actively-confined concrete is the compressive strength of such concrete and the peak axial stress equation defines the failure surface of such concrete. The following simple equation was found from a regression analysis of the test results in Table 3.1 to provide accurate predictions for the peak axial stress f'^{*}_{cc}:

$$\frac{f'^{*}_{cc}}{f'_{co}} = 1 + 3.34\left(\frac{f_l}{f'_{co}}\right)^{0.79} \qquad (3.1)$$

As mentioned earlier, f'_{co} is the unconfined concrete strength, and f_l is the constant active confining pressure. In addition, the ratio between the latter and the former is referred to as the confinement ratio.

To identify any differences between HSC and NSC, the test data of

actively-confined NSC collected by Jiang and Teng (2007) are compared with the predictions of Eq. (3.1) in Figure 3.1a. It is interesting to find that Eq. (3.1) also provides accurate predictions for NSC. Through a regression analysis of all the test results shown in Figure 3.1a, the following unified equation accurate for both NSC and HSC was obtained:

$$\frac{f'^{*}_{cc}}{f'_{co}} = 1 + 3.24\left(\frac{f_l}{f'_{co}}\right)^{0.8} \tag{3.2}$$

It is obvious from Figure 3.1a that Eqs. (3.1)-(3.2) provide very similar predictions, indicating that any difference between NSC and HSC in the peak axial stress is closely represented by Eq. (3.2).

The accuracy of Eqs. (3.1)-(3.2) is compared with that of corresponding equations of existing models (i.e. Attard and Setunge 1996; Candappa *et al.* 2001; Lu and Hsu 2006; Jiang and Teng 2007) in Table 3.2, using the present test database for HSC and that of Jiang and Teng (2007) for NSC. The root mean square deviation (RMSD) is used to evaluate the performance of each equation. The RMSD is defined by:

$$RMSD = \sqrt{\frac{\sum_{i=1}^{n}\left(P_i - E_i\right)^2}{n}} \tag{3.3}$$

where E_i is the experimental value of f'^{*}_{cc} / f'_{co}, P_i is the predicted value of f'^{*}_{cc} / f'_{co}, and n is the number of data points. A smaller RMSD implies a more accurate equation. It is evident from Table 3.2 that Eqs. (3.1-3.2) are both superior to corresponding equations in existing models, including the

one used in Jiang and Teng's (2007) model (i.e. $\frac{f'^{*}_{cc}}{f'_{co}} = 1 + 3.5\frac{f_l}{f'_{co}}$). Figure 3.1a shows that although the peak axial stress equation in Jiang and Teng's (2007) model is generally accurate for NSC and was also previously calibrated with test data of FRP-confined NSC by Teng *et al.* (2007), it does slightly underestimate the test results of actively confined HSC, especially when the confinement ratio is relatively small.

Test results of HSC with silica fume (Xie *et al.* 1995; Attard and Setunge 1996; Ansari and Li 1998; Tan and Sun 2004) are compared with Eq. (3.2) in Figure 3.1b. It should be noted that Attard and Setunge (1996) and Tan and Sun (2004) tested both HSC with and HSC without silica fume and only the results of HSC with silica fume are shown in Figure 3.1b; those of HSC without silica fume are summarized in Table 3.1 and shown in Figure 3.1a. Figure 3.1b demonstrates that these test results are scattered significantly more widely around the curve defined by Eq. (3.2): the results of Ansari and Li (1998) fall considerably below the curve while almost all the results of Xie *et al.* (1995), Attard and Setunge (1996) and Tan and Sun (2004) lie above the curve. This larger scatter of the limited existing test results has also been noted by Ansari and Li (1998), but the reasons have not been properly explored. It is thus premature to draw any firm conclusions on the behaviour of confined HSC with silica fume before further research is conducted.

3.2.3 Axial Strain at Peak Axial Stress

A similar regression analysis of the test results of actively-confined HSC led

to the following simple equation for the axial strain at peak axial stress:

$$\frac{\varepsilon_{cc}^{*}}{\varepsilon_{co}} = 1 + 18.8\left(\frac{f_l}{f'_{co}}\right)^{1.1} \tag{3.4}$$

As mentioned earlier, ε_{cc}^{*} is the axial strain at peak axial stress of concrete under a specific constant confining pressure, and ε_{co} is the axial strain at peak axial stress of unconfined concrete. The above equation also predicts closely the test data of actively-confined NSC collected by Jiang and Teng (2007) (Figure 3.2a). A regression analysis of the test data of both confined HSC (Table 3.2) and confined NSC (Jiang and Teng 2007) led to the following unified equation for the axial strain at peak axial stress:

$$\frac{\varepsilon_{cc}^{*}}{\varepsilon_{co}} = 1 + 17.4\left(\frac{f_l}{f'_{co}}\right)^{1.06} \tag{3.5}$$

As expected, Eqs. (3.4-3.5) lead to very similar predictions (Figure 3.2a). Their performance, assessed using the RMSD of $\varepsilon_{cc}^{*}/\varepsilon_{co}$, is shown to be considerably better than that of corresponding equations in existing models (see Table 3.2) including the one used in Jiang and Teng's (2007) model (i.e. $\frac{\varepsilon_{cc}^{*}}{\varepsilon_{co}} = 1 + 17.5(\frac{f_l}{f'_{co}})^{1.2}$). Nevertheless, the scatter in the test data of axial strains at peak stress is significantly larger than that of peak axial stresses.

Test results of HSC with silica fume (Xie *et al.* 1995; Attard and Setunge 1996; Ansari and Li 1998; Tan and Sun 2004) are compared with Eq. (3.5) in Figure 3.2b. It is obvious that a considerable scatter of the test results exists and most of the test results fall below the curve defined by Eq. (3.5). This observation suggests that with the presence of silica fume, the effect of confinement on the axial strain at peak axial stress is reduced; this

observation confirms the importance of differentiating HSC with silica fume from HSC without silica fume.

3.2.4 Axial Stress-Strain Equation

Most existing analysis-oriented stress-strain models employ the following axial stress-strain equation originally proposed by Popovics (1973) to describe the relationship between axial stress f_c and axial strain ε_c of confined concrete:

$$\frac{f_c}{f'^{*}_{cc}} = \frac{\left(\varepsilon_c / \varepsilon^{*}_{cc}\right) r}{r - 1 + \left(\varepsilon_c / \varepsilon^{*}_{cc}\right)^{r}} \tag{3.6}$$

where the constant r is defined by

$$r = \frac{E_c}{E_c - f'^{*}_{cc} / \varepsilon^{*}_{cc}} \tag{3.7}$$

with E_c being the elastic modulus of concrete. The value of E_c can be found from $E_c = 4730\sqrt{f'_{co}}$ (in MPa) following ACI 318-95 (1999). This formula was used in making all predictions in the present study and was found to be accurate in most cases.

Eq. (3.6) was originally proposed for NSC and some existing studies (e.g. Wee *et al.* 1996) have indicated that this equation may overestimate the post-peak stress-strain behaviour of HSC which appears to feature a steeper descending branch. By contrast, other researchers (e.g. Attard and Setunge 1996) believed that this difference between NSC and HSC is insignificant especially when they are both subjected to confinement. The latter argument appears to be reasonable, so Eq. (3.6) is adopted for both NSC and HSC in the present study. The appropriateness of this approach is demonstrated in the comparisons shown in Figure 3.3.

3.2.5 Accuracy of the New Active-Confinement Model

Eq. (3.6), together with Eqs. (3.2) & (3.5), forms a new active-confinement model applicable to both NSC and HSC. Figure 3.3 shows comparisons of the predictions of this model (identified as "Proposed Model") and three series of axial stress-strain curves from the tests conducted by Candappa *et al.* (2001) on actively-confined concrete of three different unconfined strengths (ranging from 41.9 MPa to 103.3 MPa). The predictions of the active-confinement model used by Jiang and Teng (2007) are also shown in Figure 3.3 for comparison. It is clear that the curves predicted by the proposed model are in close agreement with the experimental curves. By contrast, Jiang and Teng's (2007) model generally underestimates the experimental curves mainly because of its underestimation of the peak axial stress. The overall good performance of the new active-confinement model also supports the use of Eq. (3.6) as the axial stress-strain equation for HSC. The proposed model is thus a unified active-confinement model for both NSC and HSC.

3.3 BEHAVIOUR OF FRP-CONFINED HSC

3.3.1 General

Existing research (Berthet *et al*. 2005; Mandal *et al*. 2005; Almusallam 2006; Li 2006) on the behaviour of FRP-confined HSC is limited. Of these existing studies, Berthet *et al*. (2005) and Mandal *et al*. (2005) tested only HSC with silica fume and showed that HSC with silica fume did not benefit significantly from FRP confinement. Almusallam (2006) and Li (2006) tested a few specimens of FRP-confined HSC without silica fume, but

unfortunately they did not report the experimental lateral-to-axial strain curves. In addition, in Li's (2006) study, FRP tubes with a significant axial stiffness were employed, so the behaviour was complicated by the axial resistance and the biaxial stress state of the FRP tube. Existing test results are thus inadequate for understanding the behaviour of and the development of a stress-strain model for FRP-confined HSC. A new series of tests with appropriately detailed measurements were thus conducted as part of the present study. Details of these tests are described below.

3.3.2 New Tests

3.3.2.1 Specimens and instrumentation

A total of twelve CFRP-confined circular concrete cylinders (without any mineral admixture) with a diameter of 152 mm and a height of 305 mm were prepared and tested. These cylinders were cast in two batches (batches 1 and 2) with two different concrete mix ratios to produce two different concrete grades. Each batch included six specimens divided into three pairs which were confined with CFRP jackets (with hoop fibers only) of three different thicknesses (i.e. two identical specimens forming a pair were prepared for each CFRP jacket thickness). Details of all the specimens are summarized in Table 3.3. For each batch, three (for batch 1) or four (for batch 2) plain concrete cylinders were tested as control specimens to determine the average properties of the concrete. Both ends of the cylinders were capped with high-strength sulfur to ensure uniform loading. The CFRP jackets were formed via the wet lay-up process, with an overlapping zone spanning a circumferential distance of 150 mm. A 25 mm wide CFRP strip

was provided near each end of a CFRP-jacketed cylinder specimen to avoid unexpected failure there.

For each control specimen, two axial strain gauges with a gauge length of 120 mm and two hoop strain gauges with a gauge length of 60 mm were placed at 180^{o} apart at the mid-height of the specimen to measure the strains in both directions. For each FRP-confined specimen, six hoop strain gauges and two axial strain gauges, both with a gauge length of 20 mm, were installed at the mid-height of the specimen. Of the six hoop strain gauges, one was placed within the overlapping zone and the other 5 strain gauges were distributed evenly outside the overlapping zone. In addition, axial strains were also measured using two linear variable displacement transducers (LVDTs) at 180^{o} apart that covered the mid-height region of 120 mm for both unconfined and confined specimens. All compression tests were carried out using an MTS machine with displacement control at a rate of 0.2mm/min. All test data, including the strains, loads, and displacements were recorded simultaneously by a data logger.

3.3.2.2 Material properties

Tensile tests of five FRP coupons were conducted following the ASTM standard (ASTM D3039 2000). The test results showed that the CFRP used in the study had an average tensile strength of 2737.7 MPa and an average elastic modulus E_{frp} of 237.8 GPa, based on a nominal thickness of 0.34 mm per ply. The elastic modulus, compressive strength and compressive strain at peak axial stress of the concrete in batch 1, averaged from the four plain

concrete cylinder tests, were 39.9 GPa (ranging from 38.7 GPa to 41.4 GPa), 70.8 MPa (ranging from 69.7 MPa to 71.4 MPa) and 0.0032 (ranging from 0.0030 to 0.0033) respectively. The corresponding values in batch 2, averaged from the three plain concrete cylinder tests, were 46.4 GPa (ranging from 45.9 GPa to 47.1 GPa), 111.6 MPa (ranging from 110.9 MPa to 112.7 MPa) and 0.0034 (ranging from 0.0034 to 0.0035). These average values were used in making theoretical predictions for the tests reported later in the chapter.

3.3.2.3 Test results

All the FRP-confined specimens failed by the hoop tensile rupture of the FRP jacket with a sudden explosive noise, except one 5-ply specimen in batch 1 and two 5-ply specimens in batch 2. The test of the 5-ply specimen in batch 1 was terminated at a load of 3000 kN due to an unexpected problem with the testing machine, while the tests of the two 5-ply specimens in batch 2 were terminated at a load of 4000 kN which is close to the maximum capacity of the MTS machine. FRP rupture generally occurred outside the overlapping zone accompanied by a limited amount of delamination between the plies (Figure 3.4). The key test results, including the hoop rupture strain of the FRP jacket $\varepsilon_{h,rup}$, the ultimate axial strain ε_{cu}, the axial stress at ultimate axial strain f'_{cu}, are summarized in Table 3.3. Figure 3.5 shows the normalized axial stress-strain curves and the normalized axial stress-lateral strain curves for all twelve FRP-confined specimens, where the lateral strain ε_l is shown on the left and the axial strain ε_c is shown on the right. The axial strain was found from the readings

of the two LVDTs, and the lateral strain was averaged from the readings of the five hoop strain gauges outside the overlapping region. In Figures 3.5-3.6, the axial stress is normalized by the unconfined concrete strength f'_{co} while the strains are normalized by the axial strain at peak axial stress of unconfined concrete ε_{co}.

3.3.4 Stress Path Dependence

It is widely accepted that the behaviour of confined NSC basically complies with the assumption of path independence, which assumes that the axial stress and axial strain of concrete confined with FRP at a given lateral strain are the same as those of the same concrete actively confined with a constant confining pressure equal to that supplied by the FRP jacket. This assumption has also been the basis of most analysis-oriented stress-strain models for FRP-confined NSC (Teng and Lam 2004). To explore the validity of this assumption for confined HSC, the axial stress-strain curves of FRP-confined HSC obtained from the new tests are compared with a series of axial stress-strain curves predicted based on this assumption by adopting the procedure normally used in existing analysis-oriented models such as that of Jiang and Teng (2007), except that the lateral-to-axial relationship used is that from the corresponding test. For two nominally identical specimens, only the results of one of them are shown in Figures 3.6 for better differentiation between different curves. These predicted curves are denoted by “new ultimate equations” to indicate that in making the predictions, Eqs. (3.2) & (3.5) were used. It is evident the stress-strain curves so predicted are significantly higher than their experimental counterparts. As the new active-confinement model (including the new ultimate equations) has been

verified using a large test database of both NSC and HSC, this comparison suggests that the assumption of path independence is incorrect for confined HSC. Instead, confinement appears to be less effective for FRP-confined (passively-confined) HSC than for actively-confined HSC. It may be noted that path dependence has also been reported by some previous researchers (e.g. Bazant and Tsubakl 1980). Bazant and Tsubakl (1980) pointed out that the presence of a confining pressure in the early stage of axial loading (e.g. in the case of actively-confined concrete) tends to prevent the growth of micro-cracks. In FRP-confined concrete, the confining pressure becomes significant only when the concrete approaches its unconfined strength, and this different loading path may have a detrimental effect on concrete behaviour.

It is also worth noting that although the behaviour of confined NSC basically complies with the path independence assumption, slight deviations from the assumption have been noted. For example, the active-confinement model used in Jiang and Teng (2007) was calibrated with test data of FRP-confined NSC. Indeed, Figure 3.1a shows that the strength equation for actively-confined concrete adopted by Jiang and Teng (2007) slightly underestimates the test results of actively-confined NSC, especially when the confinement ratio is relatively small. Noting also the fact (see Figures 3.6) that the "new ultimate equations" curves in Figures 3.6 are closer to the experimental curves for specimens with a thicker FRP jacket than for those with a thinner FRP jacket, it may be concluded that the path independence assumption deviates from the actual behaviour observed in the tests more

significantly when the confining FRP jacket is softer and/or when the unconfined concrete strength is higher. Therefore, for HSC, the effect of path dependence is significant enough for it to be properly reflected in a stress-strain model.

3.3.5 Dilation Properties

Teng *et al.* (2007) found from the test data available to them that the normalized lateral-to-axial strain relationship (i.e. the lateral strain equation) of HSC can be considered to be similar to that of NSC. The lateral strain equation proposed by them based mainly on test data of confined NSC was also shown to provide reasonably accurate predictions of the test results of actively-confined HSC presented in Candappa *et al.* (2001). This relationship, defined below, was also adopted by Jiang and Teng (2007) after a critical review of existing models:

$$\Phi\left(\frac{-\varepsilon_l}{\varepsilon_{co}}\right)=\frac{\varepsilon_c}{\varepsilon_{co}}\Big/\left(1+8\frac{f_l}{f'_{co}}\right)=0.85\left\{\left[1+0.75\left(\frac{-\varepsilon_l}{\varepsilon_{co}}\right)\right]^{0.7}-\exp\left[-7\left(\frac{-\varepsilon_l}{\varepsilon_{co}}\right)\right]\right\} \tag{3.8}$$

In Figures 3.7 and 3.8, the predictions of Eq. (3.8) are shown against the new test results of unconfined HSC and FRP-confined HSC respectively, to identify any differences in dilation properties between NSC and HSC. These comparisons show that while Eq. (3.8) provides close predictions for unconfined HSC, it is much less accurate for FRP-confined HSC (Figure 3.8). The experimental curves are scattered quite widely around the prediction of Eq. (3.8), so a relationship between the results and the concrete strength cannot be identified. Indeed, the curves for a concrete compressive strength of 111.6 MPa are closer to Eq. (3.8) than those for a concrete compressive strength of 70.8 MPa although Eq. (3.8) was based mainly on

NSC test data. Therefore, it is not unreasonable to attribute the large scatter of test results to the inherent variability of concrete dilation properties, as discussed in Teng et al. (2007); given this consideration, the applicability of Eq. (3.8) to both NSC and HSC is confirmed.

3.4 MODELLING OF FRP-CONFIEND HSC

3.4.1 General

Existing models for FRP-confined concrete mainly fall into two categories (Teng and Lam 2004; Jiang and Teng 2007): (1) design-oriented stress-strain models and (2) analysis-oriented stress-strain models. The published literature contains a small number of design-oriented stress-strain models for FRP-confined HSC (Berthet *et al.* 2005; Almusallam 2006; Li 2006), but each of these models was based on the limited test data available to its originator(s) and their wide applicability is uncertain. The development of a more reliable design-oriented stress-strain model calls for a much larger amount of data obtained from either numerous experiments and/or an accurate analysis-oriented model (e.g. Teng *et al.* 2009). Analysis-oriented stress-strain models consider the responses of the concrete and the FRP jacket as well as their interaction in an explicit manner and are more versatile and powerful than design-oriented stress-strain models (Teng *et al.* 2007). Such models are applicable/easily extendable to actively-confined concrete and concrete confined by materials other than FRP. An accurate analysis-oriented stress-strain model can also be employed to generate data for the development of a design-oriented stress-strain model (Teng *et al.* 2009). This chapter is thus concerned only with the development of an

analysis-oriented stress-strain model for FRP-confined HSC.

Many analysis-oriented stress-strain models (e.g. Mirmiran and Shahawy 1997; Spoelstra and Monti 1999; Fam and Rizkalla 2001; Chun and Park 2002; Harries and Kharel 2002; Marques *et al.* 2004; Binici 2005; Jiang and Teng 2007; Teng *et al.* 2007) have been published for FRP-confined NSC. Among them, the recent model proposed by Jiang and Teng (2007) has been shown by its originators to be the most accurate; test results of FRP-confined NSC can now be closely predicted by this model (Jiang and Teng 2007). By contrast, to the best of the authors' knowledge, analysis-oriented models proposed for and/or verified using test results of FRP-confined HSC are not available in the open literature, despite the increasingly wide application of HSC in practice.

Most existing analysis-oriented stress-strain models for FRP-confined concrete are composed of the following three elements (Teng and Lam 2004; Jiang and Teng 2007): (i) an active-confinement base model, (ii) the lateral strain equation depicting the relationship between the axial strain and the lateral/hoop strain of the concrete (or hoop strain of the confining jacket), and (iii) a relationship between the lateral strain and the radial pressure supplied by the jacket. The third element can be easily defined for a linear elastic FRP jacket. It may be noted only the third element of an analysis-oriented stress-strain model for FRP-confined concrete needs to be modified if it is to be employed to predict concrete passively confined with another material. In the following sub-sections, these three elements for

HSC are examined in detail to arrive at an analysis-oriented stress-strain model for FRP-confined HSC.

3.4.2 Active-Confinement Model as the Base Model

As discussed earlier, the new active-confinement model, although having been verified using a large test database of both NSC and HSC, cannot provide accurate predictions of the present test results because of the dependence of the behaviour of confined HSC on its loading path. Therefore, a different active-confinement base model needs to be used to achieve close predictions for FRP-confined HSC. The active-confinement base model used in Jiang and Teng (2007), although slightly underestimating the stress-strain response of active-confined NSC (see Figures 3.1a and 3.3a), has been shown to work well for FRP-confined NSC. As the behaviour of actively-confined NSC is very similar to that of actively-confined HSC (see Figures 3.1 and 3.2), it is reasonable to expect that this active-confinement base model is likely to be also suitable for FRP-confined HSC. In Figure 3.6, a series of axial stress-strain curves denoted by "Jiang and Teng's ultimate equations" are also shown for comparison with the experimental curves. These curves were produced in a similar way to the curves identified as "new ultimate equations" with the only difference being that Jiang and Teng's (2007) active-confinement model was used here instead of the new active-confinement model as the base model. Figure 3.6 shows that the curves produced this way are very close to the experimental curves, indicating that Jiang and Teng's (2007) active-confinement model is also appropriate for use in the prediction of FRP-confined HSC as the base model.

3.4.3 Lateral Strain Equation and Confining Pressure

As discussed earlier, the present test results of FRP-confined HSC indicate that Eq. (3.8) is applicable to both NSC and HSC. The development of a more accurate lateral strain equation needs further research. Therefore, Eq. (3.8) is retained for the prediction of stress-strain curves of FRP-confined HSC although some errors arising from the use of Eq. (3.8) can be expected.

Once the lateral strain is known, the confining pressure f_l on a circular column from an FRP jacket is given by the following simple relationship:

$$f_l = \frac{E_{frp} t \varepsilon_h}{R} = -\frac{E_{frp} t \varepsilon_l}{R} \tag{3.9}$$

where E_{frp} is the elastic modulus of the FRP jacket in the hoop direction, ε_h and t are the hoop strain and the thickness of the FRP jacket respectively, and R is the radius of the confined concrete core.

3.4.4 Analysis-Oriented Stress-Strain Model

The above discussions suggest that Jiang and Teng's (2007) model can lead to reasonably close predictions of the stress-strain behaviour of FRP-confined HSC, with the underestimation of its active confinement base model of the stress-strain behaviour of actively-confined HSC being used to account for the detrimental effect of stress path dependence on FRP-confined HSC.

The new test results are compared with the predictions from Jiang and Teng's (2007) model in Figure 3.5. This comparison demonstrates that Jiang and Teng's (2007) model generally performs well although some small

errors exist especially for specimens with an unconfined strength of 70.8 MPa. These errors are due to the inaccuracy of the lateral-to-axial strain relationship (Figure 3.8), as discussed earlier. Further research is needed to improve the accuracy of this relationship when more test data become available. Jiang and Teng's (2007) model is thus recommended as a model for predicting the stress-strain behaviour of both FRP-confined NSC and FRP-confined HSC.

3.5 MODEL VERIFICATION USING INDEPENDENT TEST DATA

3.5.1 HSC without Silica Fume

Figure 3.9 shows comparisons between the predictions of Jiang and Teng's (2007) model and the axial stress-strain curves from tests conducted by Almusallam (2006) on HSC cylinders (150 mm x 300 mm) with an unconfined concrete strength of 50.6 MPa (with ε_{co} = 0.0029) or 60.5 MPa (with ε_{co} = 0.0030). These cylinders were confined with a one-ply or a three-ply GFRP jacket, whose elastic modulus and tensile strength were 27 GPa and 540 MPa respectively, based on a nominal thickness of 1.3 mm per ply. The experimental lateral strains at the rupture of the FRP jacket were used in making the predictions. The predictions are in reasonably close agreement with the test results.

3.5.2 HSC with Silica Fume

Figure 3.10 shows a comparison between the predictions of Jiang and Teng's (2007) model and the axial stress-strain curves from tests conducted by Berthet (2005) on HSC with silica fume. The HSC cylinders (70 mm × 140 mm) tested by Berthet (2005) had an unconfined concrete strength of

113 MPa (with ε_{co} = 0.0023) and were confined with a two-ply or a five-ply CFRP jacket whose elastic modulus and tensile strength were 230 GPa and 2,500 MPa respectively, based on a nominal thickness of 0.165 mm per ply. Again, the experimental lateral strains at the rupture of the FRP jacket were used in making the predictions. Figure 3.10 shows that Jiang and Teng's (2007) model considerably overestimates the response, especially the ultimate axial strain of these specimens (see Figure 3.10). Once again, this comparison confirms that the presence of silica fume reduces the effectiveness of confinement and a different confinement model is needed for HSC with silica fume.

Almusallam (2006) also tested HSC with silica fume but their specimens were shown to gain little strain enhancement from the confinement of FRP; Jiang and Teng's (2007) model thus cannot provide correct predictions of these test results and the comparison is not shown here.

It should be noted that predictions from Jiang and Teng's (2007) model were obtained by assuming that the elastic modulus of unconfined concrete $E_c = 4730\sqrt{f'_{co}}$ (ACI 318-95 1999). Although this equation provides accurate predictions for NSC and HSC without silica fume, it was found to underestimate the elastic modulus of HSC with silica fume based on the test results of Berthet (2005) and Almusallam (2006). If the experimental elastic modulus of unconfined concrete is used in the model, the predicted curves are further away from the experimental curves. This phenomenon reinforces the importance of differentiating HSC with silica fume from HSC without

silica fume.

3.6 SUMMARY AND CONCLUSIONS

This chapter has been primarily concerned with the behaviour and modelling of the stress-strain behaviour of confined HSC without silica fume. The behaviour of actively-confined HSC was first examined, leading to a unified active-confinement model applicable to both HSC and NSC. An experimental study on FRP-confined HSC was then presented and interpreted to examine its behaviour, which also forms the basis for the subsequent modelling work. It was shown that Jiang and Teng's (2007) model, initially developed for FRP-confined NSC, is also accurate for FRP-confined HSC. While the focus of the work was on HSC without silica fume, the effect of incoprating silica fume into HSC on its stress-strain behaviour was also given appropriate attention. The results and discussions presented in the chapter also allow the following conclusions to be drawn on the behaviour and modelling of confined HSC without silica fume:

(1) The new unified active-confinement model for actively-confined concrete is more accurate than all existing models for actively-confined HSC;
(2) The lateral-to-axial strain relationship adopted in Jiang and Teng's (2007) model, which was initially proposed in Teng et al. (2007), leads to acceptable predictions for FRP-confined HSC given the considerable variability in concrete dilation properties obtained from tests. Further studies on the dilatation properties of confined HSC are needed.

(3) The assumption of stress independence widely used in modelling the stress-strain behaviour of FRP-confined concrete can be a source of significant errors in predicting the behaviour of FRP-confined HSC, especially when the FRP jacket is relatively soft.

The presence of silica fume in HSC was shown to significantly affect the behaviour of confined HSC. While existing test data suggest that silica fume can significantly reduce the effectiveness of confinement in terms of the enhancement of strain capacity, these data are insufficient to allow more elaborate conclusions to be drawn or a separate, reliable confinement model to be developed. Much more work is needed on the behaviour of confined HSC with silica fume.

3.7 REFERENCES

ACI 318-95. (1999). *Building Code Requirements for Structural Concrete (318-95) and Commentary (318R-95)*, American Concrete Institute (ACI), Fifth Printing, Farmington Hills, Michigan, USA.

Almusallam, T.H. (2006). "Behaviour of normal and high-strength concrete cylinders confined with E-glass/epoxy composite laminates." *Composites Part B: Engineering*, 38, 629-639.

Ansari, F., and Li, Q. (1998). "High-strength concrete subjected to triaxial compression." *ACI Materials Journal*, 95(6), 747-755.

ASTM D3039. (2000). *Standard Test Method for Tensile Properties of Polymer Matrix Composite Materials*, ASTM West Conshohocken, PA.

Attard, M., and Setunge, S. (1996). "Stress-strain relationship of confined

and unconfined concrete." *ACI Materials Journal*, 93(5), 1-11.

Bazant, Z.P., and Tsubakl. (1980). "Total strain theory and path-dependence of concrete." *Journal of the Engineering Mechanics Division*-ASCE, 106(6), 1151-1172.

Berthet, J.F., Ferrier, E., and Hamelin, P. (2005). "Compressive behaviour of concrete externally confined by composite jackets, Part A: experimental study." *Construction and Building Materials*, 19, 223-232.

Binici, B. (2005). "An analytical model for stress–strain behaviour of confined concrete." *Engineering Structures*, 27(7), 1040-1051.

Candappa, D.C., Sanjayan J.G., and Setunge, S. (2001). "Complete triaxial stress-strain curves of high-strength concrete." *Journal of Materials in Civil Engineering*-ASCE, 13(3), 209-215.

Chun, S.S., and Park, H.C. (2002). "Load carrying capacity and ductility of RC columns confined by carbon fiber reinforced polymer." *Proceedings, Third International Conference on Composites in Infrastructure*, 1-12.

Fam, A.Z., and Rizkalla, S.H. (2001). "Confinement model for axially loaded concrete confined by circular fiber-reinforced polymer tubes." *ACI Structural Journal*, 98(4), 451-461.

Harries, K.A., and Kharel, G. (2002). "Behaviour and modelling of concrete subject to variable confining pressure." *ACI Materials Journal*, 99(2), 180-189.

Hollaway, L.C. and Teng, J.G. (Eds). (2008). *Strengthening and Rehabilitation of Civil Infrastructures Using FRP Composites*, Cambridge, UK: Woodhead Publishing Limited.

Holland, T.C. (2005). *Silica Fume User's Manual*, US Department of

Transportation, Report FHWA-IF-05-016, April 2005.

Imram, I., and Pantazopoulou, S.J. (1996). "Experimental study of plain concrete under triaxial stress." *ACI Materials Journal*, 93(6), 589-601.

Jiang, T., and Teng, J.G. (2007). "Analysis-oriented stress-strain models for FRP-confined concrete." *Engineering Structures*, 29, 2968-2986.

Kent, D. C., and Park, R. (1971). "Flexural members with confined concrete." *Journal of the Structural Division*-ASCE, 97(7), 1969–1990.

Lam, L., and Teng, J.G. (2002). "Strength models for fiber-reinforced plastic-confined concrete." *Journal of Structural Engineering*-ASCE, 128(5), 612-623.

Lam, L., and Teng, J.G. (2003). "Design-oriented stress-strain model for FRP-confined concrete." *Construction and Building Materials*, 17(6-7), 471-489.

Lam, L., Wong, Y.L., and Poon, C.S. (1998). "Effect of fly ash and silica fume on compressive and fracture behaviours of concrete." *Cement and Concrete Research*, 28(2), 271-283.

Li, G. (2006). "Experimental study of FRP confined concrete cylinders." *Engineering Structures*, 28, 1001-1008.

Lu, X., and Hsu, C.T.T. (2006). "Behaviour of high strength concrete with and without steel fiber reinforcement in triaxial compression." *Cement and Concrete Research*, 36, 1679-1685.

Mandal, S., Hoskin, A., and Fam, A. (2005). "Influence of concrete strength on confinement effectiveness of fiber-reinforced polymer circular jackets." *ACI Structural Journal*, 102(3), 383-392.

Mander, J. B., Priestley, M. J. N., and Park, R. (1988). "Theoretical

stress-strain model for confined concrete." *Journal of Structural Engineering*-ASCE, 114(8), 1804–1826.

Marques, S.P.C., Marques, D.C.S.C., Silva, J.L., and Cavalcante, M.A.A. (2004). "Model for analysis of short columns of concrete confined by fiber-reinforced polymer." *Journal of Composites for Construction*-ASCE, 8(4), 332-340.

Mirmiran, A., and Shahawy, M. (1997). "Dilation characteristics of confined concrete." *Mechanics of Cohesive-Frictional Materials*, 2(3), 237-249.

Popovics, S. (1973). "A numerical approach to the complete stress–strain curve of concrete." *Cement and Concrete Research*, 3(5), 583-599.

Setunge, S., Attard, M., and Darvall, P.L. (1993). "Ultimate strength of confined very high-strength concrete." *ACI Materials Journal*, 90(6), 632-641.

Spoelstra, M.R., and Monti, G. (1999). "FRP-confined concrete model." *Journal of Composites for Construction*-ASCE, 3(3), 143-150.

Tan, K.H., and Sun, X. (2004). "Failure criteria of concrete under triaxial compression. " *Proceedings, International Symposium on Confined Concrete (CD-Rom).*

Teng, J.G., and Lam, L. (2004). "Behaviour and modelling of fiber reinforced polymer-confined concrete." *Journal of Structural Engineering*, ASCE, 130(11), 1713-1723.

Teng, J.G., Chen, J.F., Smith, S.T., and Lam, L. (2002). *FRP Strengthened RC Structures*, John Wiley & Sons Ltd.

Teng, J.G., Huang, Y.L., Lam, L., and Ye, L.P. (2007). "Theoretical model for fiber reinforced polymer-confined concrete." *Journal of Composites*

for Construction, ASCE, 11(2), 201-210.

Teng, J.G., Jiang, T., Lam, L., and Luo, Y.Z. (2009). "Refinement of a design-oriented stress-strain model for FRP-confined concrete." *Journal of Composites for Construction*-ASCE, 13(4), 269-278.

Wee, T.H., Chin, M.S., and Mansur, M.A. (1996). "Stress-strain relationship of high strength concrete in compression." *Journal of Materials in Civil Engineering*, ASCE, 8(2), 70-76.

Xie, J., Elwi, A.E., and MacGregor, J.G. (1995). "Mechanical properties of three high-strength concretes containing silica fume." *ACI Materials Journal*, 92(2), 1-11.

Yu, T., Teng, J. G., Wong, Y. L., and Dong, S. L. (2010). "Finite element modelling of confined concrete-II: Plastic-damage model." *Engineering Structures*, 32(3), 680-691.

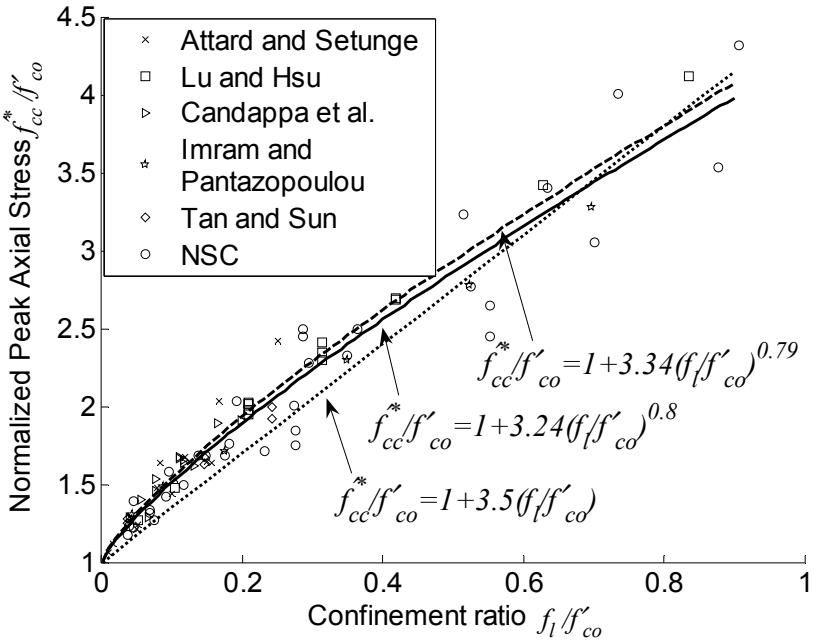

(a)

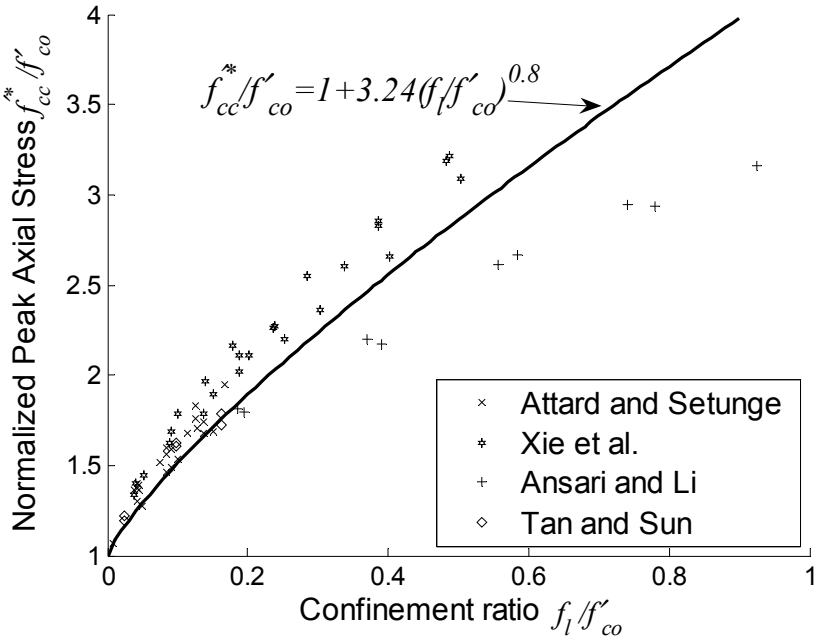

(b)

Figure 3.1 Peak axial stress of actively-confined concrete

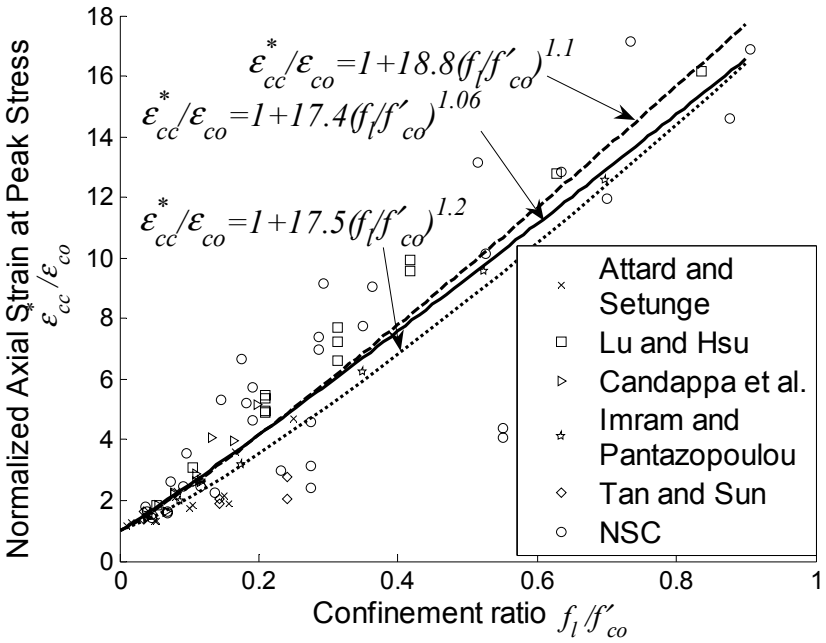

(a)

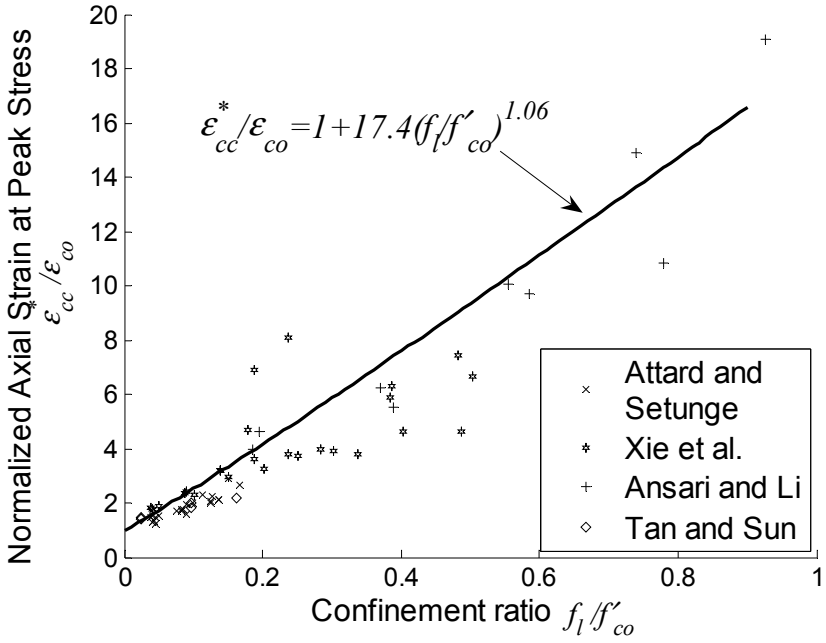

(b)

Figure 3.2 Axial strains at peak axial stress of actively-confined concrete

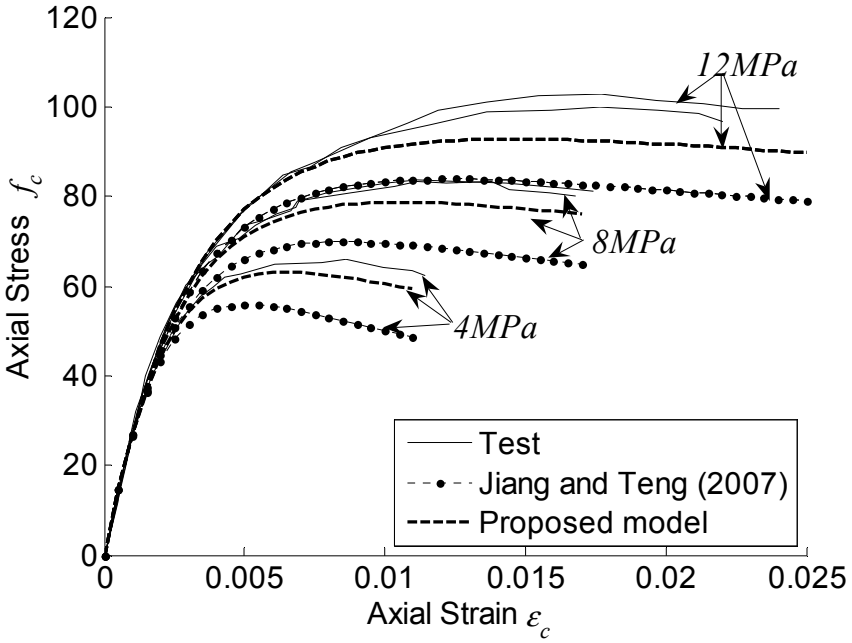
120
100
80
60
40
20
0
0
0.005
0.01
0.015
0.02
0.025
Axial Stress f_c
Axial Strain ε_c
12MPa
8MPa
4MPa
Test
Jiang and Teng (2007)
Proposed model

(a)

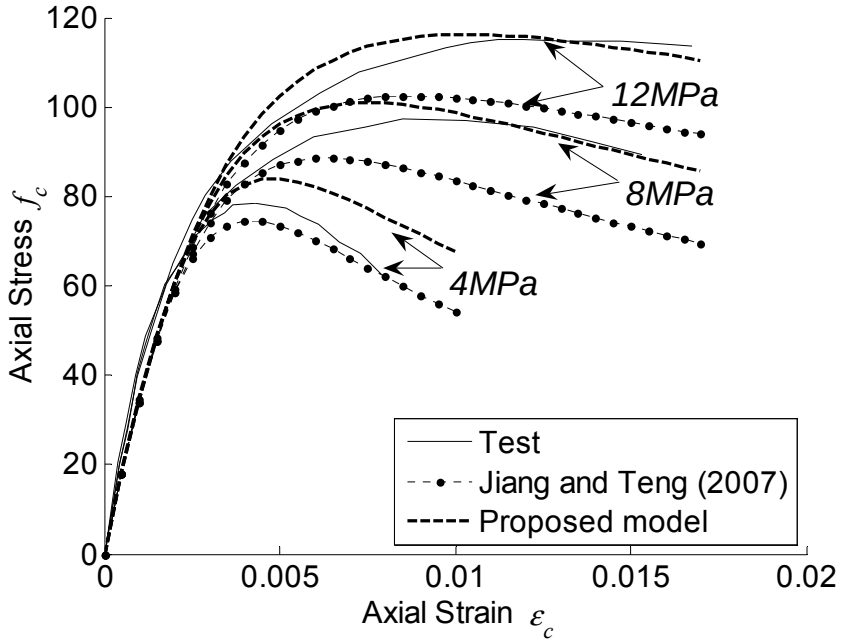
120
100
80
60
40
20
0
0
0.005
0.01
0.015
0.02
Axial Stress f_c
Axial Strain ε_c
12MPa
8MPa
4MPa
Test
Jiang and Teng (2007)
Proposed model

(b)

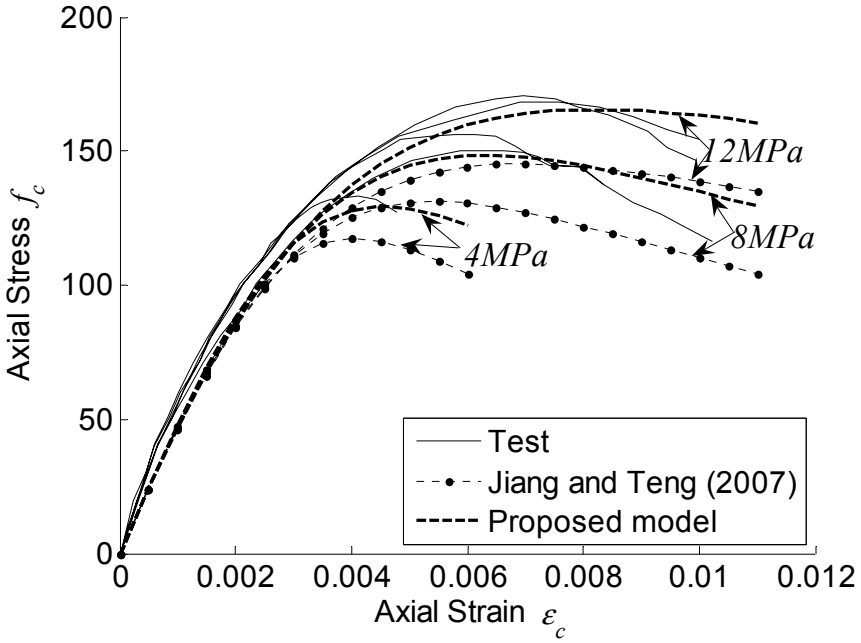

(c)

Figure 3.3 Stress-strain curves of actively-confined concrete

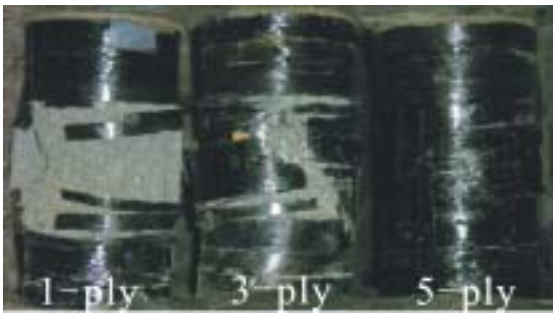

Figure 3.4 Typical failure modes of FRP-confined HSC specimens

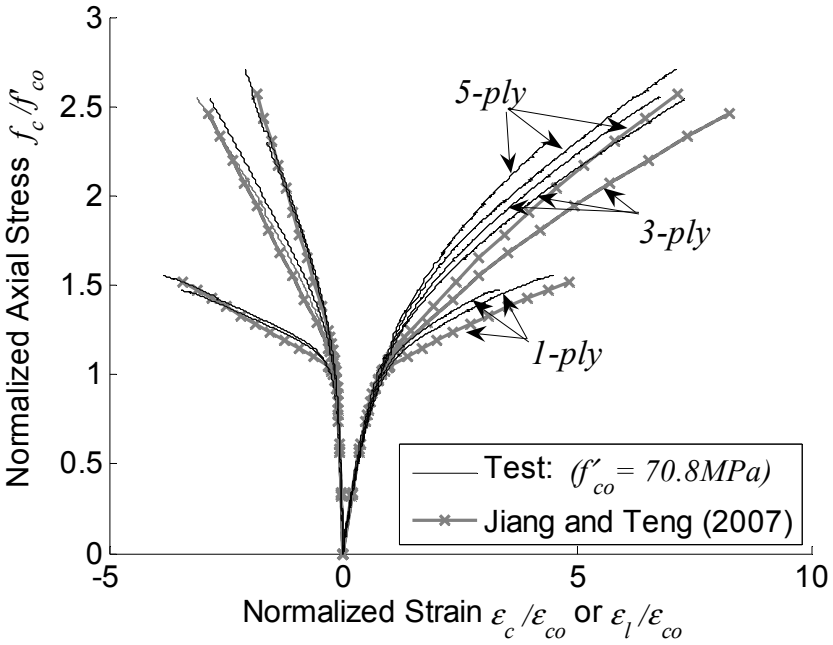

(a)

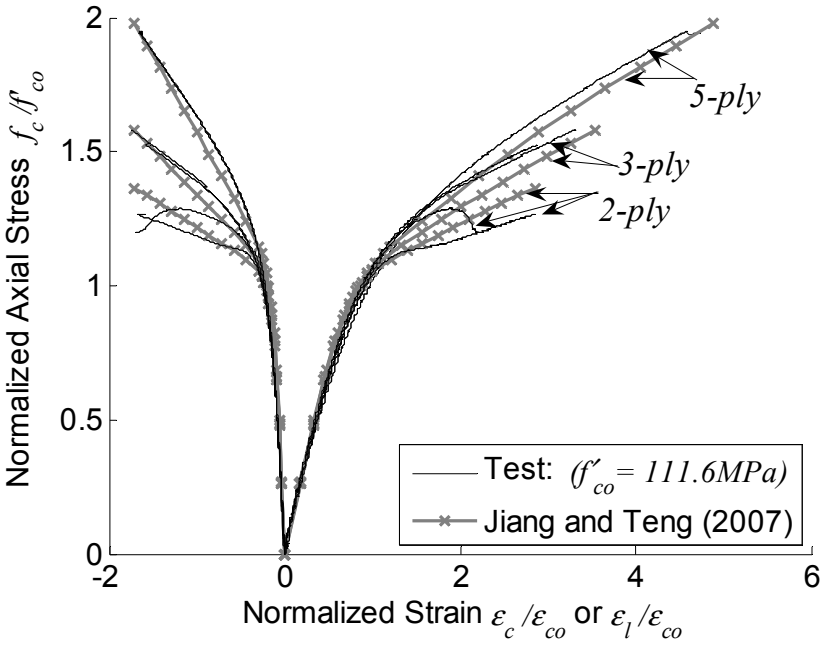

(b)

Figure 3.5 Stress-strain curves of FRP-confined HSC

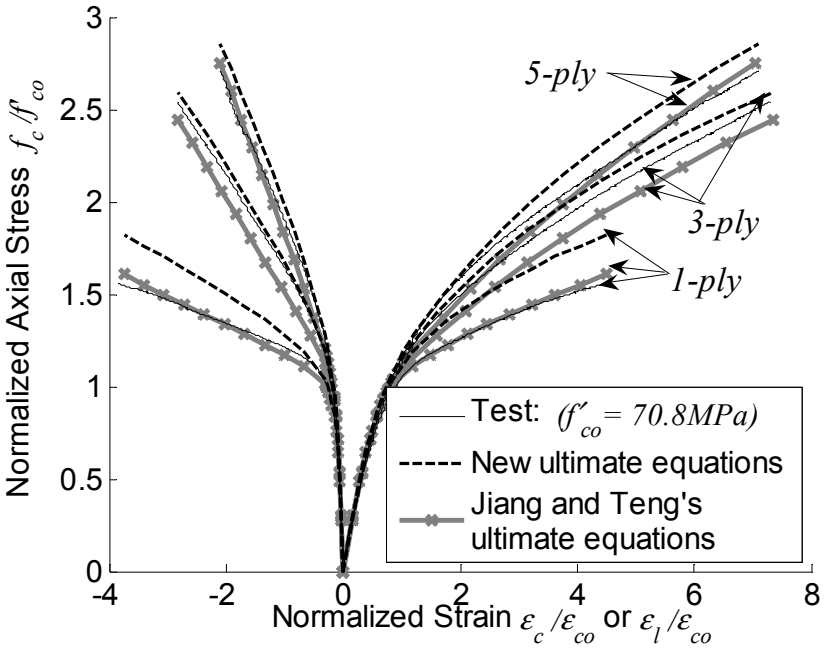

(a)

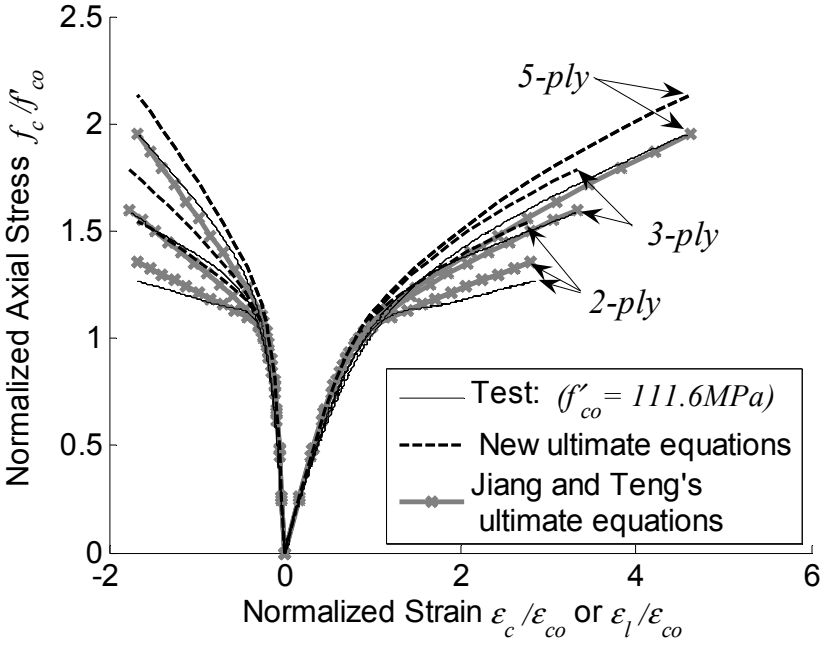

(b)

Figure 3.6 Performance of different active-confinement models

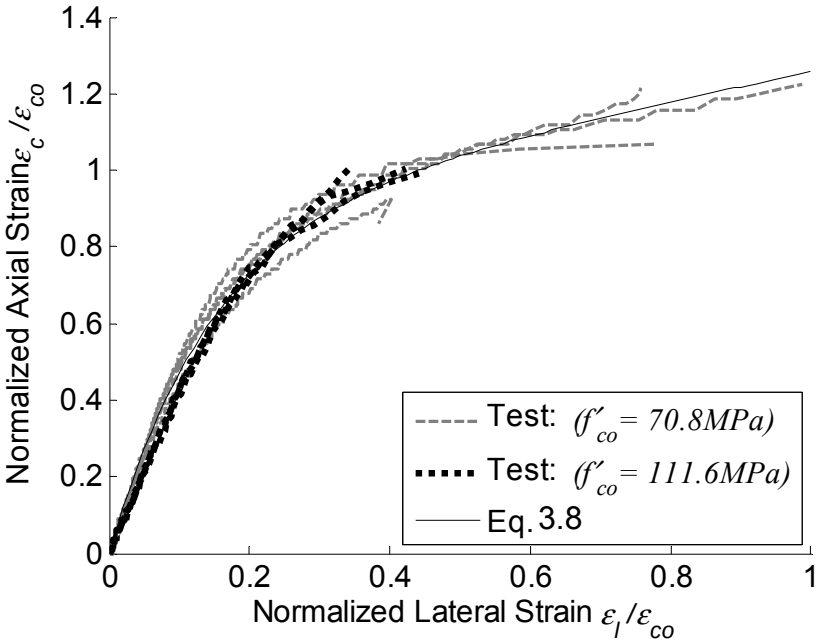

Figure 3.7 Lateral-to-axial strain curves of unconfined HSC

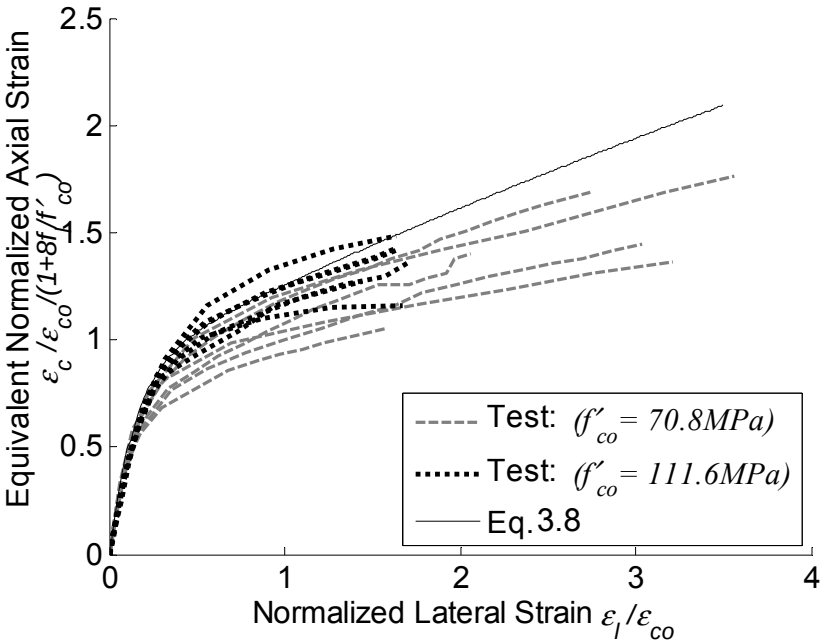

Figure 3.8 Lateral-to-axial strain curves of FRP-confined HSC

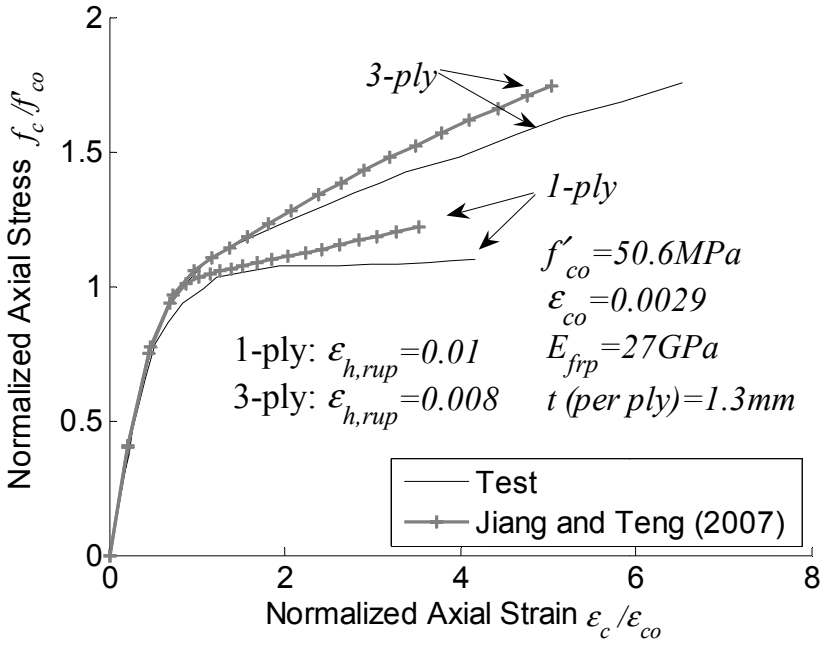

(a)

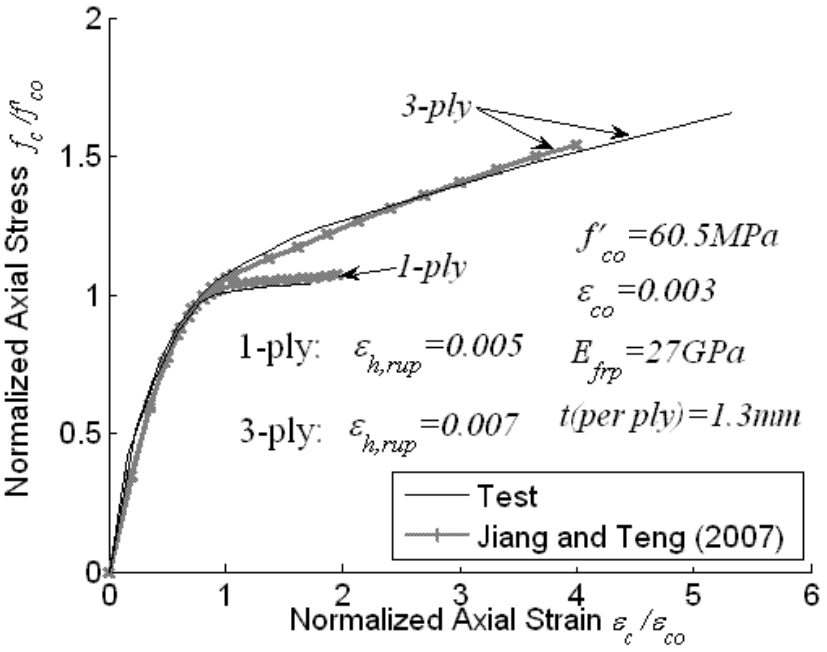

(b)

Figure 3.9 Comparison of Jiang and Teng's (2007) model with Almusallam's (2006) test results

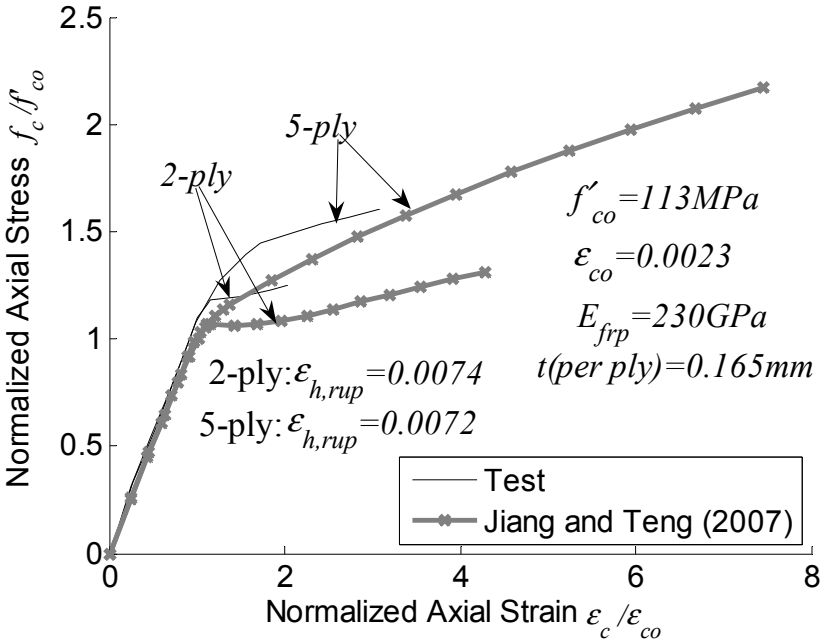

Figure 3.10 Comparison of Jiang and Teng's (2007) model with Berthet et al's (2005) test results

Table 3.1 Test results of actively-confined HSC without silica fume

No.	Diameter (mm)	Height (mm)	f'_{co} (MPa)	ε_{co} (%)	f_l (MPa)	f'^{*}_{cc} (MPa)	ε^{*}_{cc} (%)
Imram and Pantazopoulou (1996)							
1	54	115	73.4	0.33	3.2	96.1	0.50
2	54	115	73.4	0.33	6.4	108.7	0.65
3	54	115	73.4	0.33	12.8	125.6	1.05
4	54	115	73.4	0.33	25.6	168.6	2.03
5	54	115	73.4	0.33	38.4	204.0	3.11
6	54	115	73.4	0.33	51.2	240.5	4.09
Attard and Setunge (1996)							
7	100	200	100.0	0.27	1.0	106.0	0.31
8	100	200	100.0	0.27	5.0	121.0	0.36
9	100	200	100.0	0.27	10.0	144.0	0.47
10	100	200	100.0	0.27	15.0	165.0	0.58
11	100	200	126.0	0.34	5.0	162.0	0.50
12	100	200	126.0	0.34	10.0	186.0	0.71
13	100	200	126.0	0.34	15.0	211.0	0.89
14	100	200	96.0	0.28	5.0	119.0	0.37
15	100	200	96.0	0.28	10.0	147.0	0.52
16	100	200	96.0	0.28	15.0	157.0	0.53
17	100	200	60.0	0.21	1.0	67.0	0.27
18	100	200	60.0	0.21	5.0	98.0	0.48
19	100	200	60.0	0.21	10.0	122.0	0.76
20	100	200	60.0	0.21	15.0	145.0	0.99
Candappa et al (2001)							
21	100	200	60.6	0.24	4.0	78.2	0.40
22	100	200	60.6	0.24	8.0	97.8	0.98
23	100	200	60.6	0.24	12.0	115.5	1.24
24	100	200	73.1	0.24	4.0	102.6	0.45
25	100	200	73.1	0.24	8.0	121.5	0.63
26	100	200	73.1	0.24	8.0	122.3	0.69
27	100	200	73.1	0.24	12.0	138.1	0.94
28	100	200	103.3	0.30	4.0	133.1	0.43
29	100	200	103.3	0.30	8.0	151.0	0.68
30	100	200	103.3	0.30	8.0	158.0	0.67
31	100	200	103.3	0.30	12.0	171.5	0.80
32	100	200	103.3	0.30	12.0	169.3	0.78
Lu and Hsu (2006)							
33	100	200	67.0	0.25	3.5	84.9	0.47
34	100	200	67.0	0.25	7.0	99.0	0.78
35	100	200	67.0	0.25	14.0	130.7	1.24
36	100	200	67.0	0.25	14.0	132.7	1.25
37	100	200	67.0	0.25	14.0	134.9	1.35
38	100	200	67.0	0.25	14.0	135.5	1.37
39	100	200	67.0	0.25	21.0	154.0	1.66
40	100	200	67.0	0.25	21.0	157.1	1.83
41	100	200	67.0	0.25	21.0	161.2	1.94
42	100	200	67.0	0.25	28.0	180.2	2.50
43	100	200	67.0	0.25	28.0	179.9	2.41
44	100	200	67.0	0.25	42.0	229.1	3.21
45	100	200	67.0	0.25	56.0	276.0	4.06

Tan and Sun (2004)							
46	100	300	51.8	0.24	1.9	64.8	0.33
47	100	300	51.8	0.24	1.9	66.0	0.39
48	100	300	51.8	0.24	7.5	86.6	0.46
49	100	300	51.8	0.28	7.5	84.2	0.49
50	101	301	51.8	0.24	12.5	99.3	0.49
51	101	300	51.8	0.24	12.5	103.3	0.66

Table 3.2 Performance of equations for peak stress point in different active-confinement models

Source	Axial stress equation	*RMSD* HSC only	*RMSD* NSC and HSC	Axial strain equation	*RMSD* HSC only	*RMSD* NSC and HSC
Present study	$\frac{f'^{*}_{cc}}{f'_{co}} = 1 + 3.34\left(\frac{f_l}{f'_{co}}\right)^{0.79}$	0.105	0.178	$\frac{\varepsilon^{*}_{cc}}{\varepsilon_{co}} = 1 + 18.8(\frac{f_l}{f'_{co}})^{1.1}$	0.87	1.58
Present study	$\frac{f'^{*}_{cc}}{f'_{co}} = 1 + 3.24\left(\frac{f_l}{f'_{co}}\right)^{0.80}$	0.111	0.173	$\frac{\varepsilon^{*}_{cc}}{\varepsilon_{co}} = 1 + 17.4(\frac{f_l}{f'_{co}})^{1.06}$	0.89	1.55
Attard and Setunge (1996)	$\frac{f'^{*}_{cc}}{f'_{co}} = \left(1 + \frac{f_l}{0.288\left(f'_{co}\right)^{0.67}}\right)^{k}$ with $k = 1.25\left[1 + 0.062\frac{f_l}{f'_{co}}\right]\left(f'_{co}\right)^{-0.21}$	0.119	0.235	$\frac{\varepsilon^{*}_{cc}}{\varepsilon_{co}} = 1 + \left(17 - 0.06f'_{co}\right)\frac{f_l}{f'_{co}}$	1.45	1.88
Candappa et al. (2001)	$\frac{f'^{*}_{co}}{f'_{co}} = 1 + 5.3\frac{f_l}{f'_{co}}$	0.378	0.549	$\frac{\varepsilon^{*}_{cc}}{\varepsilon_{co}} = 1 + 20\frac{f_l}{f'_{co}}$	1.16	1.83

Lu and Hsu (2006)	$\frac{f_{co}^{'*}}{f_{co}^{'}} = 1 + 4.0\frac{f_l}{f_{co}^{'}}$	0.173	0.241	$\frac{\varepsilon_{cc}^{*}}{\varepsilon_{co}} = 1 + 19.21\frac{f_l}{f_{co}^{/}}$	1.04	1.71
Jiang and Teng (2007)	$\frac{f_{co}^{'*}}{f_{co}^{'}} = 1 + 3.5\frac{f_l}{f_{co}^{'}}$	0.213	0.234	$\frac{\varepsilon_{cc}^{*}}{\varepsilon_{co}} = 1 + 17.5(\frac{f_l}{f_{co}^{/}})^{1.2}$	1.06	1.67

Table 3.3 Test results of FRP-confined HSC

Specimen	t(mm)	E_{frp} (GPa)	$\varepsilon_{h,rup}$ (%)	f'_{cu} (MPa)	ε_{cu} (%)
70.8MPa					
1 ply-a	0.34	237.8	1.1	104.2	1.07
1 ply-b	0.34	237.8	1.21	110.3	1.43
3 ply-a	1.02	237.8	1.00	180.5	2.16
3 ply-b	1.02	237.8	0.90	197.7	2.33
5 ply-a	1.70	237.8	0.67	191.5	2.28
5 ply-b	1.70	237.8	0.52*	162.4	1.39
108Mpa					
2 ply-a	0.68	237.8	0.57	141.2	0.97
2 ply-b	0.68	237.8	0.58	134.0	0.75
3 ply-a	1.02	237.8	0.52	170.4	0.98
3 ply-b	1.02	237.8	0.60	176.6	1.12
5 ply-a	1.70	237.8	0.56*	217.3	1.56
5 ply-b	1.70	237.8	0.57*	217.1	1.60

*The test stopped without FRP rupture.

CHAPTER 4

NEW D-P TYPE MODEL BASED ON THE SCALING TECHNIQUE

4.1 INTRODUCTION

The behaviour of concrete in multi-axial compression is characterized by inelastic deformation. Hence, it is reasonable to apply the theory of plasticity, which is based on the split of strains into elastic and plastic parts, for simulating the behaviour of concrete. The literature review given in Chapter 2 indicates that constitutive models for concrete based on the theory of plasticity represent one of the major approaches and have met with a substantial degree of success.

Plasticity theories can be broadly divided into two groups: deformation and flow theories of plasticity (Chen and Han 2007). In the deformation theory of plasticity, the stress tensor is a function of the strain tensor alone. Such a constitutive structure is in general inappropriate for plastic deformation because when plastic deformation occurs, strains depend on both stresses and the stress history and are no longer only a function of stresses in a general sense. However, the deformation theory of plasticity has found useful applications in some special cases such as proportional or simple

loading. All the stress components under these two special loading conditions increase proportionally without elastic unloading ever occurring. Therefore, a one-to-one mapping can be found between the stress components and the strain components. The theory has been particularly successful in bifurcation studies and in the determination of necking and buckling loads (Hutchinson 1974). For the constitutive modelling of concrete, this theory was mainly employed in the period prior to the wide use of the computer. As the deformation theory of plasticity is invalid for non-proportional loading and has achieved only limited success under cyclic loading (Chen and Han 2007), it has seldom been used in commercial finite element (FE) software packages.

By contrast, the flow theory of plasticity is a more robust approach for simulating the behaviour of concrete as it does not suffer from the aforementioned limitation of the deformation theory of plasticity. The flow theory of plasticity is based on an incremental process and has the advantage that the effect of loading paths can be easily taken into account. Therefore, this theory is more versatile when used in the finite element modelling of concrete structures. Due to these reasons, the discussions of plasticity-based concrete constitutive models in this thesis are limited to those based on the flow theory of plasticity.

The flow theory of plasticity has three components: (a) the yield criterion, (b) the flow rule, and (c) the hardening (or softening) rule. The yield criterion (or yield function) for a multi-axial stress state is a generalization of the concept of the uni−axial yield stress. It defines the boundary of the elastic region, within which both unloading and reloading lead to elastic strains only. The flow rule determines the relationship between stresses and plastic strains under multi-axial loading, in which the direction of the incremental plastic strain is defined by the plastic potential function. The flow rule is referred to as an associated flow rule if the plastic potential function is the same as the yield function; otherwise, it is referred to as a non-associated flow rule. The hardening/softening rule defines the motion and new position of the yield surface (commonly referred to as the loading surface) in a stress coordinate system during plastic deformation. Two types of hardening/softening state variables are commonly used in the hardening/softening rule, which are the length of the plastic strain vector and the plastic work. The hardening/softening state variables have significant effects on the behaviour of confined concrete, which are discussed in the subsequent sections.

Over the past three decades, a number of studies have been conducted on these three components of plasticity models to improve their performance in predicting the mechanical behaviour (mainly the stress-strain response) of

confined concrete. Different yield functions have been presented to account for the inherent pressure-sensitivity of the yield stress of a concrete material. These yield criteria explored range from the simple Von Mises criterion with only one parameter to the more complex five-parameter William-Warnke yield function (Chen and Han 2007). Moreover, different plastic potential functions have also been proposed to account for the dilation characteristics of concrete in compression. More attention has recently been paid to the hardening/softening rule with the aim being to consider the effect of lateral confinement on the deformation of concrete. Different from yield functions which are normally defined in the stress space, the hardening/softening rule should be partially related to the inelastic deformation of concrete as it is commonly based on hardening/softening variables such as the equivalent plastic strain (Lubliner et al. 1989) and the equivalent plastic work (Han and Chen 1985). These two commonly used hardening/softening variables are both related to the plastic deformation of concrete. Plasticity models using these variables have succeeded in predicting the strength enhancement of concrete due to lateral confinement. However, these models have also been found to be unsuccessful in predicting the increased deformation capacity of concrete under multi-axial compression (Ohtani and Chen 1989; Yu et al. 2010a; Yu et al. 2010b). Therefore, two approaches have been suggested to address this problem (Grassl et al. 2002) as explained below.

The first approach can be referred to as the scaling approach (e.g. Barros 2001; Johansson and Akesson 2002). In the scaling approach, the hardening/softening variable is the form of a scaled length of the plastic strain vector associated with certain confinement characteristics of the current stress state. Various scaling techniques have been developed based on different confinement characteristics, including the hydrostatic pressure, the intermediate principal stress, and the mean of the two major principal stresses (Imran and Pantazopoulou 2001; Johansson and Akesson 2002; Malvar et al. 1997; Barros 2001; Yu et al. 2010a). Hereafter, plasticity-based models employing the scaling technique are referred to as scaled plasticity models.

Novel hardening/softening variables have also been adopted to deal with this issue apart from the use of a scaling technique. Recent studies (Grassl et al. 2002; Papanikolaou and Kappos 2007) have led to the plastic volume strain approach in which the plastic volumetric strain, ε_v^p, is used as the hardening/softening variable. Grassl et al. (2002) have revealed that when the plastic volumetric strain instead of the equivalent plastic strain or equivalent plastic work is utilized as the hardening/softening variable, a simple hardening/softening function is sufficient to provide reliable predictions for the increased deformation capacity of confined concrete

without using the scaling technique. The performance of this type of models will be discussed separately in Chapter 5 for clarity of presentation.

The first approach is discussed in this chapter. To simplify the discussion without loss of generality, a new D-P type model employing a scaling technique based on the hydrostatic pressure is proposed for use in the assessment process. Both the yield criterion and the flow rule in the proposed model are relatively simple, so the effect of the hardening/softening rule can be easily highlighted. The performance of this model is examined in the following sections.

As discussed above, the scaling approach can be utilized to account for the increased plastic deformation of concrete resulting from confinement. Yu et al. (2010a) assessed the capability of plasticity models of this type. In their study, D-P type models with scaled hardening variable-equivalent plastic strain relationships based on the confining pressure were assessed using experimental results for unconfined concrete, actively-confined concrete and FRP-confined concrete. Three important conclusions were drawn based on the assessment, which will be discussed in detail in Chapter 8. For this reason, only plasticity models with the equivalent plastic strain scaled to the hydrostatic pressure (Malvar et al. 1997; Wolf 2008) are discussed in this chapter. A new D-P type plasticity model employing the scaling technique

based on the hydrostatic pressure is proposed to illustrate the capability of the scaling approach in providing accurate predictions of confined concrete. This model is formulated by introducing modifications into an existing model proposed by Wolf (2008) and is calibrated with test results of actively-confined concrete. The model is then examined by comparing its predictions with test results of FRP-confined concrete. The advantages and limitations of this approach are also discussed.

It should be noted that the new model is a simplified version of that proposed by Wolf (2008) by introducing significant simplifications primarily in the yield criterion. For instance, the complex loading surface employed in Wolf (2008) is replaced by a simple D-P type failure surface in the new model. This replacement has an effect on the predicted strength enhancement as a result of confinement. The failure surface employed in Wolf's (2008) model implies a nonlinear relationship between the strength increment and the confining pressure, whereas the D-P type failure surface employed in the new model implies a linear relationship. The accuracy of this linear approximation is acceptable within a certain range of confinement ratios. In addition, the influence of the Lode angle on the failure surface is not considered in the new model. Therefore, the new model is only expected to be capable of providing accurate predictions for uniformly confined concrete. Uniform confinement is a specific case of

confinement as is found in confined circular concrete columns and is a simpler case than non-uniform confinement. If a constitutive model cannot even predict the response of concrete under uniform confinement, it is meaningless to examine its capacity for non-uniform confinement. With the above modifications, the most complex part of the new model is the hardening/softening rule, and most of the parameters requiring calibration are associated with the hardening/softening rule. Therefore, attention can be focused on this part to examine the capability of the scaling approach.

4.2 PROPOSED CONSTITUTIVE MODEL

4.2.1 Loading Surfaces

Following Malvar et al. (1997) and Wolf (2008), the backbone of the proposed model consists of three distinct loading surfaces. These three surfaces correspond to the yield, peak and residual stress states of the concrete. They reduce to the yield, peak and residual stress states for concrete under uni-axial compression as shown in Fig. 4.1. The current loading surface located between two of these three surfaces can be determined using a so-called damage parameter (Malvar et al. 1997; Wolf 2008). Equations defining these loading surfaces are assumed to have a D-P type shape in the proposed model (see Figs. 4.2 & 4.3) so that the differences between these equations are only due to the hardening/softening parameter k_n. Based on this simplification, the loading surface, f^n, can be

expressed as

$$f^n = \tan\theta\, I_1 + \sqrt{J_2} - k_n \tag{4.1}$$

where θ is the frictional angle, I_1 is the first invariant of the stress tensor which can be defined in the stress space as

$$I_1 = \sigma_x + \sigma_y + \sigma_z \tag{4.2}$$

and J_2 is the second invariant of the deviatoric stress tensor which can be defined as

$$J_2 = \frac{1}{6}\left[(\sigma_x - \sigma_y)^2 + (\sigma_y - \sigma_z)^2 + (\sigma_z - \sigma_x)^2\right] + \tau_{xy}{}^2 + \tau_{yz}{}^2 + \tau_{zx}{}^2 \tag{4.3}$$

The parameter k_n is defined as

$$k_n = \begin{cases} k_{n,yield} + \beta(k_{n,peak} - k_{n,yield}) & \psi < \psi_{peak} \\ k_{n,peak} + \beta(k_{n,residual} - k_{n,yield}) & \psi \geq \psi_{peak} \end{cases} \tag{4.4}$$

where $k_{n,yield}$, $k_{n,peak}$, $k_{n,peak}$ are the values of parameter k_n at the points of initial yielding, peak stress and residual stress respectively. The parameter ψ_{peak} defines the damage level when the failure surface (i.e. peak stress surface) is reached, and the parameter β is defined as a function of the so-called damage parameter ψ (Wolf 2008):

$$\beta = \left(\frac{\psi}{\psi_{peak}}\right)^{\kappa} e^{1-\left(\frac{\psi}{\psi_{peak}}\right)^{\kappa}} \tag{4.5}$$

Here, the parameter κ, controls the rate at which the failure surface travels from one loading surface to the next (Wolf 2008).

The value for ψ is integrated along the loading path of the material in order to obtain the current total damage level. The incremental damage $d\psi$ is defined as a scaled equivalent plastic strain increment $d\varepsilon^p$ with respect to the hydrostatic pressure:

$$d\psi = \frac{d\varepsilon^p}{\emptyset + \alpha\left(\frac{I_1}{\sqrt{3}f'_{co}}\right)^{\gamma}} \tag{4.6}$$

The parameter $\emptyset$, defines the accumulation of damage at very low levels of stress, and the parameters α, and γ reflect the effect of confinement on the damage accumulation of concrete. The effective plastic strain increment $d\varepsilon^p$ is defined as

$$d\varepsilon^p = \sqrt{\frac{2}{3}d\varepsilon^p_{ij}d\varepsilon^p_{ij}} \tag{4.7}$$

In Eq. (4.6), the scaling technique is employed, in which the incremental damage $d\psi$ is defined as a scaled variable of the effective plastic strain increment $d\varepsilon^p$. The denominator of Eq. (4.6) is defined as a function of the hydrostatic stress (I_1) to scale the effective plastic strain increment $d\varepsilon^p$.

4.2.2 Flow Rule

It has been demonstrated (e.g. Chan and Han 2007) that the use of an associated flow rule for concrete results in unrealistic predictions for plastic volume expansions which exceed those from tests. Hence, a non-associated flow rule is employed in the present constitutive model. There are several

different ways to define a non-associated flow rule. One typical approach is to use a potential surface similar to the yield surface but with a dilation angle θ_1 different from the frictional angle θ. Another approach is that suggested by Han and Chen (1985) in which the flow rule is defined as a combination of the associated flow rule and the Prandtl-Reuss flow rule (Malvar et al. 1997; Wolf 2008) (i.e. the J_2 flow rule) which does not allow for any plastic volume expansion. The latter approach is adopted in the present model. The potential surface, G^n, is therefore defined as follows:

$$G^n = \Omega \tan\theta \, I_1 + \sqrt{J_2} \tag{4.8}$$

where Ω is a parameter controlling the amount of plastic volume expansion and lies between 0 and 1. In the extreme case when Ω is equal to 0, the J_2 flow rule, which is a non-associated flow rule for Eq. (4.1), is utilized; when Ω is equal to 1, the associated flow rule is applied.

4.3 CALIBRATION OF PARAMETERS

The proposed constitutive model was implemented in ABAQUS by writing a user-defined material subroutine (UMAT). A total of eleven parameters are used in the proposed constitutive model for the definition of the behaviour of concrete. Four of these eleven parameters are basic to concrete and can be directly determined from material properties of unconfined concrete. These parameters include the unconfined concrete strength f'_{co}, the axial strain at unconfined concrete strength ε_{co}, the elastic modulus of concrete

E, and the Poisson ratio μ. The remaining seven parameters need to be identified from experimental results of actively-confined concrete. These parameters are $\theta, \emptyset, \Omega$, α, γ, κ and ψ_{peak}. The process for determining these seven parameters is discussed below.

In the finite element modelling of actively-confined concrete under uniform confinement, the concrete in a circular cylindrical specimen in a standard equal tri-axial compression test can be modeled using a single cubic element. This is because the stress state at any material point within such a uniformly confined specimen is identical, and a single-element finite element model is sufficient to reflect the stress-strain behaviour of the concrete. In the present study, symmetry was exploited so that only one-eighth of a small cube was included in the finite element model with symmetric boundary conditions imposed on the three symmetry planes; these planes are perpendicular to each other and the displacements perpendicular to each plane were set to be zero. The use of symmetric conditions is not essential but makes it easier for the application of loading. The same pressure was applied on the two lateral surfaces to represent the hydrostatic confining pressure acting on the surface of the concrete specimen; displacements were then imposed on the top surface of the cubic element to simulate compressive loading. The finite element model is illustrated in Fig. 4.4.

As discussed earlier, the failure surface of the model is of the D-P type. The value of parameter θ can be determined from the confinement effectiveness factor k_1 using equations developed in previous research (Yu et al. 2010a):

$$\theta = \tan^{-1}\frac{k_1 - 1}{\sqrt{3(k_1 + 2)}} \tag{4.9}$$

The least-squares method was utilized in the process of parameter calibration to obtain the value of k_1 from test data.

The parameters $\emptyset$ and γ control incremental damage $d\psi$ (see Eq. 4.6) as affected by confinement. Wolf (2008) suggested a constant value of 0.5 for $\emptyset$, which is employed as the default value in the proposed model. For γ, Wolf (2008) adopted the following power law relationship:

$$\frac{\varepsilon_{cc}}{\varepsilon_{co}} = a_W \left(\frac{I_1}{\sqrt{3}f'_{co}}\right)^{\gamma} + b_W \tag{4.10}$$

where a_W and b_W are constants used to fit the test data of axial strains at peak stress ε_{cc}, and an estimated value of 1.720 was used for γ. However, it was found in the present study that this γ value is less than optimal. Therefore, this parameter together with four other parameters (i.e. Ω, α, κ, ψ_{peak}), were identified via a simple trial-and-error procedure of fitting the experimental results of actively-confined concrete.

Using the above process of parameter calibration, the test results for

actively-confined concrete reported by Candappa et al. (1999) were used for the determination of the eleven material parameters; that is, these test results were taken as the benchmark results. This set of tests was chosen because of their consistent stress-strain curves and the large range of strain values covered by these experiments. These test specimens had an unconfined concrete strength of 41.9 MPa and were subjected to three different confining pressures (4 MPa, 8 MPa and 12 MPa).

Axial stresses of Candappa et al.'s (1999) specimens are shown against their axial strains and lateral strains in Figure 4.5. In this figure, compressive stresses/strains are taken to be positive while tensile stresses/strains are taken to be negative. Indeed, these definitions are adopted throughout this thesis for concrete unless otherwise specified. Parameters f'_{co}, ε_{co}, E, and μ were obtained from the control specimens (unconfined concrete specimens), and their values are shown in the same Fig. 4.5. Based on the experimental peak stresses of confined specimens, k_1 was found to be 5.3. Using Eq. (4.9), the value of θ was found to be 0.3267. The other five parameters except $\emptyset$, for which the default value of 0.5 was used, were adjusted to fit the axial stress-strain curves and axial stress-lateral strain curves; the deduced value are also given in Fig. 4.5. As interaction exists among these five parameters, a trial-and-error process was employed to determine these parameters. The predicted stress-strain curves using the

values of parameters so identified are compared with the experimental results in Fig. 4.5. The numerical results are seen to be in close agreement with the experimental results. This agreement, achieved consistently for three different confining pressures using a single set of parameters, indicates that the proposed model can capture the major characteristic of concrete under uniform active confinement.

4.4 COMPARISON WITH TEST RESULTS OF FRP-CONFINED CONCRETE

Experimental results of FRP-confined circular concrete cylinders reported by Lam and Teng (2004) are compared with the numerical results obtained using the proposed constitutive model in this section. Similar to the case of actively-confined concrete, the concrete in this case is also taken to be under uniform confinement so that the one-element finite element model was still applicable. The same symmetric conditions were also imposed on the three symmetric planes as explained earlier. The two lateral surfaces, which were subjected to hydrostatic pressure in the case of actively-confined concrete, were tied to 4-node membrane elements, which were used to model the FRP jacket. The difference between FRP confinement and active confinement is that the confining pressure provided by the FRP jacket is related to the lateral deformation of the concrete core. In the finite element model, the FRP jacket was taken as a linear elastic material, which can thus provide a

gradually increasing confining pressure. An equivalent thickness t_{eq} calculated from the following equation was specified for the membrane element to provide an in-plane stiffness that is identical to the confining stiffness equal to that of the cylindrical jacket:

$$t_{eq} = \frac{1}{R} t_{FRP} \tag{4.11}$$

Here, R is the radius of the concrete core and t_{FRP} is the original thickness of the FRP jacket.

In the process of parameter calibration described above, test results for both unconfined and actively-confined concrete were required for identifying the values of all the unknown parameters. To investigate the predictive capability of the proposed constitutive model, it is desirable to have a series of tests that include unconfined concrete, actively-confined concrete and passively-confined concrete. The first two types of experimental result can be used to determine all the material parameters while the last type of experimental results can be used to check the accuracy of the constitutive model in providing predictions for FRP-confined concrete. This is because the predictions for FRP-confined concrete in this case are independent of the process of parameter calibration. To the best of the author's knowledge, the only series of tests which included all three types of experiments were conducted by Cetisli and Naito (2009). In their experiments, confining pressures which varied linearly with the lateral deformation were provided

by a tri-axial cell to mimic FRP confinement. Unfortunately, their experimental results of passively-confined concrete showed significantly larger variations than those of FRP-confined concrete and are therefore unsuitable for use as verification data for the proposed constitutive model. For instance, Cetisli and Naito (2009) observed smaller ultimate axial strains at larger confinement stiffnesses, which is contrary to experimental observations of FRP-confined concrete [e.g. Lam and Teng (2004)].

Based on the above considerations, test results of FRP-confined concrete were employed to assess the capability of the proposed constitutive model. In the absence of objective tests (test series including actively-confined concrete) to determine the values of the material parameters, these material parameters were estimated by fitting the stress-strain curves (using least-square method) generated by an empirical model developed for actively-confined concrete. The analysis-oriented stress-strain model developed by Jiang and Teng (2007) has been shown by the authors to provide close predictions for FRP-confined concrete, so the actively-confined concrete model employed as the base model in Jiang and Teng (2007) model was adopted in the present study to identify the parameters for the proposed constitutive model which are mainly related to the behaviour of actively-confined concrete. Other parameters which are mainly related to the dilation characteristics were determined by fitting the

experimental results of FRP-confined concrete. Similar approaches of parameter calibration were also adopted in identifying parameters for other constitutive models considered in Chapters 5 & 6.

In the proposed constitutive model, the most significant parameter related to the active-confinement model is the parameter θ. By adopting the value of 3.5 for the confinement effectiveness factor as given in Teng et al.'s (2007) model in Eq. (4.9), the value of θ is found to be 0.2624. Other parameters were then determined by fitting the axial strains at peak stress of control specimens and the experimental stress-strain curves of FRP-confined specimens using a trial-and-error process. From this point of view, the assumption of path-independence is only partially fulfilled in the process of parameter calibration for the current constitutive model as the test results of FRP-confined concrete are employed in the determination of some of the parameters (e.g. Ω).

Fig. 4.6 shows the test results of all six FRP-confined concrete specimens reported by Lam et al. (2006). These six specimens are used in the present thesis as the benchmark specimens for FRP-confined circular concrete cylinders; that is, unless otherwise specified, the test results of FRP-confined concrete cylinders employed in comparisons with numerical predictions are the results of these six specimens. The predicted stress-strain

curves in Fig. 4.6 were obtained by using the proposed constitutive model with calibrated parameters. In analysis, the finite element model was loaded to the point at which the experimental hoop rupture strain of the FRP jacket was reached. The comparisons show that the finite element results with the same set of calibrated parameters provide close predictions for the specimens with a confinement stiffness equal to 1086 MPa, but deviate significantly from the experimental results for the specimens with a confinement stiffness equal to 543 MPa. Here, the confinement stiffness is defined as $\frac{E_{FRP}t_{FRP}}{R}$, where E_{FRP} is the elastic modulus of FRP. For the latter specimens (Fig. 4.6a), the ultimate axial strain is significantly overestimated. This overestimation indicates that the corresponding lateral strain and hence the confining pressure at a given axial strain are significantly underestimated. This comparison shows that the constitutive model can only provide accurate prediction for specimens with specific confinement stiffness, i.e. the proposed constitutive model cannot reflect the effect of confinement stiffness on the stress-strain response of passively-confined concrete.

4.5 CONCLUSIONS

This chapter has been concerned with the performance and capability of a D-P type plasticity model based on the equivalent plastic strain scaling approach. For the assessment purpose, a new simple D-P type plasticity

model was proposed to highlight the effect of the strain hardening/softening rule on predictions. From the performance study of the new D-P type model presented in this chapter, a number of conclusions can be reached. These conclusions are summarized as follows:

- For actively-confined concrete, the proposed model can provide accurate predictions for the stress-strain behaviour of concrete at different confining pressures.
- For FRP-confined concrete, the proposed model is not successful in predicting the stress-strain behaviour of concrete unless the confining stiffness happens to be at a specific level. The incorrect predictions are due to the incapability of the proposed model in capturing the dilation behaviour of FRP-confined concrete.
- Although the scaling approach can correctly predict the increased deformation capacity of actively-confined concrete, no simple method exists for determining the values of the material parameters except for the material parameter θ. As interaction exists among the material parameters controlling the scaling function and the flow rule, they need to be determined through a trial-and-error process. It is also complicated to adjust these parameters to provide accurate predictions for FRP-confined concrete under different confining stiffness.

4.6 REFERENCES

Barros, M. H. F. (2001). "Elasto-plastic modelling of confined concrete elements following MC90 equations." *Engineering Structures*, 23(4), 311-318.

Candappa, D. P., Setunge, S., and Sanjayan, J. G. (1999). "Stress versus strain relationship of high strength concrete under high lateral confinement." *Cement and Concrete Research*, 29(12), 1977-1982.

Cetisli, F., and Naito, C. J. (2009). "Concrete subjected to varying confinement, I: Experimental evaluation." *Journal of Advanced Concrete Technology*, 7(2), 239-249.

Chen, W. F., and Han, D. J. (2007). *Plasticity for Structural Engineers*, J Ross Pub.

Grassl, P., Lundgren, K., and Gylltoft, K. (2002). "Concrete in compression: a plasticity theory with a novel hardening law." *International Journal of Solids and Structures*, 39(20), 5205-5223.

Han, D. J., and Chen, W. F. (1985). "A nonuniform hardening plasticity model for concrete materials." *Mechanics of Materials*, 4(3-4), 283-302.

Hutchinson, J. W. (1974). "Plastic buckling." *Advances in Applied Mechanics*, 14, 67-144.

Imran, I., and Pantazopoulou, S. J. (2001). "Plasticity model for concrete under triaxial compression." *Journal of Engineering Mechanics*,

ASCE, 127(3), 281-290.

Jiang, T., and Teng, J. G. (2007). "Analysis-oriented stress-strain models for FRP-confined concrete." *Engineering Structures*, 29(11), 2968-2986.

Johansson, M., and Akesson, M. (2002). "Finite element study of concrete-filled steel tubes using a new confinement-sensitive concrete compression model." *Nordic Concrete Research -Publications*, 27, 43-62.

Lam, L., and Teng, J. G. (2004). "Ultimate condition of fiber reinforced polymer-confined concrete." *Journal of Composites for Construction*, ASCE, 8(6), 539-548.

Lam, L., Teng, J. G., Cheung, C. H., and Xiao, Y. (2006). "FRP-confined concrete under axial cyclic compression." *Cement & Concrete Composites*, 28(10), 949-958.

Lubliner, J., Oliver, J., Oller, S., and Onate, E. (1989). "A plastic-damage model for concrete." *International Journal of Solids and Structures*, 25(3), 299-326.

Malvar, L. J., Crawford, J. E., Wesevich, J. W., and Simons, D. (1997). "A plasticity concrete material model for DYNA3D." *International Journal of Impact Engineering*, 19(9-10), 847-873.

Ohtani, Y., and Chen, W. F. (1989). "A plastic-softening model for concrete materials." *Computers & Structures*, 33(4), 1047-1055.

Teng, J. G., Huang, Y. L., Lam, L., and Ye, L. P. (2007). "Theoretical model for fiber-reinforced polymer-confined concrete." *Journal of Composites for Construction*, ASCE, 11(2), 201-210.

Wolf, J. (2008). *A plasticity model to predict the effects of confinement on concrete*, California Institute of Technology.

Yu, T., Teng, J. G., Wong, Y. L., and Dong, S. L. (2010a). "Finite element modelling of confined concrete-I: Drucker-Prager type plasticity model." *Engineering Structures*, 32(3), 665-679.

Yu, T., Teng, J. G., Wong, Y. L., and Dong, S. L. (2010b). "Finite element modelling of confined concrete-II: Plastic-damage model." *Engineering Structures*, 32(3), 680-691.

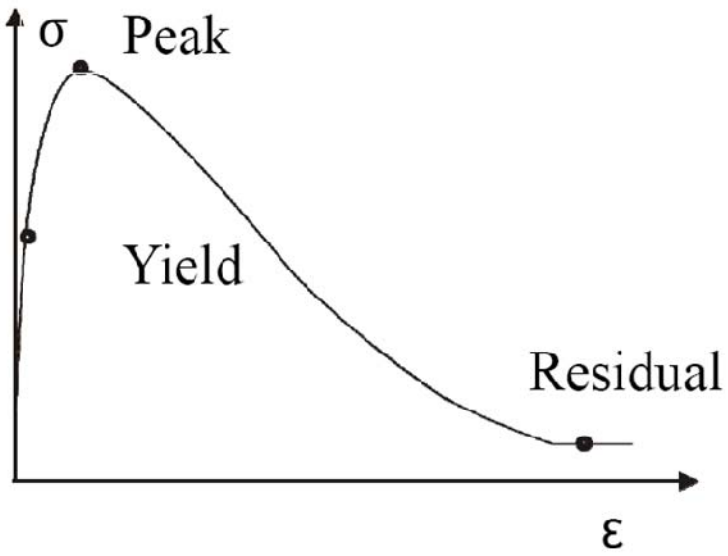

Figure 4.1 Loading surface locations for unconfined concrete

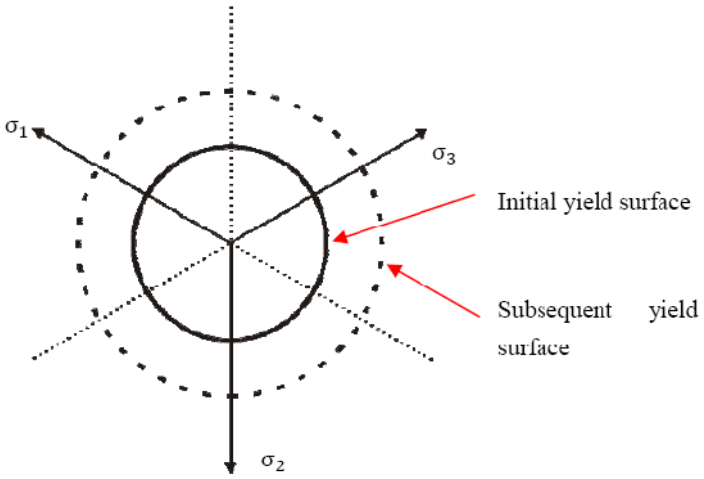

Figure 4.2 Yield surfaces of the D-P type model in the deviatoric plane

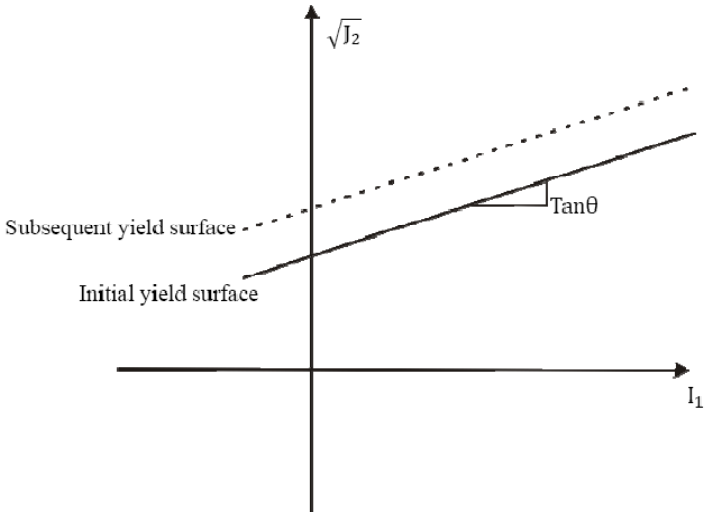

Figure 4.3 Yield surfaces of the D-P type model in the $I_1 - \sqrt{J_2}$ plane

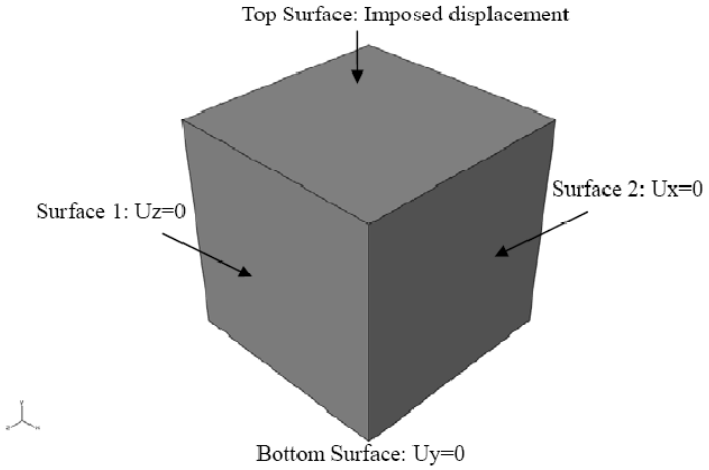

Figure 4.4 Displacement boundary conditions for a cube element

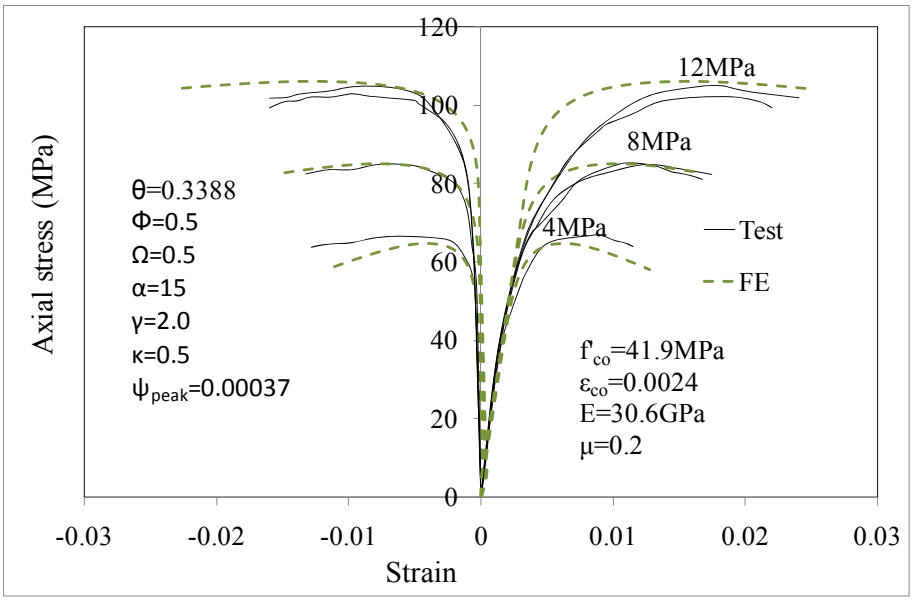

Figure 4.5 Finite element predictions based on the new D-P type model versus test results of actively-confined concrete from Candappa et al.(1999)

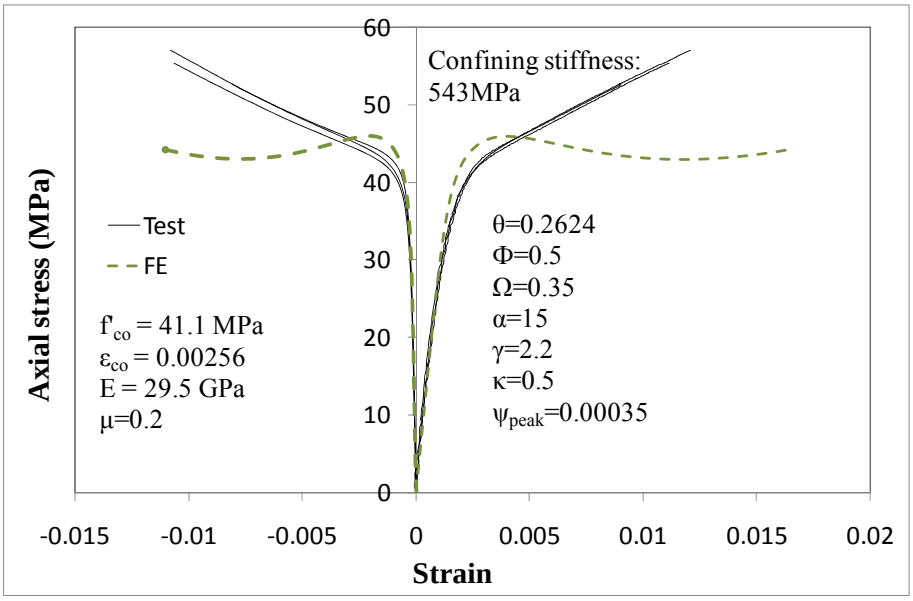

(a) FRP-confined concrete with a confining stiffness equal to 543 MPa

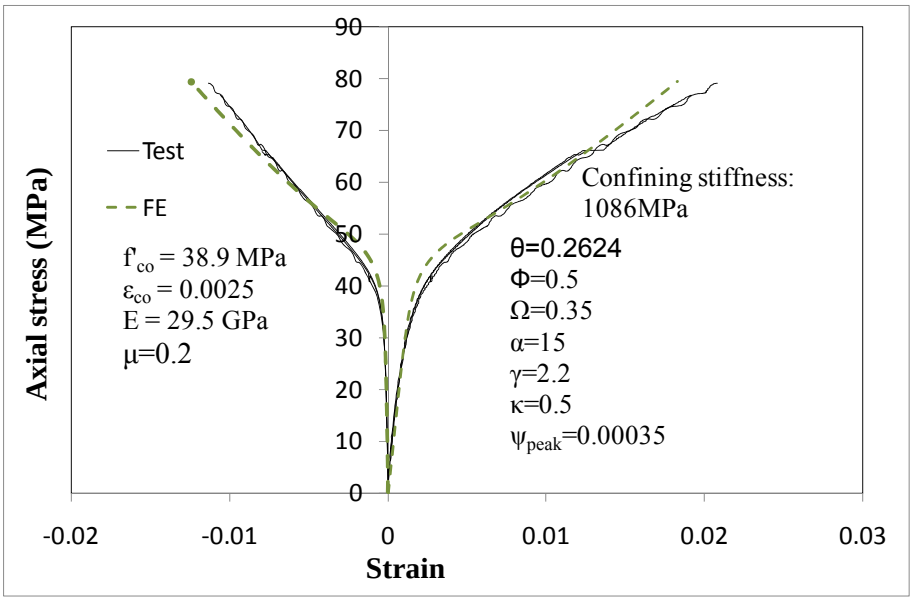

(b) FRP-confined concrete with a confining stiffness equal to 1086 MPa

Figure 4.6 Finite element results based on the new D-P type model versus test results of FRP-confined concrete from Lam et al. (2006)

CHAPTER 5

PLASTICITY MODEL CONTROLLED BY THE PLASTIC VOLUMETRIC STRAIN

5.1 INTRODUCTION

The literature review given in Chapter 2 indicates that two approaches have been suggested by researchers (e.g. Imran and Pantazopoulou 2001; Barros 2001; Grassl et al. 2002; Johansson and Akesson 2002) to improve the capability of plasticity-based models in predicting the increased deformation capacity of concrete due to confinement. The first approach (i.e. the scaling approach) has been discussed in Chapter 4. In the present chapter, the performance of a constitutive model based on the second approach is discussed.

As mentioned in Section 4.1, Papanikolaou and Kappos's (2007) model employs the plastic volumetric strain, ε_v^p, as the hardening/softening variable and has the capability of providing accurate predictions for actively-confined concrete with a simple process of parameter calibration. In the present study, Papanikolaou and Kappos's (2007) model was implemented into ABAQUS as a UMAT subroutine. The parameters of the constitutive model were calibrated from the experimental results reported by Candappa et al. (1999) for actively-confined concrete and an empirical

active confinement model (Teng et al. 2007). The predictions of Papanikolaou and Kappos's (2007) model for FRP-confined concrete were then compared with test results.

5.2 PAPANIKOLAOU AND KAPPOS' (2007) MODEL

5.2.1 Loading Surface

Papanikolaou and Kappos (2007) developed a plasticity model to study the response of confined concrete. In this model, the loading surface is based on the three-parameter failure criterion proposed by Menetrey and Willam (1995), which is defined in the Haigh-Westergaard coordinates (ξ, ρ, θ) (these three coordinates have been defined in Chapter 2) as follows:

$$f^{p}(\xi,\rho,\theta) = \left(\sqrt{3/2}\frac{\rho}{h(\kappa)f'_{co}}\right)^{2} + m\left(\frac{\rho}{\sqrt{6}h(\kappa)f'_{co}}r(\theta,e) + \frac{\xi}{\sqrt{3}h(\kappa)f'_{co}}\right) - c(\kappa) \quad (5.1)$$

where *m* is a cohesion parameter of the concrete which is given by

$$m = 3\frac{(h(\kappa)f'_{co})^{2} - (f_t)^{2}}{h(\kappa)f'_{co}f_t}\frac{e}{e+1} \quad (5.2)$$

and $r(\theta, e)$ is an elliptic function used for the description of the out-of-roundness of the deviatoric section

$$r(\theta,e) = \frac{4(1-e^{2})\cos^{2}\theta + (2e-1)^{2}}{2(1-e^{2})\cos\theta + (2e-1)[4(1-e^{2})\cos^{2}\theta + 5e^{2} - 4e]^{1/2}} \quad (5.3)$$

In the above three equations, f_t is the tensile strength of concrete, and e is the eccentricity coefficient. Parameters $h(\kappa)$ and $c(\kappa)$ are the hardening and the softening functions of the hardening/softening rule used to determine the instantaneous shape and location of the loading surface,

which are dependent on the value of the hardening/softening parameter(κ). The parameter κ in this model is set equal to the plastic volumetric strain ε_v^p as suggested by Grassl et al.(2002):

$$d\kappa = d\varepsilon_v^p = d\varepsilon_1^p + d\varepsilon_2^p + d\varepsilon_3^p \tag{5.4}$$

where ε_i^p(i=1-3) is the principal plastic strain in the *i*th direction.

Eq. (5.3) indicates that the value of $r(\theta, e)$ is controlled by parameter e which has a recommended value of 0.52 (Menetrey and Willam 1995) calculated from a default equal biaxial concrete strength $f_{bc}^{'} = 1.14 f_{co}^{'}$. Moreover, Eqs. (5.1) and (5.3) show that the effect of the Lode angle has been considered in the loading surface. This feature is included mainly to improve the capability of the loading surface to consider the difference between uniform confinement and non-uniform confinement. For concrete under uniform confinement, in which the Lode angle is equal to $\pi/3$ (on the compressive meridian), r(θ,e) is equal to 1.0, which corresponds to the most effective confinement effect. For concrete under equal bi-axial compression, in which the Lode angle is equal to zero (on the tensile meridian and is a typical non-uniform confinement case), r(θ,e) is equal to 1/e, which corresponds to the most ineffective confinement effect in the compression zone. The loading surface thus has a non-circular shape in the deviatoric plane (see Fig. 5.1). In addition, the effects of parameters h and c on the tensile meridian and the compressive meridian of the loading surface are

given in Figs. 5.2 and 5.3.

For the hardening parameter $h(\kappa)$, an elliptic-type function is adopted, which was originally proposed by Cervenka et al. (1998):

$$h(\kappa) = \begin{cases} h_0 + (1 - h_0)\sqrt{1 - \left(\left(\varepsilon_{v,t}^{p} - \varepsilon_{v}^{p}\right)/\varepsilon_{v,t}^{p}\right)^2}, & \kappa \le \varepsilon_{v,t}^{p} \\ 1, & \kappa > \varepsilon_{v,t}^{p} \end{cases} \tag{5.5}$$

where h_0 is a constant that defines the onset of yielding and $\varepsilon_{v,t}^{p}$ is the plastic volumetric strain at the uni-axial concrete strength. The following function originally proposed by Van Gysel and Taerwe (1996) is adopted for the softening parameter $c(\kappa)$ for uni-axial compression:

$$c(\kappa) = \begin{cases} 1, & \kappa \le \varepsilon_{v,t}^{p} \\ \left(1/\left(1 + \left((n_1 - 1)/(n_2 - 1)\right)^2\right)\right), & \kappa > \varepsilon_{v,t}^{p} \end{cases} \tag{5.6}$$

where:

$$n_1 = \varepsilon_{v}^{p}/\varepsilon_{v,t}^{p} \tag{5.7}$$

$$n_2 = \left(\varepsilon_{v,t}^{p} + t_p\right)/\varepsilon_{v,t}^{p} \tag{5.8}$$

and t_p is a constant which controls the slope of the softening function.

5.2.2 Failure Surface

Eqs. (5.1) and (5.5-5.8) indicate that when the hardening/softening variable κ is equal to $\varepsilon_{v,t}^{p}$, both the hardening parameter $h(\kappa)$ and the softening parameter $c(\kappa)$ are equal to unity. The loading surface function

described by Eq. (5.1) hence reaches its failure state and reduces to

$$f^{p}(\xi,\rho,\theta)=\left(\sqrt{3/2}\frac{\rho}{f'_{co}}\right)^{2}+m\left(\frac{\rho}{\sqrt{6}f'_{co}}r(\theta,e)+\frac{\xi}{\sqrt{3}f'_{co}}\right)-1 \qquad (5.9)$$

Eq. (5.9) is the three-parameter failure criterion originally proposed by Menetrey and William (1995). If only uniform confinement is taken into consideration, Eq. (5.9) further reduces to

$$\frac{f^{*}_{cc}}{f'_{co}}=\frac{f_{l}}{f'_{co}}+\sqrt{1+m\frac{f_{l}}{f'_{co}}} \qquad (5.10)$$

where f_l is the confining pressure, and f^{*}_{cc} is the concrete strength under confining pressure f_l . Eq. (5.10) is in the form of the Hoek and Brown failure criterion and can be used in the calibration of the parameter m.

5.2.3 Flow Rule

A non-associated flow rule is employed in Papanikolaou and Kappos's (2007) model. In the Haigh-Westergaard coordinates, the plastic potential function is defined as follows:

$$g=A\left(\frac{\rho}{k\sqrt{c}f'_{co}}\right)^{n}+\left[C+\frac{1}{2}(B-C)(1-\cos3\theta)\right]\frac{\rho}{k\sqrt{c}f'_{co}}+\frac{\xi}{k\sqrt{c}f'_{co}} \qquad (5.11)$$

where A, B and C are three parameters controlling the shape of the plastic potential function in the stress space. Calibration of these parameters for the flow rule is based on the assumption that both the incremental plastic strain vector and the total plastic strain vector have identical inclinations for stress states within the failure surface. The detailed procedure of parameter calibration is explained below.

5.3 CALIBRATION

The following steps were adopted in the process of parameter calibration:

a. Determine the value of parameter *m* to fit the peak stress of actively-confined concrete f_{cc}^{*} and calculate the value of artificial concrete tensile strength f_t;
b. Calculate the values of A, B, C which control the axial strain at peak stress;
c. Adjust the value of $\varepsilon_{v,t}^{p}$ to fit the dilation behaviour of confined-concrete;
d. Adjust the value of t_p to fit the slope of the axial stress-strain curves.

The detailed process of calibration for a selected set of experiments is as follows. First, using the test data of peak stresses under different confining pressures and considering Eq. (5.10), the value of *m* can be determined by using the Least Squares Method. Then, the value of f_t can be calculated from Eq. (5.2) once the value of *m* is known. As this study is focused on the compressive behaviour of confined concrete, an artificial f_t value was adopted to obtain the required value of *m* from a regression of experimental results. Here, f_t does not have a direct physical meaning, and it is just employed to reflect the corresponding value of *m*. Actually, if *m* is directly adopted as a parameter, it is unnecessary to calculate the value of f_t.

Therefore, f_t is just retained as a parameter so that the model has the same parameters as those suggested by Papanikolaou and Kappos (2007). After the value of f_t is determined, the values of A, B and C can be calculated based on the assumption that the inclination of the total plastic strain is equal to that of the incremental plastic strain (Grassl et al. 2002). This assumption means that

$$\frac{\rho'}{\xi'} = -\frac{d\xi}{d\rho} \tag{5.12}$$

where ξ' and ρ' are the hydrostatic and deviatoric lengths of the total plastic strain vector, respectively. The inclination Ψ (i.e. gradient) of the plastic strain vector of the plastic potential surface on the compressive meridian with respect to the deviatoric axis can be expressed as:

$$\Psi = -\frac{d\xi}{d\rho} = nA\left(\frac{\rho}{f'_{co}}\right)^{n-1} + B \tag{5.13}$$

Ψ_1, and Ψ_2 are the inclinations of the plastic strain vector, and ρ_1 and ρ_2 are the deviatoric lengths of the stress vector under the states of uni-axial compression and equal tri-axial compression, respectively. Substituting ρ_1 and ρ_2 into Eq. (5.13) leads to

$$\Psi_1 = nA\left(\frac{\rho_1}{f'_{co}}\right)^{n-1} + B \tag{5.14}$$

$$\Psi_2 = nA\left(\frac{\rho_2}{f'_{co}}\right)^{n-1} + B \tag{5.15}$$

Based on the previous assumption of identical inclinations, Ψ can also be determined from the total plastic strain vector:

$$\Psi = \frac{\rho'}{\xi'} = \frac{\sqrt{\left(\varepsilon_1^p - \varepsilon_2^p\right)^2 + \left(\varepsilon_2^p - \varepsilon_3^p\right)^2 + \left(\varepsilon_3^p - \varepsilon_1^p\right)^2}}{\varepsilon_1^p + \varepsilon_2^p + \varepsilon_3^p} \tag{5.16}$$

The plastic strains for the uni-axial stress state and the equal tri-axial stress state can be calculated by the following steps described below. The axial plastic strain component is equal to the axial total strain component minus the elastic part. For the uni-axial stress state, the components of the principal plastic strain vector are:

$$\varepsilon_3^p = \varepsilon_{co} - \frac{f'_{co}}{E} \tag{5.17}$$

The lateral plastic strain is calculated as

$$\varepsilon_1^p = \varepsilon_2^p = \frac{\varepsilon_{v,t}^p - \varepsilon_3^p}{2} \tag{5.18}$$

For the equal tri-axial stress state, the components of the principal plastic strain vector are:

$$\varepsilon_3^p = \varepsilon_{cc}^* - \frac{\left(f_{cc}^* - 2\mu f_l\right)}{E} \tag{5.19}$$

$$\varepsilon_1^p = \varepsilon_2^p = \frac{\varepsilon_{v,t}^p - \varepsilon_3^p}{2} \tag{5.20}$$

As mentioned earlier, ε_{cc}^* is the axial strain at peak stress for concrete in an equal tri-axial stress state (i.e. active confinement). It was found by Papanikolaou and Kappos (2007) that a linear relationship between the confinement level $\left(f_l / f_{cc}^*\right)$and the strain amplification $\left(\varepsilon_{cc}^*/\varepsilon_{co}\right)$ can be obtained as long as the parameter *n* is equal to 3.0. Using test data of axial strains at peak stress under different confining pressures from the selected

experimental results, a linear relationship was determined as follows:

$$\frac{\varepsilon_{cc}^{*}}{\varepsilon_{co}} = 1 + k_2 \frac{f_l}{f_{co}^{*}} \tag{5.21}$$

where k_2 represents the confinement effectiveness factor for axial strains at peak stress.

Substituting Eqs. (5.17-5.21) into Eq. (5.16), the values of Ψ_1, and Ψ_2 can be obtained based on the assumption of the total plastic strain vector. The values of A and B can then be calculated as

$$A = \frac{\Psi_1 - \Psi_2}{n\left(\left(\frac{\rho_1}{f_{co}'}\right)^{n-1} - \left(\frac{\rho_2}{f_{co}'}\right)^{n-1}\right)} \tag{5.22}$$

$$B = \Psi_1 - nA\left(\frac{\rho_1}{f_{co}'}\right)^{n-1} \tag{5.23}$$

The coefficient C can be calibrated based on results of concrete under equal biaxial stress-states. Ψ_3 and ρ_3 are the inclination of the plastic strain vector and the deviatoric length of the stress vector at equal biaxial compression, respectively. The inclination under equal biaxial compression, Ψ_3, based on the incremental principal plastic strain vector can be calculated as

$$\Psi_3 = nA\left(\frac{\rho_3}{f_{co}'}\right)^{n-1} + C \tag{5.24}$$

The components of the total principal plastic strain vector under equal biaxial compression are

$$\varepsilon_3^p = \varepsilon_2^p = \varepsilon_{bc} - \frac{f_{bc}(1-\mu)}{E} \tag{5.25}$$

$$\varepsilon_1^p = \varepsilon_{v,t}^p - 2\varepsilon_3^p \tag{5.26}$$

where f_{bc} and ε_{bc} are the concrete strength and the corresponding axial strain. The value of f_{bc} can be calculated from Eq. (5.9) once the values of *m* and *e* are determined. The value of ε_{bc} is assumed to have the same amplification as the value of f_{bc}:

$$\frac{\varepsilon_{bc}}{\varepsilon_{co}} = \frac{f_{bc}}{f'_{co}} \tag{5.27}$$

By solving Eq. (5.24), the following value for coefficient C is derived:

$$C = \Psi_3 - nA\left(\frac{\rho_3}{f'_{co}}\right)^{n-1} \tag{5.28}$$

In the above process of computation, the value of $\varepsilon_{v,t}^p$ is required in Eqs. (5.18), (5.20) and (5.26) to calculate the plastic potential coefficients (i.e. A, B and C). The initial value of $\varepsilon_{v,t}^p$ is assumed to be equal to $f'_{co}(1-2\mu)/E$, which means that the volumetric strain at peak stress under uni-axial compression, equal biaxial compression and equal tri-axial compression are all equal to zero. This value can be changed to fit the overall dilation behaviour of the full-range stress-strain response of confined concrete. After the values of A, B and C are determined, the value of t_p can be found by fitting the slope of the post-peak stress-strain curve. A Matlab Program was developed to calculate the values of A, B, and C based on the process described above. The code of this program is given as Appendix A1 of this thesis.

The present constitutive model was also implemented into ABAQUS by writing a user-defined material subroutine (UMAT). Finite element models using this constitutive model were then employed to predict the response of confined concrete. Test results of actively-confined concrete reported by Candappa et al. (1999) were once again used as benchmark results to verify the validity of the constitutive model.

The values of various parameters were determined from Candappa et al.'s (1999) test data as follows. First, from the test data of peak stresses under different confining pressures, the value of *m* was found to be 12.95 using the least squares method, and the value of f_t was then calculated to be 3.3 MPa. Second, from the test data of axial strains at peak stress, the value of k_2 was found to be 21.8. The value of $\varepsilon_{v,t}^{p}$ was modified from the initial value of 0.00082 to 0.0025 to fit the overall dilation behaviour of confined-concrete. Finally, using Eqs. (5.22), (5.23) and (5.28), the values of A, B, and C were determined to be 4.776, -6.179, and -3.923, respectively. The finite element predictions obtained with the present calibrated constitutive model are compared with the test results in Fig. 5.4. The values of the model parameters are also shown in the figures. These figures show that the predicted stress-strain curves are in close agreement with the test results.

Finally, the present constitutive model was utilized to predict the response of FRP-confined concrete as was done using the modified DP type model presented earlier in Chapter 4. The same finite element model as described in Section 4.3 for FRP-confined concrete was employed with the present constitutive model replacing the D-P type plasticity model. The active-confinement model used in Teng et al. (2007) was adopted to identify values of parameters for the concrete constitutive model. Here, Teng et al.'s (2007) model instead of Jiang and Teng's (2007) model is used as it employs a linear-form equation to predict the axial strain at the peak axial stress of actively confined concrete. This linear-form equation can be reproduced by the present constitutive model when its parameter n is equal to 3. In Teng et al.'s (2007) model, the following equations were adopted for the peak stress and the axial strain at peak stress:

$$\frac{f_{cc}^{*}}{f_{co}^{'}} = 1 + 3.5\frac{f_l}{f_{co}^{'}} \tag{5.29}$$

$$\frac{\varepsilon_{cc}^{*}}{\varepsilon_{co}} = 1 + 17.5\frac{f_l}{f_{co}^{*}} \tag{5.30}$$

Eq. (5.29) is in a form different from that of Eq. (5.10), so it cannot be directly employed to determine the value of *m*. A least squares method was adopted to determine the value of *m* which can satisfy the least squares approximation between these two equations within certain range of confinement levels. This range was selected as 0~0.25 which is a common definition for the range of low confinement (Attard and Setunge 2002).

Based on this additional assumption, the value of *m* for FRP-confined concrete was determined to be 6.13 as shown in Fig. 5.5.

After the value of *m* was determined, Eq. (5.30) and the initial value of $f'_{co}(1-2\mu)/E$ for $\varepsilon_{v,t}^{p}$ were used to determine the values of A, B and C. The test results of Lam et al. (2006) were selected as the benchmark results for comparison. Two confinement stiffnesses, 543 MPa and 1086 MPa, were once again considered in the comparison. Fig. 5.6b shows that for the higher confinement stiffness, the finite element model provides close predictions for stress-strain curves including both the axial stress-strain curves and the axial stress-lateral strain curves. However, Fig. 5.6a shows that for the lower confinement stiffness, the finite element model only provides close predictions for the axial stress-lateral strain curve. The axial strain can be observed from Fig. 5.6a of being overestimated so that the axial stress- strain curve is still underestimated although the axial stress at a given lateral strain is close to the test result.

To refine the predictions of the finite element model, the parameters which control the dilation characteristics of the constitutive model need to be modified to fit the experimental results more closely. As discussed earlier, the most important parameter that controls the dilation characteristics is $\varepsilon_{v,t}^{p}$. This parameter needs to be revised from the initial assumed value to a new

value so as to predict the test result of FRP-confined concrete with lower confinement stiffness accurately. As $\varepsilon_{v,t}^{p}$ also influences the slope the post-peak branch of the stress-strain curve, the parameter t_p also needs to be revised to remedy the change induced by the revised value for $\varepsilon_{v,t}^{p}$. The need for these possible revisions means that in the case of FRP confinement, the values of $\varepsilon_{v,t}^{p}$ and t_p can no longer be taken as constant for different confinement stiffnesses; instead, their values need to vary with the confinement stiffness. The behaviour of the finite element model with the revised parameter values is shown in Fig. 5.7. This figure shows that once lateral dilation was properly predicted, the constitutive model with revised value of $\varepsilon_{v,t}^{p}$ provided comparatively more accurate predictions for stress-strain curves of weakly-confined concrete than that with default value. Although the ultimate state of the FRP-confined concrete was adequately predicted, difference still existed between the predicted result and the experimental results. This difference is reflected in the axial stress before the ultimate axial strain. In this range, the lateral strain at a given axial strain tends to be overestimated (see the left part of Fig. 5.7) resulting in an overestimated axial stress. It can be expected that using a gradually increased $\varepsilon_{v,t}^{p}$ can provide more accurate prediction. However, this modification leads to a much more complex constitutive model and is not the major concern in the present study.

5.4 CONCLUSIONS

This chapter has been concerned with the performance of Papanikolaou and Kappos's (2007) model on actively confined concrete and FRP-confined concrete. As Papanikolaou and Kappos's (2007) model is a relatively new constitutive model and is not available in existing commercial software, this model was first implemented into ABAQUS as a UMAT subroutine. Then, this UMAT subroutine was employed in finite element models for simulating confined concrete. The results of these finite element models were utilized for evaluating the performance of actively confined concrete and FRP-confined concrete.

Twelve parameters are employed in this model for describing the behaviour of concrete under confinement. Compared to the D-P type model based on the scaling approach discussed in Chapter 4, this model uses a more complex loading surface and a flow rule which can account for the effect of the Lode angle on the confinement effect. A major advantage of this model is that each parameter can be determined using a relatively simple process which allows the role of each parameter to be properly considered.

This model can provide accurate predictions for the stress-strain behaviour of actively-confined concrete under different confining pressures. For FRP-confined concrete, the model with a constant value for $\varepsilon_{v,t}^{p}$ is

unsuccessful in predicting the stress-strain behaviour of concrete confined with FRP jackets of different confining stiffnesses although the predictions are accurate for a certain confining stiffness. For this model to provide close predictions for FRP-confined concrete over a wide range of confining stiffnesses, the value of $\varepsilon_{v,t}^{p}$ needs to vary with the confining stiffness.

In summary, the discussions presented in Chapter 4 and this chapter show that plasticity-based constitutive models for concrete that employ either the scaling technique or the plastic volumetric strain approach can both provide accurate predictions for actively-confined concrete, but improvements are still needed before they can deliver accurate predictions for FRP-confined concrete. It has been found that refinement of the hardening/softening rule has an insignificant effect on the prediction of lateral deformation.

5.5 REFERENCES

Attard, M. M., and Setunge, S. (1996). "Stress-strain relationship of confined and unconfined concrete." *ACI Materials Journal*, 93(5), 432-442.

Barros, M. H. F. (2001). "Elasto-plastic modelling of confined concrete elements following MC90 equations." *Engineering Structures*, 23(4), 311-318.

Candappa, D. P., Setunge, S., and Sanjayan, J. G. (1999). "Stress versus

strain relationship of high strength concrete under high lateral confinement." *Cement and Concrete Research*, 29(12), 1977-1982.

Cervenka, J., Cervenka, V., and Eligehausen, R. "Fracture-plastic material model for concrete, application to analysis of powder actuated anchors." *Proceedings of the 3rd International Conference on Fracture Mechanics of Concrete Structures-FRAMCOS 3, Gifu, Japan*, 1107-1116.

Grassl, P., Lundgren, K., and Gylltoft, K. (2002). "Concrete in compression: a plasticity theory with a novel hardening law." *International Journal of Solids and Structures*, 39(20), 5205-5223.

Imran, I., and Pantazopoulou, S. J. (2001). "Plasticity model for concrete under triaxial compression." *Journal of Engineering Mechanics*-ASCE, 127, 281.

Johansson, M., and Akesson, M. (2002). "Finite element study of concrete-filled steel tubes using a new confinement-sensitive concrete compression model." *Nordic Concrete Research -Publications*, 27, 43-62.

Lam, L., Teng, J. G., Cheung, C. H., and Xiao, Y. (2006). "FRP-confined concrete under axial cyclic compression." *Cement & Concrete Composites*, 28(10), 949-958.

Menetrey, P., and Willam, K. J. (1995). "Triaxial failure criterion for concrete and its generalization." *ACI Structural Journal*, 92(3),

311-318.

Papanikolaou, V. K., and Kappos, A. J. (2007). "Confinement-sensitive plasticity constitutive model for concrete in triaxial compression." *International Journal of Solids and Structures*, 44(21), 7021-7048.

Teng, J. G., Huang, Y. L., Lam, L., and Ye, L. P. (2007). "Theoretical model for fiber-reinforced polymer-confined concrete." *Journal of Composites for Construction*-ASCE, 11(2), 201-210.

Van Gysel, A., and Taerwe, L. (1996). "Analytical formulation of the complete stress-strain curve for high strength concrete." *Materials and Structures*, 29(9), 529-533.

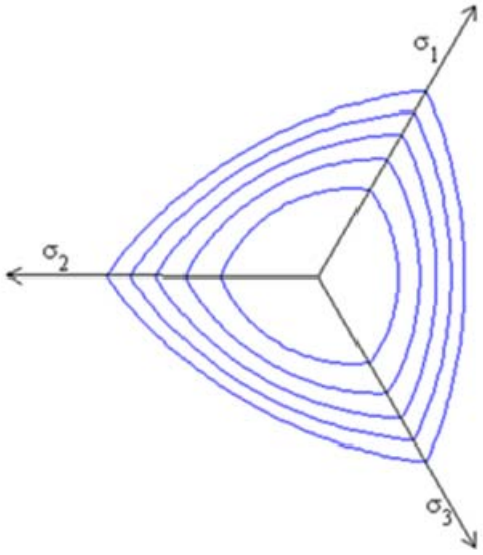

Figure 5.1 Yield surfaces of Papanikolaou and Kappos (2007)'s model in the deviatoric plane

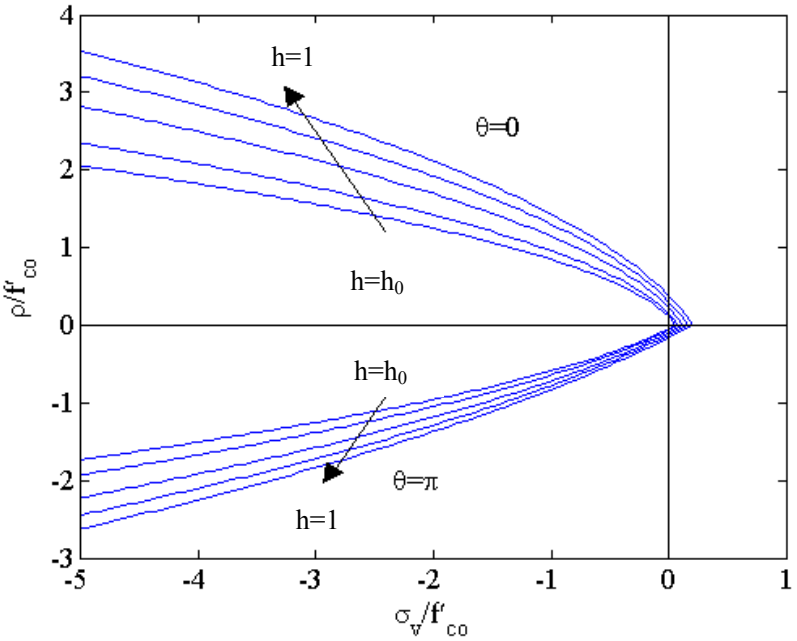

Figure 5.2 Effect of parameter k on the yield surfaces of Papanikolaou and Kappos's (2007) model

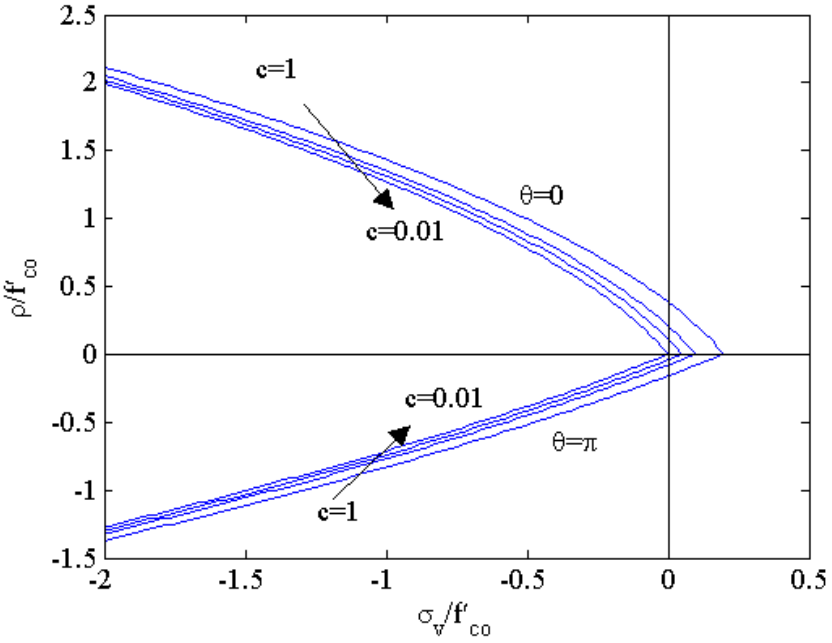

Figure 5.3 Influence of parameter c on the yield surfaces of Papanikolaou and Kappos's (2007) model

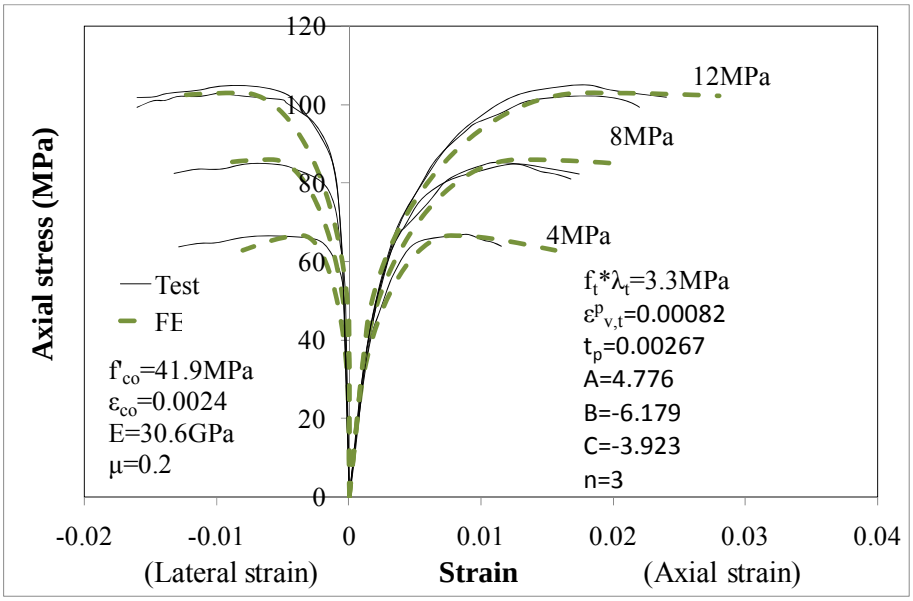

Figure 5.4 Comparison between finite element predictions and test results of Candappa et al. (1999)

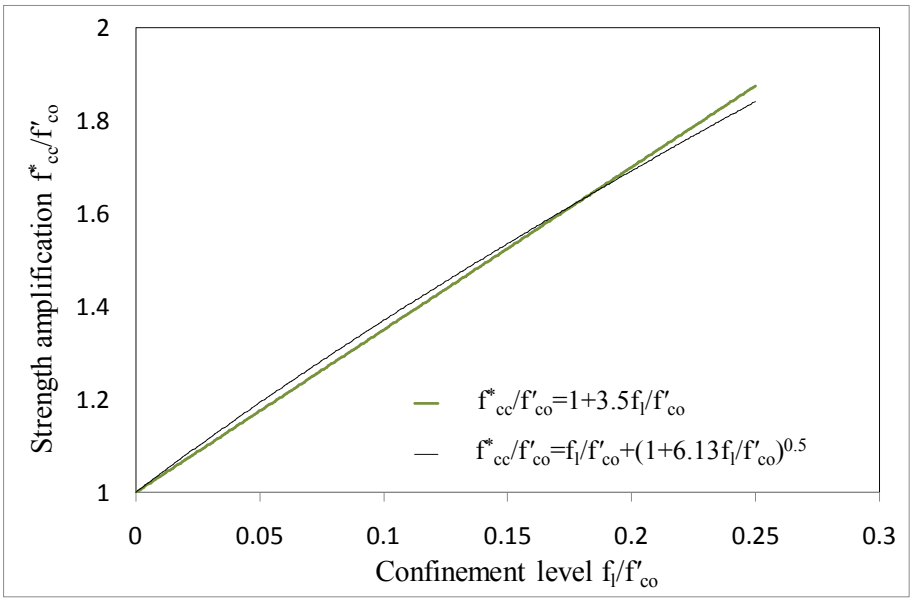

Figure 5.5 Determination of m using the least squares approach

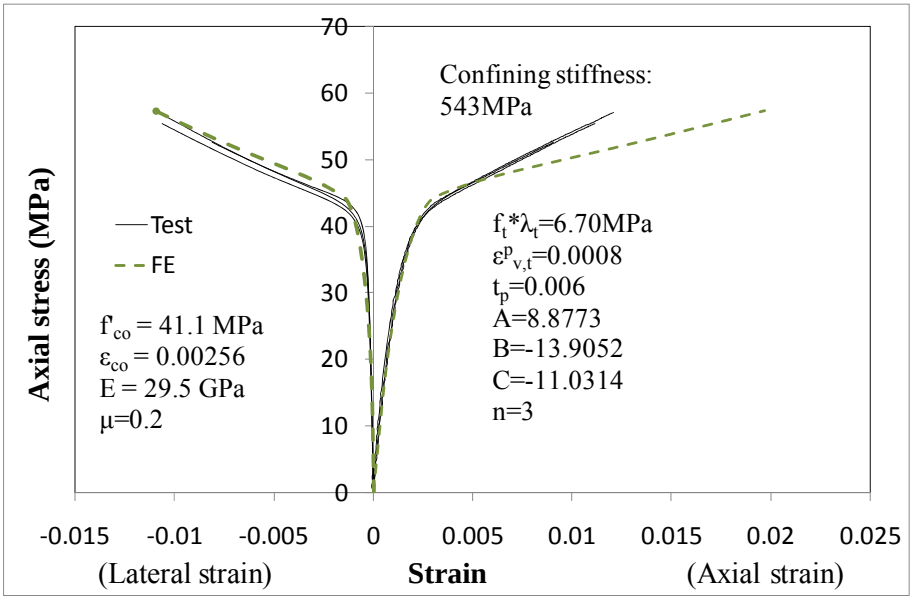

(a) FRP-confined concrete with confining stiffness equal to 543 MPa

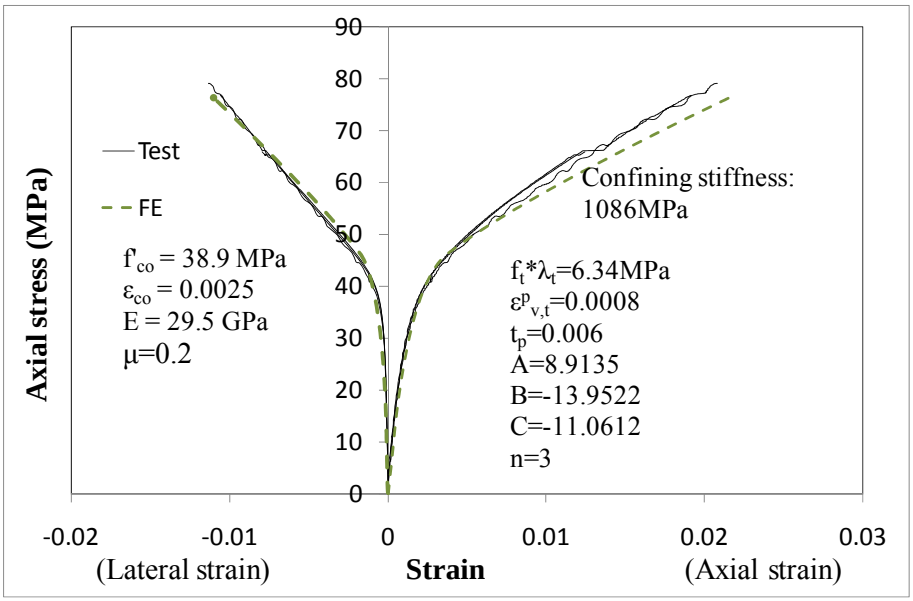

(b) FRP-confined concrete with confining stiffness equal to 1086 MPa

Figure 5.6 Comparison between finite element results and test results of Lam et al. (2006)

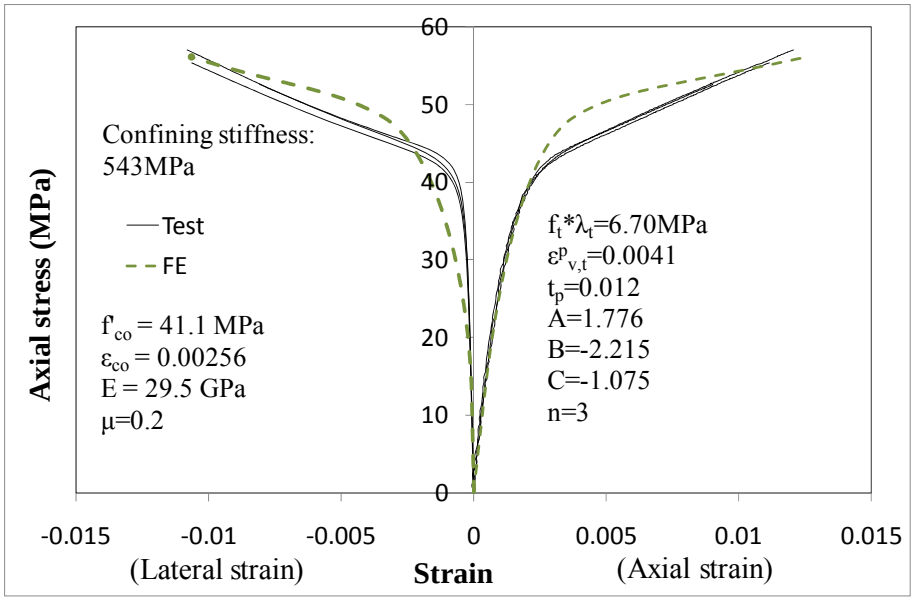

Figure 5.7 Comparison between finite element results from the refined model and test results of Lam et al. (2006)

CHAPTER 6

PLASTIC-DAMAGE MODELS FOR CONFINED CONCRETE

6.1 INTRODUCTION

It has been concluded in Chapters 4 and 5 that a plasticity-based constitutive model for concrete, employing either the scaling technique or a novel hardening variable (e.g. the plastic volumetric strain) in the hardening/softening rule (referred to as the hardening rule for brevity), leads to accurate predictions of the behaviour of actively-confined concrete, but fails to capture the lateral deformation characteristics and hence the stress-strain behaviour of FRP-confined concrete.

Elastic unloading is assumed in the theory of plasticity, which does not reflect the elastic stiffness degradation of concrete observed in laboratory experiments. In contrast, this stiffness degradation can be described using the theory of damage mechanics. Moreover, concrete exhibits considerable irreversible deformation which cannot be described by the theory of damage mechanics alone. That is, either plasticity or damage alone, cannot achieve a satisfactory description of the complex failure process of concrete which is characterized by both stiffness degradation and irreversible deformation. Consequently, plastic-damage models, which are based on a combination of

the flow theory of plasticity and the theory of damage mechanics, have emerged as a popular approach for the constitutive modelling of concrete. The combination of plasticity theory and damage mechanics is believed to be capable of closely representing most of the important features of concrete failure. This chapter is therefore concerned with the constitutive modelling of concrete using the plastic-damage (or damaged plasticity) approach.

While the inclusion of damage in a constitutive model is for the simulation of the elastic stiffness reduction of concrete as deformation increases, it also affects the hardening rule employed in the plasticity part of a plastic-damage constitutive model. For instance, the softening behaviour of concrete in some plastic-damage models (e.g. Grassl and Jirasek 2006) is described as damage, so the hardening rule in the plasticity part only describes the hardening behaviour of concrete. This process overcomes the possible numerical difficulty which may be encountered when plasticity model was employed for simulating the strain-softening behaviour of concrete. Therefore, even if elastic stiffness reductions are not of major concern, a plastic-damage model may provide an attractive alternative approach for the modelling of concrete with strain-softening regime. This chapter is concerned with the exploration of this possibility in the modelling of confined concrete.

In formulating the hardening rule of the plasticity part of a plastic-damage model for confined concrete, the two techniques examined in Chapters 4 & 5 (i.e. the scaling technique and the plastic volumetric strain technique) are still required to consider the increased ductility of concrete due to lateral confinement. Otherwise, the ascending branch of the concrete response which is controlled by the hardening rule of the plasticity part cannot be properly predicted. Based on the above discussion, it can be concluded that the contributions of these two parts (i.e. the hardening rule and the damage variable) in plastic-damage models should be properly formulated to accurately predict the increased deformation capacity of concrete under lateral confinement.

Existing plastic-damage models are usually based on plasticity with isotropic hardening enriched by either isotropic (scalar) (e.g. Lubliner et al. 1989) or anisotropic (vector) (Carol et al. 2001) damage. Compared to isotropic damage, an anisotropic damage model for concrete is more complex and is harder to combine with plasticity; in addition, its application in structural analysis is also not straightforward. Moreover, there are insufficient experimental data for verifying this type of damage models. Due to these limitations of an anisotropic damage model, the isotropic damage model has been widely used instead for combination with plasticity to develop plastic-damage models following various approaches. In the

present study, all considerations of concrete damage are limited to isotropic damage.

Two approaches have been commonly employed in combining plasticity with damage in the existing literature. The first approach comprises the combination of plasticity based on nominal stresses with damage whose evolution is defined by the total or plastic strain (Lubliner et al. 1989; Imran and Pantazopoulou 2001). Here, the term “nominal stress” refers to a macro-level stress and is defined as a force divided by the total area acted upon by the force. The plasticity part in the second approach is based on effective (undamaged) stresses and is combined with damage whose evolution is also defined by the total strain or plastic strain . Here, the term “effective stress” refers to an average micro-level stress in the undamaged material between defects and is defined as a force divided by the undamaged part of total area acted upon by the force.

Based on the so-called local uniqueness conditions, Grassl and Jirasek (2006) assessed the performance of the two approaches mentioned above. They found that the second approach is numerically more stable and attractive for developing plastic-damage models (Grassl and Jirasek 2006). When plasticity is defined based on effective stresses, the plasticity part and the damage part of a plastic-damage model is uncoupled, and no further

restriction on the specific form of the plastic part and the damage part is required. However, if plasticity is defined based on nominal stresses, the evolution of the damage variable requires a positive plastic modulus in the plastic part to achieve local uniqueness. This restriction makes the approach unsuitable for materials with softening behaviour. A more in-depth discussion of the issue can be found in Grassl and Jirasek (2006). Due to this advantage of the second approach, this chapter is only concerned with plastic-damage models formulated in the effective stress space and based on a scalar damage variable.

Two plastic-damage models representing two different approaches are considered in this chapter, which is similar to the work presented in Chapters 4 & 5. In the first model, the scaling technique is employed to describe the behaviour of confined concrete; whereas in the second model, the plastic volumetric strain technique is employed instead. The two plastic-damage models examined in this chapter include: (a) the plastic-damage model proposed by Grassl and Jirasek (2006) which is based on the first approach; and (b) a new plastic-damage model formulated on the basis of the framework of Papanikolaou and Kappos's (2007) plasticity model. Details of these two models are given in the following sections.

6.2 GRASSL AND JIRASEK'S (2006) MODEL

Grassl and Jirasek (2006) developed a plastic-damage model for concrete based on their assessment of different types of plastic-damage models. The plasticity part of the model is given in the effective stress space, and the damage part of the model is driven by the scaled plastic volumetric strain. The equations used to define the basic components of the plasticity and the damage parts of this model are given in the subsequent sub-sections.

6.2.1 Components of the Plasticity Model

The plasticity part of this model is defined by a pressure-sensitive yield function, a non-associated flow rule, and a hardening rule based on the scaling technique. In this model, the scaling law is referred to as the ductility measure. The hardening law, which is an important feature of this model, is given in detail below.

6.2.1.1 Yield surface

The yield function was modified from that proposed by Etse and Willam (1994). Its expression, defined in the Haigh-Westergaard effective stress space, is as follows:

$$f_p(\bar{\sigma}_V, \bar{\rho}, \bar{\theta}; \kappa_p) = \left\{ [1 - q_h(\kappa_p)] \left(\frac{\bar{\rho}}{\sqrt{6} f'_{co}} + \frac{\bar{\sigma}_V}{f'_{co}} \right)^2 + \sqrt{\frac{3}{2}} \frac{\bar{\rho}}{f'_{co}} \right\}^2 + m q_h^2(\kappa_p) \left[\frac{\bar{\rho}}{\sqrt{6} f'_{co}} r(\cos \bar{\theta}) + \frac{\bar{\sigma}_V}{f'_{co}} \right] - q_h^2(\kappa_p) \quad (6.1)$$

where $\bar{\sigma}_V, \bar{\rho}, \bar{\theta}$ are the volumetric effective stress, the deviatoric effective stress, and the Lode angle in the effective stress space, respectively. The $\bar{\sigma}_V, \bar{\rho}, \bar{\theta}$ can be defined by Eqs. (2.96-2.98) using the corresponding effective stress components instead of the total stress components. The parameter r is the same as that defined by Eq. (5.3) except that the corresponding components defined in the total stress space in Eq. (5.3) should be replaced by those defined in the effective stress space. The parameter m is the same as that defined by Eq. (5.2). The parameter q_h controls the hardening rule of this model and is defined as a function of the hardening variable κ_p. When the variable q_h is equal to one, the yield function turns into the failure surface proposed by Menetrey and Willam (1995); for uniform confinement, this equation can be further reduced to the Hoek and Brown failure criterion. Thus, it is clear that the value of m can be calibrated using the same approach as that suggested in Chapter 5.

6.2.1.2 Flow rule

A non-associated flow rule is adopted in Grassl and Jirasek's (2006) model, which means that the yield function and the plastic potential do not coincide.

Therefore, the direction of the plastic flow is not normal to the yield surface, which is important for the realistic modelling of the lateral deformation of concrete under compression. As discussed in previous chapters (e.g. Chapters 2 and 4), an associated flow rule tends to give unrealistically high volumetric expansions in compression. Based on these considerations, the plastic potential in the model is given as

$$g_p(\bar{\sigma}_V, \bar{\rho}, \bar{\theta}; \kappa_p) = \left\{ \left[1 - q_h(\kappa_p)\right] \left(\frac{\bar{\rho}}{\sqrt{6} f'_{co}} + \frac{\bar{\sigma}_V}{f'_{co}} \right)^2 + \sqrt{\frac{3}{2}} \frac{\bar{\rho}}{f'_{co}} \right\}^2 + q_h^2(\kappa_p) \left[\frac{m\bar{\rho}}{\sqrt{6} f'_{co}} + \frac{m_g(\bar{\sigma}_V)}{f'_{co}} \right] \tag{6.2}$$

Eq. (6.2) does not depend on the Lode angle so as to increase the efficiency of the implementation of the model. This feature partially limits the capability of the flow rule for describing the response of concrete in complex multi-axial compression. To properly reflect the plastic volumetric expansion, the parameter m_g which controls the ratio of the volumetric and the deviatoric parts of the flow direction, is defined based on the volumetric stress as follows:

$$m_g(\bar{\sigma}_V) = A_g B_g f'_{co} \exp \frac{\bar{\sigma}_V - f_t/3}{B_g f'_{co}} \tag{6.3}$$

where A_g and B_g are parameters determined from lateral plastic

deformations under the two conditions of uni-axial tension and compression. They are given as follows:

$$A_g = \frac{3f_t}{f'_{co}} + \frac{m}{2} \tag{6.4}$$

$$B_g = \frac{1/3(1+f_t/f'_{co})}{\ln A_g - \ln(2D_f - 1) - \ln\left(\frac{m}{2}+3\right) + \ln(D_f+1)} \tag{6.5}$$

Here, D_f should be determined by fitting the results of uni-axial compression.

6.2.1.3 Hardening law

The dimensionless variable q_h controls the evolution of the yield surface, and thereby the elastic range. q_h is defined as a function of the hardening variable κ_p as follows:

$$q_h(\kappa_p) = \begin{cases} q_{h0} + (1 - q_{h0})\kappa_p(\kappa_p^2 - 3\kappa_p + 3), & \kappa_p < 1 \\ 1, & \kappa_p \geq 1 \end{cases} \tag{6.6}$$

The scaling technique was adopted in the Grassl and Jirasek (2006) model to capture the increase in ductility due to lateral confinement. The increment of the hardening variable is defined as

$$d\kappa_p = \frac{d\varepsilon_p}{x_h(\bar{\sigma}_V)} \cos^2\bar{\theta} \tag{6.7}$$

where x_h is a hardening ductility measure used to scale the plastic strain increment $d\varepsilon_p$ [the definition $d\varepsilon_p$ is the same as that used in Wolf (2008)], a more complex x_h is defined as follows:

$$x_h(\bar{\sigma}_V) = \begin{cases} E_h \exp(-R_h(\bar{\sigma}_V)/F_h) + D_h, & R_h(\bar{\sigma}_V) < 0 \\ A_h - (A_h - B_h)\exp(-R_h(\bar{\sigma}_V)/C_h), & R_h(\bar{\sigma}_V) \geq 0 \end{cases} \quad (6.8)$$

where A_h, B_h, C_h, and D_h are calibrated using values of strain at peak stress under uni-axial tension, uni-axial compression and equal tri-axial compression, whereas E_h and F_h are given by the following equations to ensure a smooth transition between the two parts of Eq. (6.8) at $R_h = 0$:

$$E_h = B_h - D_h \quad (6.9)$$

$$F_h = \frac{(B_h - D_h)C_h}{A_h - B_h} \quad (6.10)$$

6.2.2 Components of the Damage Model

Isotropic scalar damage is employed to formulate the damage part of the Grassl and Jirasek (2006) model. A salient feature of this damage model is that damage is driven by the scaled volumetric plastic strain instead of the total strain which is employed in a pure damage model. The individual components of the damage model are presented in the following sub-sections.

6.2.2.1 Loading function and equivalent strain

The damage loading function is based on the scaled volumetric plastic strain which is defined as

$$d\tilde{\varepsilon} = \begin{cases} 0, & \kappa_p < 1 \\ \frac{d\kappa}{x_s(\bar{\sigma}_V)}, & \kappa_p > 1 \end{cases} \quad (6.11)$$

where x_s is a softening ductility measure defined as

$$x_s(\bar{\sigma}_V) = \begin{cases} 1 + A_s R_s^2(\bar{\sigma}_V), & R_s(\bar{\sigma}_V) < 1 \\ 1 - 3A_s + 4A_s\sqrt{R_s\,(\bar{\sigma}_V)}, & R_s(\bar{\sigma}_V) \geq 1 \end{cases} \tag{6.12}$$

In the above equation, A_s is a parameter that controls the softening response in uni-axial compression, and R_s is defined as $\hat{\kappa}/\kappa$. Here $\hat{\kappa}$ is the so-called "negative" volumetric plastic strain and is defined as

$$\hat{\kappa} = \sum_{I=1}^{3} \langle -d\varepsilon_{pI} \rangle \tag{6.13}$$

where $d\varepsilon_{pI}$ are the principal components of the plastic strain increments and as mentioned earlier $\langle \cdot \rangle$ denotes the McAuley bracket (positive-part operator). Compressive strains are defined as negative in the Grassl and Jirasek (2006) model. Eq. (6.13) indicates that only the contribution of compressive plastic strains is considered in the definition of $\hat{\kappa}$.

6.2.2.2 Evolution law

To describe the evolution of damage, an exponential equation is employed to relate the damage variable ω_d to the internal variable $\tilde{\varepsilon}$

$$\omega_d = 1 - \exp(-\tilde{\varepsilon}/\varepsilon_f) \tag{6.14}$$

where ε_f is a parameter that controls the slope of the softening curve.

6.2.3 Implementation in Finite Element Analysis

An existing finite element program named OOFEM and written by Patzak (Patzák and Bittnar 2001) was adopted for use in the numerical analyses of the present study. OOFEM is a free finite element code with an

object-oriented architecture for solving mechanical, transport and fluid mechanics problems. In OOFEM, the present constitutive model was not directly provided. Instead, a non-local version of this model was offered. The non-local version and the local version of a constitutive model require different processes of parameter calibration. In the present study, only the local version of the constitutive model is of interest. Therefore, the non-local version in this program was revised to become a local version. The process suggested in the subsequent sub-sections can then be used to calibrate the parameters for the present constitutive.

The present constitutive model is the only model examined in this PhD project which has been implemented in OOFEM; other constitutive models examined in the project were implemented in ABAQUS. Using OOFEM, the same finite element model as described in Chapter 4 were employed to model the selected experiments except that the element types were replaced by the same types of elements available in OOFEM. For instance, the C3D8 element in ABAQUS to model the concrete was replaced by the LSPACE element in OOFEM, and the T3D2 element in ABAQUS to model the confining material was replaced by the TRUSS3D element in OOFEM.

6.2.4 Parameter Calibration and Comparison with Test Results

6.2.4.1 General

A total of fifteen parameters are used in the Grassl and Jirasek (2006) model to define the general response of concrete. These parameters can be divided into four groups: the elastic properties, the hardening regime, the strength envelope, and the softening regime. The elastic properties are defined by the Young's modulus E and Poisson's ratio μ, which can be obtained directly from experimental results. The strength envelope of the Grassl and Jirasek (2006) model in the effective stress space is defined by three parameters, including the uni-axial tensile strength f_t, the uni-axial compressive strength f'_{co}, and the eccentricity parameter e. The hardening rule is characterized by five independent parameters. Among these parameters, q_{h0} defines the initial value of the hardening variable, and A_h, B_h, C_h, and D_h define the hardening ductility measure. The softening regime is characterized by ε_f and A_s for the softening ductility measure. Furthermore, both the hardening and softening regimes are affected by the parameters of the flow rule, A_g and B_g, which can be calculated from Eqs. (6.4) & (6.5).

6.2.4.2 Default values for some parameters

To determine all the fifteen parameters from experimental results is a huge

task. Default values have thus been suggested by Grassl and Jirasek (2006) to simplify the procedure of parameter calibration. q_{h0} is defined as $q_{h0} = f_{ini}/f'_{co}$ where f_{ini} is the initial yield strength of concrete under uniaxial compression. Usually, f_{ini} is set to be $0.3f'_{co}$. Explicit relationships between A_h, B_h, C_h, and D_h (which affect the hardening ductility measure) and measurable material properties do not exist. Based on the fitting of selected sets of experimental results (e.g. Kupfer et al. 1969; Imran and Pantazopoulou 1996), Grassl and Jirasek (2006) suggested the following default values for these three parameters: $A_h = 0.08$, ,$C_h = 2$, and $D_h = 1e-6$. Besides these three parameter, a linear relationship between B_h and the axial plastic strain at peak stress ε_p^{peak}under uni-axial compression was provided:

$$B_h = -2.29\varepsilon_p^{peak} + 0.00046 \tag{6.15}$$

D_f has a significant influence on the lateral-to-axial strain relationship for both unconfined and confined concrete. Based on a long trial-and-error process, a default value of 0.85 was suggested by these authors for D_f. ε_f and A_s control the softening regime of the stress-strain behaviour of concrete. Their values should be determined from the fracture energy G_f and from the softening part of the stress-strain curve under uni-axial compression. The expressions for these two parameters are similar. Grassl and Jirasek (2006) recommended a default value of 15 for A_s to simplify the process of parameter calibration. Finally, Grassl and Jirasek (2006)

proposed a default value of 0.525 for the eccentricity parameter e to achieve an equal biaxial concrete strength close to Kupfer et al.'s (1969) experimental results. The eccentricity parameter controls the shape of the deviatoric section as discussed in the previous chapter.

6.2.4.3 Calibration of the remaining parameters

With the default parameter values detailed above, only the values of the following parameters are unknown: E, μ, f'_{co}, f_t, and ε_f. Among these parameters, E, μ, and f'_{co} are material properties of unconfined concrete and can be determined from standard tests. If the experimental value for μ, is unavailable, a default value of 0.2 may be adopted, which should lead only to negligible errors in the finite element results. As illustrated in Chapter 5, f_t relates to m, e, and f'_{co} as described by Eq. (6.2). If $h(\kappa)$ in Eq. (5.2) is equal to 1, this equation can be rewritten as

$$m = 3\frac{f'^2_{co} - f_t^2}{f'_{co} f_t}\frac{e}{e+1} \tag{6.16}$$

The value of m can be determined from a selected set of test data using the least squares method. The artificial f_t value can then be calculated from Eq. (6.16).

The parameter ε_f is used to fit (using a trial-and-error process) the slope of the softening part of the stress-strain curve under uni-axial compression. If localization of failure occurs, this parameter should change with the element

size. As only concrete under uniform confinement was modeled using a single solid element in the present study, there was no such localization failure. Therefore, the value of ε_f in the present study did not need to vary with the element size.

Test results for actively-confined concrete reported by Candappa et al. (1999) were used to assess the stress-strain curves obtained from finite element analysis using Grassl and Jirasek's (2006) model with calibrated parameters. The detailed process of calibration for this set of experiments is described in the subsequent paragraphs.

As presented in Chapter 5, the value of m can be determined to be 12.95. Based on this value of m, the value of f_t can then be found to be 3.3 MPa. For ε_f, a value of 1.65e-4 was obtained from a trial-and-error process for the descending branch of the stress-strain curves of confined concrete . For the other parameters, their default values as suggested by Grassl and Jirasek (2006) were adopted. The same finite element model as described in Chapter 4 for actively-confined concrete was employed in the numerical analysis. Fig. 6.2 shows that the predicted stress-strain responses using the final calibrated parameters compare favorably with the test results. This comparison indicates that the present constitutive model can provide close predictions for actively-confined concrete.

Grassl and Jirasek's (2006) model was next utilized in predicting the response of FRP-confined concrete. The same finite element model as described in Section 4. 4 for FRP-confined circular concrete cylinders was adopted, but the present concrete constitutive model was used to replace the D-P type model. Eq. (5.29) was adopted to identify the value of m and then to calculate the value of f_t using Eq. (6.16). As the present constitutive model has the same failure surface as that of Papanikolaou and Kappos's (2007) model, the same values for f_t as those adopted in Papanikolaou and Kappos's (2007) model for FRP-confined concrete cylinders were obtained. The values of E, μ, and f'_{co} were determined from the control cylinder tests; these values are the same as those adopted in the D-P type model and are shown in Fig. 6.2. To better fit the value of ε_{co}, the value of B_h was adjusted from the default value of 0.003 to 0.00325. The value of ε_f was set to be 9.6e-4 to fit (using a trial-and-error process) the slope of the second branch of stress-strain curves for FRP-confined concrete. All other parameters retained their default values. The experimental stress-strain curves are compared with the predicted curves in Figs. 6.3. The predicted results are similar to the finite element results based on Papanikolaou and Kappos's (2007) concrete model. For the specimens with the confinement stiffness equal to 1086 MPa, the finite element results are in close agreement with the experimental results for both the axial stress-strain curve

and the axial stress-lateral strain curve. For the specimens with the confinement stiffness equal to 543 MPa, the finite element predictions differ substantially from the experimental results for the axial stress-strain curves although the two sets of results are in agreement for the axial stress-lateral strain curves. This inconsistency indicates that the finite element model cannot accurately capture the lateral-to-axial strain relationship for concrete at different confinement stiffness levels.

The above discussion indicates a plastic-damage model with its hardening part based on the scaling technique cannot provide accurate predictions for the lateral-to-axial strain response of FRP-confined concrete. The inclusion of isotropic damage in this type of plastic-damage model seems to have little influence on the volumetric response of concrete.

6.3 PLASTIC-DAMAGE MODEL BASED ON PAPANIKOLAOU AND KAPPOS' (2007) PLASTICITY MODEL

6.3.1 General

As shown in Chapter 5, Papanikolaou and Kappos's (2007) plasticity model is capable of providing accurate predictions for actively-confined concrete, and the values of its parameters can be determined via a simple and clear process of parameter calibration. In the softening part of this constitutive model, a plastic softening model is adopted. As explained earlier, for the

description of the softening characteristics of concrete, a damage model has advantages over a plasticity model. Therefore, in this section, a plastic-damage model based on Papanikolaou and Kappos's (2007) plasticity model is presented. This plastic-damage model is referred to as PDPK model in this thesis. The advantages of Papanikolaou and Kappos's (2007) plasticity model are retained in the proposed plastic-damage model. For instance, the process of determining the values of A, B and C remains the same. The equations used for the definition of this model are given in the following sub-sections.

6.3.2 Components of the Plasticity Model

The plasticity model includes a pressure-sensitive yield function, a non-associated flow rule, and a hardening rule with a novel hardening variable.

6.3.2.1 Loading surface

The loading function proposed by Papanikolaou and Kappos (2007) is given by Eq. (5.1) which is applicable to both hardening and softening responses. In the present model, only the hardening response of concrete is considered in the plasticity part, while the softening part is accounted for by the damage model.

By assigning a value of 1 to $c(\kappa)$ in Eq. (5.1), the yield function is

obtained as follows:

$$f^{p}(\xi,\rho,\theta)=\left(\sqrt{3/2}\frac{\rho}{h(\kappa)f'_{co}}\right)^{2}+m\left(\frac{\rho}{\sqrt{6}h(\kappa)f'_{co}}r(\theta,e)+\frac{\xi}{\sqrt{3}h(\kappa)f'_{co}}\right)-1 \quad (6.17)$$

As previously discussed, a similar approach has previously been adopted by Grassl and Jirasek (2006) and Yu et al (2010b). After the attainment of peak stress, no strain-hardening/softening is defined in the plasticity part, and the yield surface remains unchanged. For the hardening parameter $h(\kappa)$, an elliptic-type function (i.e. Eq. 5.5) is still adopted. This elliptic-type function is an important part to ensure that the condition used to determine the values of A, B, and C is still satisfied.

6.3.3.2 Flow rule

For the definition of the flow rule, a constant value of 1 replaces $c(\kappa)$ in Eq. (5.11) so that it becomes

$$g=A\left(\frac{\rho}{kf'_{co}}\right)^{n}+\left[C+\frac{1}{2}(B-C)(1-\cos3\theta)\right]\frac{\rho}{kf'_{co}}+\frac{\xi}{kf'_{co}} \quad (6.18)$$

The values of other parameters are determined in the same way as in Papanikolaou and Kappos (2007). Eqs. (5.5), (6.17) and (6.18) ensure that the plasticity part of the PDPK model is the same as that of Papanikolaou and Kappos's (2007) model before the peak stress of confined concrete is reached. Therefore, the values of A, B, and C can be determined using the same approach as in Papanikolaou and Kappos's (2007) model.

6.3.4 Components of the Damage Model

6.3.4.1 General

The isotropic scalar damage concept is once again adopted in the damage part of the proposed model. In this new damage model, a new loading function was employed for the definition of the damage evolution. A major feature of this loading function is that it is driven by the plastic volumetric strain. This feature is different from that of some pure damage models which is usually driven by the total strain (e.g. Mazars and Pijaudier-Cabot 1989).

6.3.4.2 Evolution law

The evolution law of damage is applied in the proposed model to describe the descending branch of the stress-strain behaviour of concrete. It is assumed to have the same form as that used to describe the softening part of the hardening rule adopted in Papanikolaou and Kappos's (2007) plasticity model. The following equation relates the damage variable ω_d to the internal variable κ:

$$\omega_d = 1 - c(\kappa) \tag{6.19}$$

where $c(\kappa)$ has the same form as that of Eq. (5.6).

A process similar to that suggested by Grassl and Jirasek (2006) was

adopted to calculate stress components from corresponding strain increments. More detailed information such as the evaluation of nominal stresses from effective stresses based on the calculated value of the damage variable can be found in Grassl and Jirasek (2006).

6.3.5 Calibration

Papanikolaou and Kappos's (2007) model was implemented in ABAQUS through a user-defined material subroutine (UMAT). The test results for actively-confined concrete reported by Candappa et al. (1999) were again used to verify the proposed constitutive model. The process of parameter calibration for the PDPK model is the same as that of Papanikolaou and Kappos's (2007) model. The values previously determined for A, B, and C for Papanikolaou and Kappos's (2007) model were directly used in the proposed model. Only the value of t_p needed to be revised from 0.003 to 0.009 to fit the slope of the descending branch. The same finite element model as described in Chapter 4 was still used except that the constitutive model was replaced by the present constitutive model. The finite element predictions based on the present model are compared with the test results in Fig. 6.4; values of the model parameters are given in the figure. It can be found that the predicted stress-strain curves compare favorably with the test results. Indeed, the performance of the PDPK model is similar to that of Papanikolaou and Kappos's (2007) model.

Finally, test results of FRP-confined concrete were used for assessing the capability of the proposed constitutive model. Except for the value of t_p, the values for other parameters are the same as those previously determined for Papanikolaou and Kappos's (2007) model. The value of t_p was determined to fit the axial stress- strain and axial stress-lateral strain curves of FRP-confined concrete with a confinement stiffness equal to 1086 MPa; a value of 0.018 was found from this process. A comparison of the finite element results with the experimental results for this confinement stiffness is given in Fig. 6.5a. It is seen that the finite element results are accurate. However, when this value for t_p was used to provide predictions for FRP-confined concrete with a confinement stiffness equal to 543 MPa, the finite element predictions overestimate the experimental axial strains. The performance of the PDPK model for FRP-confined concrete is also similar to that of the original plasticity model proposed by Papanikolaou and Kappos (2007). This phenomenon indicates that although different approaches (softening plasticity and damage) were used for the description of the softening behaviour of concrete, no significant difference is observed from the predicted lateral deformation response. Therefore, it can be concluded that as long as proper values for the model parameters are employed, a plasticity model and a plastic-damage model provide similar results for confined concrete under monotonic loading. It should be noted that if unloading becomes important, only a plastic-damage model can

predict stiffness degradation as the degree of damage increases.

6.3.6 Discussions

Based on the parameter calibration and the model assessment presented above, it can be concluded that the PDPK model provides predictions which are similar to those obtainable from Papanikolaou and Kappos's (2007) plasticity model. The values of all parameters except t_p can be the same as those in Papanikolaou and Kappos's (2007) model; the value of t_p should be approximately three times its value in Papanikolaou and Kappos's (2007) model. According to existing studies such as Grassl and Jirasek (2006), the proposed model is a more stable model than Papanikolaou and Kappos's (2007) model as it simulates stress reductions after the peak stress by reductions in elastic constants instead of retractions of the yield surface in the stress space (Yu et al. 2010). The plastic damage model does, however, still suffer from the same incapability in modelling FRP-confined concrete as the plasticity model is based on. This shortcoming may be overcome by employing a more complex damage model such as a vector damage model (e.g. Carol et al. 2001).

6.4 CONCLUSIONS

In this chapter, the performance of two types of plastic-damage models in predicting the stress-strain response of plain concrete in uniaxial and equal tri-axial compression has been examined. In both approaches, the yield

surface is assumed to remain unchanged after the attainment of the peak stress of concrete, the plasticity part is based on isotropic hardening described in the effective stress space, and the damage part is driven by the plastic volumetric strain or normalized plastic volumetric strain.

Comparisons between the finite element predictions and the experimental results have been presented to assess the capability of these two approaches. It seems that both approaches can provide accurate predictions for both unconfined concrete and actively-confined concrete provided that properly calibrated parameters are used. However, they both fail to provide accurate predictions for FRP-confined concrete with different confinement stiffnesses. This weakness is inherited from the plasticity model they are based on and has not been overcome or alleviated by the use of an isotropic damage model to describe the post-peak softening behaviour of concrete. An anisotropic damage model may be necessary so that the predicted lateral-to-axial strain relationship for confined concrete can be significantly changed. This is beyond the scope of the present chapter.

Based on the assessment of the four types of concrete constitutive models as presented in Chapters 4, 5 and 6, it may be concluded that both the scaling technique and the use of a novel hardening variable only help in the modelling of concrete under active confinement where the confining

pressure is independent of lateral deformation. For FRP-confined concrete, which is a typical form of passive confinement, the accurate prediction of lateral deformation is an important issue, but improvement in the hardening rule or inclusion of damage has insignificant effects on the predicted lateral deformation. As the accurate prediction of lateral deformation of confined concrete is the key to the accurate prediction of the behaviour of passively-confined concrete, this aspect will be examined in detail in the subsequent chapters.

6.5 REFERENCES

Candappa, D. P., Setunge, S., and Sanjayan, J. G. (1999). "Stress versus strain relationship of high strength concrete under high lateral confinement." *Cement and Concrete Research*, 29(12), 1977-1982.

Carol, I., Rizzi, E., Willam, K.J. (2001). "On the formulation of anisotropic elastics degradation. II. Generalized pseudo-Rankine model for tensile damage." *International Journal of Solids and Structures*, 38, 519–546.

Etse, G., and Willam, K. (1994). "Fracture energy formulation for inelastic behaviour of plain concrete." *Journal of Engineering Mechanics*-ASCE, 120(9), 1983-2011.

Grassl, P., and Jirasek, M. (2006). "Damage-plastic model for concrete failure." *International Journal of Solids and Structures*, 43(22-23),

7166-7196.

Imran, I., and Pantazopoulou, S. J. (1996). "Experimental study of plain concrete under triaxial stress." *ACI Materials Journal*, 93(6), 589-601.

Imran, I., and Pantazopoulou, S. J. (2001). "Plasticity model for concrete under triaxial compression." *Journal of Engineering Mechanics*-ASCE, 127, 281.

Jason, L., Huerta, A., Pijaudier-Cabot, G., and Ghavamian, S. (2006). "An elastic plastic damage formulation for concrete: Application to elementary tests and comparison with an isotropic damage model." *Computer Methods in Applied Mechanics and Engineering*, 195(52), 7077-7092.

Kupfer, H., Hilsdorf, H. K., and Rusch, H. (1969). "Behaviour of concrete under biaxial stresses." *ACI Journal Proceedings*, 66, 656-666.

Lee, J. H., and Fenves, G. L. (1998). "Plastic-damage model for cyclic loading of concrete structures." *Journal of Engineering Mechanics*-ASCE, 124(8), 892-900.

Lubliner, J., Oliver, J., Oller, S., and Onate, E. (1989). "A Plastic-damage model for concrete." *International Journal of Solids and Structures*, 25(3), 299-326.

Mazars, J., and Pijaudier-Cabot, G. (1989). "Continuum damage theory: Application to concrete." *Journal of Engineering Mechanics*-ASCE,

115(2), 345-365.

Menetrey, P., and Willam, K. J. (1995). "Triaxial failure criterion for concrete and its generalization." *ACI Structural Journal*, 92(3), 311-318.

Papanikolaou, V. K., and Kappos, A. J. (2007). "Confinement-sensitive plasticity constitutive model for concrete in triaxial compression." *International Journal of Solids and Structures*, 44(21), 7021-7048.

Patzák, B. and Bittnar Z. (2001). "Design of object oriented finite element code." *Advances in Engineering Software*, 32(10-11),759-767.

Wolf, J. (2008). *A plasticity model to predict the effects of confinement on concrete,* California Institute of Technology.

Yu, T., Teng, J. G., Wong, Y. L., and Dong, S. L. (2010). "Finite element modelling of confined concrete-II: Plastic-damage model." *Engineering Structures*, 32(3), 680-691.

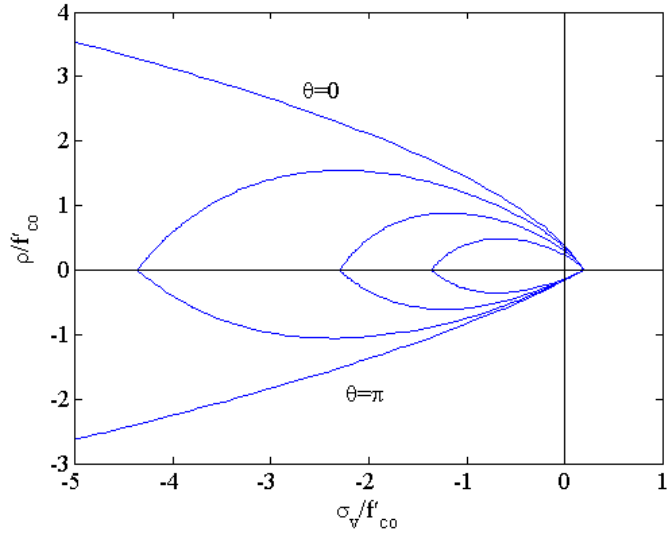

Figure 6.1 Yield surface of the constitutive model proposed by Grassl and Jirasek (2006)

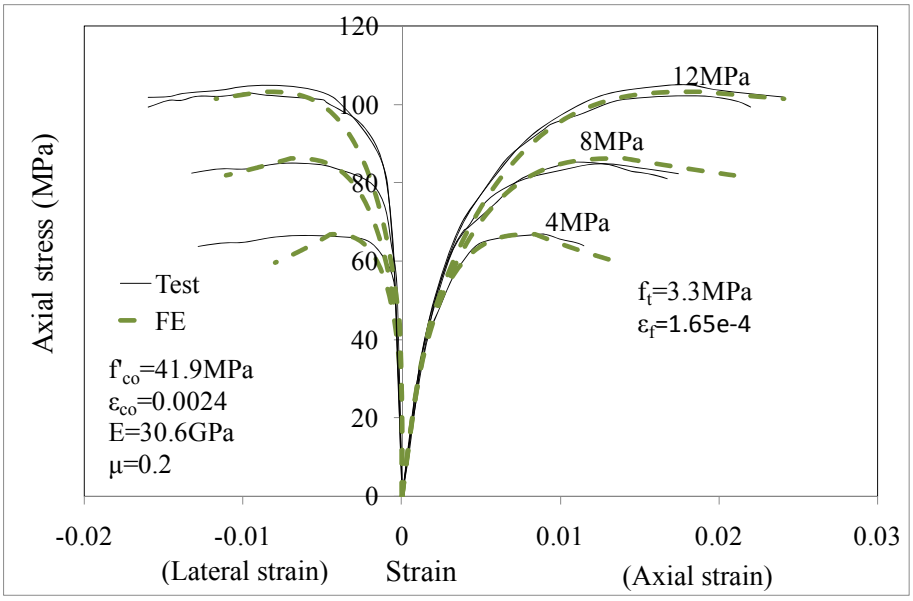

Figure 6.2 Comparison between finite element results based on Grassl and Jirasek's (2006) model and test results from Candappa et al. (1999) for actively-confined concrete

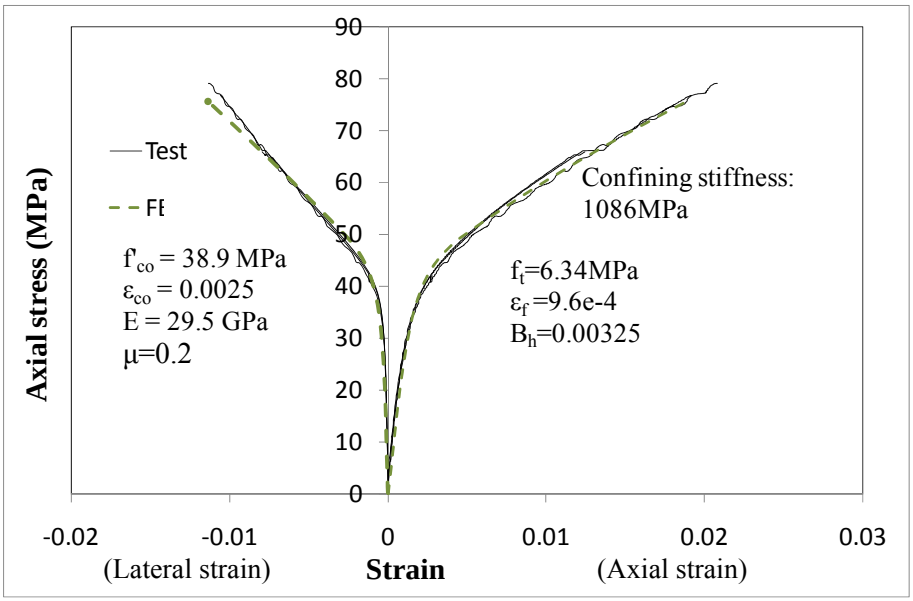

(a) FRP-confined concrete with the confining stiffness equal to 1086 Mpa

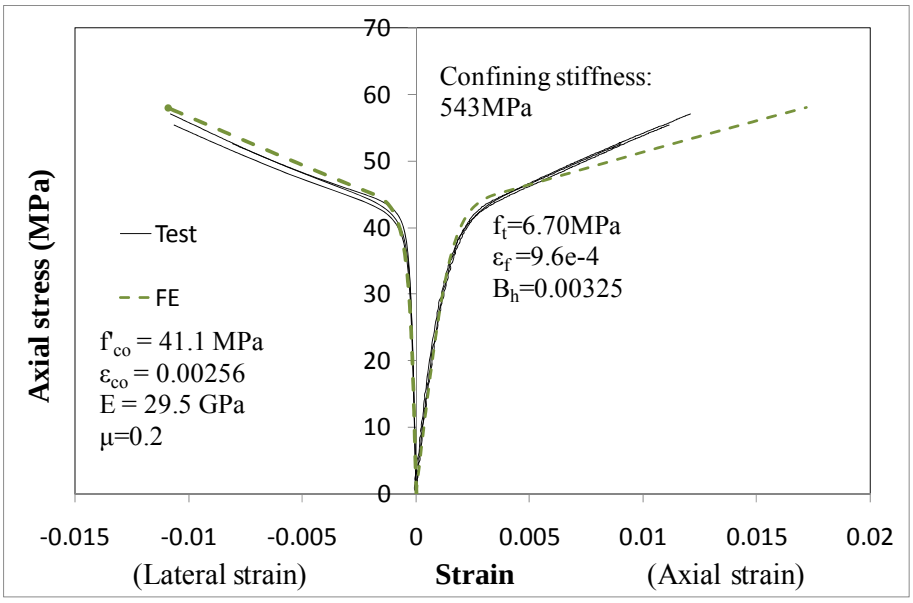

(b) FRP-confined concrete with the confining stiffness equal to 543 MPa

Figure 6.3 Comparison between finite element results based on Grassl and Jirasek's (2006) model and test results from Lam et al. (2006) for FRP-confined concrete

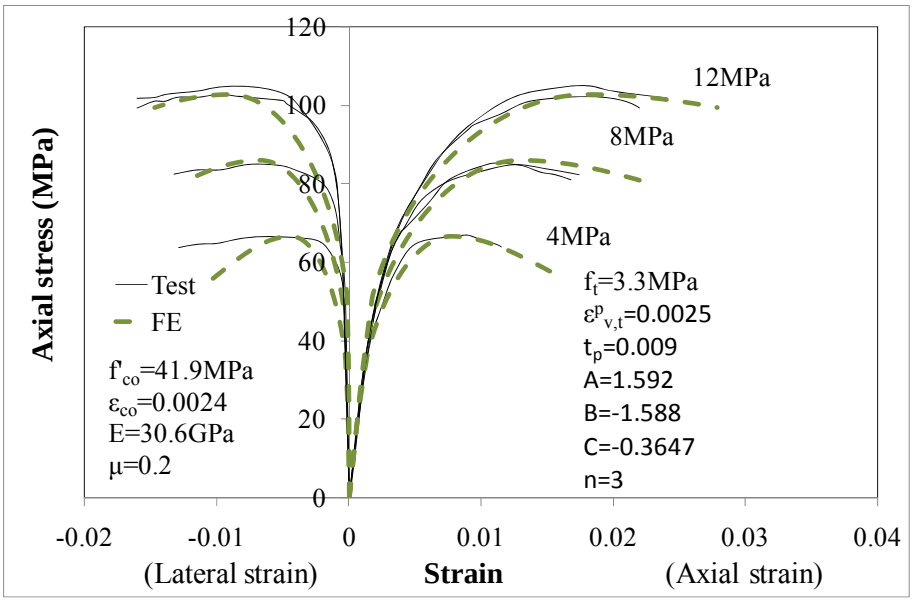

Figure 6.4 Comparison between finite element results based the PDPK model and test results from Candappa et al. (1999) for actively-confined concrete

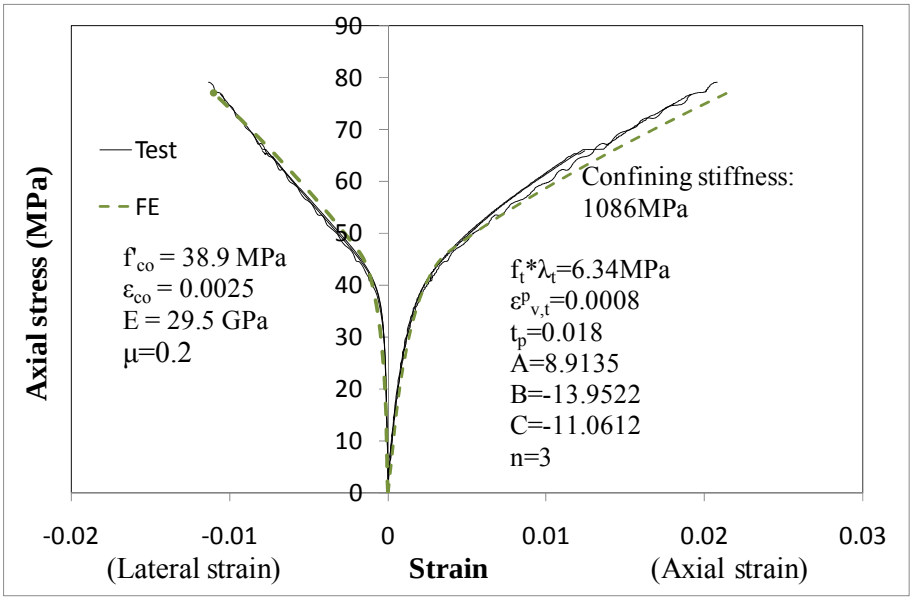

(a) FRP-confined concrete with the confinement stiffness equal to 1086 MPa

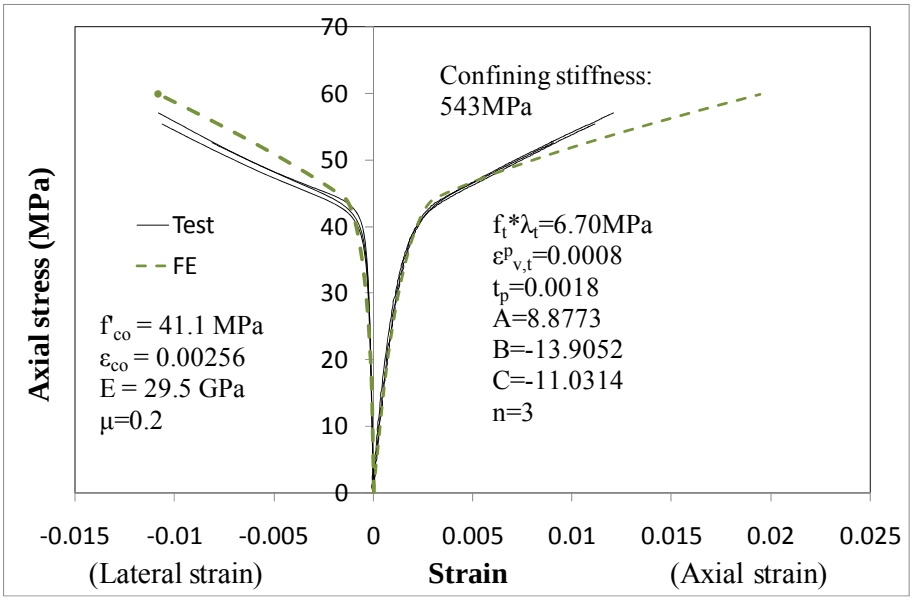

(b) FRP-confined concrete with the confinement stiffness equal to 543 MPa

Figure 6.5 Comparison between finite element results based on the PDPK model and test results from Lam et al. (2006) for FRP-confined concrete

CHAPTER 7

MICROPLANE MODEL FOR CONFINED CONCRETE

7.1 INTRODUCTION

Based on the discussions in the previous chapters, one important application of FRP composites is as wraps or jackets for the confinement of reinforced concrete (RC) columns for enhanced strength and ductility. To consider the effect of confining stresses which act orthogonally to the direction of the main compressive stresses, particularly when the stresses vary over the section (i.e. non-uniform confinement), a three-dimensional (3-D) concrete constitutive model is required. Many constitutive models have already been proposed for concrete under multi-dimensional stress states (see Chapters 2, 4-6). Different theoretical frameworks have been used in formulating these models, including nonlinear elasticity models, plasticity models, plastic-damage models, and endochronic models for concrete (Chen and Han 2007). Although, great achievements have been made in the modelling of concrete by applying these macroscopic constitutive models such as nonlinear elastic and elasto-plastic models for both actively confined concrete (i.e. confined by a constant confining pressure) and passively confined concrete (i.e. confined by an increasing confining pressure as the concrete dilates)(Mirmiran et al. 2000; Yeh and Chang 2007; Yu et al. 2010a; Yu et al. 2010b), there is still the need to

develop better approaches for modelling the confinement mechanism of concrete.

In recent years, the microplane model (Bazant et al. 2000) has attracted increasing attention from researchers interested in modelling the stress-strain behaviour of confined concrete due to its intrinsic advantages(Liu and Foster 2000; Ghazi et al. 2002; Baky et al. 2010). The microplane model is a general 3-D constitutive model which describes the complicated inelastic properties of concrete based on one dimensional (1-D) stress-strain models defined on planes at various orientations at a material point. On each of those micro planes, the microstrains are obtained through the projection of the strain tensor based on the concept of kinematic constraint. The micro stresses can be calculated from the corresponding micro strains (using the previously defined 1-D stress-strain models), and finally the stress tensor is derived from these micro stresses using the principle of virtual work. This process avoids the direct description of the complex relationships between the stress tensor and the strain tensor, at the expense of a larger amount of calculation. The major advantage of the microplane model is its conceptual simplicity. Another salient feature of this approach is that it relies on relationships at the microscopic level instead of the macroscopic level. The so-called micro planes may be imagined to represent damage planes or weak planes in the micro-structure of concrete material. It is well-known that certain macroscopic phenomena of concrete can be reasonably well interpreted using microscopic mechanisms.

For instance, the shear dilation effects of concrete can be easily explained by the difference between the magnitudes of the tensile and the compressive deviatoric boundaries. Due the intrinsic advantages mentioned above, the microplane model is a promising constitutive model for predicting the mechanical response of concrete, especially its confinement mechanism.

Despite the advantages listed above, some drawbacks also exist in the original microplane models such as model M4 (Bazant et al. 2000).These drawbacks primarily exist in the computational aspects as summarized by Nemecek et al. (2002) and Tue et al. (2008). Existing investigations on confined concrete using microplane models (Liu and Foster 2000; Ghazi et al. 2002; Baky et al. 2010) are all based on their original versions without eliminating the associated drawbacks. To achieve reliable predictions using microplane models, it is necessary to eliminate these drawbacks from the analysis. The aim of this chapter is to present a modified version of microplane model M4 to whose associated drawbacks have been eliminated.

In the following sections, the concepts and corresponding equations for the microplane model M4 are first briefly recalled for the completeness. This is then followed by presenting the remedies for the M4 model. In the following sections, the microplane model M4 is referred to as the M4 model for brevity.

7.2 FORMULATION FOR THE M4 MICROPLANE MODEL

7.2.1 Formulations for Microplane Model Proposed by Bazant et al. (2000)

Seven versions of the microplane model have been developed by Bazant and his co-workers (Bazant and Caner 2005). These seven versions are named as M1 through M7, with M7 being the latest version. The most frequently used versions are M2 and M4 (Liu and Foster 2000; Ghazi et al. 2002; Di Luzio 2007; Baky et al. 2010) instead of the latest version M7. For confined concrete, the M4 model is preferred as it has almost the same stress-strain behaviour within the compression regime as that of the latter version (i.e. microplane model M5) but has a relatively simple formulation.

As mentioned earlier, the formulation used in the microplane approach describes the complicated inelastic properties of concrete through individual micoplanes which can be at all possible orientations at a material point. The kinematic constraint, which is a basic hypothesis of the microplane model, is applied to determine the micro-strains from the macro-strain tensor. Based on the kinematic constraint assumption, the micro-strains on a microplane are projections of the macro strain tensor on that plane. As a result, the normal and the shear strain components on each microplane according to the M4 model are as follows(Bazant et al. 2000):

$$\varepsilon_N = N_{ij}\varepsilon_{ij},\ \varepsilon_M = M_{ij}\varepsilon_{ij},\ \varepsilon_L = L_{ij}\varepsilon_{ij} \tag{7.1}$$

$$N_{ij} = n_i n_j, M_{ij} = \frac{m_i n_j + m_j n_i}{2}, L_{ij} = \frac{l_i n_j + l_j n_i}{2} \quad (7.2)$$

Where ε_{ij} is the macro-strain tensor, ε_N is the normal strain on a microplane, and ε_L and ε_M are components of shear strains on the same microplane; m_i and l_i (i=1-3) are the two orthogonal unit coordinate vectors lying within the microplane,and n_i is the unit normal vector characterizing the orientation of the microplane. Fig. 7.1 shows the definition of a microplane and its corresponding micro-strain components.

The normal strain component can be further decomposed into a volumetric strain ε_V and a deviatoric strain ε_D within the small strain regime [for finite strain, different equation was proposed (see Bazant et al. 1996)]; that is (Bazant et al. 2000)

$$\varepsilon_V = \varepsilon_{kk} \quad (7.3)$$

and

$$\varepsilon_D = \varepsilon_N - \varepsilon_V \quad (7.4)$$

The governing relationships between the micro-stresses and the micro-strains are defined using incremental elastic relations and stress-strain boundaries that cannot be exceeded. The incremental elastic relations within the boundaries are given by (Bazant et al. 2000):

$$d\sigma_V = E_V d\varepsilon_V, d\sigma_D = E_D d\varepsilon_D, d\sigma_M = E_T d\varepsilon_M, d\sigma_L = E_T d\varepsilon_L \quad (7.5)$$

and

$$E_V = \frac{E}{1-2\mu},\ E_D = \frac{5E}{(1+\mu)(2+3v)},\ E_T = vE_D \tag{7.6}$$

where E is the initial modulus of elasticity of concrete; E_V, E_D and E_T are the volumetric, deviatoric and tangential muduli of elasticity, respectively; μ is the Poisson's ratio and v is the ratio of the tangential modulus (modulus in the tangential direction of the microplane) to the deviatoric modulus; σ_V and σ_D are the volumetric and deviatoric stress components on the microplane; and σ_L and σ_M are components of shear stresses on the microplane. The stress boundaries are given by the following equations(Bazant et al. 2000):

$$\sigma_v^b = \begin{cases} -Ek_1k_3e^{\left(-\frac{\varepsilon_V}{k_1k_4}\right)},\ \sigma_v < 0 \\ \frac{E_v k_1 c_{13}}{[1+(c_{14}/k_1)\langle\varepsilon_V - k_1c_{13}\rangle]^2},\ \sigma_v \geq 0 \end{cases} \tag{7.7}$$

$$\sigma_D^b = \begin{cases} \frac{Ek_1c_8}{1+[\langle-\varepsilon_D - k_1c_8c_9\rangle/k_1c_7]^2},\ \sigma_D < 0 \\ \frac{Ek_1c_5}{1+[\langle-\varepsilon_D - k_1c_5c_6\rangle/k_1c_{18}c_7]^2},\ \sigma_D \geq 0 \end{cases} \tag{7.8}$$

$$\sigma_N^b = Ek_1c_1\exp\left(-\frac{\langle\varepsilon_N - c_1c_2k_1\rangle}{c_3k_1+\langle-c_4(\sigma_V/E_v)\rangle}\right) \tag{7.9}$$

$$\sigma_T^b = \frac{E_Tk_1k_2c_{10}\langle-\sigma_N+\sigma_N^0\rangle}{E_Tk_1k_2+c_{10}\langle-\sigma_N+\sigma_N^0\rangle} \tag{7.10}$$

with

$$\sigma_N^0 = \frac{E_Tk_1c_{11}}{1+c_{12}\langle\varepsilon_V\rangle} \tag{7.11}$$

In the above equations, σ_v^b, σ_D^b, σ_N^b, and σ_T^b are the volumetric, deviatoric, normal and shear stress boundaries, respectively. The parameters k_1 to k_4

and c_{18} are the adjustable parameters, used to define the concrete strength and the general stress-strain behaviour. Parameter c_1 to c_{17} are the fixed or weakly adjustable parameters which have already been calibrated by some standard tests. Their values as recommended by Caner and Bazant(2000) and their main roles are summarized in table 7.1.

After determining the micro-stresses on a microplane, the macroscopic stress tensor is derived from the micro-stresses based on the principle of virtual work for the surface Ω of a unit hemisphere (due to the symmetry of the stress tensor and the strain tensor)(Bazant et al. 2000):

$$\sigma_{ij} = \sigma_V \delta_{ij} + \frac{3}{2\pi}\int_\Omega s_{ij}^D \, d\Omega \tag{7.12}$$

$$s_{ij}^D = \sigma_D \left(n_i n_j - \frac{\delta_{ij}}{3}\right) + \sigma_L L_{ij} + \sigma_M M_{ij} \tag{7.13}$$

$$\frac{3}{2\pi}\int_\Omega s_{ij}^D \, d\Omega \approx 6\sum_{mp=1}^{N_m} w_{mp}\left(\sigma_D^{mp}\left(n_i n_j - \frac{\delta_{ij}}{3}\right) + \sigma_L^{mp} L_{ij} + \sigma_M^{mp} M_{ij}\right) \tag{7.14}$$

The integral of the micro-stresses over the unit hemisphere in Eq. (7.12) is approximated by Gaussian integration in numerical calculations as shown in Eq. (7.14). Integration formulas proposed by Bazant and Oh (1985) with the number of microplanes N_m equal to 21 and 28 on the hemisphere are commonly used. In these integration schemes, each microplane is identified by its corresponding plane number mp with the orientations (n_i) and the weights (w_{mp}). After sweeping through all the microplanes (i.e. $mp = 1, \dots, N_m$), the stress tensor σ_{ij} can be calculated. The detailed values of the n_i, w_{mp}, and

N_m for a selected integration scheme can be found in the published literature such as Bazant and Oh (1985).

7.2.2 Remedies for the Computational Aspects of the M4 Model

As mentioned earlier, drawbacks exist in the M4 model mainly in the computational aspects; these drawbacks have been identified by previous researchers (Nemecek et al. 2002; Di Luzio 2007; Tue et al. 2008) during numerical implementation and testing. These drawbacks compromise the accuracy and reliability of the microplane model and need to be addressed before the constitutive model can be used for providing accurate predictions for the material behaviour of concrete. These deficiencies include: (1) directional bias for micro shear stress, (2) strain increment magnitude dependence of model, (3) integration scheme dependence; and (4) significant loading direction dependence of the numerical results. These issues are examined and the remedies are proposed in the remainder of this sub-section.

For the original M4 model (Bazant et al., 2000), two alternative algorithms (namely Alt-I and Alt-II) were developed to calculate the micro-shear stresses in the orientations of the two orthogonal vectors, $\vec{l}$ and $\vec{m}$, within the microplane. Alt-I calculates the shear stresses in the $\vec{l}$ and $\vec{m}$ directions and imposes on the two components the following stress boundaries: $\sigma_L = \mathrm{Sign}(\sigma_L^e)\min\left(|\sigma_T^b|, |\sigma_L^e|\right)$ and $\sigma_M = \mathrm{Sign}(\sigma_M^e)\min\left(|\sigma_T^b|, |\sigma_M^e|\right)$. Alt-II calculates the resultant of the elastic shear stress as $\sigma_T^{eR} = \sqrt{(\sigma_L^e)^2 + (\sigma_M^e)^2}$

and determines the two shear stress components as $\sigma_L = \min\left(\sigma_T^b, \sigma_T^{eR}\right)\frac{\sigma_L^e}{\sigma_T^{eR}}$ and $\sigma_M = \min\left(\sigma_T^b, \sigma_T^{eR}\right)\frac{\sigma_M^e}{\sigma_T^{eR}}$ according to the boundary $[\min\left(\sigma_T^b, \sigma_T^{eR}\right)]$ and the unit vector in the direction of the resultant (e.g. $\frac{\sigma_L^e}{\sigma_T^{eR}}$).

Compared to Alt-II, Alt-I is a numerically more effective approach in terms of computational efficiency; it can reduce the computational cost significantly and up to about 50% (Cancer and Bazant 2000). For this reason, in numerical implementations using the M4 microplane model such as ATENA, Alt-I is frequently used. However, it has been revealed by Di Luzio (2007) that Alt-I leads to predictions which are direction-dependent (Fig. 7.2): the predictions are sensitive to the direction of the applied displacement. This direction bias is due to the identical stress-strain relationship adopted for the two components of the micro shear stresses and the non-symmetric distribution of the directions of the $\vec{l}$ and $\vec{m}$ vectors due to the limitation of the integration scheme. These non-symmetric distribution of the directions results from the definitions of the direction vectors of $\vec{l}$ and $\vec{m}$. Within a given micro plane, the direction of $\vec{l}$ and $\vec{m}$ can be defined arbitrarily so long as they are perpendicular to each other. To eliminate this uncertainty, one of the direction vectors such as $\vec{m}$ is chosen to be normal to the axes (i.e. X, Y, Z axis); other direction vector $\vec{l}$ is thus obtained as the vector product, $\vec{l}=\vec{m}\times\vec{n}$. To minimize the direction bias of $\vec{l}$ and $\vec{m}$, $\vec{m}$ is often chosen to be normal to

axis X, Y, or Z alternatively. However, in most integration schemes, the number of integration point is not in multiples of three. Therefore, this direction bias cannot be totally eliminated. Due to this direction bias, the constitutive model becomes sensitive to the direction of the applied displacement. Fig. 7.2a shows that the predicted stress-strains for the uni-axial compression are different when displacements are applied in three selected orthogonal direction (i.e. X, Y, Z axis) if Alt-I is adopted. This discrepancy disappears if Alt-II is used (see Fig. 7.2b). Based on these observations, Alt-II was subsequently used in all numerical analyses of the present study instead of Alt-I to eliminate this directional bias problem.

In addition to the use of Alt-II to remove the directional dependence of the M4 model for the case of loading in three arbitrary orthogonal directions, it has also been revealed by Tue et al. (2008) that if the orientations of the microplanes cannot be evenly distributed with respect to the three directions of the X, Y, Z coordinates, more than 480 microplanes are required in the integration scheme to eliminate the directional dependence of the M4 model for all possible loading directions, leading to a highly costly process. In practical applications, directional dependence can be partly remedied by the use of a large number of finite elements, and as a result, the integration scheme with 61 microplanes has been recommended by Tue et al. (2008) as an optimal scheme.

Furthermore, it has been shown by Nemecek et al. (2002) that the response of the M4 model under uni-axial compression is dependent on the magnitudes of strain increments. The Alt-II algorithm predicts different stress-strain responses for small and large strain increments after the point of peak stress has been reached (Fig. 7.3). It is difficult to find a single critical strain increment value which yields a stable response as this critical strain value depends on the loading condition. This drawback can be eliminated by using a revised algorithm for the evaluation of the micro volumetric stress. This method, which was first proposed by Tue et al. (2008), involves an additional step used to ensure the convergence of the micro volumetric stress σ_v within the strain increment. In the original M4 model, σ_v is recalculated as the average of the microplane normal stress; it is often different from that calculated from the volumetric stress boundary. This difference is found to be the main reason of the strain-increment-magnitude-dependency. A detailed description of this algorithm can be found in Tue et al. (2008). This algorithm is also employed in the M4 model presented in this chapter to eliminate the possible dependence of predictions on the strain increment.

As mentioned above, the stress tensor σ_{ij} is derived through summation of the micro-stresses over all spatial orientations. Only a finite number of orientations can be used in the numerical process so that numerical Gaussian integration schemes with 21, 28, 37 and 61 integration points (i.e. microplanes)

are commonly used. Starting from the M2 version, it has been found that these integration schemes cannot achieve convergence for the axial stress-volumetric strain response (Badal and Leblond 2004). This drawback also exists in the M4 model as has been described by Nemecek et al. (2002) and Tue et al. (2008). For the M2 microplane model, it was found that at least 120 Guassian integration points are required to achieve a macroscopic response independent of the integration scheme (Badal and Leblond 2004). Fig. 7.4 shows that the axial stress-volumetric strain curves obtained from the M4 model with different integration schemes but with the same values for the material parameters. Although only integration schemes of up to 61 integration points were proposed by by Bazant's group, results from higher order integration schemes (with 132 and 208 integration points) proposed by Heo and Xu (1998) are also considered in the comparison. It can be found from Fig. 7.4 that although it is hard to achieve strict convergence of the axial stress-volumetric strain relationship due to the localization of micro stress-strain behaviour when a limited number of microplanes is used, the response of the integration scheme with 61 points can be approximately taken as the convergent result. Increasing the number of integration points further to 132 or even 208 only has a small effect on the far post-peak range of the overall axial stress-volumetric strain curve; these three curves (corresponding to 61, 132 and 208 integration points) are nearly identical for the majority of the full range. In the subsequent analyses, the parameters of the M4 model

were calibrated based on the integration scheme with 61 integration points.

The numerical tests presented in this chapter were conducted using an in-house code based on Matlab, and all the revisions of the M4 model as discussed above were implemented. In the present study, as the focus is on the stress-strain behaviour of concrete under uniform confinement, only the stress-strain behaviour of a single material point needs to be investigated due to the uniformity of the stress and strain distributions within a specimen (e.g. a circular concrete cylinder confined by an FRP jacket). Therefore, a driver of a material subroutine is enough for the numerical analyses undertaken for this chapter.

For concrete under active confinement, the confinement is simply a constant confining pressure; for a circular concrete cylinder confined by an FRP jacket (a typical case of passively confined concrete), the confinement can be represented by a constant confining stiffness ($k_{stiff} = \frac{2E_j t_j}{D}$ where E_j and t_j are respectively the elastic modulus and the thickness of the FRP jacket); the confining stiffness represents the rate of confinement increase at a material point. For brevity, in the following descriptions, the term "FRP-confined concrete" is used to refer to concrete in a circular solid concrete cylinder confined with an FRP jacket unless otherwise specified. A salient feature of the M4 model is that the calculation of a stress increment corresponding to a

strain increment is generally explicit. Once the strain loading paths are given, it is easy to calculate the corresponding stresses. However, some special strain loading paths used in calibrating the parameters of the material model, such as uni-axial compression and equal tri-axial compression etc. cannot be represented by an explicit strain loading paths. For these purposes, an outer iteration algorithm was adopted in the present study to obtain the required strain loading paths for concrete under uni-axial compression, equal tri-axial compression (i.e. concrete under active confinement), and axial compression with FRP confinement. The procedure consists of the following 4 steps:

- Step1: Consider the previous strain vector $\varepsilon^{pre} = \{\varepsilon_1^{pre} \quad \varepsilon_2^{pre} \quad \varepsilon_3^{pre} \quad 0 \quad 0 \quad 0\}$ and the previous stress vector $\sigma^{pre} = \{\sigma_1^{pre} \quad \sigma_2^{pre} \quad \sigma_3^{pre} \quad 0 \quad 0 \quad 0\}$
- Step 2: Assume a strain vector increment $\Delta\varepsilon^0 = \{-\Delta\varepsilon_1 \quad \Delta\varepsilon_1 \quad \Delta\varepsilon_1 \quad 0 \quad 0 \quad 0\}$;
- Step3: Using the modified microplane algorithm to calculate the stress vector $\sigma = \{\sigma_1 \quad \sigma_2 \quad \sigma_3 \quad 0 \quad 0 \quad 0\}$. If $|\sigma_2 + f_l| < \delta$ & $|\sigma_3 + f_l| < \delta$, $\sigma^{pre} = \sigma$ & $\varepsilon^{pre} = \varepsilon^{pre} + \Delta\varepsilon^0$ and return to step 2; if not, go to step 4;
- Step 4: $\Delta\varepsilon^i = \Delta\varepsilon^{i-1} + \{0 \quad f_l - \sigma_2 \quad f_l - \sigma_3 \quad 0 \quad 0 \quad 0\}/E$, and return to step 3.

Through this iterative algorithm, a strain increment in each loading step satisfying the strain and the stress boundaries was found so that spurious loading and unloading path does not appear in the overall strain loading path (i.e. the strain increment is tried until a stress increment which satisfies the stress boundary condition is achieved). The confining pressure f_l varies with the specified stress boundaries. For unconfined concrete, it equals to zero; for actively confined concrete, it equals to the confining pressure; and for FRP confined concrete, it equals to $k_{stiff} * \varepsilon_2^{pre}$, in which k_{stiff} is the confining stiffness provided by the FRP jacket.

This chapter aims to clarify the effects of the parameters of the M4 model on its performance in predicting the behaviour of both actively confined concrete and FRP-confined concrete, and to identify the key characteristics that the M4 model need to possess in order to provide accurate predictions of experimental results for confined concrete. A thorough assessment is presented of the M4 model including the previous modifications with the same coefficients for both actively-confined concrete and FRP-confined concrete; further refinements to achieve even closer predictions for experimental data are also presented.

7.3 IDENTIFICATION OF PARAMETERS OF THE M4 MODEL

As mentioned earlier, for the M4 model, seventeen of the parameters ($c_1 - c_{17}$) are weakly adjustable parameters whose values can be used to describe the

intrinsic behaviour of the concrete material. The other five adjustable parameters ($k_1 - k_4$ and c_{18}) as well as the initial modulus E are commonly used to fit the experimental data. For any stress-strain curve, E controls its vertical scaling transformation, k_1 controls its radial scaling transformation, c_{18} controls the slope of the post-peak range of the uni-axial compressive stress-strain response, and $k_2 - k_4$ mainly influence the shape of the stress-strain curve at very high levels of confinement. At a lower confinement level, which covers the majority of cases encountered in civil engineering applications, the roles of $k_2 - k_4$ are less important.

In the present study, k_1, E, and c_{18} were firstly assigned appropriate values to fit the axial stress-strain curve of concrete under uni-axial compression. Next, the axial stress-strain relationship of confined concrete predicted using the values for k_1, E, and c_{18} obtained from uni-axial compression was examined to check the performance of the M4 model before refinement; this examination is based on comparison between predictions using the M4 model and those using an analysis-oriented stress-strain model proposed by Jiang and Teng (2007). As mentioned earlier, this analysis-oriented stress-strain model (an analytical model) was derived from a test database that includes unconfined concrete, actively confined concrete and FRP-confined concrete; as a result, and in general it can closely predict experimental results.

Fig. 7.5 compares the results of the M4 model with those of the analytical model for unconfined concrete, indicating that the M4 model can represent the overall axial stress-strain behaviour of unconfined concrete quite well. In Fig. 7.6, the predictions of the M4 model are compared with those of the analytical model for actively-confined concrete, indicating that the M4 model is not so accurate for concrete under relatively low levels of confinement, which was also noted by Ghazi et al. (2002). Ghazi et al. (2002) found that the M4 model tends to underestimate the effect of confinement on concrete at low confinement levels as the parameters of the M4 model were calibrated using test data at very high confinement levels (i.e. with the confinement pressure being close to 2 times of the concrete strength). When employed for low confinement cases, some parameters require appropriate modifications to better predict the peak stress and the post-peak response of confined concrete. New formulas for parameters k_1, c_7 and c_{10} were proposed as functions of the confining pressure in Ghazi et al. (2002) to fit the results of their own analytical model (an empirical model for the stress-strain behaviour of actively-confined concrete).

In the present study, a similar approach to that of Ghazi et al. (2002) is employed to improve the performance of the M4 model for confined concrete including both actively-confined concrete and FRP-confined concrete. After a significant number of trials, the following functions were determined for

parameters k_1 and c_7:

$$k_1 = k_1^0 \text{ for } \frac{f_l}{f'_{co}} \leq 0.1 \tag{7.13}$$

$$k_1 = k_1^0 \left(1 + \frac{3}{5}\left(\frac{f_l}{f'_{co}} - 0.1\right)\right) \text{for} \frac{f_l}{f'_{co}} > 0.1 \tag{7.14}$$

$$c_7 = 50\left(1 + 28\frac{f_l}{f'_{co}}\right) \text{ for} \frac{f_l}{f'_{co}} \leq 0.05 \tag{7.15}$$

$$c_7 = 50\left(48\frac{f_l}{f'_{co}}\right) \text{ for} \frac{f_l}{f'_{co}} > 0.05 \tag{7.16}$$

where k_1^0 is the initial value of k_1 and it is commonly obtained by fitting the stress-strain curve of unconfined concrete.

Eqs.(7.13)-(7.14) are different from the corresponding equations in Ghazi et al. (2002) due to the following reasons. First, the algorithm of the M4 model used in this chapter is different from that used in Ghazi et al. (2002) as has been explained earlier (including revisions in the computational aspects). Secondly, different analytical models have been adopted to calibrate the parameters of the M4 model: in Ghazi et al. (2002), the calibration was based on the analytical model proposed by Attard and Setunge (1996) for actively confined concrete while in the present study, the calibration was based on an analytical model proposed by Jiang and Teng (2007) which is accurate for both actively-confined concrete and passively-confined concrete. In addition, the analytical model adopted in Ghazi et al. (2002) for parameter calibration includes a nonlinear equation for the peak stress, and as a result the coefficient c_{10} is thus a variable related to the confining pressure, while in Jiang and

Teng's (2007) model, a linear equation is used for the peak stress and as a result, c_{10} is a constant. The results of the modified M4 model and those of the analytical model proposed by Jiang and Teng (2007) are compared in Fig. 7.7. This figure shows that the modified M4 model is in good agreement with the analytical model proposed by Jiang and Teng (2007) for actively-confined concrete.

The performance of the modified M4 model for passively confined concrete is further examined in Fig. 7.8, where three confining stiffness values, being 600 MPa, 400MPa and 200 MP, are considered. This figure shows that the modified M4 model results in good agreement with Jiang and Teng's (2007) analytical model at higher confinement stiffness levels (e.g. with the confining stiffness equal to 600MPa) but underestimates the results of the analytical model at smaller confinement stiffness levels (e.g. with the confining stiffness equal to 400MPa or 200MPa). For a confining stiffness equal to 600MPa, the modified M4 model can closely predict the lateral strains at corresponding axial strains, Fig 7.9. When the confinement stiffness is equal to 400MPa or 200MPa, the modified model underestimates lateral strains significantly, Fig. 7.9. These results indicate that the modified M4 model, which provides accurate predictions for actively confined concrete, tends to underestimate the lateral dilation of FRP-confined concrete at relatively small confining stiffness levels. As FRP-confined concrete is subjected to a passive confining pressure

where the confinement is determined by the amount of lateral dilation of concrete, the dilation characteristics of concrete have a strong influence on the axial stress-strain response of FRP-confined concrete. Underestimations of lateral strains lead to underestimations of passive confinement and consequently inaccurate stress-strain responses even though the same model can closely predict the behaviour of actively-confined concrete. The inelastic volumetric dilation of FRP-confined concrete is thus of prime importance for the accurate prediction of stress-strain behaviour of FRP-confined concrete. The influences of the parameters of the M4 model on lateral strains and hence volumetric expansions are examined below.

In the M4 model, the dilation characteristics of concrete under compression is controlled by the normal or deviatoric boundary, mainly through the values of c_5, c_8, and c_{18}. Three other parameters, namely c_2, c_6, and c_9, also have some effect on the dilation characteristics, but their effect on the overall stress-strain behaviour is not so significant. Fig. 7.10 shows the effect of c_5 on the axial stress-strain and the axial stress-lateral strain responses. It can be observed that the lateral dilation and the overall axial stress-strain responses are substantially affected by c_5 which has a recommended value of 2.5. If this parameter is used to adjust the lateral strain behaviour, the previously calibrated parameters such as k_1 or E need be re-adjusted for unconfined concrete. This parameter is thus not suitable for fine-tuning the lateral

behaviour of the M4 model. Similar issues exist with c_{18} as it has been calibrated for the descending branch of unconfined concrete.

Fig. 7.11 shows the influence of c_8 on the axial stress-strain and axial stress-lateral strain responses. It is shown that changing the value of c_8 from the recommended value of 8 up to 16 or even 32 has negligible effect on axial stress-strain response but significantly changes lateral strains after the peak axial stress. Similarly, Fig. 7.12 shows that the axial stress-strain response of FRP-confined concrete is insensitive to c_8 and the predicted axial stress-strain curve is also close to the result of the analytical model. Due to these reasons, c_8 is thus used to adjust the dilation characteristics for FRP-confined concrete.

After a significant number of trials, the following functions were found to be suitable to define c_8:

$$c_8 = 8\left(5.8 - 0.56\frac{k_{stiff}}{f'_{co}}\right) \text{ for } 4 \le \frac{k_{stiff}}{f'_{co}} \le 7.5 \tag{7.17}$$

$$c_8 = 8\left(2.56 - 0.128\frac{k_{stiff}}{f'_{co}}\right) \quad \text{for} \frac{k_{stiff}}{f'_{co}} \le 12 \tag{7.18}$$

$$c_8 = 8\left(1.984 - 0.08\frac{k_{stiff}}{f'_{co}}\right) \quad \text{for} \frac{k_{stiff}}{f'_{co}} \le 19 \tag{7.19}$$

The performance of the final revised version of the M4 model for FRP-confined concrete (referred to as the $M4^+$ model) is examined in Figs. 7.13-7.14. The model provides close predictions of both the stress-strain

curves and the lateral-to-axial strain relationships predicted by Jiang and Teng's (2007) model. The success of this model confirms that an accurate prediction of the dilation properties is essential in modelling the behaviour of FRP-confined concrete or other passively-confined concrete.

In Fig. 7.15, the predictions of the $M4^+$ model are compared with the test results taken from Jiang and Teng (2007). The unconfined concrete strengths f'_{co} and the corresponding axial strains ε_{co} of the specimens as well as the confining stiffness of by the FRP jacket are shown in the figure. A major difference between the microplane model (including versions M1 to M7) and other constitutive models such as nonlinearly elastic models and plasticity models is that in the former f'_{co} and ε_{co} are not input parameters but are predicted by adjusting the values of k_1, E, and c_{18} as described earlier. The values of these three parameters used to fit the unconfined stress-strain curves are also given in the figure. The values of other parameters can be found in Table 7.1. Fig. 7.15 shows that the stress-strain curves predicted by the $M4^+$ model are in excellent agreement with the test results, and the bilinear property of FRP-confined concrete stress-strain curves can be properly captured by the $M4^+$ model.

When compared with the experimental results, the $M4^+$ model slightly underestimates the axial stress at the initiation of the second branch (i.e. the

transition point). This underestimation of axial stress may be still due to the underestimation of the lateral strain. As can be seen from Fig. 7.14, although the predicted axial strain-lateral strain response is close to that from the analytical model overall, the lateral strain near the transition point is still underestimated. A further refinement of the M4 model by relating c_8 to not only the confining stiffness but also other variables such as the confining pressure may be needed; such a further revision will however further increase the complexity of the $M4^+$ model. The accuracy of the $M4^+$ model is deemed to be acceptable for most practical applications.

7.4 CONCLUSIONS

The general behaviour of the M4 version of the microplane model (Bazant et al. 2000) (i.e. the M4 model) for confined concrete has been assessed in this chapter using both numerical results from an existing analytical model and experimental results. This assessment has shown that in order to achieve accurate prediction of the behaviour of FRP-confined and other passively confined concrete, the M4 model needs to be modified to possess at least the following two features: (a) the parameters which control the slope of the descending branches such as k_1 and c_7 should be dependent on the confining pressure; (b) the parameters which control the lateral dilation such as c_8 should be dependent on the rate of confinement increment. Parameter c_8 is recommended for achieving the second feature because its value has

insignificant effect on the predictions for the unconfined concrete strength and the corresponding axial strain. A modified M4 model possessing these two features, referred to as the $M4^+$ model, has been presented in this chapter and implemented into an in-house Matlab code. Comparisons between numerical predictions obtained using the $M4^+$ model and test results have shown that the $M4^+$model can provide accurate predictions for both actively-confined concrete and FRP-confined concrete. A step by step process of calibrating the parameters of the M4 model to achieve such accurate predictions for the stress-strain behaviour of FRP-confined concrete has also been explained in the chapter. The $M4^+$ model is a predictive model with sufficient accuracy for most practical applications. Further refinement of the $M4^+$model is possible to improve its predictions for the lateral strain near the transition point of the bi-linear stress-strain curve, but such refinement will come with additional complexity which may not be worthwhile.

7.5 REFERENCES

Attard, M. M., and Setunge, S. (1996). "Stress–strain relationship of confined and unconfined concrete."*ACI Material Journal*, 93(5), 432-442.

Baky, A., Demer, M., Yahiaoui, A., and Neale, K. W. (2010). "Nonlinear micromechanics-based finite element analysis of FRP-wrapped concrete columns subjected to axial load " *Proceeding of the 5th*

International Conference on FRP Composites in Civil Engineering, September 27-29, 2010, Beijing, China, 626-629.

Bazant, Z. P., and Caner, F. C. (2005). "Microplane model M5 with kinematic and static constraints for concrete fracture and anelasticity. I: Theory." *Journal of Engineering Mechanics*-ASCE, 131(1), 31-40.

Bazant, Z. P., Xiang, Y. Y., and Prat, P. C. (1996). "Microplane model for concrete. I: Stress-strain boundaries and finite strain." *Journal of Engineering Mechanics*-ASCE, 122(3), 245-254.

Bazant, Z. P., Caner, F. C., Carol, I., Adley, M. D., and Akers, S. A. (2000). "Microplane model M4 for concrete. I: Formulation with work-conjugate deviatoric stress." *Journal of Engineering Mechanics*-ASCE, 126(9), 944-953.

Bazant, Z. P., and Oh, B. H. (1985). "Microplane model for progressive fracture of concrete and rock." *Journal of Engineering Mechanics*-ASCE, 111(4), 559-582.

Caner, F. C., and Bazant, Z. P. (2000). "Microplane model M 4 for concrete. II: Algorithm and calibration." *Journal of Engineering Mechanics*, 126(9), 954-961.

Chen, W. F., and Han, D. J. (2007). *Plasticity for Structural Engineers*, J Ross Pub.

Di Luzio, G. (2007). "A symmetric over-nonlocal microplane model M4 for fracture in concrete." *International Journal of Solids and Structures*,

44(13), 4418-4441.

Ghazi, M., Attard, M. M., and Foster, S. J. (2002). "Modelling triaxial compression using the Microplane formulation for low confinement." *Computers & Structures*, 80(11), 919-934.

Liu, J., and Foster, S. J. (2000). "A three-dimensional finite element model for confined concrete structures." *Computers & Structures*, 77(5), 441-451.

Mirmiran, A., Zagers, K., and Yuan, W. Q. (2000). "Nonlinear finite element modelling of concrete confined by fiber composites." *Finite Elements in Analysis and Design*, 35(1), 79-96.

Nemecek, J., Patzak, B., Rypl, D., and Bittnar, Z. (2002). "Microplane models: computational aspects and proposed parallel algorithm." *Computers &Structures*, 80(27), 2099-2108.

Teng, J. G., Chen, J. F., Smith, S. T., and Lam, L. (2002). *FRP-Strengthened RC Structures*, John Wiley and Sons, Inc., UK.

Teng, J. G., Yu, T., Wong, Y. L., and Dong, S. L. (2007). "Hybrid FRP-concrete-steel tubular columns: Concept and behaviour." *Construction and Building Materials*, 21(4), 846-854.

Tue, N. V., Li, J. B., Schenk, G., Mucha, S., and Puschel, T. (2008). "Computational aspects of microplane model M4 for concrete: deficiencies and improvements." *Proceedings of the 3rd International Conference on the Concrete Future*, X. G. Zhou, C. T.

Tam, L. H. Han, and Y. B. Shao, eds., Ci-Premier Pte Ltd, Singapore, 411-418.

Yeh, F. Y., and Chang, K. C. (2007). "Confinement efficiency and size effect of FRP confined circular concrete columns." *Structural Engineering and Mechanics*, 26(2), 127-150.

Yu, T., Teng, J. G., Wong, Y. L., and Dong, S. L. (2010a). "Finite element modelling of confined concrete-I: Drucker-Prager type plasticity model." *Engineering Structures*, 32(3), 665-679.

Yu, T., Teng, J. G., Wong, Y. L., and Dong, S. L. (2010b). "Finite element modelling of confined concrete-II: Plastic-damage model." *Engineering Structures*, 32(3), 680-691.

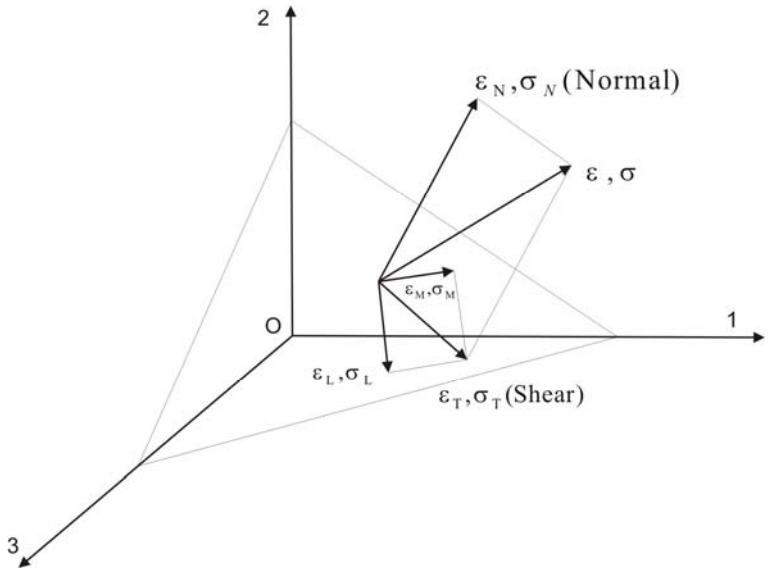

Figure 7.1 Stress and strain vectors on a typical microplane

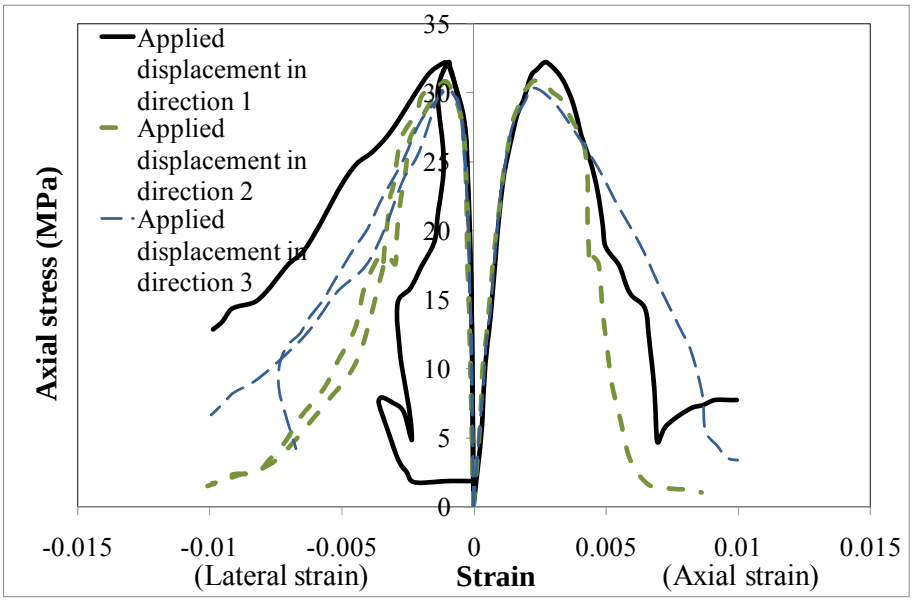

(a) From Alt-I

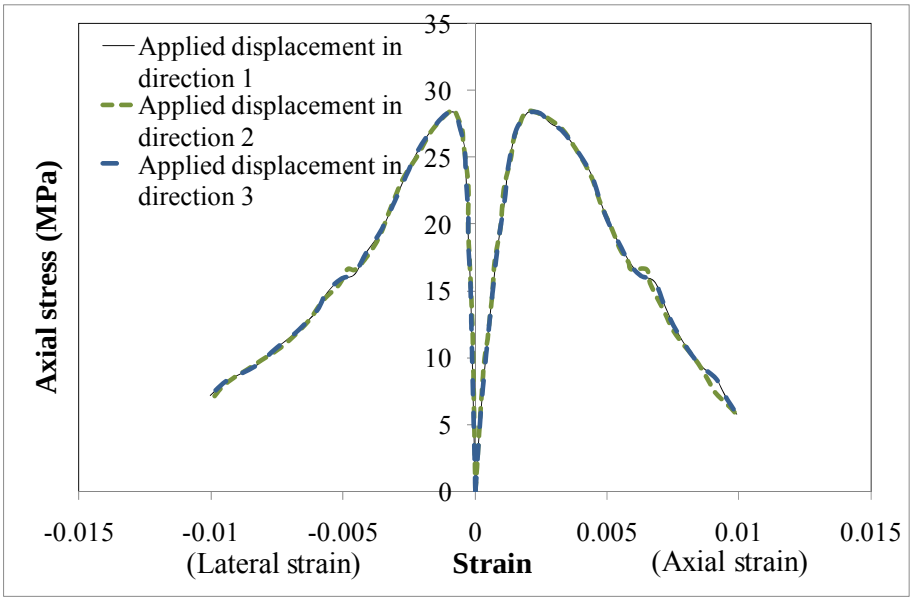

(b) From Alt-II

Figure 7.2 Stress-strain curves for uniaxial compression with displacements applied at different directions (three orthogonal directions such as X, Y, Z axes)

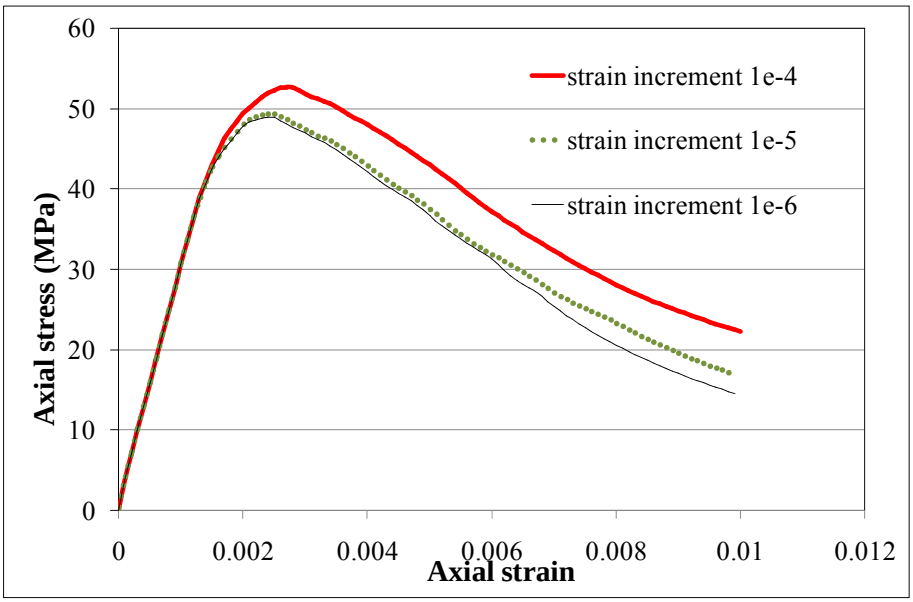

(a) Using the original algorithm

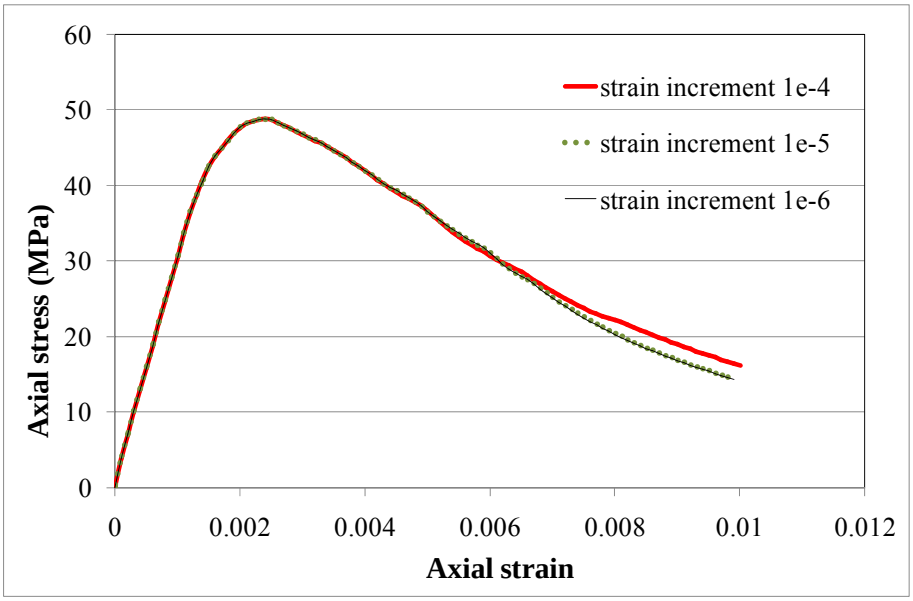

(b) Using the revised algorithm

Figure 7.3 Effect of strain increment magnitude on predicted response

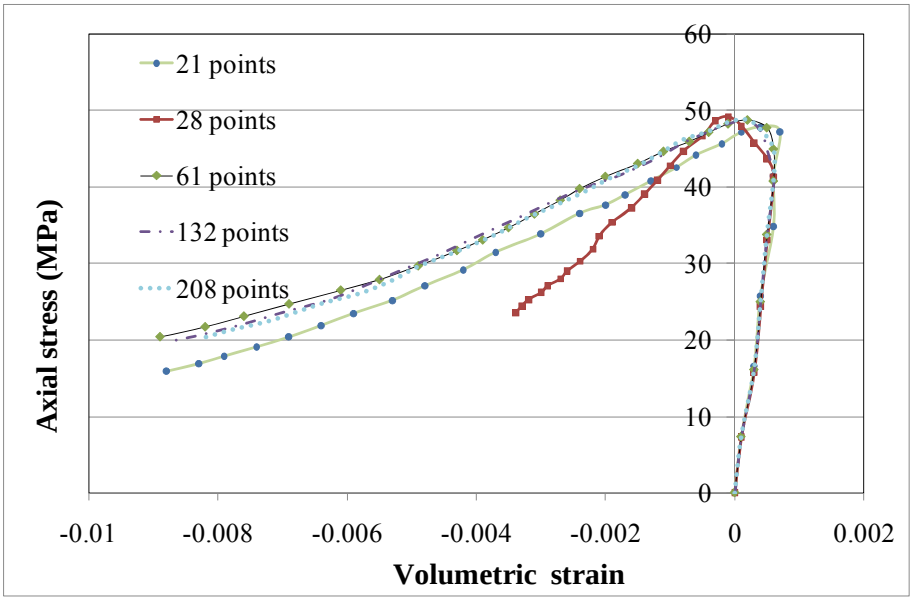

Figure 7.4 Effect of integration scheme on volumetric response under uni-axial compression

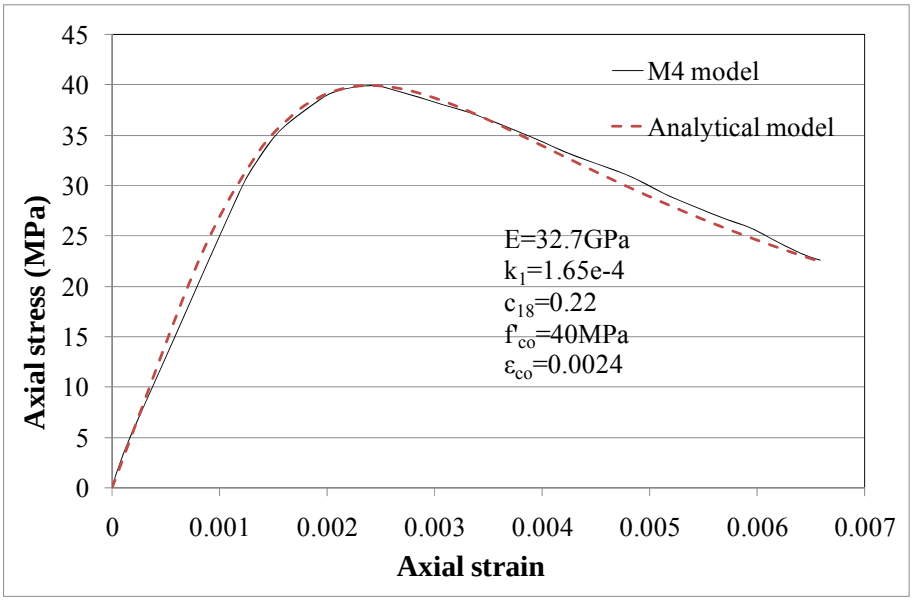

Figure 7.5 The M4 model versus Jiang and Teng's (2007) model for un-confined concrete

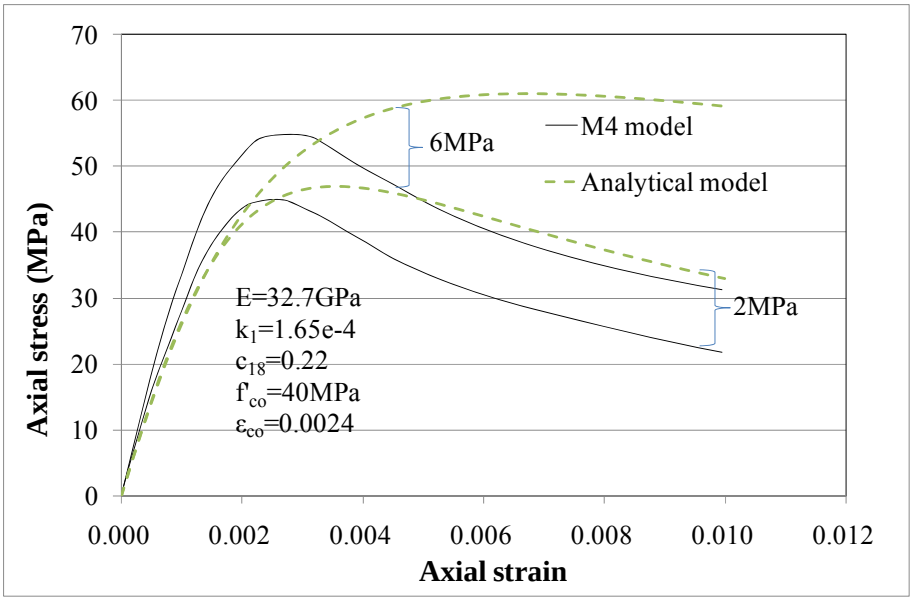

Figure 7.6 The M4 model versus Jiang and Teng's (2007) model for actively-confined concrete

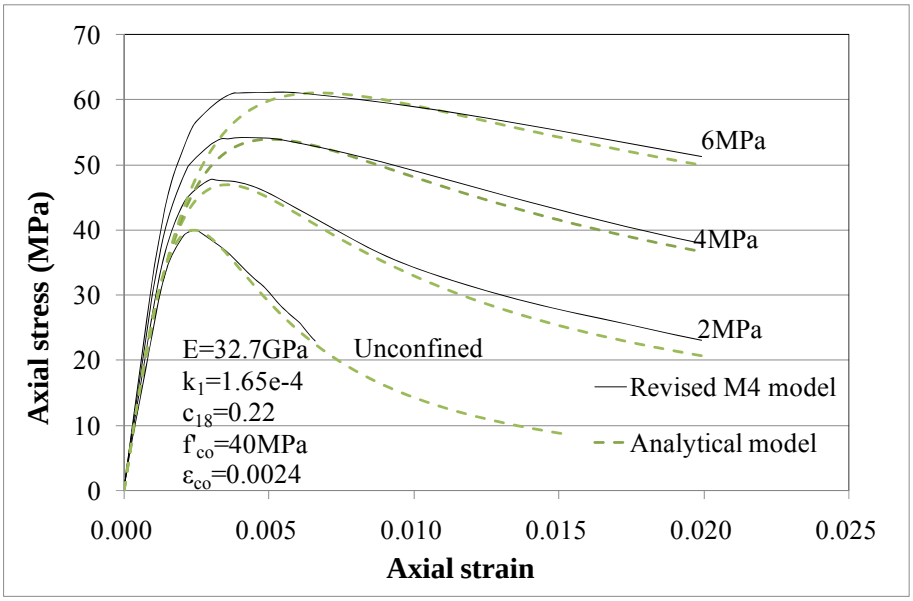

Figure 7.7 The revised M4 model versus Jiang and Teng's (2007) for actively-confined concrete

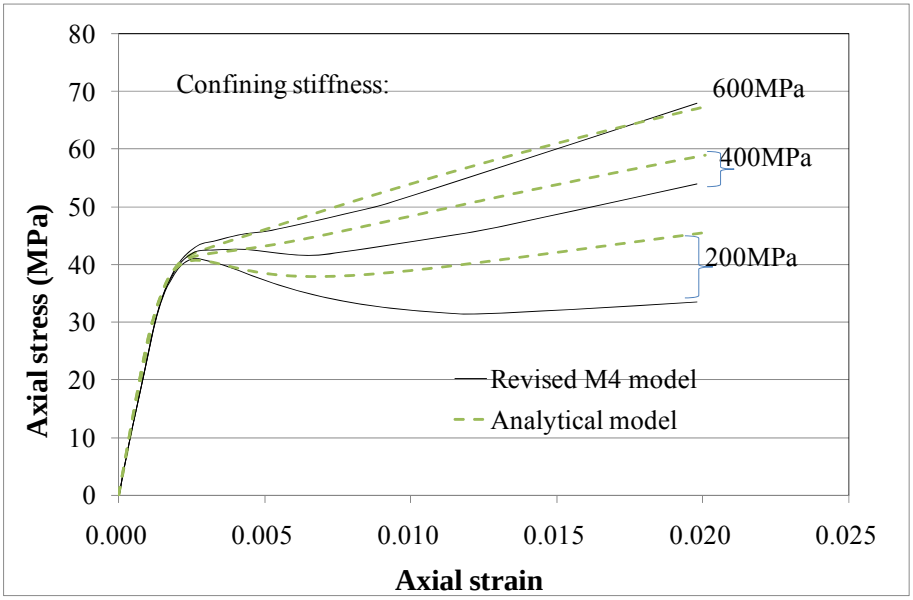

Figure 7.8 The revised M4 model versus Jiang and Teng's (2007) for FRP-confined concrete

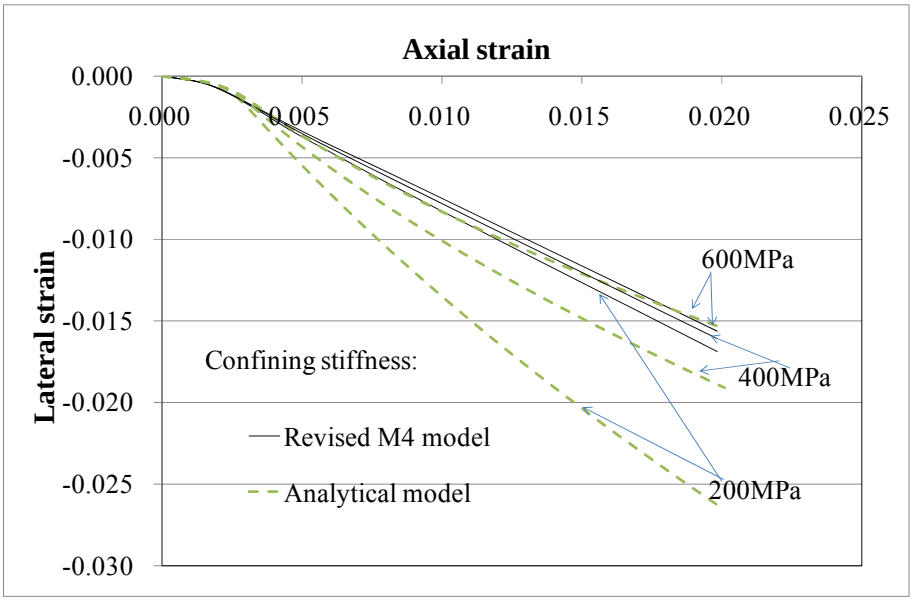

Figure 7.9 Lateral-to-axial strain curves: the revised M4 model versus Jiang and Teng's (2007) model for FRP-confined concrete

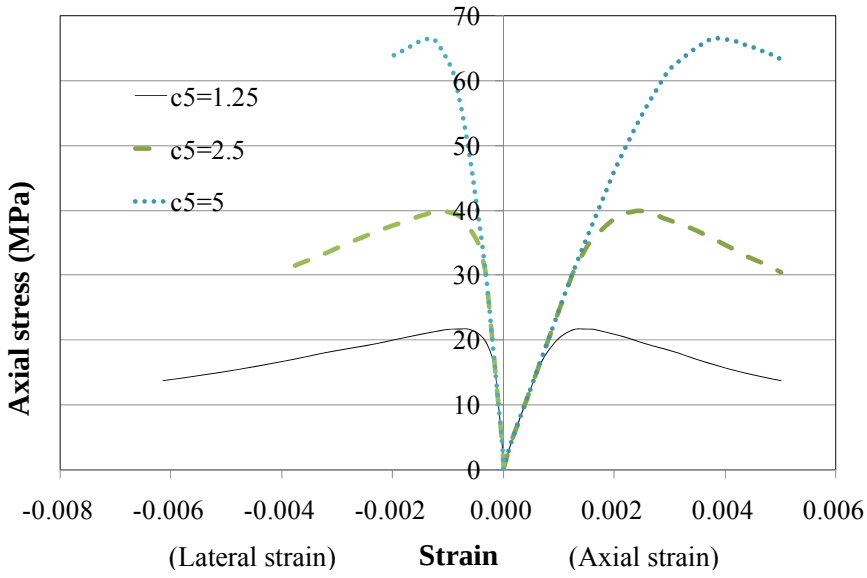

Figure 7.10 Effect of c_5 on the stress-strain behaviour of concrete predicted by the M4 model

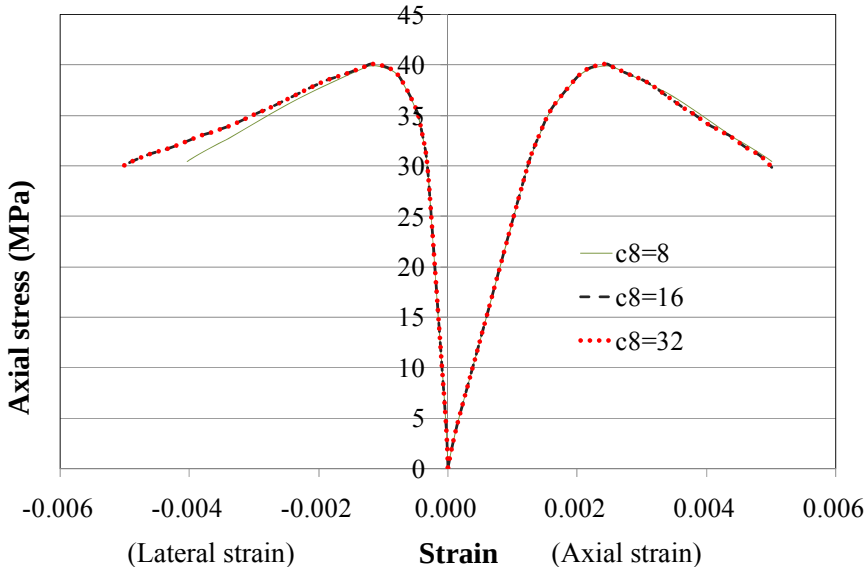

Figure 7.11 Effect of c_8 on the stress-strain behaviour of concrete predicted by the M4 model

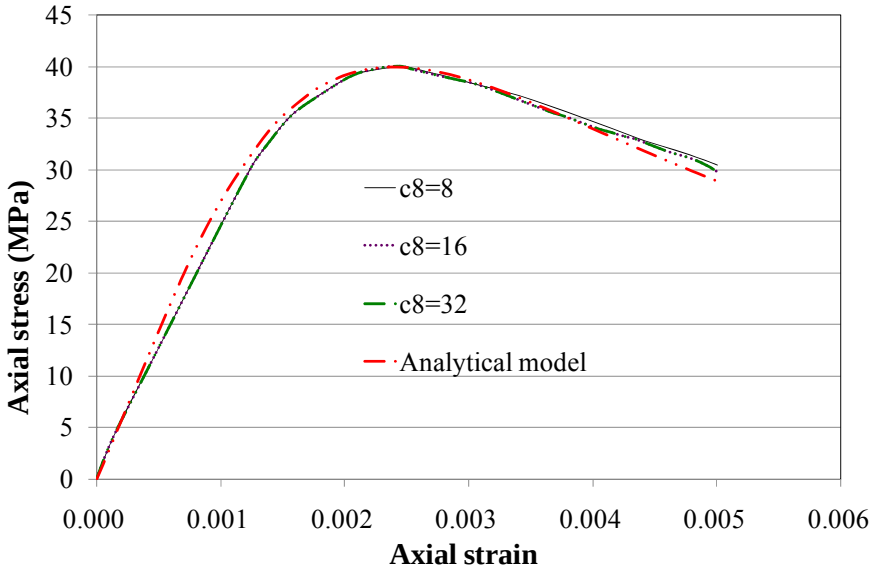

Figure 7.12 Axial stress-strain curves from the M4 model with different c_8 values versus predictions of Jiang and Teng's (2007) model

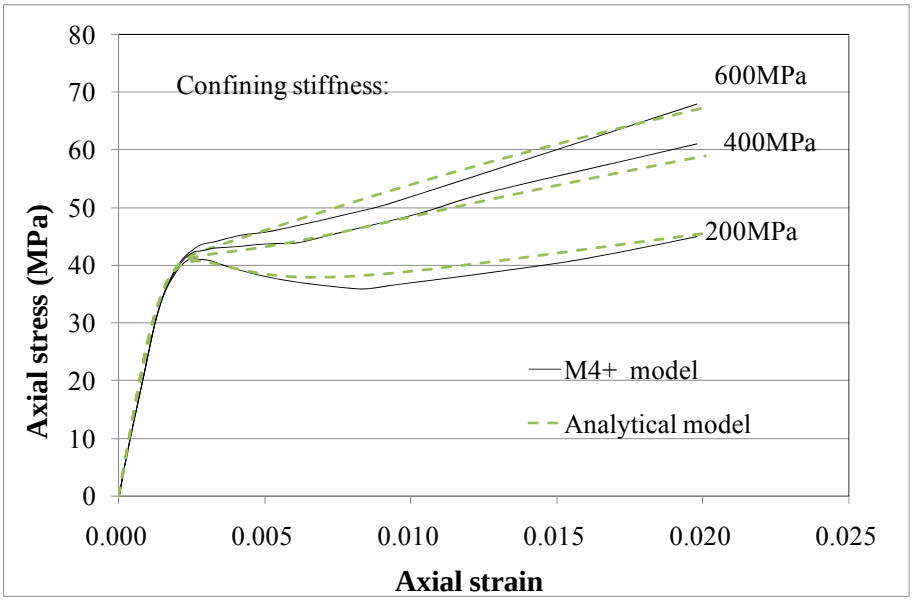

Figure 7.13 Comparison of axial stress-strain curves between the M4^{+} model and Jiang and Teng's (2007) for FRP-confined concrete

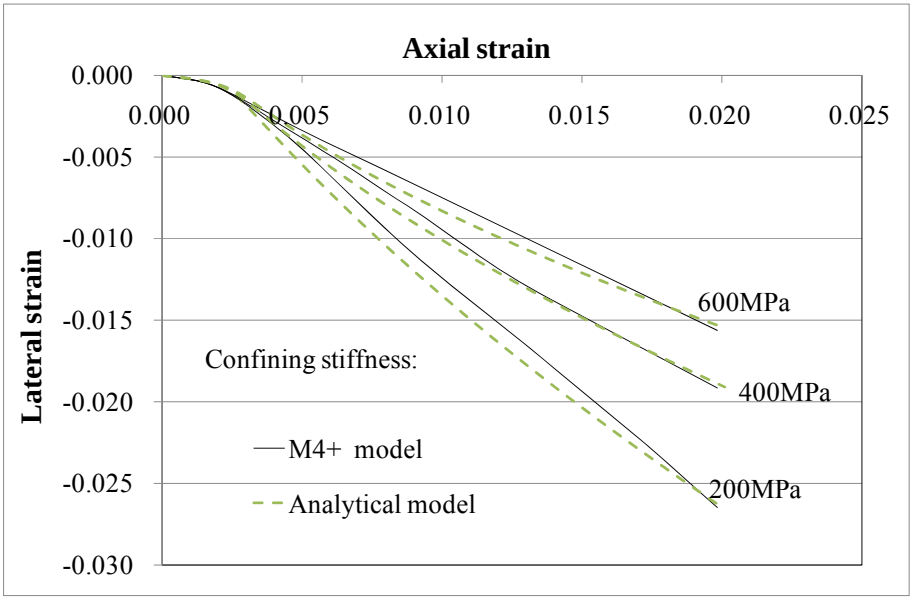

Figure 7.14 Comparison of lateral-to-axial strain curves between the M4^{+} model and Jiang and Teng's (2007) model for FRP-confined concrete

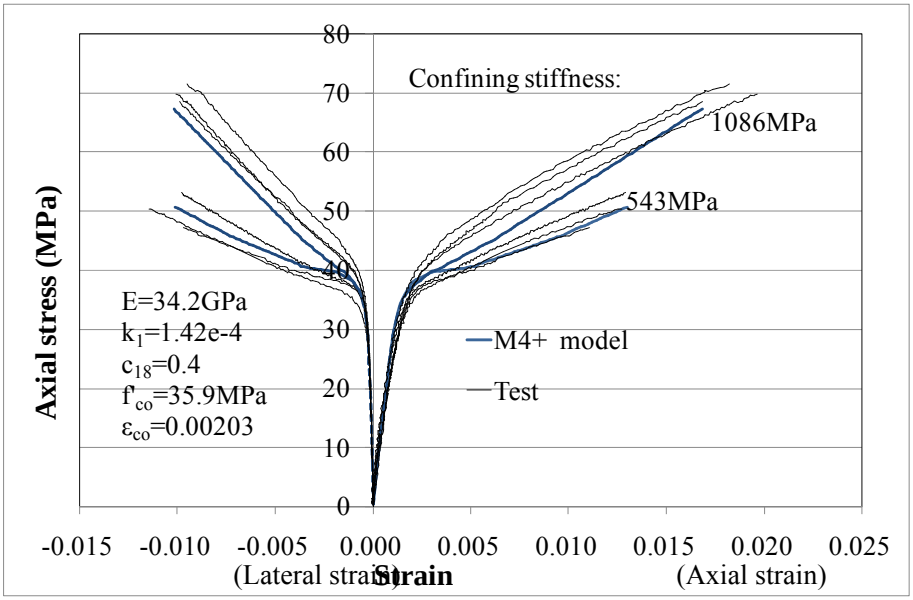

(a) $f'_{co} = 35.9\text{MPa}$

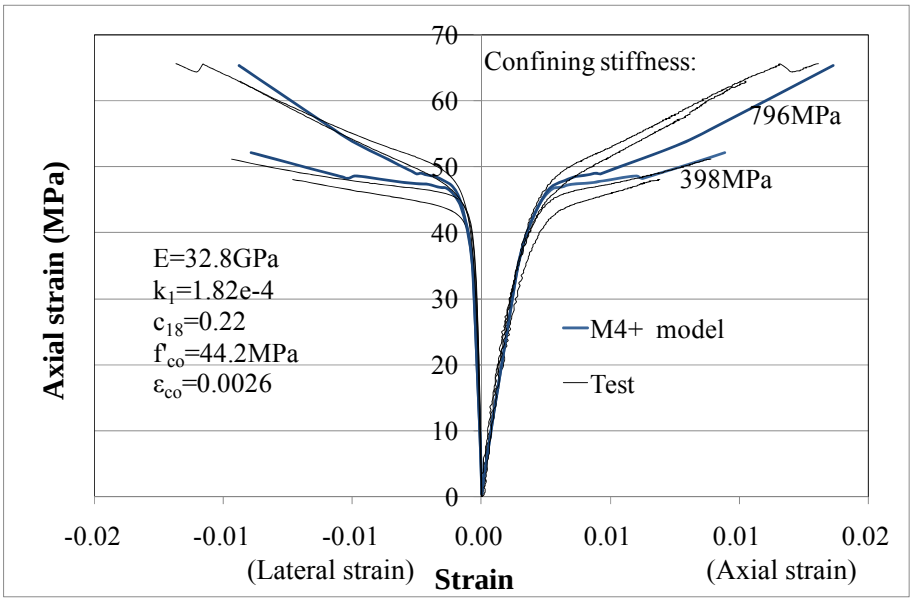

(b) $f'_{co} = 44.2\text{MPa}$

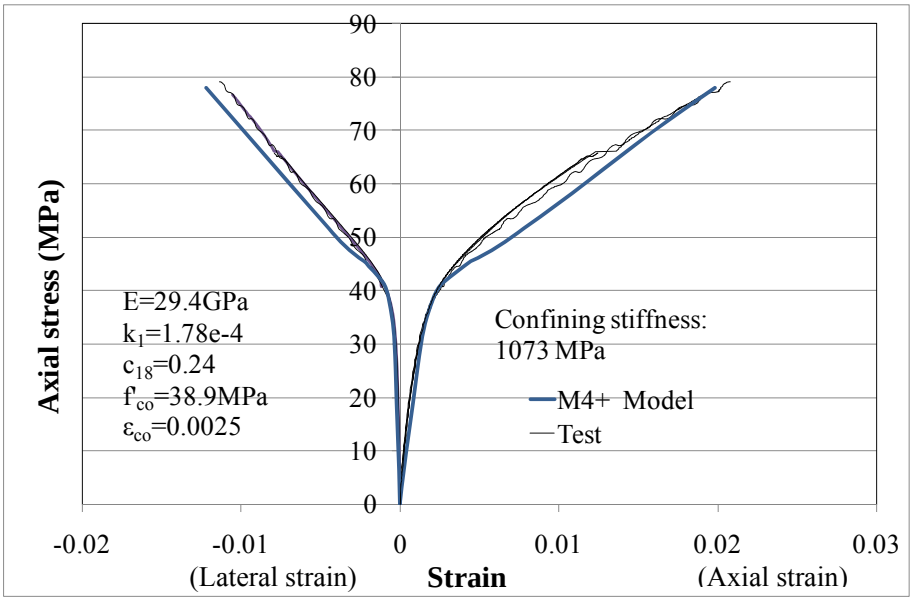

(c) $f'_{co} = 38.9\text{MPa}$

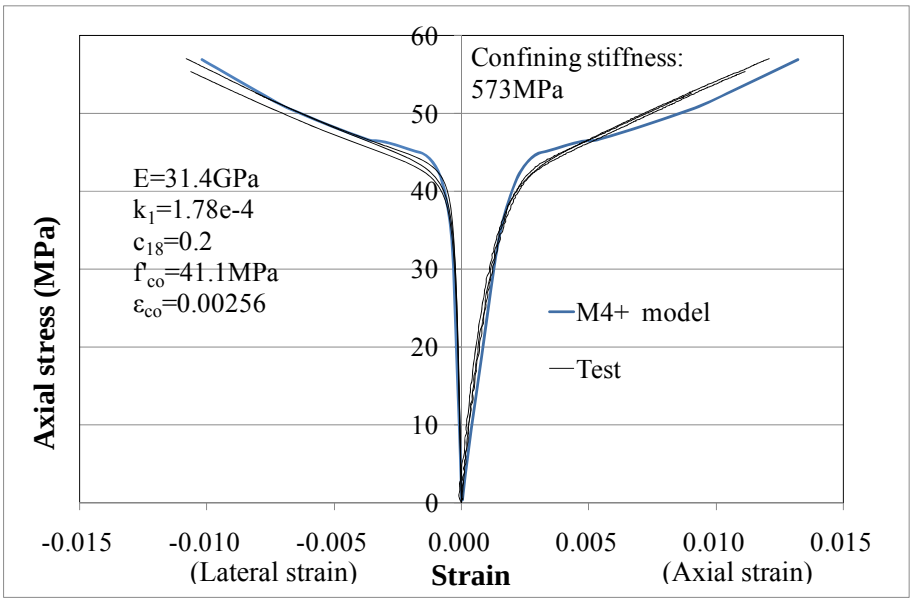

(d) $f'_{co} = 41.1\text{MPa}$

Figure 7.15 Comparison of axial stress-strain curves between the $M4^+$ model and test results

Table 7.1 Parameters of the M4 model

Parameter	Discription of parameter	Suggested value	Adopted value
c_1	Controls peak stress magnitude under uniaxial (unconfined)tension	0.62	0.62
c_2	Controls roundness of peak in uniaxial tension	2.76	2.76
c_3	Controls steepness of postpeak descent in uniaxial tension	4.00	4.00
c_4	Same as c_3 but for tensile volumetric strain	70	70
c_5	controls volumetric expansion in compressive uniaxial stress test	2.5	2.5
c_6	Controls roundness of peak of volumetric expansion in compressive uniaxial stress test	1.3	1.3
c_7	controls steepness of postpeak descent in compressive uniaxial stress test	50	Eqs. (7.15-7.16)
c_8	Controls peak magnitude in compressive uniaxial stress test	8	Eqs. (7.17-7.19)
c_9	Controls peak roundness in compressive uniaxial stress test	1.3	1.3
c_{10}	Controls pressure effect in standard triaxial tests	0.73	0.73
c_{11}	Sets magnitude of initial cohesion in frictional response	0.2	0.2
c_{12}	Controls decrease of cohesion with increasing volume expansion (frictional cohesion damage)	7000	7000
c_{13}, c_{14}	Control lateral contraction in uniaxial tension	0.2,0.5	0.2,0.5
c_{15}, c_{16}	Control effects of volumetric strain and volumetric stress on unloading slope in hydrostatic compression tests	0.02,0.01	0.02,0.01
c_{17}	Controls degree of damage manifested in unloading slopes	0.4	0.4
c_{18}	Similar as c_7	Adjustable	Adjustable
k_1	Scales all boundary		
k_2	Affects friction boundary		
k_3, k_4	Affect volumetric boundary		

*suggested value means parameter values suggested by Bazant et al., (2000). Adopted value means parameter values adopted in this chapter.

CHAPTER 8

EFFECT OF CROSS-SECTIONAL SHAPE ON BEHAVIOUR OF FRP-CONFINED CONCRETE

8.1 INTRODUCTION

The literature review given in Chapter 2 indicates that a large number of experiments have been conducted on circular concrete columns/cylinders uniformly confined by an FRP jacket. Based on this extensive amount of experimental data, many empirical and semi-empirical models have been developed primarily for such uniformly confined concrete columns/cylinders (see Chapter 2). By contrast, the vast majority of columns in reinforced concrete buildings and other structures are of non-circular sections (e.g. rectangular columns), and the amount of available test data is considerably less than that for circular ones. It is also well known that the degree of confinement varies over a non-circular section, and the average degree of confinement in a non-circular section is much less than that in a corresponding circular section (e.g. Lam and Teng 2003). Obviously, stress-strain models developed for confined concrete in circular sections cannot be used for concrete in non-circular sections.

Several empirical and semi-empirical stress-strain models for FRP-confined concrete in non-circular columns have been proposed (Harajli 2006; Lam

and Teng 2003b) to predict the average axial stress- strain response of a given cross-section. These models were generally extended from stress-strain models originally developed for FRP-confined concrete in circular columns. Factors related to confinement effectiveness in this type of models are commonly employed to consider the efficiency of confinement in non-circular sections. These factors account for the reduced effectiveness of confinement in non-circular sections compared to their circular counterparts and are generally determined by regression of available test data and/or by assuming a certain confinement mechanism (e.g. the arching action assumption). Hence, these models usually suffer from a common and fundamental drawback that they are not based on a rigorous understanding of the confinement mechanism in non-circular cross-sections. As a result, the current understanding of the confinement mechanism of FRP-confined non-circular sections, derived from experiments, is still very limited. To improve our understanding of this type of confinement mechanism, the finite element modelling offers a powerful tool as it can capture the complex stress distribution over the whole cross-section. With a suitable numerical model, it is possible to study the confinement mechanism in all types of column sections.

A number of researchers have presented finite element models for FRP-confined concrete in non-circular columns (e.g. Kiousis et al. 1994;

Malvar et al. 2004; Doran et al. 2009). Chapter 2 and Chapters 4-7 have indicated that most of the constitutive models for the concrete material adopted in existing finite element studies can only explain certain specific features of the behaviour of confined concrete and/or predict this behaviour for some specific conditions (e.g. providing accurate predictions for a certain confining stiffness). In the finite element analysis of concrete under passive confinement (e.g. FRP-confined concrete), the concrete constitutive model plays a fundamental role in accurately reproducing the mechanical response of concrete members. Due to the limitation of existing constitutive models, modelling the mechanical response of FRP-confined concrete in non-circular columns subjected to axial loading is still a challenging issue.

It is well known that in a non-circular section the confining pressure provided by the FRP jacket varies around the perimeter and the axial stress in the concrete varies over the whole section. Therefore, the stress distribution in a non-circular section is much more complex than that in a circular section. As can be seen from Chapter 2 and Chapters 4-7, most existing constitutive models of concrete cannot even provide accurate predictions for FRP-confined concrete in circular columns, so their capability in providing accurate predictions for FRP-confined concrete in non-circular columns is questionable. As the performance of different types of constitutive models of concrete in modelling circular FRP-confined

concrete cylinders has been assessed or discussed in the previous chapters (i.e. Chapters 2, 4-7), only those constitutive models which can provide accurate predictions for FRP-confined concrete in circular columns are examined in this chapter. It has also been mentioned in Chapter 2 that the modified compression field theory has provided a potential framework to capture the major characteristics of the stress-strain behaviour of concrete under uniform confinement. However, it has also been pointed out that this method is not very accurate for the stress-strain behaviour of FRP-confined circular concrete columns as it overestimates the hoop strain of FRP-confined concrete. Moreover, this method is not convenient for implementation into a finite element model driven by strain or displacement increments. As a result, this approach is also not included in the comparisons given in the present chapter. Based on the above considerations, only two constitutive models (i.e. the modified CDPM model and the $M4^{+}$ model) were used in the finite element studies presented in this chapter on the effects of cross-sectional shapes on confinement effectiveness.

In practice, the rectangular section is commonly adopted in structural design for columns. As a special case of FRP-confined rectangular columns, FRP-confined square columns show superior performance in terms of confinement effect than rectangular columns of other sectional aspect ratios.

Therefore, most of the experiments on rectangular columns have been conducted on square columns. In addition, since FRP confinement is much less effective for rectangular sections than for circular sections, the possibility of modifying a rectangular section into an elliptical section has been explored. For these reasons, in the present study, test specimens with square and elliptical sections were selected for investigation in the numerical modelling work. Using the numerical results, the confinement mechanism in these two typical non-circular sections (i.e. square and elliptical sections) is examined.

To study the confinement effects in non-circular sections, the accuracy of constitutive models employed in finite element analyses needs to be verified first. Therefore, comparisons between test results and finite element predictions obtained using the two constitutive models identified above are first presented in this chapter for FRP-confined concrete in square and elliptical columns. Axial stress-strain curves, axial stress-hoop strain curves, and axial force-strain curves were generated using finite element analysis for different concrete strengths and confinement levels. The cross-sections and loading details are described in section 8.2.

As two alternative constitutive models were employed in the prediction of the behaviour of confined concrete, their corresponding predictions for

FRP-confined concrete in non-circular columns are separately assessed in this chapter. The numerical results obtained from finite element analysis using the modified CDPM model are presented in Section 8.3, and those obtained from finite element analysis using the $M4^+$ model are given in Section 8.4. Next, a performance comparison between these two constitutive models in reflecting the effects of sectional shape is given in Section 8.5. Finally, the predicted distribution of stresses in selected sections is examined in Section 8.6.

The numerical results presented in this chapter can be used to highlight the advantages and disadvantages of the different section shapes and the capability of the two constitutive models in simulating the behaviour of FRP-confined concrete. In the design of RC columns, designers need to make many decisions. For each specific application, understanding the effect of sectional shapes can help the designer to choose the most suitable sectional shape that exhibits more optimal performance for a given application.

8.2 DISCUSSION OF SECTIONS USED FOR PERFORMANCE COMPARISON

8.2.1 Selection of Experimental Data

Experimental data for FRP-confined non-circular concrete columns have

been collected to verify the numerical results and to examine the effects of cross-sectional shapes. The experimental data include the axial stress-strain curves, axial stress-hoop strain curves (for FRP-confined concrete in square columns), and axial force-strain curves (for FRP-confined concrete in elliptical columns). These experimental curves were chosen based on the following criteria: a) the selected specimens showed good ductility and deformability (i.e. a relatively large axial strain); b) the selected axial stress-strain curves or axial force-strain curves have an ascending second branch or a slowly descending second branch. These two criteria were adopted due to the following considerations. First, if an FRP-confined concrete column has only limited ductility, the second branch of the stress-strain curve is generally very short, and the slope of the second branch tends to show large variations. As the second branch slope is a key indicator for assessing the deformation capacity of a concrete specimen under hoop confinement, it is hard to assess the performance of a constitutive model if test data for this slope show a large scatter. Second, the parameters of those two constitutive models for use in finite element analysis were both calibrated from Jiang and Teng's (2007) analysis-oriented stress-strain model which is more accurate for concrete with sufficient confinement than that for concrete with insufficient confinement despite that Jiang and Teng's (2007) model is superior to its earlier version proposed by Teng et al. (2007) in predicting the behaviour of

FRP-confined concrete.

Based on the above two criteria, 21 specimens, including 12 square specimens and 9 elliptical specimens, were collected for inclusion in the database. The basic information of these specimens, including their geometric and material parameters, is given in Tables 8.1-8.2; Table 8.1 summarizes the information of square specimens while Table 8.2 summarizes the information of elliptical specimens. What should be noted is that these selected specimens are all small-scale specimens with dimensions close to the commonly used standard cylinders. Therefore, the possible size effect these 21 selected specimens need not to be considered.

Within these 21 specimens, the 12 square specimens were selected from the published literatures (Masia et al. 2004; Hosotani et al. 1996; Wang 2008). The major parameters controlling the confinement effect in FRP-confined square columns are considered. Four square specimens were selected from Masia et al. (2004). These specimens were divided into two groups, depending on the dimensions of the cross-section. These four square specimens had the same corner radius of 25 mm but two different section sizes (section side lengths of 100 mm and 150 mm). The specimens with a side length of 100 mm are named WS while the specimens with a side length of 150 mm are named WL.

In Hosotani et al.'s (1996) study on FRP-confined square columns, the parameter varied was the elastic modulus of the confining material; normal modulus CFRP ($E_{frp} = 252GPa$) and high modulus CFRP ($E_{frp} = 439GPa$) were both used. The corner radius of these two specimens was both 38 mm, and their side length was 200 mm. It should also be noted that these two specimens were FRP-confined RC columns, which means they included longitudinal steel bars and steel hoops. The confinement effect of the steel hoops is negligible as large hoop spacing was used. It was found that when the hoop spacing is larger than 1.25 times the centerline of the spiral, the effect of steel hoops can be neglected (Binici 2005). Longitudinal bars also have an insignificant effect on the confinement behaviour of concrete as will be discussed in detail in Chapter 9. Therefore, in the present study, this feature was neglected in the finite element models. In connection with this assumption, the contribution of the longitudinal steel bars was removed from the test results of Hosotani et al. (1996) to produce the experimental axial stress-strain and axial stress-hoop strain curves for comparison with the finite element predictions.

Eight square specimens were also selected from Wang (2008) for comparison. The parameters varied in Wang's (2008) study include the unconfined concrete strength f'_{co}, the section corner radius *r*, and the

thickness of the FRP jacket t_j. Within these 8 specimens, the concrete strength ranged from 30.7 MPa to 52.7 MPa; the corner radius ranged from 30 mm to 60 mm; the thickness of the FRP jacket ranged from 0.165 mm to 0.33 mm. In Wang's (2008) test, for the FRP-confined concrete with unconfined concrete strength equal to 30.7 MPa, all the specimens have ascending second branches and they were also selected into the database; for the FRP-confined specimens with unconfined concrete strength equal to 52.7 MPa, only two specimens with their corner radius equal to 60mm have ascending second branches and they were selected into the database. The names of these 8 specimens include three parts. The first three characters represent the concrete cylinder strength. For instance, C30 means the concrete cylinder compressive strength was about 30 MPa. The subsequent three characters represent the section corner radius *r*. For instance, R30 means the section corner radius was 30mm. The last two characters represent the thickness of the FRP jacket. For instance, P1 means the square column was wrapped by a one-ply of FRP jacket.

Finally nine elliptical specimens recently tested at The Hong Kong Polytechnic University were included into the test database (Stefano 2011). The major parameters influencing the confinement effect in the FRP-confined elliptical columns were considered in these tests. Three ratios between the major axis length, *a,* and the minor axis length, *b*, ranging from

1.3 to 2, were considered. The thickness of the FRP jacket was another important parameter. Two different thicknesses, 0.171 mm and 0.342 mm, were considered in this series of experiments. The concrete strength ranged from 32.64 MPa to 35.92 MPa. These elliptical specimens are distinguished by their batches and a/b ratios.

8.2.2 Overview of Finite Element Models

The main objective of the present study is to examine the effect of cross-sectional shape through finite element modelling. Similar to that suggested by Yu et al. (2010), the finite element models in this study included only a horizontal slice of the specimens and consisted of a single layer of 3D solid elements to represent the concrete. The effect of end restraints will be discussed in Chapter 9 in detail. The finite element models followed closely the geometry and the FRP jacket arrangement of these short-column specimens, using 8-node solid elements for the concrete and 2-node elements (truss or beam elements) for the FRP jacket. Considering the symmetry of the specimen under an idealized condition, only a quarter of the horizontal slice is needed to be modeled.

Although two alternative constitutive models were used to model the concrete material, it was found that the constitutive models have insignificant influence on the convergence of the finite element mesh. Therefore, in the finite element models used to obtain the results given in

Sections 8.3 and 8.4, the same mesh was used for the same specimen regardless of the constitutive model employed. Two typical finite element meshes used to represent these non-circular cross-sections are illustrated in Figs. 8.1-8.2, for square and elliptical shapes, respectively. It should also be noted that in finite element analysis, the details of the corners of a square section were modelled to consider its influence on the confinement effect. In some earlier studies (e.g. Malvar et al. 2004; Koksal et al. 2008), the features of the corner were neglected in their finite element analyses. Therefore, their explanation of the confinement mechanism is questionable, although their numerical models may still be able to provide accurate predictions for the experimental stress-strain response. These important features were properly captured in the present study, and the corner radius was taken as an important parameter which has significant influence on the confinement effect in a section.

In all the finite element models, the C3D8R solid element was used to model the concrete. This type of solid element is available with either ABAQUS implicit or explicit. A 2-node element was used in the hoop direction to model the FRP jacket as a unidirectional material. In ABAQUS implicit, membrane elements without compressive stiffness are also available for modelling the FRP jacket; however, this option is unavailable in ABAQUS explicit. As the same finite element mesh was intended for use

with both ABAQUS implicit and ABAQUS explicit, a 2-node element was thus the preferred choice.

Two types of 2-node elements are available with ABAQUS for the modelling of the FRP jacket: the truss element and the beam element. For FRP-confined square columns, the flat sides of the FRP jacket are subjected to bending deformation. The use of the truss element in the finite element model neglects the influence of this bending deformation. In most cases, as the thickness of the FRP jacket is small, the effect of this bending deformation is negligible. In order to clarify the effect of this bending deformation, the beam element was first used in the finite element model to examine the influence of bending deformation. The element B31 provided by ABAQUS was used for this purpose. These beam elements were tied to the solid elements to consider the interaction between the concrete and the FRP jacket. Compared to the 8-node solid element, the beam element B31 has additional rotational degrees of freedom. These rotational degrees of freedom need to be properly addressed, especially at the symmetry planes. The actual thickness of the FRP jacket was used in defining the beam elements. In this part of the study focused on the influence of bending deformation of the FRP jacket, the concrete constitutive model was not the major issue of concern, and the concrete material was modeled using the modified CDPM model.

Figs. 8.3-8.4 show the influence of jacket bending deformation for two square specimens (C30R30P2 and C30R45P2) as revealed by numerical simulations. In these two figures, three locations were selected for comparison, which include a point at the center of one of the flat sides, one of the points of intersection between the corner zone and the flat part, and the point at the center of the corner. These three points can be seen as the characteristic points for the deformed configuration. Fig. 8.5 shows the shape of the deformed section for specimen C30R45P2. It can be observed from this figure that the first point (i.e. one of the points at the center of a flat side) experiences the largest outward curvature; the second point (i.e. one of the points of intersection between the corner zone and the flat part) is a point of contra-flexure for the bending deformation; the last point (i.e. the point at the center of the corner) experiences the largest inward curvature.

At these three selected points, the magnitudes of the hoop strain on the inner surface and the outer surface of the beam element are shown against the axial strain in Figs. 8.3-8.4, where compressive axial strains and tensile hoop strains are both shown as positive values. These two figures show that the difference between the hoop strains on the inner and the outer surfaces at these three points is negligible, which indicates that in these two specimens the influence of the bending deformation is very small. Therefore, it is unnecessary to use beam elements instead of truss elements in the finite

element modelling of such columns. Using truss elements instead of beam elements to model the FRP jacket has another advantage: the truss element T3D2 has the same nodal degrees of freedom as those of the solid element C3D8R. Therefore, when truss elements are tied to solid elements to consider the interaction between the concrete and the FRP jacket, no additional restraints need to be imposed on the truss elements. Therefore, in the subsequent finite element analyses, the truss element T3D2 was used to model the FRP jacket, and the hoop strain obtained from this element can be taken as the average hoop strain obtained from the inner and the outer surfaces of the FRP jacket.

To model the confinement effect provided by the FRP jacket, in the finite element slice models with a single layer of solid elements, two layers of truss elements were placed at the top and the bottom nodes of the solid elements. Furthermore, the cross-sectional areas of these truss elements were set to be the product of the height of the solid element (in the axial direction) and half of the thickness of the FRP jacket. As the height of the horizontal slice has no effect on the numerical results, a fixed value of 8 mm was always used in the finite element analyses. Trial analyses were conducted to find the optimal mesh for the discretization of the cross-section. It was found that an element size of around 5 mm for the solid elements was suitable for all the finite element models. The size of the

truss elements was set to be compatible with the solid elements, so that the distances between the adjacent nodes of the truss element and the solid element are equal to zero.

As mentioned above, when truss elements were used to model the FRP jacket, restraints needed only to be applied to the concrete core. Symmetry boundary conditions were imposed on the corresponding symmetry planes shown in Figs. 8.1-8.2. The displacements in the z-direction on the bottom surface were all prevented. On the top surface, displacements were applied in the z-direction to realize axial loading.

In this study, the FRP jacket in all the finite element models was modeled as an elastic material. In both ABAQUS implicit and ABAQUS explicit, two material parameters, namely the elastic modulus E_{frp} and Poisson's ratio μ_f, are required to define an elastic material. The values of E_{frp} used in the study are given in Table 8.1 or 8.2. For truss elements, the parameter μ_f does not have any influence on their confinement effect. Hence, in this study, the value of the parameter μ_f was always set to be 0. In summary, the choice of element types and material parameters for the FRP jacket ensured that they were only modeled as a confining material with mechanical resistance only in the hoop direction. When ABAQUS explicit was used, the density of the FRP was set to be 1.85e-5 g/mm^3.

8.3 FINITE ELEMENT RESULTS BASED ON THE MODIFIED CDPM MODEL

8.3.1 Concrete Model

As discussed in Chapter 2, a number of studies exist on the finite element analysis of FRP-confined concrete. Among these studies, most of them have been based on a Drucker-Prager (D-P) type plasticity model for the concrete (Lan 1998; Mirmiran et al. 2000; Mahfouz et al. 2001; Karabinis and Rousakis 2002; Oh 2002; Rousakis et al. 2007; Eid and Paultre 2007). A recent review and comprehensive assessment of existing D-P type models for FRP-confined concrete showed that none of them could properly capture all the key features of FRP-confined concrete (Yu et al. 2010a). Therefore, Yu et al. (2010b) developed a new plastic-damage model for FRP-confined concrete, in which the deficiencies of the previous D-P type plasticity models were eliminated.

In this part of the study, the modified CDPM model proposed by Yu et al. (2010) was used to reproduce the stress-strain response of FRP-confined concrete in non-circular columns. Unlike empirical and semi-empirical models, the modified CDPM model is based on the plastic-damage theory and provides a sound theoretical basis for modelling the confinement mechanism. In Chapter 2, it has been pointed out that the behaviour of FRP-confined circular concrete cylinders (i.e. uniform confinement) can be

accurately predicted using this modified CDPM model. In the remainder of this section, the capability of the modified CDPM model in predicting the behaviour of FRP-confined concrete in non-circular sections (i.e. effect of the cross-sectional shape) is examined. Before presenting the numerical results, a short summary of the modified CDPM model and some necessary refinements are introduced.

8.3.2 Yu et al.'s Model and Refinements

Yu et al.'s (2010b) model was based on the knowledge of FRP-confined concrete developed at The Hong Kong Polytechnic University (e.g Teng and Lam 2004; Teng et al. 2007) and formulated within the theoretical framework of the concrete damaged plasticity model (CDPM) provided in ABAQUS. Similar to other plastic-damage models used for FRP-confined concrete (Lubliner et al. 1989; Luccioni and Rougier 2005; Grassl and Jirasek 2006), Yu et al.'s (2010b) model includes four components: the yield criterion, the hardening rule, the flow rule, and the damage variable. These four components are all confinement-dependent, which is the key feature of this model. An analysis-oriented stress-strain model for FRP-confined concrete (Teng et al. 2007) was used by them to derive input parameters for the plastic damage model. The four components of Yu et al.'s (2010b) model are described in detail in the subsequent sub-sections.

8.3.2.1 Yield criterion and hardening rule

The yield function adopted in the CDPM model was first proposed by Lubliner et al. (1989) and later modified by Lee and Fenves (1998) in terms of the effective stress. The yield function is given by:

$$F = \frac{1}{1-A}\left(\sqrt{3\bar{J}_2} - A\bar{I}_1 + B\langle -\bar{\sigma}_{min}\rangle - C\langle -\bar{\sigma}_{min}\rangle\right) - \bar{\sigma}_{cn}(\tilde{\varepsilon}^{pl}) \quad (8.1)$$

with

$$A = \frac{\frac{f'_b}{f'_{co}} - 1}{2\frac{f'_b}{f'_{co}} - 1}; \ 0 \le A \le 0.5, \quad (8.2)$$

$$B = \frac{\bar{\sigma}_{cn}(\tilde{\varepsilon}^{pl})}{\bar{\sigma}_{tn}(\tilde{\varepsilon}^{pl})}(1 - A) - (1 + A), \quad (8.3)$$

$$C = \frac{3(1-K)}{2K-1} \quad (8.4)$$

where $\bar{I}_1$ is the first invariant of effective stresses, $\bar{J}_2$ is the second invariant of deviatoric effective stresses. $\bar{\sigma}_{min}$ is the minimum principal effective stress, $\bar{\sigma}_{cn}$ and $\bar{\sigma}_{tn}$ are the effective compressive and tensile cohesion stresses respectively, $\tilde{\varepsilon}^{pl}$ is the equivalent plastic strain, and K is the strength ratio between equal biaxial compression and equal tri-axial compression. As mentioned earlier, f'_{co} is the uniaxial compressive strength of concrete (unconfined concrete strength), f'_b is the biaxial compressive strength of concrete with f'_b/f'_{co} =1.16 as the default value (Kupfer et al. 1969). In addition, the equivalent plastic strain increment is defined by the

following equation:

$$d\tilde{\varepsilon}^{pl} = -d\tilde{\varepsilon}^{pl}_{min} \tag{8.5}$$

where $\tilde{\varepsilon}^{pl}_{min}$ is the minimum eigenvalues of the plastic strain ε^{p}.

Yu et al. (2010b) suggested that $\overline{\sigma}_{cn}$ should depend not only on $\tilde{\varepsilon}^{pl}$ but also on the effective confining pressure $\sigma_{l,eff}$ given by:

$$\sigma_{l,eff} = \frac{2(\sigma_2+\alpha f'_{co})(\sigma_3+\alpha f'_{co})}{\sigma_2+\sigma_3+2\alpha f'_{co}} - \alpha f'_{co} \tag{8.6}$$

where σ_2 and σ_3 are the two principal hoop stresses; and α is a constant to be determined based on test results. It was suggested by Yu et al. (2010b) that the best-fit value for α is 0.0039 based on experimental stress-strain responses of concrete under bi-axial compression (Kupfer et al. 1969). This value was adopted in the present study as a default value if not otherwise specified. The hardening rule is thus defined as:

$$\overline{\sigma}_{cn} = \overline{\sigma}_{cn}\left(\tilde{\varepsilon}^{pl}, \sigma_{l,eff}\right) \tag{8.7}$$

Yu et al. (2010b) determined that K = 0.725 based on the following equation describing the failure surface of concrete under equal tri-axial compression (Teng et al. 2007):

$$f'^{*}_{cc} = f'_{co} + 3.5\sigma_l \tag{8.8}$$

where f'^{*}_{cc} is the peak stress of concrete under a uniform hoop confining

pressure σ_l.

8.3.2.2 Flow rule and damage variable

In the CDPM model provided by ABAQUS, the flow rule is described by the following expressions:

$$d\varepsilon_j^p = d\lambda \frac{\partial G}{\partial \sigma_j} \tag{8.9}$$

and

$$G = \sqrt{(\ni\ \sigma_{to} \tan\psi) + \bar{J}_2} - \bar{I}_1 \tan\psi \tag{8.10}$$

where $d\lambda$ is a non-negative scalar, σ_j is the current stress vector, G is the potential function (ABAQUS 2004), σ_{to} is the uniaxial tensile strength, $\ni$ is referred to as the eccentricity which has a default value of 0.1, and ψ is the dilation angle which is constant in ABAQUS. Yu et al. (2010b) suggested that the dilation angle should depend on the equivalent plastic strain $\tilde{\varepsilon}^{pl}$ and the equivalent confinement stiffness k_{eq} as follows

$$\psi = \psi\left(k_{eq}, \tilde{\varepsilon}^{pl}\right) \tag{8.11}$$

where k_{eq} can be calculated from

$$k_{eq} = -2\sigma_{l,eff}/(\varepsilon_2 + \varepsilon_3) \tag{8.12}$$

with ε_2 and ε_3 being the two principal hoop strains.

In addition, Yu et al. (2010b) proposed the following equation for the

damage variable d which is also confinement-dependent:

$$d = 1 - \frac{\sigma_c - \frac{1+C+2A}{1-A}\sigma_l}{f'^{*}_{cc} - \frac{1+C+2A}{1-A}\sigma_l} \tag{8.13}$$

where σ_c is the axial stress of concrete on the descending branch. The two newly defined parameters, the effective confining pressure $\sigma_{l,eff}$ and the equivalent confinement stiffness k_{eq}, were implemented into ABAQUS as "user-defined solution dependent field variables".

8.3.2.3 Implementation into ABAQUS

In the CDPM model provided in ABAQUS, $\bar{\sigma}_{cn}$ is independent of the confinement characteristics and only a single $\bar{\sigma}_{cn}$ - $\tilde{\varepsilon}_c^{pl}$ curve is required for a given concrete, which can be obtained from the uniaxial compressive stress-strain curve of concrete. In Yu et al.'s (2010b) model, as $\bar{\sigma}_{cn}$ is a function of both $\tilde{\varepsilon}_c^{pl}$ and $\sigma_{l,eff}$, a family of $\bar{\sigma}_{cn}$ - $\tilde{\varepsilon}_c^{pl}$ curves, each corresponding to a given value of $\sigma_{l,eff}$, is required for a given concrete. Such $\bar{\sigma}_{cn}$ - $\tilde{\varepsilon}_c^{pl}$ curves can be derived from an analysis-oriented stress-strain model for FRP-confined concrete (e.g. Teng et al. 2007; Jiang and Teng 2007). Such an analysis-oriented stress-strain model usually includes an active confinement base model to describe the axial stress-strain relationship of concrete under a constant hoop confining pressure (Teng and Lam 2004).

Similarly, a series of d-$\tilde{\varepsilon}_c^{pl}$ curves for different values of $\sigma_{l,eff}$ is required in Yu et al.'s (2010b) model, as d is also confinement-dependent. In determining d, the post-peak yield surface is assumed to be the same as the yield surface at peak stress determined from Eq. (8.1). The d - $\tilde{\varepsilon}_c^{pl}$ curve for a given state of stresses is determined by means of interpolation, based on the value of $\sigma_{l,eff}$ calculated from the hoop strains (ε_2 and ε_3) determined in the previous step of analysis.

It should be noted that when the axial deformation of concrete in compression is uniform over the cross-section, the equivalent plastic strain $\tilde{\varepsilon}^{pl}$ is equal to the plastic compressive strain of concrete ε_c^p (positive according to the sign convention of this thesis). This is because that in this specific case, one of the principal directions coincides with the axial direction for both stresses and strains, and the other two principal directions are always perpendicular to this axial direction. For this situation, a finite element model containing only a horizontal slice of the concrete specimen/column can be used in analysis, and $\tilde{\varepsilon}^{pl}$ can be replaced by ε_c^p. However, if the axial deformation is non-uniform, which may be due to non-uniform confinement, load eccentricity or other factors, shear stresses develop between adjacent horizontal slices. Consequently, the axial

direction is not necessarily one of the principal directions. In such a more general situation, a 3D finite element model of the entire concrete specimen/column needs to be used in analysis, and $\tilde{\varepsilon}^{pl}$ is no longer equal to ε_c^p.

In addition, it should also be mentioned if the axial deformation of concrete in compression is uniform over the cross-section, $\varepsilon_2 < 0$ and $\varepsilon_3 < 0$ hold, and the equivalent confinement stiffness k_{eq} given by Eq. (8.12) is always positive, according to the sign convention adopted in this thesis as the concrete experiences lateral expansion. However, if the axial deformation of concrete in non-uniform over the cross-section, $\varepsilon_2 > 0$ or $\varepsilon_3 > 0$ may happen. This may lead to a negative value for k_{eq} and may cause convergence problems in the finite element analysis.

For the present finite element models, the following assumptions were added when implementing Yu et al.'s (2010b) plastic-damage model into ABAQUS without compromising the generality of the model for practical applications:

a) σ_2 and σ_3 in Eq. (8.9) are the two smaller principal stresses while ε_2 and ε_3 used in the flow rule are the two smaller principal strains (according to the sign convention of this thesis);

b) σ_2 (or σ_3) is ignored in calculating $\sigma_{l,eff}$ if it becomes negative (i.e. $\sigma_2 < 0$ or $\sigma_3 < 0$), as the effect of tensile stresses on confined concrete is unclear; and

c) $\varepsilon_2 + \varepsilon_3 < 0$. If $\varepsilon_2 + \varepsilon_3$ is found to be positive or zero, it is taken as a very small negative value in determining the flow rule.

The purpose of these assumptions is to limit the revised part of the CDPM model in the compressive zone. In addition, two material parameters, the unconfined concrete strength f'_{co} and the corresponding axial strain ε_{co}, are required to generate the input parameters for the CDPM model in ABAQUS. For the specimens listed in Table 8.1, the reported strengths of plain concrete cylinders/prisms were directly adopted, which means that the size effect on the behaviour of these specimens was not considered as their sizes were close to that of standard concrete cylinders. However, the size effect on the behaviour of large concrete columns deserves attention.

8.3.3 Stress-Strain Curves

A finite element numerical study was conducted using the modified CDPM as explained above to evaluate the capability and limitation of the modified CDPM model in reproducing the response of FRP-confined concrete in non-circular columns subjected to axial compression. The numerical modelling procedure for all the columns followed that described above. Average axial stress-strain curves and axial stress-hoop strain curves for FRP-confined concrete in square sections are shown in Figs. 8.6-8.8. All

numerical analyses were terminated at the rupture of the FRP jacket (failure of the FRP jacket). The predicted axial stress-strain curves are compared with the experimental curves in Fig. 8.6 for Masia et al.'s (2004) tests, in Fig. 8.7 for Hosotani et al.'s (1997) tests, and in Figs. 8.8 for Wang's (2008) tests, respectively.

Fig. 8.6a shows the predicted and the experimental axial stress-strain and axial stress-hoop strain responses for FRP-confined concrete in square columns marked as WS and tested by Masia et al. (2004). This figure shows that some variation exists within the experimental results. The numerical results fall in-between the experimental results and correlate well with the experimental results. Fig. 8.6b shows the predicted axial stress-strain and axial stress-hoop strain responses of FRP-confined concrete in two square columns named WL and tested by Masia et al. (2004). Although the numerical results slightly underestimate the deformation capacity of these two square columns, they still show adequate agreement with the experimental curves including the stiffness of the second branch of the axial stress-strain curve.

Fig. 8.7a shows the predicted and experimental axial stress-strain and axial stress-hoop strain responses of FRP-confined concrete in a square column named S-12 and tested by Hosotani et al. (1997), indicating excellent

agreement between experimental and numerical results. The first ascending branch of the experimental stress-strain curves is accurately predicted by the numerical model. Although the numerical model seems to slightly underestimate the axial stress near the transition point of the stress-strain curves, the ultimate state of the experimental curves is properly predicted. Fig. 8.7b shows a similar comparison for another column (column H-8); close agreement is seen and the axial stress in the transition zone is more closely predicted.

Fig. 8.8 shows comparisons between predicted and experimental stress-strain curves for specimens tested by Wang (2008). These figures indicate that in general the numerical model closely predicts the actual behaviour of these specimens. Fig. 8.8a shows comparisons for specimens C30R30P1 and C30R30P2. For specimen C30R30P2, close agreement is observed. For specimen C30R30P1, the ultimate stress is properly captured by the numerical model which however underestimates the deformation capacity. Fig. 8.8b shows the numerical predictions versus test results for specimens C30R45P1 and C30R45P2. For specimen C30R45P1, close agreement is observed. For specimen C30R45P2, close agreement in the shape of stress-strain curves is seen although the axial stress is slightly underestimated. Fig. 8.8c shows comparisons for specimens C30R60P1 and C30R60P2. For these two specimens, the predicted stress-strain curves are

in close agreement with the experimental results. Fig. 8.8d shows comparisons for specimens C50R60P1 and C50R60P2. For specimen C50R60P1, close agreement between the numerical and the experimental results is seen. For specimen C50R60P2, close agreement in the shape of stress-strain curves is seen although the axial stress is slightly underestimated.

As mentioned above, nine new elliptical specimens were selected for simulation. These specimens were divided into three batches. Among the different batches, the varied parameters were the unconfined concrete strength and the thickness of the FRP jacket; within each batch, the varied parameter was the a/b ratio. The variation of the a/b ratio was achieved through changing the value of b. Therefore, as b is increased, the a/b ratio becomes smaller while the cross-sectional area of the specimen becomes larger. Axial force-strain curves for FRP-confined elliptical concrete columns from both numerical analysis and experiments are shown in Fig. 8.9. The physical meaning of the axial force is similar to that of the average axial stress. Compared to the axial stress-strain curves, the difference between the axial force-strain curves for the same set of test results is more significant. The difference is most significant for the elliptical columns compared to the previous square columns. That is because for an elliptical column with a smaller a/b ratio, it is under more effective confinement and

has a larger cross-sectional area. Therefore, it can resist a much larger axial force. Hence, for FRP-confined elliptical concrete columns, axial force-strain curves are adopted for comparison instead of their corresponding axial stress-strain curves.

For these elliptical specimens, the finite element analysis was terminated when the reported ultimate experimental axial strain was reached. Some observations can be made from the experimental and the numerical results. All of these columns are predicted to have a bilinear axial force-strain curve, which is similar to the behaviour of circular concrete cylinders with a sufficient amount of FRP confinement. By contrast, the experimental results for some columns with a large aspect ratio (i.e. a large a/b ratio) show a descending post-peak branch although the descending trend is very mild. For instance, specimens with their *a/b* ratio equal to 2 in batch III and batch IV show a descending trend after their peak stress, but the specimen with the same *a/b* ratio from batch II does not show such a descending branch. The concrete strengths in these three batches are close, and the thickness of the FRP jackets in Batch III and IV are twice that of batch II. Therefore, the specimen of batch II should have a larger chance of displaying a descending response, but the experimental results are to the contrary. This may be attributed to the scatter of experimental results as the second branch is close to being horizontal in all three cases. Although the overall axial force-strain

curves of all the specimens are properly predicted by the finite element models, the ultimate axial forces of these specimens are all slightly overestimated. This trend of overestimation needs to be further examined using more experimental results.

8.4 RESULTS OF FE MODELS BASED ON THE MICROPLANE MODEL

8.4.1 Implementation of the M4$^+$ Model in ABAQUS

As indicated in Chapter 7, the M4$^+$ model was implemented into the Matlab software as an in-house code to predict the stress-strain behaviour of concrete under uniform confinement. In that case, the M4$^+$ model was only used as a material driver. A material driver is sufficient to describe the mechanical response of concrete under uniform confinement, because the stress state of the whole specimen can be represented by that of any material point. In addition, the definitions of the confining pressure and the confining stiffness for concrete under uniform confinement are clear. The detailed explanations are as follows: 1) for concrete under uniform active confinement, the confining pressure f_l is a constant; 2) for concrete under uniform passive confinement provided by a linear elastic material such as FRP, the confining stiffness k_{stiff} is a constant. In addition, the confining stresses over the cross-section are the same.

For concrete under non-uniform confinement (e.g. FRP-confined square

columns), however, the definition of the confining pressure or the confining stiffness becomes much less clear and different definitions have been proposed by previous researchers. For the confining pressure, various definitions were suggested by different researchers (e.g. Barros 2001; Johansson and Akesson 2002; Oh 2002; Montoya et al. 2006; Yu et al. 2010b), and were commonly based on a principal stress or a combination of two principal stresses. For instance, Oh (2002) used the smallest principal stress (i.e. σ_3) as the confining pressure; Barros (2001) employed the intermediate principal stress (i.e. σ_2); Johansson and Akesson (2002) and Montoya et al. (2006) used the mean value of the two smaller principal stresses (i.e. $(\sigma_2 + \sigma_3)/2$); Yu et al. (2010b) suggested a more complicated definition of the confining pressure which has been discussed in Section 8.3.2.1 in detail. For the confining stiffness, the only definition is the one proposed by Yu et al. (2010b). The expression of this confining stiffness has been given in Eq. (8.10). Although there has been some research following that of Yu et al. (2010b) (e.g. Jiang et al. 2011), no other definition exists as much of the research has focused on FRP-confined circular concrete cylinders (i.e. uniform confinement), and therefore it has not been necessary to define a new expression for the confining stiffness.

In the present study, the effects of the above four types of definitions of confining pressure on the predicted stress-strain responses of FRP-confined

concrete under non-uniform confinement have been assessed through comparison with test results. It has been found that the most suitable definition for the confining pressure in the $M4^+$ model is the smallest principal stress σ_3. The confining stiffness k_{stiff} is defined as $-\sigma_3/\varepsilon_3$ in the current model to be consistent with the definition for the confining pressure. Here, ε_3 represents the third principal strain. To avoid any numerical problems, if the k_{stiff} is smaller than a predefined value of 50, it is set to be 50.

Besides the definitions of the confining pressure and the confining stiffness, other difficulties also exist in implementing the microplane model into a finite element model. Among these, the most challenging one is probably the tangential stiffness matrix of the M4 model. In the early versions of the microplane model, such as M1 and M2, smooth curves are employed to define the relationships between micro stresses and micro strains, and their corresponding tangential stiffness matrices can be obtained directly. Using these explicit tangential stiffness matrices, the microplane model can be employed in implicit finite element models with high efficiency. In other words, nonlinear static analysis is more efficient when an explicit material tangential stiffness matrix exists. However, due to certain insufficiencies (Jirasek 1993) of these microplane models, the concept of smooth micro-stress-strain relationships has been abandoned since the M3 model,

and formulations of stress–strain boundaries were used in the later microplane models such as the M3 and the M4 models. Due to the non-smooth micro-stress-micro-strain relationship introduced by the stress-strain boundaries, an explicit tangential stiffness matrix cannot be obtained. To address this problem, Caner and Bazant (2000) suggested constructing the tangential stiffness matrix from its definition (i.e. defining the component of the tangential stiffness as the ratio between a strain increment and its induced stress increment). This is a computationally intensive approach. To reduce the computational burden, Nemecek et al. (2002) suggested using the initial elastic stiffness matrix instead of the tangential stiffness matrix. This approach is still not very effective as a large number of iterations are usually required. Moreover, this approach is prone to convergence problems during the numerical calculation. Another way which is easier is to use the $M4^{+}$ model in an explicit finite element model, where the tangential stiffness matrix becomes unnecessary.

Static problems can be solved using explicit finite element methods as long as an appropriate load time function is used to keep the inertia forces small. It is much more effective to use an explicit analysis especially when the constitutive model used is also formulated as explicit. Based on the above discussion, the $M4^{+}$ model is thus implemented in ABAQUS using the user-defined material subroutine (VUMT). Within this $M4^{+}$ model, the

definitions of the confining pressure and the confining stiffness explained in this section are used.

The $M4^+$ model was then employed to simulate the behaviour of FRP-confined concrete in non-circular columns. The $M4^+$ model is considered to be more promising and conceptually more transparent than other types of constitutive models such as plasticity-based models in modelling the responses of concrete. It also provides a more fundamental explanation of the behaviour of concrete with some reference to the material microstructure. In Chapter 7, it has been demonstrated that the behaviour of FRP-confined circular concrete cylinders can be accurately predicted using the $M4^+$ model. As mentioned in that chapter, the parameters k_1, c_7, and c_8 of the $M4^+$ model are dependent on the confining pressure and the confining stiffness. Moreover, these parameters were calibrated based on a material driver, in which the effects of end restraints were not taken into account. Considering this specific situation, a horizontal slice of concrete columns was also employed in the current finite element analysis. As the current finite element model also neglected the effects of end restraints, it thus has similar boundary conditions in the vertical direction as the previous material driver. Therefore, the empirical equations developed for the parameters k_1, c_7, and c_8 of the $M4^+$ model can be used in the finite element analysis without any modification. Another advantage of the slice

model is that it can avoid possible spurious localization at the structural level.

In the modified CDPM model, f'_{co} and ε_{co} are employed as input material parameters. However, in the M4^{+} model, three parameters E, k_1^0, and c_{18} are used as input material parameters instead of f'_{co} and ε_{co}. The values of these three parameters are determined by fitting the axial stress-strain curves of unconfined concrete. The detailed values of these three parameters for each batch of concrete are summarized in Tables 8.3 and 8.4. Other parameters required by the M4^{+} model were assigned their default values as suggested in Chapter 7. As in Section 8.3, the effects of size on the behaviour of confined concrete are still neglected here.

8.4.2 Stress-Strain Curves

The VUMAT was used in finite element analysis to model the mechanical responses of FRP-confined concrete in non-circular columns subjected to axial loading. As explained in Section 8.2, the finite element models adopted the same finite element mesh and element types as those used in Section 8.3, but were executed using ABAQUS explicit instead of ABAQUS implicit.

To evaluate the capability of the M4^{+} model in reproducing the mechanical responses of FRP-confined concrete in non-circular columns, the predicted

average axial stress-strain and axial stress-hoop strain curves along with the corresponding experimental curves are shown in Figs. 8.10-8.12. The same termination criterion as described in Section 8.3 was adopted. The predicted axial stress-strain curves are compared with the experimental curves in Fig. 8.10 for Masia et al.'s (2004) tests, in Fig. 8.11 for Hosotani et al.'s (1997) tests, and in Fig. 8.12 for Wang's (2008) tests.

Fig. 8.10a shows the predicted and the experimental axial stress-strain and axial stress-hoop strain responses of FRP-confined concrete in a square columns marked as WS and tested by Masia et al. (2004). As can be seen, there is a good agreement between the numerical and the experimental results. In addition, the ultimate states of these specimens were also accurately predicted. Fig. 8.10b shows the axial stress-strain and axial stress-hoop strain responses of the specimens marked as WL, which were also tested by Masia et al. (2004). Although the deformation capability of these specimens is slightly overestimated, the numerical results correlate remarkably well with the experimental results.

Figs. 8.11 show the predicted and the experimental axial stress-strain and axial stress-hoop strain responses of FRP-confined concrete in square columns as tested by Hosotani et al. (1997). As mentioned in Section 8.2, these two specimens were confined with two different types of FRP jackets

(Normal modulus and high modulus). These figures show that the finite element model overestimates the ultimate stress of these two specimens, but they predict the deformation capability of these specimens accurately. That is, the finite element model tends to overestimate the stiffness of the second branch of the axial stress-strain curves. The possible reason for this overestimation is that the confining stiffness involved in these two specimens are far beyond the scope of those used to calibrate the parameters of the $M4^+$ model (i.e. k_1, c_7 and c_8). In these two specimens, the FRP jacket is much thicker than other specimens selected from the database. Moreover, for specimen H-8, the elastic modulus of the FRP jacket is much larger than that of other specimens. Therefore, the confining stiffness provided by the FRP jacket in these two specimens is much larger than other specimens selected for comparison. Due to this reason, the finite element models cannot provide accurate predictions for these two specimens.

Fig. 8.12 shows the comparisons between the predicted and the experimental stress-strain curves for the specimens tested by Wang (2008). Unlike the numerical results obtained using the modified CDPM model, which tend to slightly overestimate the axial stress, especially the ultimate axial stress, the numerical results obtained using the $M4^+$ model tend to slightly underestimate the axial stress. However, the extent of this

underestimation is very small. Therefore, excellent agreement between the experimental and the numerical results is still achieved for these specimens.

Axial force-strain curves for FRP-confined elliptical concrete columns from both numerical analysis and experiments are shown in Figs. 8.13. The following observations can be made from these figures: 1) the numerical model can predict the overall behaviour of the experimental responses; 2) unlike the numerical results obtained using the modified CDPM, where all the elliptical specimens show bilinear axial force-strain curves, some of the numerical results obtained using the $M4^{+}$ model show a descending branch in axial force-strain curves for the specimens with larger values of the a/b ratio. The variations obtained using these two different constitutive models may be due to the fact that they are based on different theories.

8.5 COMPARISON WITH ANALYTICAL RESULTS FROM DIFFERENT CONSTITUTIVE MODELS AND EMPIRICAL MODELS

As mentioned above, a number of empirical or semi-empirical models have been proposed to predict the stress-strain behaviour of FRP-confined concrete in non-circular columns. Two representative models among them (i.e. Lam and Teng 2003; Wei and Wu 2012), were selected for comparison with results from the finite element models. Lam and Teng's (2003) model was chosen because it is a simple but relatively accurate model, and Wei

and Wu's (2012) model was chosen as most of the experimental data used in this chapter had already been used in building this model. The formulations of these two empirical models are summarized below.

In Lam and Teng's (2003) design-oriented stress-strain model, two shape factors, k_{s1} and k_{s2}, were adopted to consider the impact of section shapes. The equation of the ultimate axial stress is as follows:

$$f_{cu} = f'_{co} + k_1 k_{s1} f_{l,a} \tag{8.14}$$

For the ultimate axial strain, the following expression is used

$$\frac{\varepsilon_{cu}}{\varepsilon_{co}} = 1.75 + k_2 k_{s2} \frac{f_{l,a}}{f'_{co}} \left(\frac{\varepsilon_{h,rup}}{\varepsilon_{co}}\right)^{0.45} \tag{8.15}$$

Here, $k_1 = 3.3$ and $k_2 = 12$. In addition, the value of $\varepsilon_{h,rup}$ was suggested to be $0.586\varepsilon_j$ (Lam and Teng 2003). The definitions of other parameters can be found in Chapter 2.

Wei and Wu (2012) proposed a unified stress-strain model for FRP-confined concrete in both circular and rectangular columns. This empirical model is the most updated one for FRP-confined concrete in non-circular columns. Compared to Lam and Teng's (2003) design-oriented stress-strain model, more complex expressions are employed to consider the ultimate state of the FRP-confined concrete in non-circular columns. In this model, the equation of the ultimate axial stress is as follows:

$$\frac{f_{cu}}{f'_{co}} = 0.5 + 2.7\left(\frac{2r}{b_{sq}}\right)^{0.4}\left(\frac{f_l}{f'_{co}}\right)^{0.73}\left(\frac{h}{b_{sq}}\right)^{-1} \quad (8.16)$$

where f_l, is calculated by

$$f_l = \frac{2f_{frp}t}{b_{sq}} = \frac{2E_j\varepsilon_{frp}t}{b_{sq}} \quad (8.17)$$

For a square column, b_{sq} is the width of the column.

For the ultimate axial strain, the following expression is used:

$$\frac{\varepsilon_{cu}}{\varepsilon_{co}} = 1.75 + 12\left(\frac{f_l}{f'_{co}}\right)^{0.75}\left(\frac{f_{30}}{f'_{co}}\right)^{0.62}\left(0.36\frac{2r}{b_{sq}} + 0.64\right)\left(\frac{h}{b_{sq}}\right)^{-0.3} \quad (8.18)$$

where f_{30} is the concrete strength of unconfined grade C30 concrete. In Eq. (8.18), the following equation is adopted to calculate ε_{co}.

$$\varepsilon_{co} = 0.000937\sqrt[4]{f'_{co}} \quad (8.19).$$

In Sections 8.3 & 8.4, the axial stress-strain and axial stress-hoop strain curves or axial force-strain curves obtained from finite element analysis using the two different constitutive models are compared with the experimental results separately. To further demonstrate the capability of these two constitutive models, predictions for the ultimate state of the concrete are compared in Tables 8.5 and 8.6.

In Table 8.5, the predictions are normalized by the corresponding experimental results. Here, 'theo1' represents the numerical results obtained

using the modified CDPM model; 'theo2' represents the results obtained using the $M4^+$ model; 'theo3' represents the results obtained from Lam and Teng's (2003b) design-oriented stress-strain model; 'theo4' represents the results obtained from Wei and Wu's (2012) design-oriented stress-strain model. The same definitions for 'theo1' and 'theo2' are also adopted in Table 8.6.

The third and the fourth columns in Table 8.5 show the finite element results obtained using the modified CDPM model; the fifth and the sixth columns of this table show the finite element results obtained using the $M4^+$ model; the seventh and the eighth columns of this table show the results obtained from Wei and Wu's (2012) design-oriented stress-strain model; the ninth and the tenth columns of this table show the results obtained from Lam and Teng's (2003b) design-oriented stress-strain model. Two statistical indicators, i.e. the average value and the standard deviation, were calculated to assess the capability of these four approaches in predicting the ultimate state.

The average values of the ultimate stress obtained from these four approaches are 0.97, 1.1, 0.98, and 0.89, respectively. It seems that for the ultimate strength, Wei and Wu's (2012) design-oriented stress-strain model and the modified CDPM model show better performance than the other two

models. Within these two models, the results obtained from the modified CDPM model shows a relatively small standard deviation equal to 0.08, indicating that its prediction suffers a smaller variation compared to Wei and Wu's (2012) design-oriented stress-strain model (a standard deviation equal to 0.11). Wei and Wu's (2012) design-oriented stress-strain model shows even better performance for the ultimate stress than the $M4^{+}$ model. Generally, the accuracy of the empirical models strongly depends on the test database employed in the process of regression analysis. As most of the experimental data summarized in Table 8.1 except those of Hosotani et al. (1997) have been used in the process of regression analysis in calibrating Wei and Wu's (2012) model, the high accuracy of Wei and Wu's (2012) design-oriented stress-strain model for these test data is to be expected. In addition, although the numerical results obtained using the $M4^{+}$ model give a slightly larger average value, they show the smallest standard deviation among the results of all these four models.

The average values of the ultimate axial strain obtained from these four models are 0.94, 1.1, 0.86, and 0.66, respectively. For the ultimate axial strain, the modified CDPM model shows the best performance among these four models. Its predicted average value is 0.94 which is very close to 1, indicating a good agreement between the predicted values and the experimental data. In addition, its predicted values possess the smallest

standard deviation of 0.14, which means they are highly consistent. Similarly, the ultimate axial strains obtained using the $M4^+$ model also show better performance than the other two design-oriented stress-strain models. In summary, for the ultimate axial strains, the constitutive models used in finite element analyses demonstrate their advantages in providing more accurate predictions.

Another thing that should be noted is that for both the ultimate stress and the ultimate axial strain, the predicted results using the $M4^+$ model tend to slightly overestimate the experimental results, while those obtained using the other three models tend to underestimate the corresponding experimental results.

Table 8.6 summarizes the predicted ultimate axial stress obtained using the two different concrete constitutive models for FRP-confined concrete in elliptical columns. The ultimate axial strain is not compared as the finite element analysis for these elliptical specimens was terminated based on the ultimate axial strain itself. The two design-oriented stress-strain models discussed above are not directly applicable to elliptical specimens, and thus they are also not included in the comparison. In Table 8.6, the first column of data gives the numerical results obtained from the finite element analysis based on the modified CDPM model. The upper boundary of the data is

1.42; the lower boundary of the data is 1.02; the average value is 1.13 with a standard deviation of 0.12. These statistics indicate that the numerical results obtained by using the modified CDPM model tend to overestimate the ultimate axial stress. Moreover, these data indicate that for specimens with a large a/b ratio, the prediction error tends to be large. The second column of data in this table gives the numerical results obtained using the $M4^+$ model. The upper boundary of the data is 1.24; the lower boundary of the data is 0.82; the average value is 1.08 with a standard deviation of 0.16. These statistics indicate that the numerical results obtained using the $M4^+$ model also tend to slightly overestimate the ultimate axial stress. What is different from the numerical results obtained by using the modified CDPM model, in which the ultimate axial stresses for all 9 specimens are overestimated, the predictions obtained by using the $M4^+$ model do not show this systematic error. Thus, although the scatter of the predictions obtained using the $M4^+$ model is larger than that obtained using the modified CDPM model, its average error (8%) is still smaller than that obtained using the modified CDPM models (13%).

8.6 CONFINING STRESS DISTRIBUTION OVER THE WHOLE SECTION

The confining stress distribution over a non-circular section reflects the confining effects of the FRP jacket in an intuitive way. It is physically understood that a uniformly-distributed confining stress has a better

confining effect than a non-uniformly distributed confining stress. For instance, the confining effect in a circular section is better than that in a square/rectangular section with an identical cross-sectional area.

The stress distribution over a non-circular section of interest can hardly be obtained using an experimental approach. Therefore, in developing empirical models, a simplified approach is generally employed to introduce an assumed distribution (e.g. Mander et al. 1988, Lam and Teng 2003). This assumption often includes two uniformly-distributed stress zones. In one of these zones, the concrete is assumed to be under effective uniform confinement, while in the other zone, the concrete is assumed to be under no confinement. Due to the simple treatment of the stress zones, this assumption can only be seen as a rough approximation of the actual stress distribution. By contrast, the numerical results from finite element analysis enable a detailed examination of the stress distribution at any stage of loading. Therefore, in this section, the distribution of the stress over the whole cross-sections of some selected specimens is examined to provide some intuitive understanding.

Although similar numerical results were obtained using the two different constitutive models in modelling the behaviour of FRP-confined concrete in non-circular columns, in this section, only those obtained using the

modified CDPM model are examined to reveal the stress distribution. That is because for the numerical results obtained using the $M4^+$ model, their predicted stress distributions lose symmetry at relatively large values of axial deformation. To further illustrate this phenomenon, the axial stress distributions of specimen C30R30P2 based on the numerical results obtained using the $M4^+$ model are shown in Fig. 8.14. The distribution of the axial stress at an early stage before reaching the strength of unconfined concrete is shown in Fig. 8.14a. At this specific stage, the distribution of the axial stress remains symmetric. However, it can be observed that the distribution of the axial stress loses its symmetry to some extent at the ultimate state when the rupture of the FRP jacket is achieved (see Fig. 8.14b). To check whether this loss of symmetry is due to the use of the explicit finite element method, the $M4^+$ model was also implemented into the implicit finite element models with a tangential stiffness matrix as suggested by Caner and Bazant (2000). The same phenomenon still exists. Therefore, a possible reason of this asymmetry of stress may be due to the inherent characteristics of the $M4^+$ model. For an explicit material model, with the increase of the calculation time, the errors of the constitutive model may accumulate and thus the distribution of the axial stress may lose symmetry, although the accumulated errors have an insignificant effect on the overall average stress-strain behaviour.

Figs. 8.15 and 8.16 show the contours of the axial stress over two selected cross-sections, namely the sections of C30R30 and C30R45. In these two figures, the contours correspond to the stress states where the failure of the FRP jacket is achieved, which is of interest. The magnitude of the axial stress is given in MPa. In addition, the gray areas in Figs. 8.15-8.16 indicate the zones with the magnitude of the axial stress smaller than the corresponding unconfined concrete strength f'_{co} (i.e. non-effective confinement zone).

From the axial stress contour plots, some basic characteristics of the stress distribution can be observed. It seems that the distribution of the axial stress shows the pattern of an arch shape. It is typical of stress distribution of a square section that the highest axial stress occurs at the corners of the section. In addition, along the diagonal direction, the magnitude of the axial stress drops gradually, although the concrete within this zone (the zone along the diagonal direction) is still effectively confined as the smallest axial stress predicted is still larger than the unconfined concrete strength. On the other hand, the constraint on both sides of the diagonal zone becomes not so effective and the magnitude of the axial stress drops further. Therefore, the weakest confinement zones appear in the middle of the sides. As a result, the contour plot of the whole section shows an X-shape, which is similar to what is commonly assumed for a square concrete column

confined by steel hoops (Mander et al. 1988).

Furthermore, it can also be observed from Figs. 8.15 and 8.16 that the amount of FRP affects the stress distribution. With the increase of the thickness of the FRP jacket, the ineffective confinement zones (gray zones in the figures) become smaller, indicating an increased effective confinement zone. This factor has not been taken into consideration in the arching action assumption. The neglect of the effect of the thickness of the FRP jacket may be due to an implicit assumption adopted in the arching assumption. In the arching assumption, the concrete is implicitly taken as an elastic material, which means that increasing the thickness of the FRP jackets does not introduce stress redistribution. By contrast, in the finite element analysis, the concrete material experiences inelastic behaviour. Therefore, the concrete displays a nonlinear performance and the change of the thickness also affects the stress distribution.

What is more, the radius of the corner is another important factor which affects the stress distribution. Figs. 8.15 and 8.16 show that the magnitude of the axial stress is higher for the specimen with a larger corner radius. For instance, for the specimen C30R45P2 which has a relatively large corner radius of 45mm, no gray zones exist in the contour plot and the whole section can be seen as effectively confined. Generally, the effects of this

factor have been considered in the empirical model (e.g. Lam and Teng 2003).

To further illustrate the confining effect, the contours of the third principal stress are selected to represent the confining pressure and are shown in Figs. 8.17-8.18 for the above four specimens. Similarly, the distribution of the confining pressure also shows a clear pattern of an arch shape. Furthermore, as can be seen from these figures, no tensile stress appears on any of the sections, indicating that the whole section is under effective confinement. In the low confining zone, the axial stress is smaller than the unconfined concrete strength f'_{co} because the axial strain at the failure stage is much larger than ε_{co}. Therefore, concrete experienced a long stress softening process, although its peak stress is still larger than the unconfined concrete strength f'_{co}.

Similar to that of square sections, Fig. 8.19 shows the contours of the axial stress over two elliptical cross-sections of batch II with two different a/b ratios. It can be observed from these figures that the axial stress near the vertex of the major axis of the ellipse is larger than that near the minor axis of the ellipse. Moreover, along the major axis of the ellipse, there is a significant gradient existing in the axial stress. With the increase of the a/b ratio, the gradient of the axial stress becomes large, indicating an increased

non-uniformity of the stress distribution. This observation may explain why a larger a/b results in a less effective confinement effect.

8.7 CONCLUSIONS

This chapter has been concerned with the development of finite element models for the analysis of FRP-confined non-circular concrete columns. These finite element models can be employed to perform a large number of numerical experiments for detailed examinations of the underlying mechanism of confinement. Two constitutive models, i.e. the modified CDPM model and the $M4^+$ model were employed to describe the behaviour of concrete under confinement. These two constitutive models were selected as their accuracy for FRP-confined circular concrete cylinders had already been verified, and therefore they were considered to be more promising in predicting the mechanical responses of FRP-confined concrete in non-circular columns compared to other constitutive models.

The finite element models using the above two constitutive models were verified by comparison with experimental results of FRP-confined concrete in non-circular columns. The comparison showed that the finite element models were capable of reproducing the axial stress-strain or axial force-strain response of FRP-confined concrete in non-circular columns. In addition, the high accuracy of these finite element models indicates that the

finite element models can capture the major characteristics of the experimental results.

Furthermore, the corner radius of the square section was properly considered in the finite element model. In this way, it is possible to trace the hoop strains at any place of the square section to determine the onset of rupture of the FRP jacket. In addition, the presence of a corner radius has a significant effect on the confinement effect. Therefore, this detail plays an important role in the confinement mechanism.

For FRP-confined concrete in square columns, the numerical results were also compared with results from existing empirical models. For the ultimate stress, the empirical model developed by Wei and Wu (2012) has similar accuracy as the finite element model using the modified CDPM model. However, for the ultimate axial strain, the finite element models using the two constitutive models both have better performance than the empirical models.

The numerical results enabled a comprehensive examination of the distribution of the axial stress and that of the confining pressure in the hoop direction. It was found that both the corner radius and the thickness of the FRP jacket have a significant effect on the stress distribution in the concrete.

The effect of corner radius has already been widely accepted by researchers and considered in some empirical models (e.g. Lam and Teng 2004). By contrast, the effect of the thickness of the FRP jacket on the stress distribution is not so intuitive. This effect exists because concrete is a non-linear material and the thickness of the FRP jacket changes the stress state of concrete at failure.

8.8 REFERENCES

Barros, M. H. F. (2001). "Elasto-plastic modelling of confined concrete elements following MC90 equations." *Engineering Structures*, 23(4), 311-318.

Binici, B. (2005). "An analytical model for stress-strain behaviour of confined concrete." *Engineering Structures,* 27(7),1040-1051.

Caner, F. C., and Bazant, Z. P. (2000). "Microplane model M4 for concrete. II: Algorithm and calibration." *Journal of Engineering Mechanics*-ASCE, 126(9), 954-961.

Doran, B., Koksal, H. O., and Turgay, T. (2009). "Nonlinear finite element modelling of rectangular/square concrete columns confined with FRP." *Materials & Design*, 30(8), 3066-3075.

Harajli, M. H. (2006). "Axial stress-strain relationship for FRP confined circular and rectangular concrete columns." *Cement and Concrete*

Composites, 28(10), 938-948.

Hosotani, M., Kawashima, K., and Hoshikuma, J. "Seismic retrofit of reinforced concrete bridge piers by carbon fiber sheets." *In: Proc., 3rd US-Japan Workshop of Seismic Retrofit of Bridges*, 217-242.

Jiang, J., Wu, Y., and Zhao, X. (2011). "Application of Drucker-Prager Plasticity Model for Stress-Strain Modelling of FRP Confined Concrete Columns." *Procedia Engineering*, 14, 687-694.

Jiang, T., and Teng, J. G. (2007). "Analysis-oriented stress-strain models for FRP-confined concrete." *Engineering Structures*, 29(11), 2968-2986.

Jirasek, M. (1993). *Modelling of fracture and damage in quasi-brittle materials*, Northwestern University.

Johansson, M., and Akesson, M. (2002). "Finite element study of concrete-filled steel tubes using a new confinement-sensitive concrete compression model." *Nordic Concrete Research Publications*, 27, 43-62.

Karabinis, A. I., and Kiousis, P. D. (1994). "Effects of confinement on concrete columns-plasticity approach." *Journal of Structural Engineering*-ASCE, 120(9), 2747-2767.

Lam, L., and Teng, J. G. (2003). "Design-oriented stress-strain model for FRP-confined concrete in rectangular columns." *Journal of Reinforced Plastics and Composites*, 22(13), 1149-1186.

Malvar, L. J., Morrill, K. B., and Crawford, J. E. (2004). "Numerical modelling of concrete confined by fiber-reinforced composites." *Journal of Composites for Construction*-ASCE, 8(4), 315-322.

Mander, J. B., Priestley, M. J. N., and Park, R. (1988). "Theoretical stress-strain model for confined concrete." *Journal of Structural Engineering*-ASCE, 114(8), 1804-1826.

Masia, M. J., Gale, T. N., and Shrive, N. G. (2004). "Size effects in axially loaded square-section concrete prisms strengthened using carbon fibre reinforced polymer wrapping." *Canadian Journal of Civil Engineering*, 31(1), 1-13.

Montoya, E., Vecchio, F. J., and Sheikh, S. A. (2006). "Compression field modelling of confined concrete: Constitutive models." *Journal of Materials in Civil Engineering*, 18(4), 510-517.

Nemecek, J., Patzak, B., Rypl, D., and Bittnar, Z. (2002). "Microplane models: computational aspects and proposed parallel algorithm." *Computers & Structures*, 80(27), 2099-2108.

Oh, B. (2002). *A plasticity model for confined concrete under uniaxial loading*, Lehigh University.

Stefano, C. (2011). *Experimental study on carbon FRP-confined elliptical concrete columns*, MPh Thesis, University of Bologna.

Teng, J. G., Huang, Y. L., Lam, L., and Ye, L. P. (2007). "Theoretical model for fiber-reinforced polymer-confined concrete." *Journal of*

Composites for Construction-ASCE, 11(2), 201-210.

Wang, L. (2008). *Effect of corner radius on the performance of CFRP-confined square concrete columns*, City University of Hong Kong.

Wei, Y. Y., and Wu, Y. F. (2012). "Unified stress-strain model of concrete for FRP-confined columns." *Construction and Building Materials*, 26, 381-392.

Yu, T., Teng, J. G., Wong, Y. L., and Dong, S. L. (2010a). "Finite element modelling of confined concrete-I: Drucker-Prager type plasticity model." *Engineering Structures*, 32(3), 665-679.

Yu, T., Teng, J. G., Wong, Y. L., and Dong, S. L. (2010b). "Finite element modelling of confined concrete-II: Plastic-damage model." *Engineering Structures*, 32(3), 680-691.

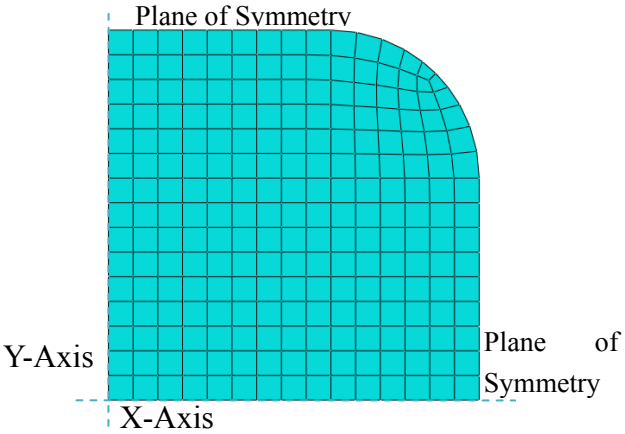

(a) Plan view

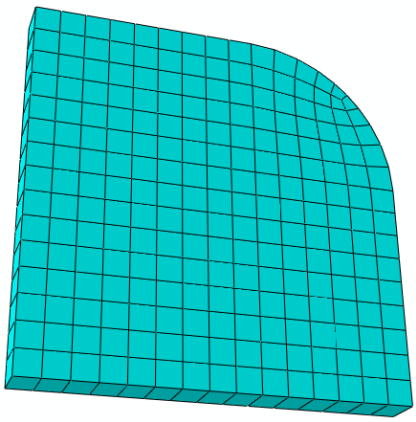

(b) 3D view

Figure 8.1 Mesh details for specimens C30R30 from Wang (2008)

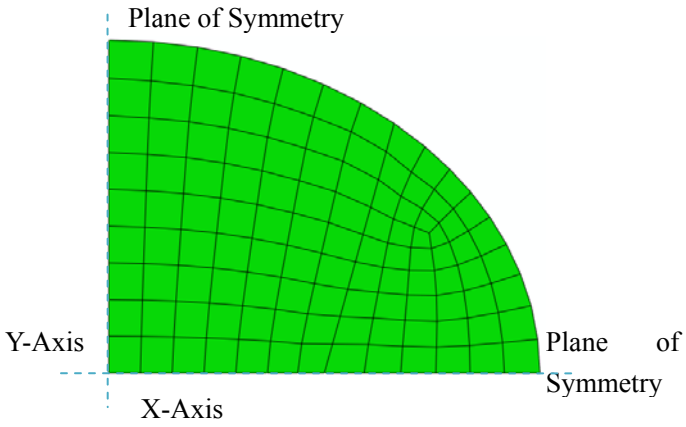

(a) Plan view

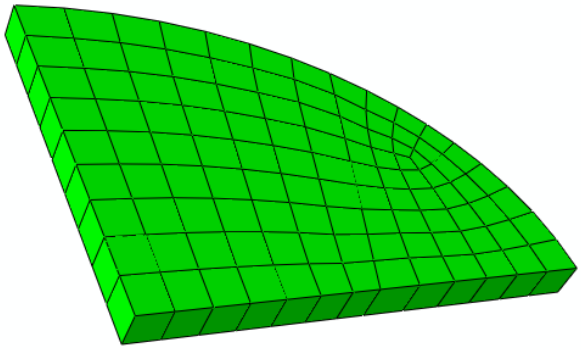

(b) 3D view

Figure 8.2 Mesh details for Stefano's (2011) Batch II elliptical specimens (a/b=1.3)

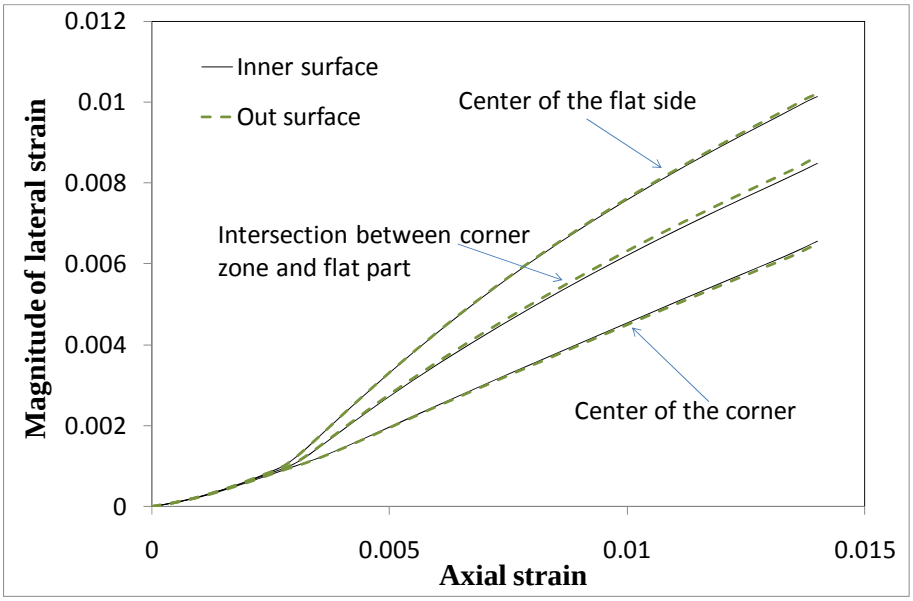

Figure 8.3 Effect of bending deformation on the CDPM finite element results for specimen C30R30P2

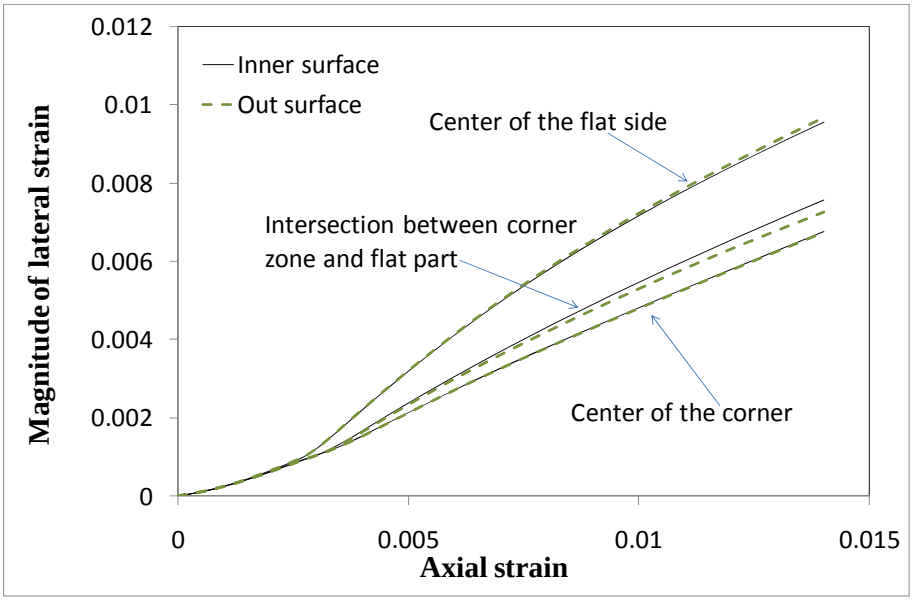

Figure 8.4 Effect of bending deformation on the CDPM finite element results for specimen C30R45P2

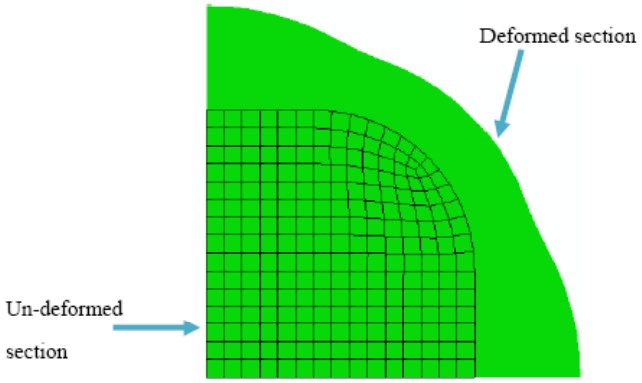

Figure 8.5 Un-deformed section and deformed section of specimen C30R45P2 from a CDPM finite element model

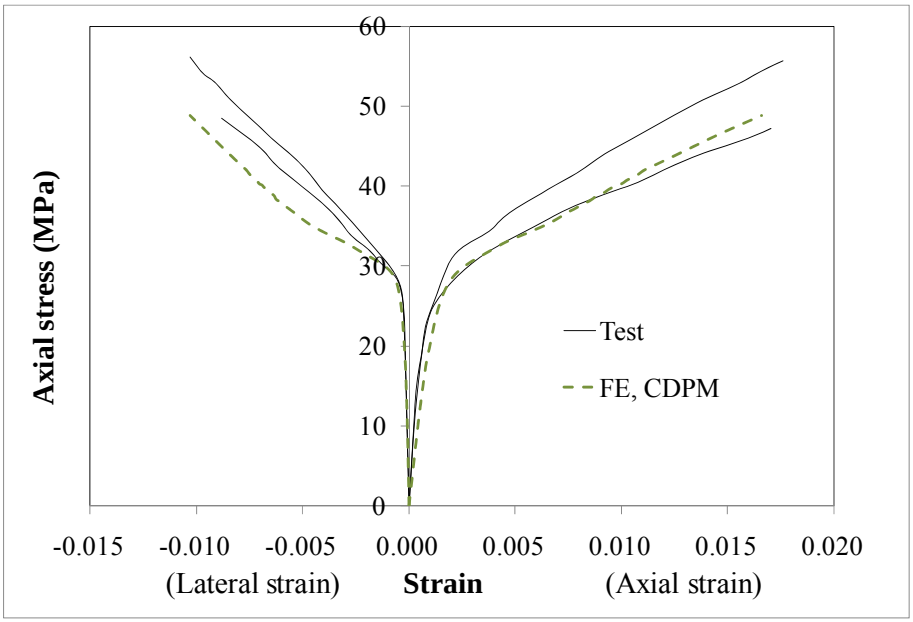

(a) Specimens WS

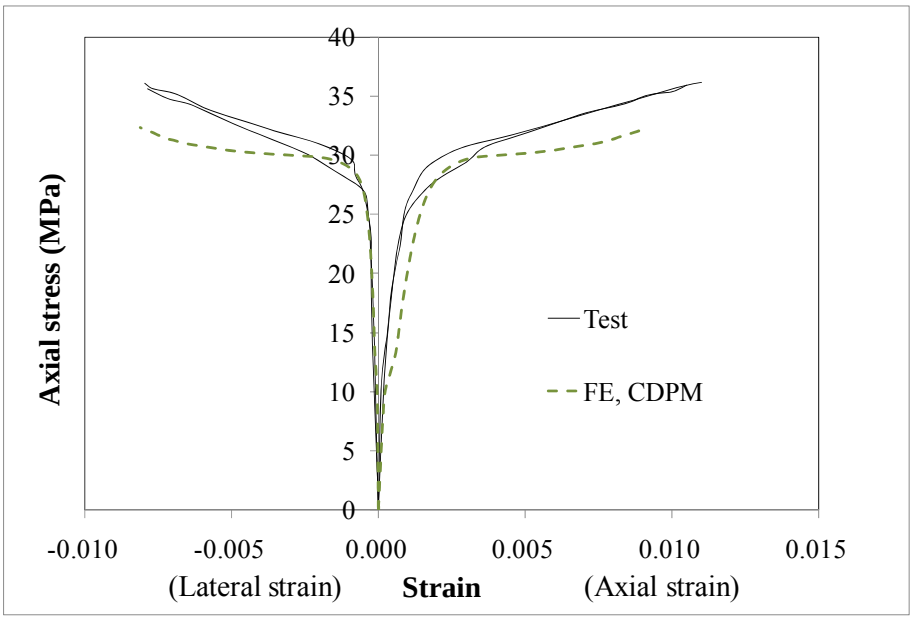

(b) Specimens WL

Figure 8.6 Axial stress-strain and axial stress-hoop strain curves for Masia et al.'s (2004) tests (Based on the CDPM model)

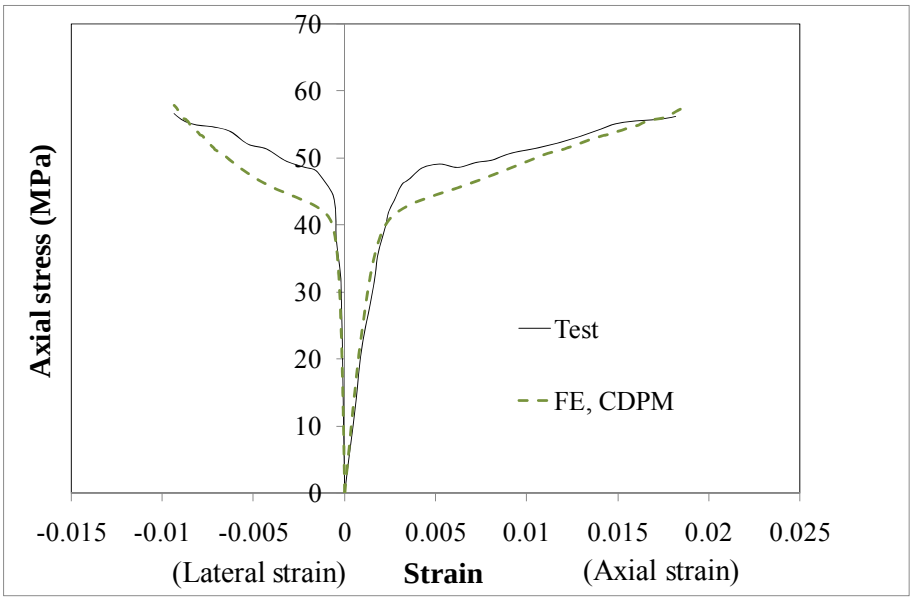

(a) Specimen S-12

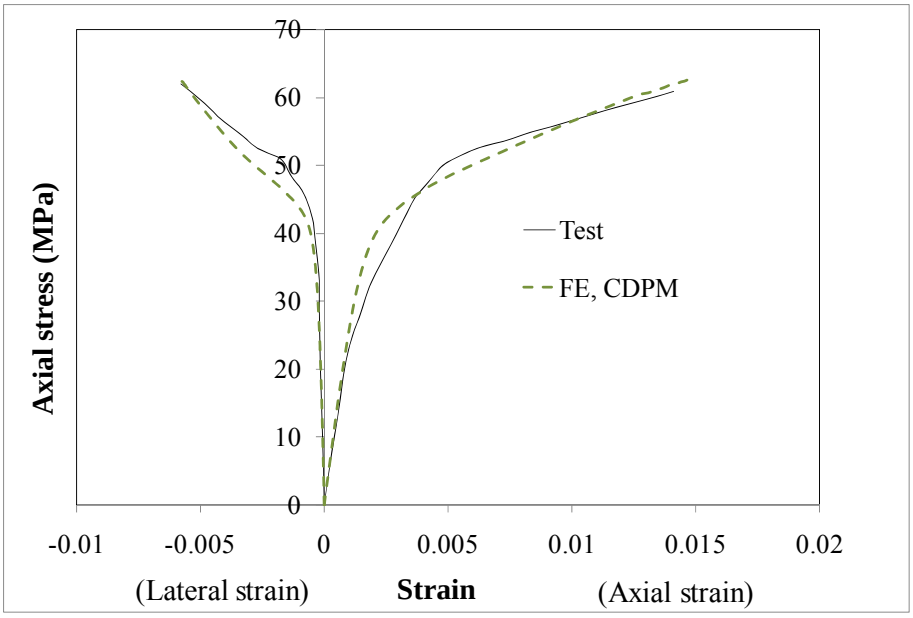

(b) Specimen H-8

Figure 8.7 Axial stress-strain and axial stress-hoop strain curves for Hosotani et al.'s(1997) tests (Based on the CDPM model)

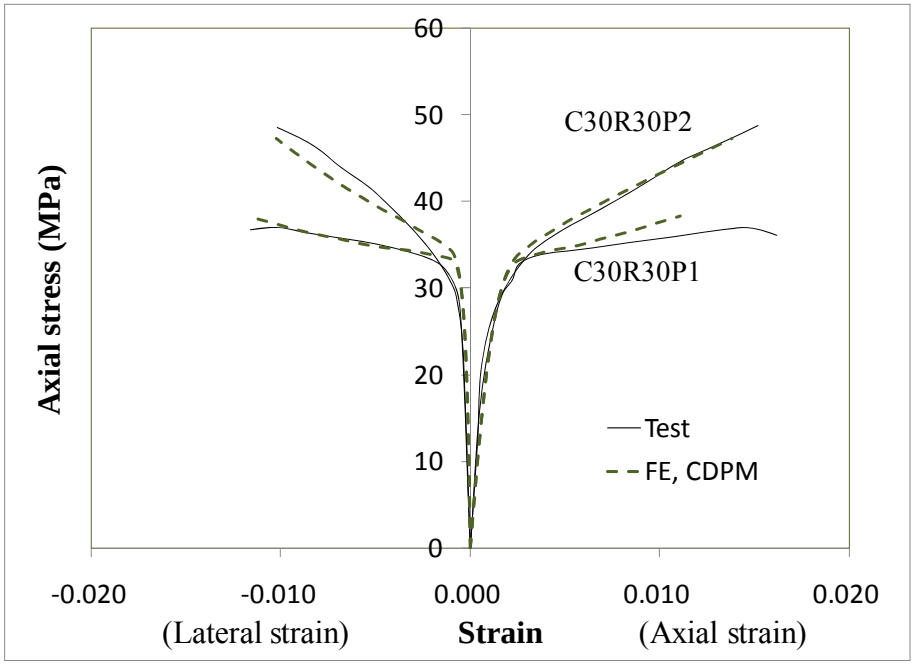

(a) Specimens C30R30

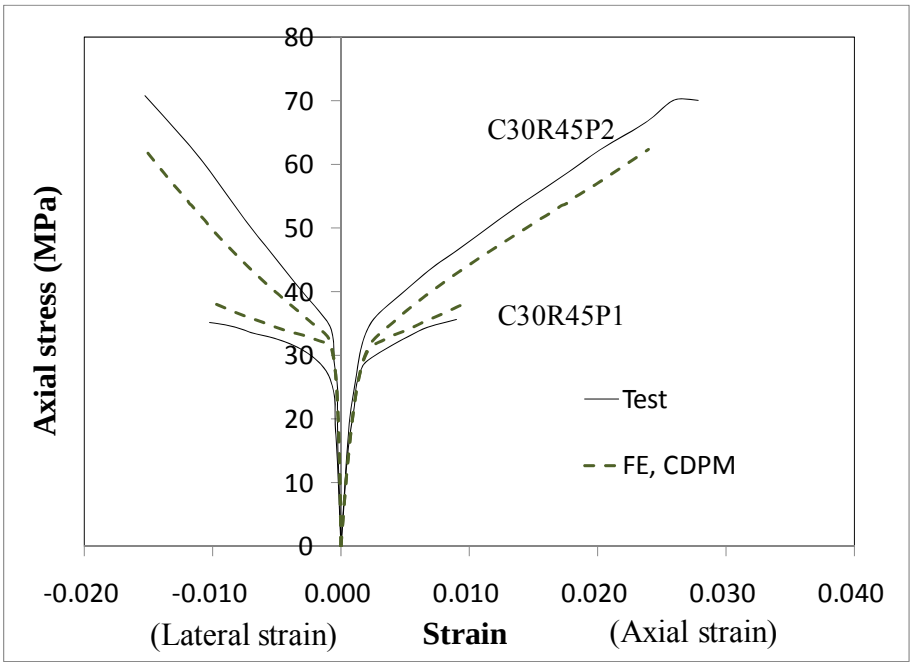

(b) Specimens C30R45

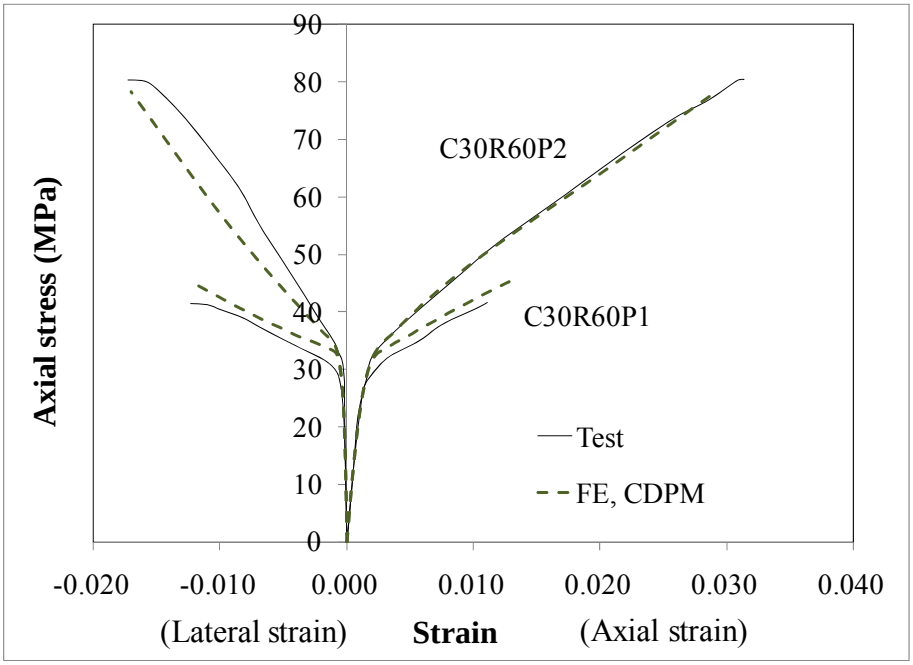

(c) Specimens C30R60

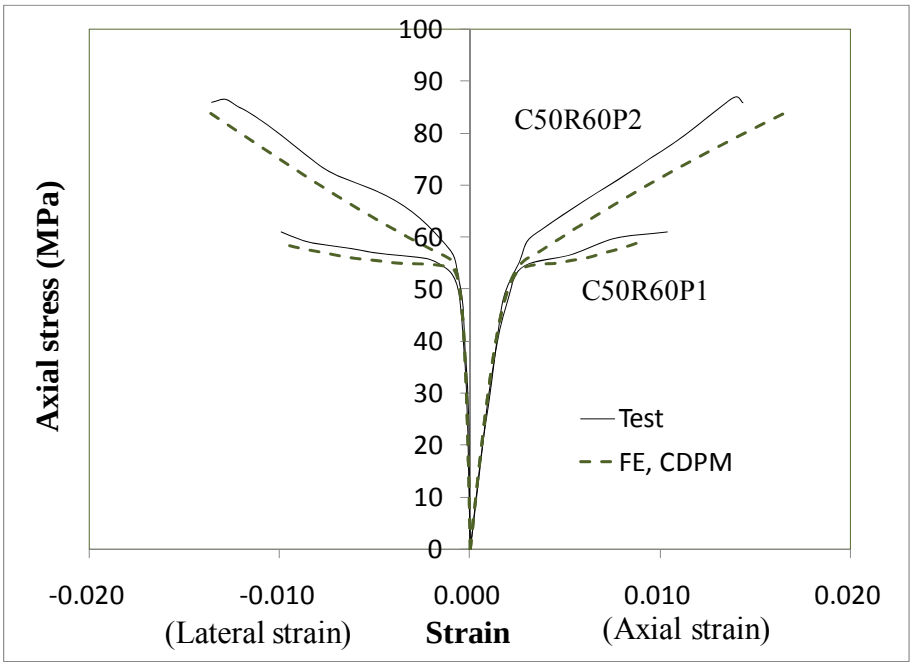

(d) Specimens C50R60

Figure 8.8 Axial stress-strain and axial stress-hoop strain curves for Wang's (2008) tests (Based on the CDPM model)

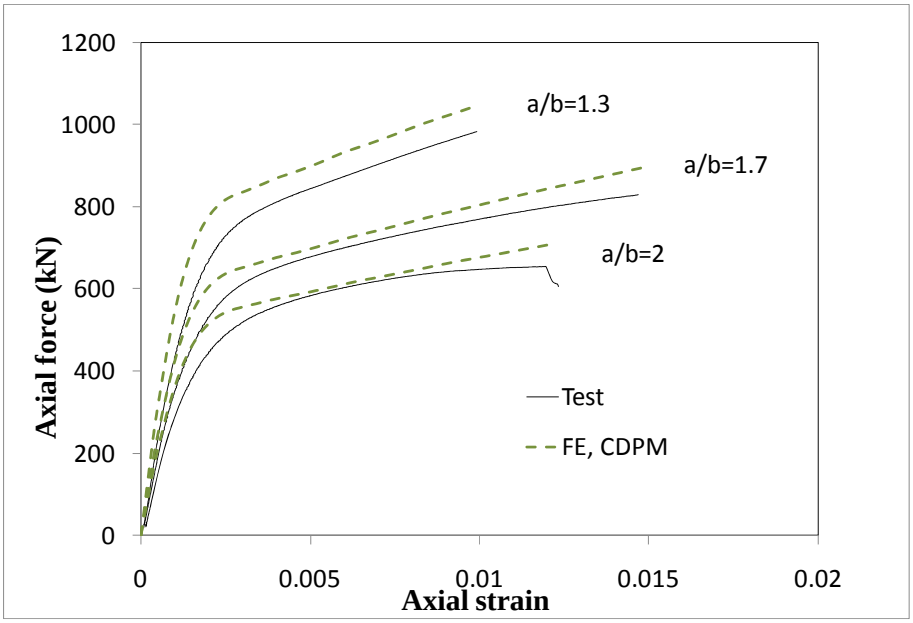

(a) Batch II

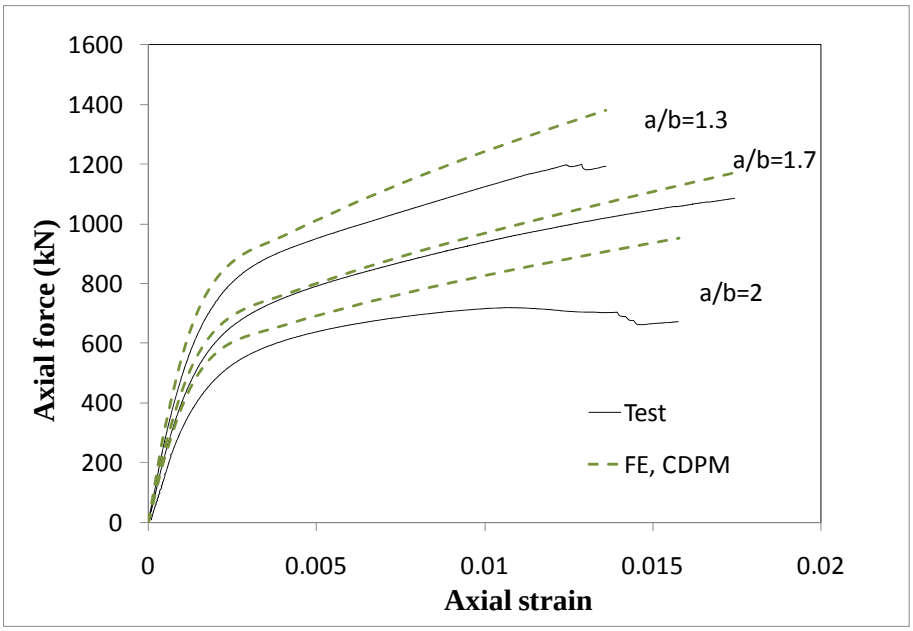

(b) Batch III

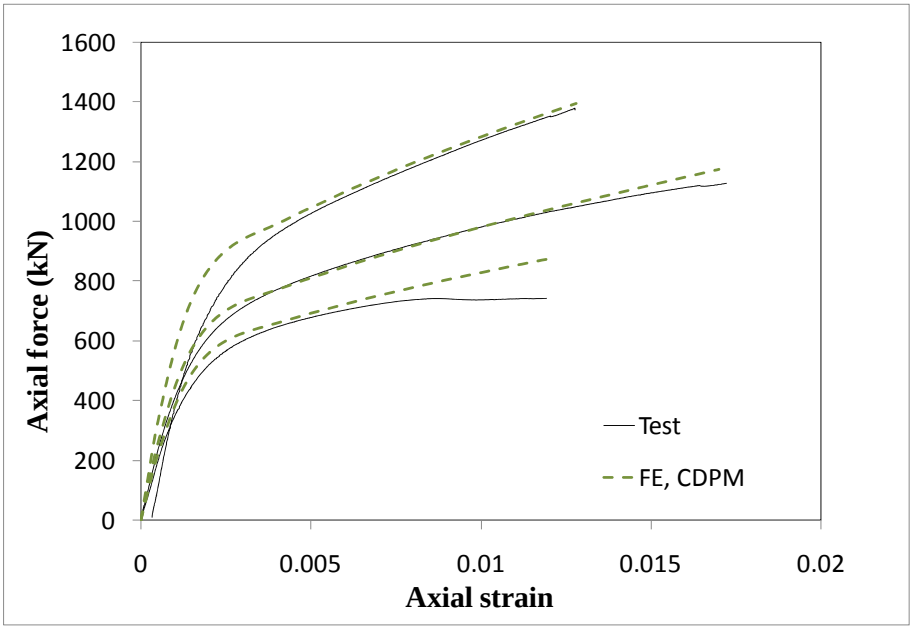

(c) Batch IV

Figure 8.9 Axial force-strain curves for Stefano's (2011) elliptical specimens (Based on the CDPM model)

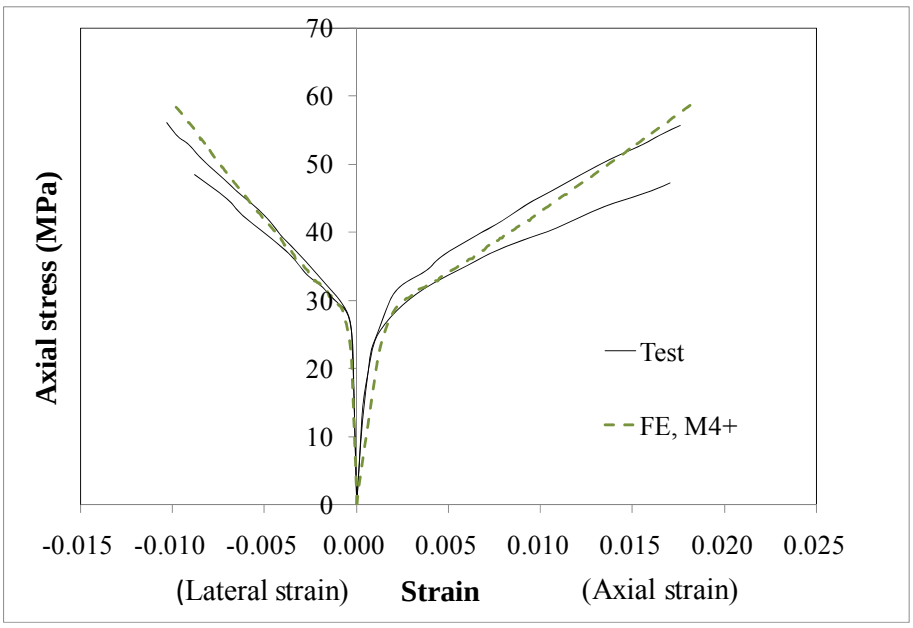

(a) Specimens WS

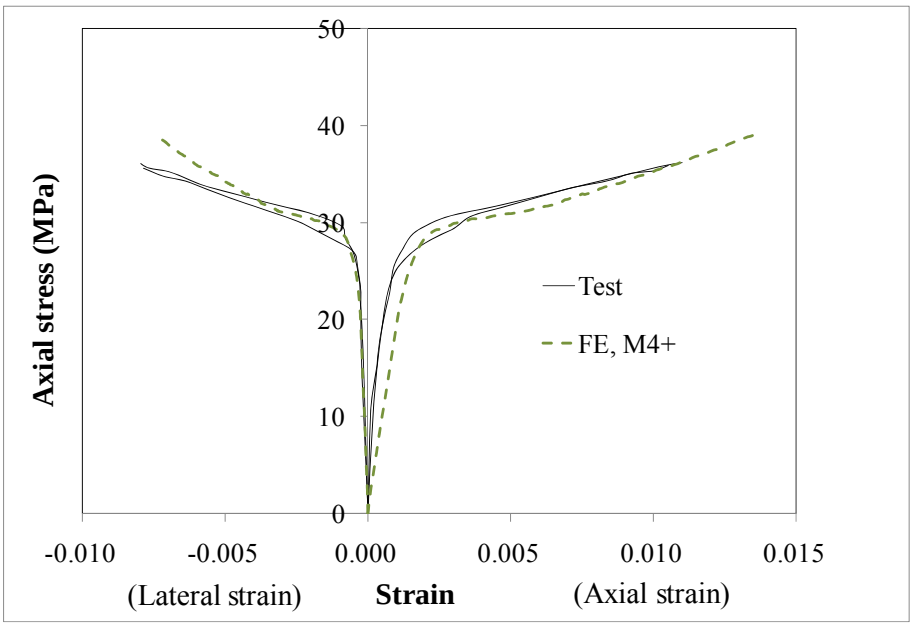

(b) Specimens WL

Figure 8.10 Axial stress-strain and axial stress-hoop strain curves for Masia et al.'s(2004) tests (Based on the $M4^{+}$ model)

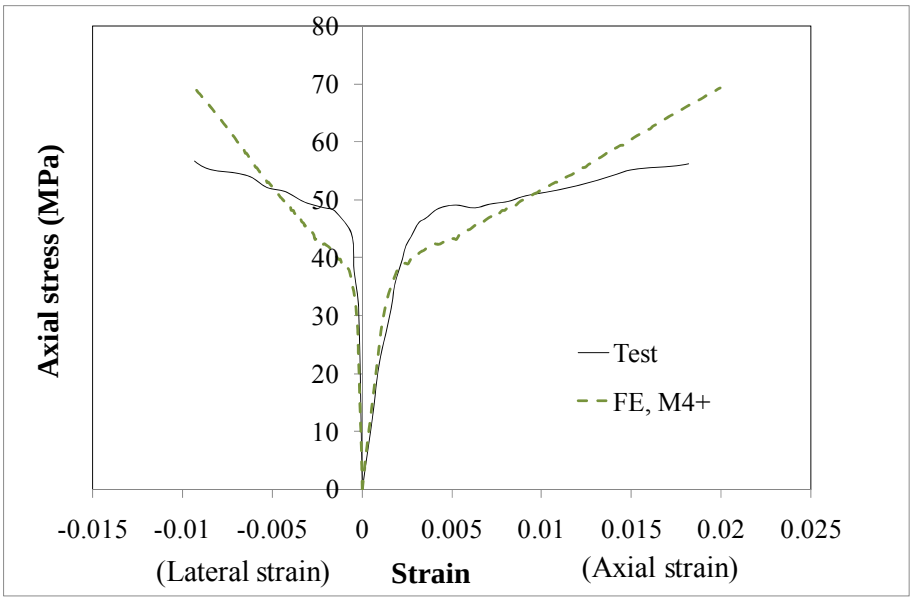

(a) Specimen S-12

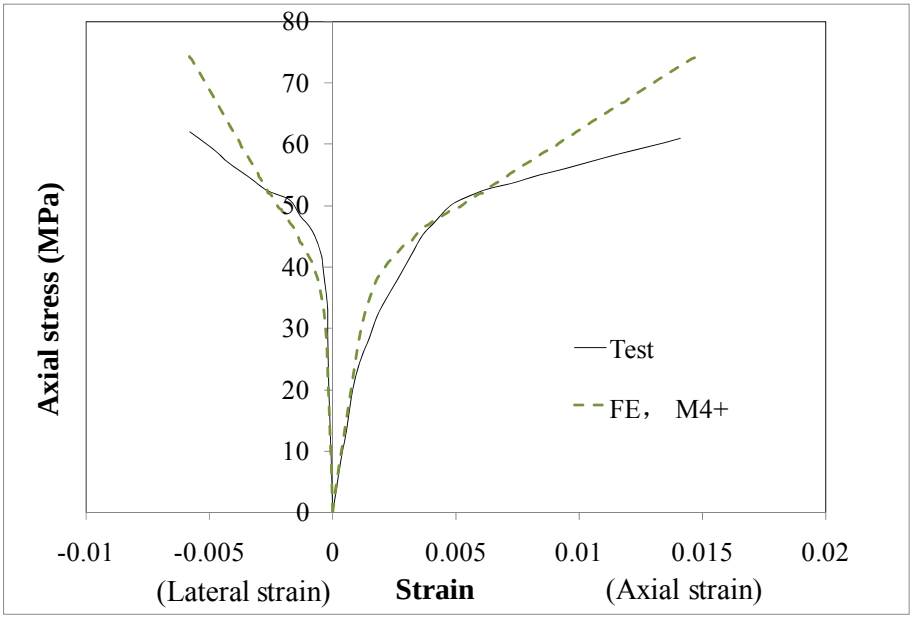

(b) Specimen H-8

Figure 8.11 Axial stress-strain and axial stress-hoop strain curves for Hosotani et al.'s(1997) tests (Based on the $M4^{+}$ model)

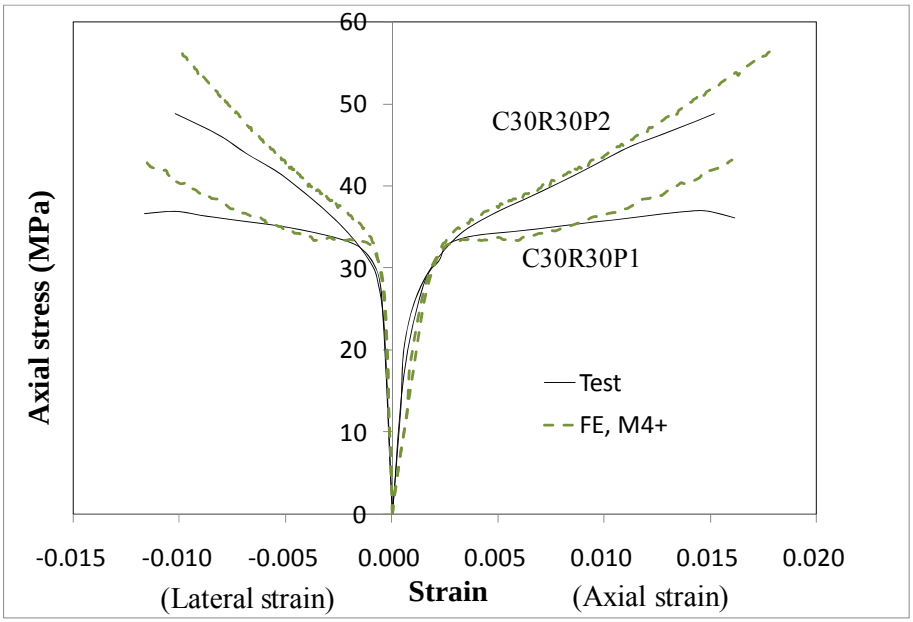

(a) Specimens C30R30

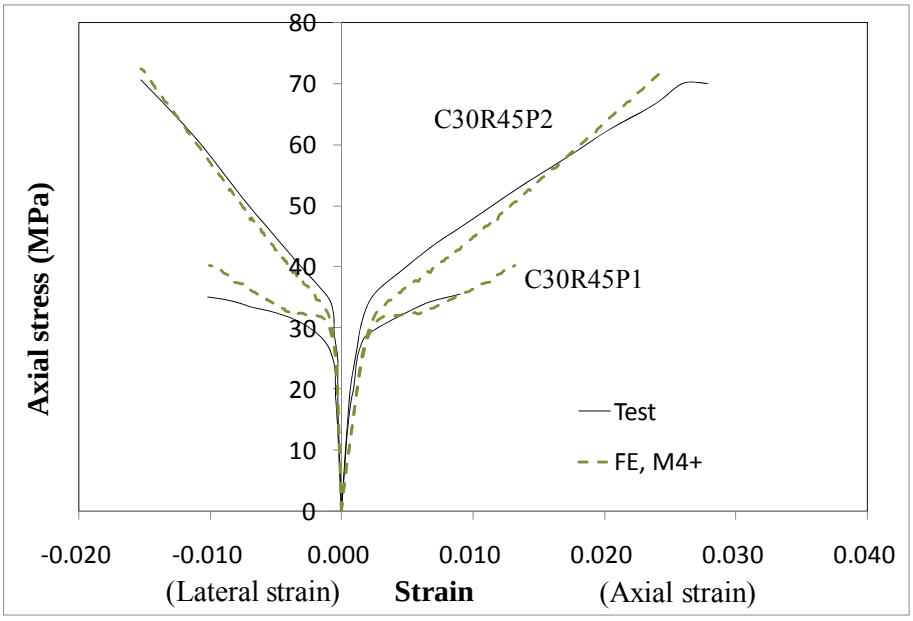

(b) Specimens C30R45

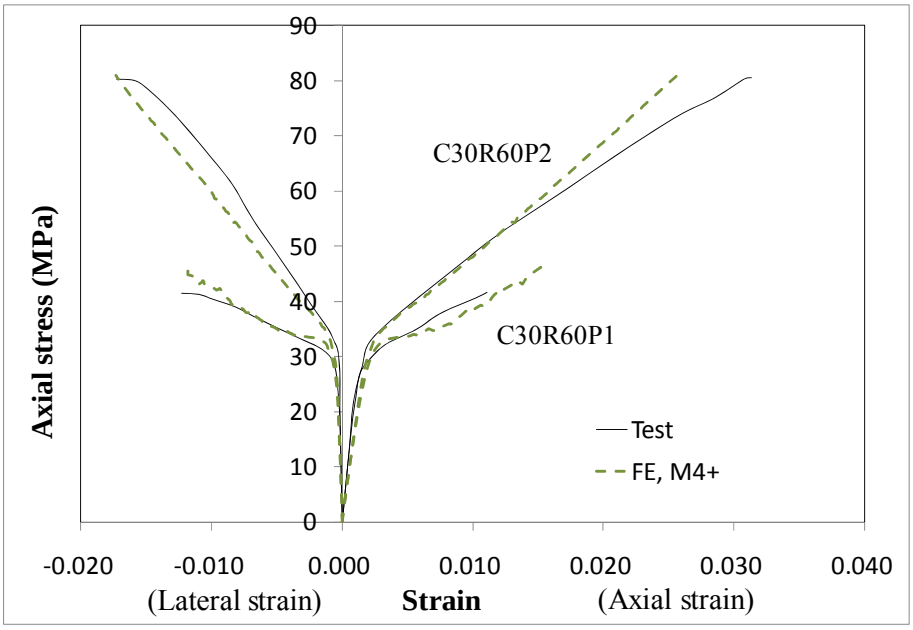

(c) Specimens C30R60

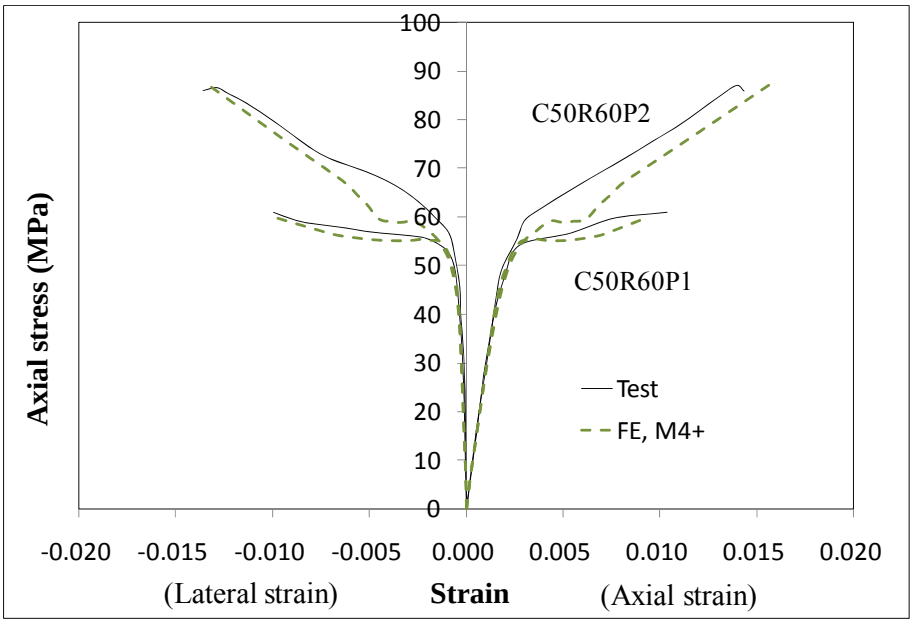

(d) Specimens C50R60

Figure 8.12 Axial stress-strain and axial stress-hoop strain curves for Wang's (2008) tests (Based on the $M4^{+}$ model)

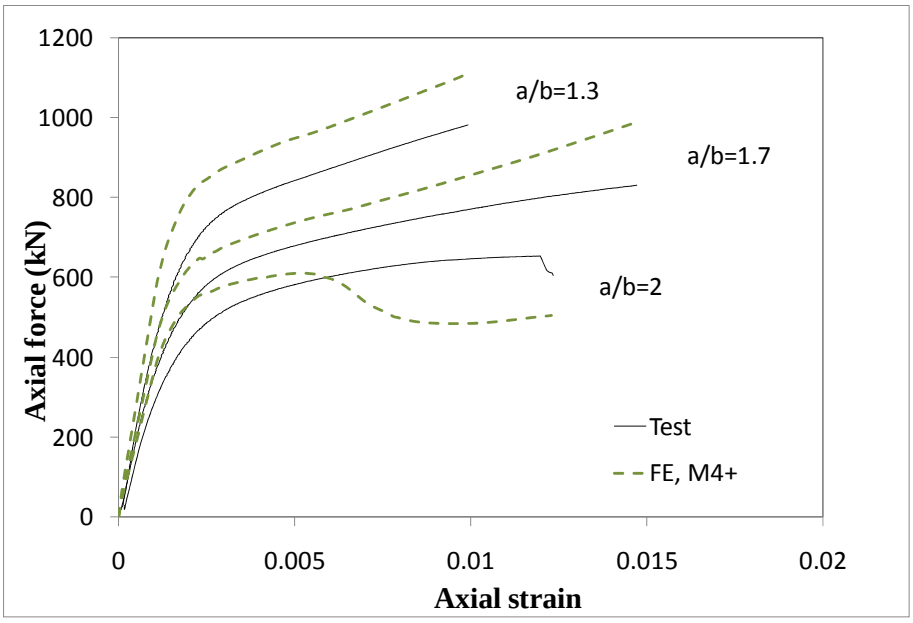

(a) Batch II

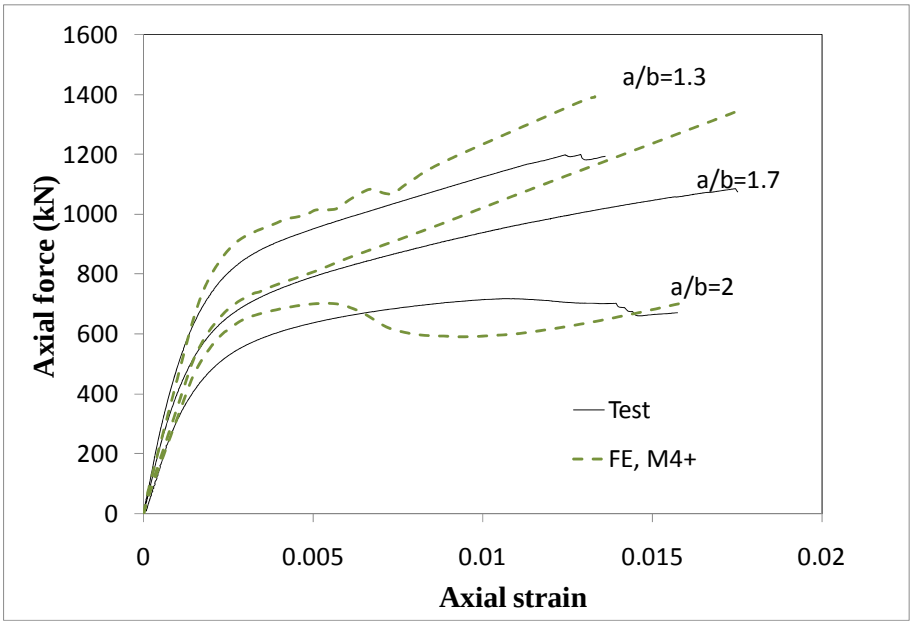

(b) Batch III

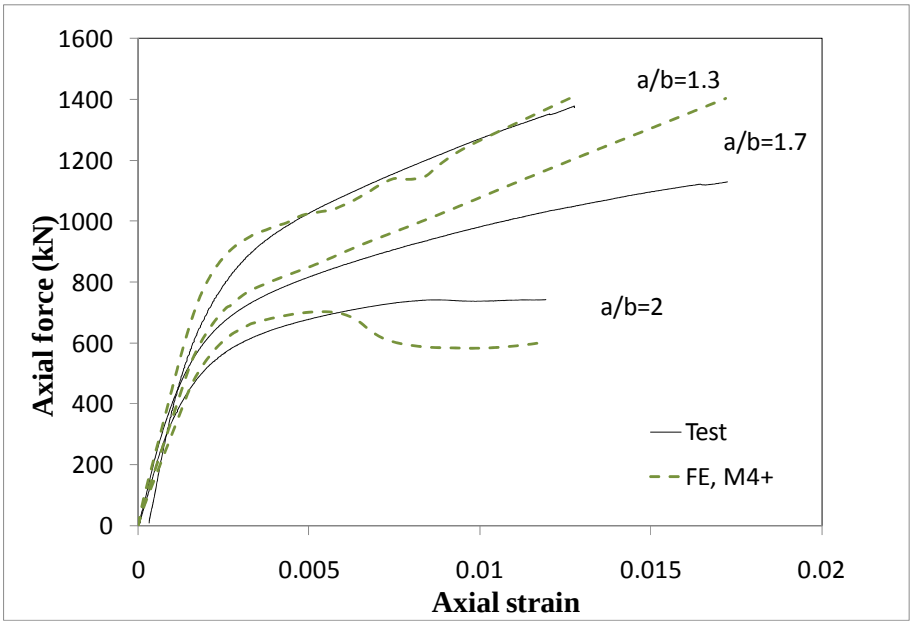

(c) Batch IV

Figure 8.13 Axial force-strain curves for Stefano's (2011) elliptical specimens (Based on the $M4^{+}$ model)

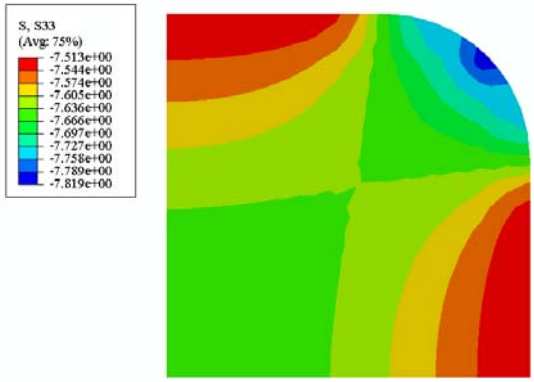

(a) Early stage

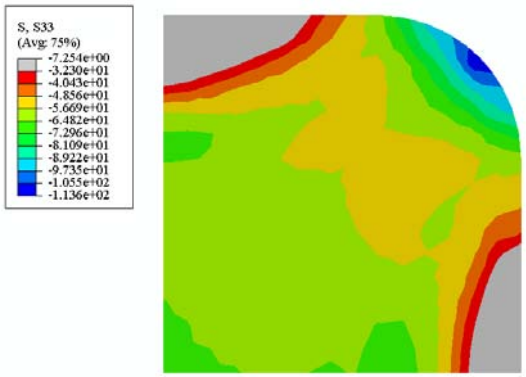

(b) Ultimate stage

Figure 8.14 Contours of axial stress over the cross-section of specimen C30R30P2 (Based on the $M4^{+}$ model)

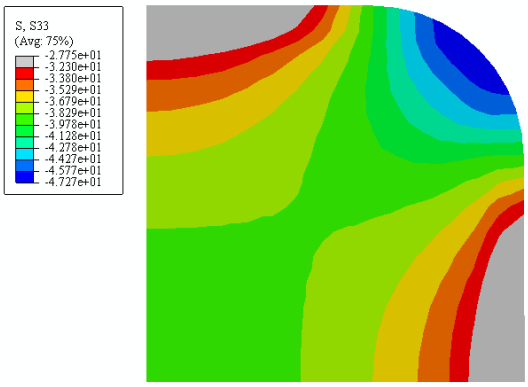

(a) 1-ply

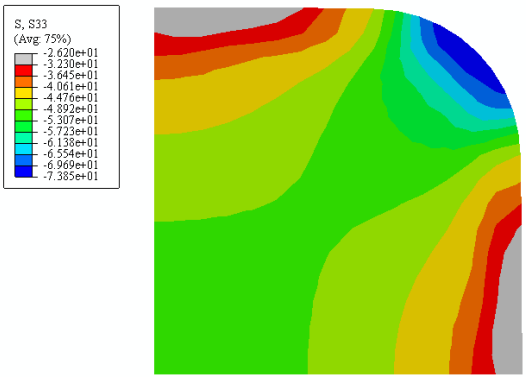

(b) 2-ply

Figure 8.15 Contours of axial stress over the cross-section of specimens C30R30 (Based on the CDPM model)

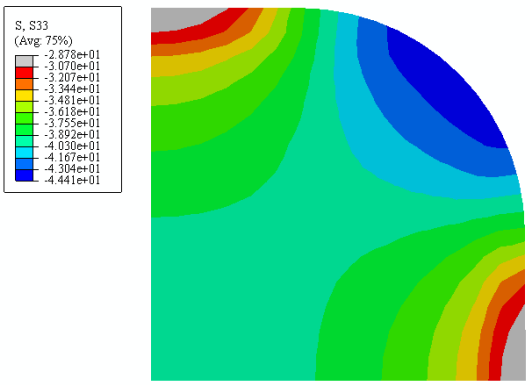

(a) 1-ply

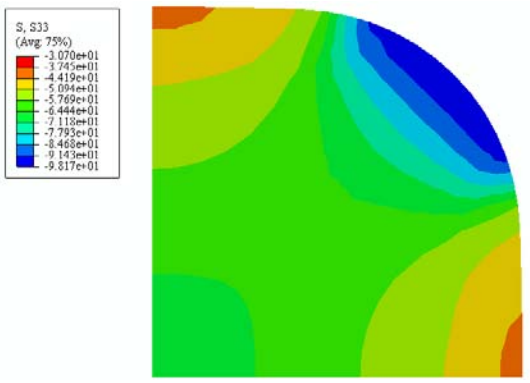

(b) 2-ply

Figure 8.16 Contours of axial stress over the cross-section of specimens C30R45 (Based on the CDPM model)

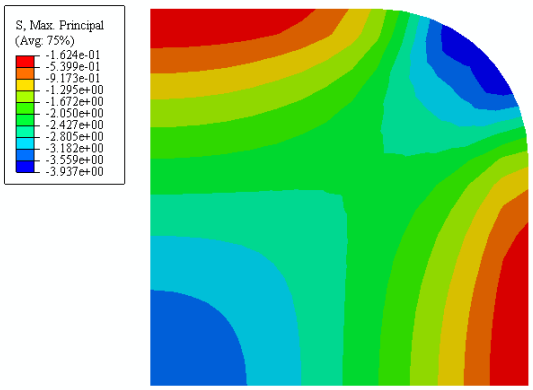

(a) 1-ply

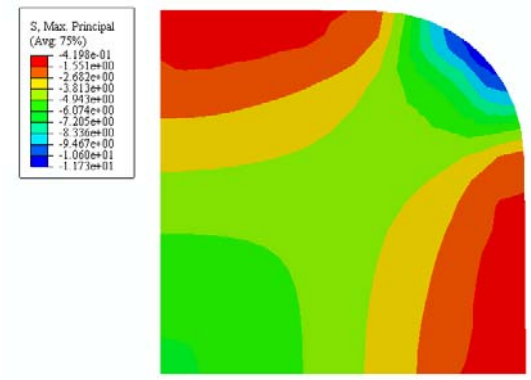

(b) 2-ply

Figure 8.17 Contours of confining stress over the cross-section of specimens C30R30 (Based on the CDPM model)

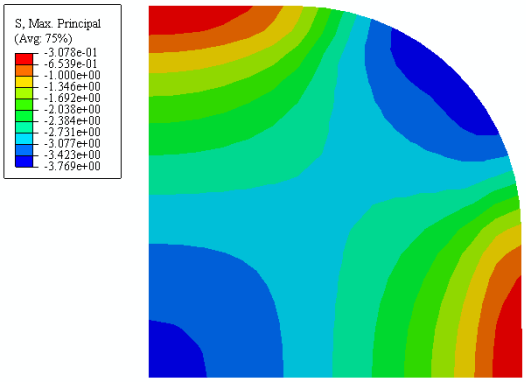

(a) 1-ply

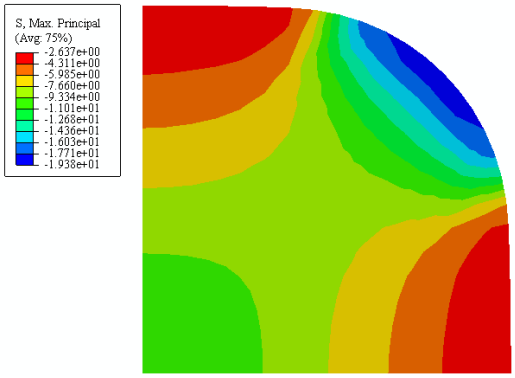

(b) 2-ply

Figure 8.18 Contours of confining stress over the cross-section of specimens C30R45 (Based on the CDPM model)

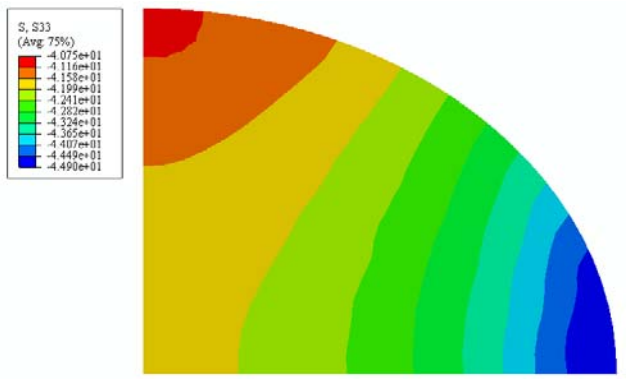

(a) Batch II, a/b=1.3

(b) Batch II, a/b=2

Figure 8.19 Contours of axial stress over the cross-sections of elliptical specimens (Based on the CDPM model)

Table 8.1 Properties of FRP-confined square columns

Researchers	Specimen index	Dimension,B*L, mm	Corner radius r, mm	B/r	f'_{co}, Mpa	ε_{co}	Ej, Gpa	t_j, mm	f_{frp} (MPa)	ε_{frp} (%)
Masia et al. (2004)	WS	100*300	25	4	27	0.002	230	0.26	3500	1.5
	WL	150*450		6						
Hosotani et al. (1997)	H-8	200*600	30	6.7	38	0.0021	439	0.68	4433	1.76
	S-12						252	0.67	3972	0.9
Wang (2008)	C30R30P1	150*300	30	5	32.3	0.0027	219	0.165	4364	1.99
	C30R30P2							0.33		
	C30R45P1		45	3.3	30.7	0.0027		0.165		
	C30R45P2							0.33		
	C30R60P1		60	2.5	31.8	0.0027		0.165		
	C30R60P2							0.33		
	C50R60P1				52.7	0.0027	225.7	0.165	3788	1.92
	C50R60P2							0.33		

Table 8.2 Properties of FRP-confined elliptical columns

Batch	a/b	H, mm	a, mm	b, mm	f'_{co}, Mpa	ε_{co}	Ej, Gpa	t_j, mm
II	1.3	398.8	201	154.7	32.64	0.0027	242	0.171
	1.7	400.6	200.1	120.8				
	2	398.9	201.7	101.9				
III	1.3	398.5	202.9	156	35.69	0.0027		0.342
	1.7	399.7	200.8	120.2				
	2	399.5	202.9	102.1				
IV	1.3	397.9	200.7	155.4	35.92	0.0029		
	1.7	399.4	199.9	120.9				
	2	399.2	200.3	101.9				

Table 8.3 Properties of FRP-confined square columns and parameters for the M4^{+} model

Researchers	Specimen index	Dimension,B*L, mm	Corner radius r, mm	B/r	f'_{co}, Mpa	ε_{co}	Ej, Gpa	t_j, mm	k_1^0	E, Gpa	c_{18}
Masia et al. (2004)	WS	100*300	25	4	27	0.002	230	0.26	0.00015	24.3	0.2
	WL	150*450		6							
Hosotani et al. (1997)	H-8	200*600	30	6.7	38	0.0021	439	0.68	0.000162	31.7	0.2
	S-12						252	0.67			
Wang (2008)	C30R30P1	150*300	30	5	32.3	0.0027	230.5	0.165	0.000192	22.6	0.2
	C30R30P2							0.33			
	C30R45P1		45	3.3	30.7	0.0027		0.165	0.000192	21.5	0.2
	C30R45P2							0.33			
	C30R60P1		60	2.5	31.8	0.0027		0.165	0.000192	22.3	0.2
	C30R60P2							0.33			
	C50R60P1				52.7	0.0027		0.165	0.000192	37	0.2
	C50R60P2							0.33			

Table 8.4 Properties of FRP-confined elliptical columns and parameters for the $M4^{+}$ model

Batch	a/b	H, mm	a, mm	b, mm	f'_{co}, Mpa	ε_{co}	Ej, Gpa	t_j, mm	k_1^0	E, Gpa	c_{18}
II	1.3	398.8	201	154.7	32.64	0.0027	242	0.171	0.000145	29	0.4
	1.7	400.6	200.1	120.8							
	2	398.9	201.7	101.9							
III	1.3	398.5	202.9	156	35.69	0.0027		0.342	0.000192	25.3	0.2
	1.7	399.7	200.8	120.2							
	2	399.5	202.9	102.1							
IV	1.3	397.9	200.7	155.4	35.92	0.0029			0.000206	23.7	0.2
	1.7	399.4	199.9	120.9							
	2	399.2	200.3	101.9							

Table 8.5 Predictions from finite element models and empirical models for FRP-confined square columns

Researchers	Specimen index	$f_{cu,theo1}/f_{cu,exp}$	$\varepsilon_{cu,theo1}/\varepsilon_{cu,exp}$	$f_{cu,theo2}/f_{cu,exp}$	$\varepsilon_{cu,theo2}/\varepsilon_{cu,exp}$	$f_{cu,theo3}/f_{cu,exp}$	$\varepsilon_{cu,theo3}/\varepsilon_{cu,exp}$	$f_{cu,theo4}/f_{cu,exp}$	$\varepsilon_{cu,theo4}/\varepsilon_{cu,exp}$
Masia et al. (2004	WS-1	0.93	0.79	1.05	1.05	0.96	1.02	0.82	0.74
	WS-2	0.87	0.91	1.13	0.96	1.05	1.27	0.88	0.88
	WL-1	0.90	0.84	1.09	1.29	1.06	1.48	1.01	0.95
	WL-2	0.89	0.84	1.08	1.24	0.97	1.68	0.90	1.02
osotani et al. (199	H-8	1.01	1.05	1.20	1.06	0.75	0.55	0.73	0.42
	S-12	1.02	1.06	1.22	1.10	0.81	0.43	0.80	0.30
Wang (2008)	C30R30P1	1.05	0.69	1.17	0.99	1.11	0.72	1.06	0.56
	C30R30P2	0.98	0.91	1.16	1.19	1.02	0.65	0.92	0.56
	C30R45P1	1.09	1.11	1.13	1.45	1.06	0.82	0.97	0.65
	C30R45P2	0.86	0.88	1.03	0.89	0.93	0.66	0.79	0.58
	C30R60P1	1.09	1.15	1.12	1.37	1.02	0.69	0.89	0.56
	C30R60P2	0.98	0.93	1.01	0.82	0.89	0.61	0.72	0.55
	C50R60P1	0.97	0.85	0.98	0.90	1.12	0.80	1.04	0.78
	C50R60P2	0.98	1.17	1.02	1.10	0.96	0.62	0.87	0.68
Average value		0.97	0.94	1.10	1.10	0.98	0.86	0.89	0.66
Standard deviation		0.08	0.14	0.07	0.18	0.11	0.37	0.11	0.20

Table 8.6 Predictions from finite element models for FRP-confined elliptical column

Batch	a/b	$f_{cu,theo1}/f_{cu,exp}$	$f_{cu,theo2}/f_{cu,exp}$
II	1.3	1.07	1.13
	1.7	1.08	1.19
	2	1.08	0.83
III	1.3	1.16	1.17
	1.7	1.08	1.24
	2	1.42	1.04
IV	1.3	1.02	1.03
	1.7	1.04	1.24
	2	1.19	0.82
Average value		1.13	1.08
Standard deviation		0.12	0.16

CHAPTER 9

FINITE ELEMENT ANALYSIS OF FRP-CONFINED CONCRETE COLUMNS USING THE MODIFIED CDPM MODEL FOR CONCRETE

9.1 INTRODUCTION

As discussed in Chapter 8, the plastic-damage model proposed by Yu et al. (2010b) for FRP-confined concrete was further refined to make it applicable to 3D finite element modelling. This refined model has been referred to as the modified CDPM model in the previous chapter. An additional assumption of uniform axial deformation was adopted in Yu et al. (2010b) so that the finite element model only needs to include a horizontal slice of the column represented by a single-layer of solid elements. Such a slice model can closely represent the mid-height region of an FRP-confined circular concrete cylinder. Having been successfully employed in the nonlinear finite element analysis of hybrid FRP-concrete-steel double-skin tubular columns (DSTCs) in Yu et al. (2010b), it can also be used to model the responses of FRP-confined concrete in non-circular columns, so long as the end restraints existing in the column can be neglected (see Chapter 8). This slice model provides an efficient approach for modelling interactions within the chosen transverse plane provided that axial non-uniformity is un-important. However, it is impossible for the slice model to capture the axial non-uniformity in both deformations and stresses. For instance, when concrete is only confined by steel hoops, the slice model cannot be directly applied.

Therefore, Yu et al.'s model was first extended to the 3D case in the study reported in this chapter. At the beginning of the study, particular attention was paid to the effects of end restraints and a recalibration process was adopted to eliminate their impact on the numerical results. After that, the recalibrated model is used in finite element models to examine the effects of internal and external passive confinement provided by both transverse steel bars and FRP jackets. Finally, the finite element models were utilized to check the assumption of arching action, which is commonly used in concrete confined by transverse steel bars.

The present study was focused on the performance of a concrete constitutive model in the finite element analysis of concrete columns. FRP and steel are the other two materials which are commonly used in concrete columns. Therefore, constitutive models for these two materials are also briefly described here. In the finite element models presented below, the FRP jacket is treated as a linear elastic material that fails when its rupture strain is reached; the steel bar is considered as an elastic-perfectly-plastic material and bar buckling is not considered. The material parameters for both materials are given for each column specimen. Additionally, a perfect bond is assumed between concrete and steel (or FRP) if not specifically mentioned.

9.2 ANALYSIS OF FRP-CONFINED CONCRETE CYLINDERS

9.2.1 Finite Element Model

The finite element model was to simulate the behaviour of FRP-confined concrete cylinders using ABAQUS. Circular concrete cylinders, each with a diameter (D) of 150 mm and a length (L) of 300 mm, were considered. The modified CDPM model as described in Chapter 8 was adopted as the constitutive model for concrete in the finite element simulation. For FRP jackets, only the confinement stiffness in the hoop direction was considered. The Poisson's ratio of the FRP jacket was set to be zero and this value was always used in the numerical simulations of this study. These settings ensured that the FRP jacket only functioned as a confining device in the finite element model.

Based on the symmetry conditions of FRP-confined circular cylinders, an axi-symmetric model was used and only half of the column height was included in the finite element model. A 4-node axi-symmetric solid element and a 2-node axi-symmetric membrane element were adopted for the concrete and the FRP jacket respectively. Both the concrete and the FRP jacket had elements' size of about 6.25 mm, which was chosen on the basis of a mesh convergence study. In all these finite element models, axial displacements were uniformly imposed on the top surface of the concrete cylinder until the maximum hoop strain in the FRP jacket reached its rupture strain. (e.g. 0.9%)

9.2.2 Effects of End Restraints

In standard compression tests of concrete specimens such as standard cylinders or cubes, the horizontal displacements at the ends of the specimen are restrained by the friction between the end surfaces and the loading platens. It has been well established that the end restraints affect the failure mode and load carrying capacity of the concrete specimen (Sangha and Dhir 1972), and the characteristic "shear cone failure" is a result of the end restraints. As it is not realistic to completely eliminate the end restraints in laboratory tests, it is generally recommended that the compressive strength of concrete be obtained from tests with end restraints, and the axial compressive strain of concrete in cylindrical tests be based on the average shortening in the mid-height region within a gauge length no more than two thirds the height of the specimen (ASTM 2010). This is also the normal practice for the compression tests of FRP-confined concrete cylinders.

In this sub-section, the effects of end restraints are first discussed based on numerical examples of typical FRP-confined concrete cylinders. It is generally assumed for these numerical examples that, for concrete, its unconfined strength f'_{co} is 40 MPa and its axial strain at peak stress ε_{co} is 0.0025; for FRP jackets, its thickness t_{frp}, modulus of elasticity E_{frp} and average hoop rupture strain $\varepsilon_{h,rup}$ are 0.34mm, 240GPa and 0.009, respectively. The finite element model presented in Section 9.2.1 was utilized for the simulation. To achieve more accurate predictions, input parameters required by the modified CDPM model (Yu et al. 2010b) were derived using Jiang and Teng's (2007) analysis-oriented stress-strain model,

which has been verified as a more accurate model for FRP-confined concrete in circular cylinders.

Fig. 9.1 shows that without end restraints, the distributions of both axial displacements and stresses are uniform; however, when the horizontal displacements at the end are precluded by restraints, the distributions of both axial displacements and axial stresses become highly non-uniform. Fig. 9.2 shows that without end restraints, the finite element model reproduced the stress-strain curves predicted by Jiang and Teng's (2007) model. However, when horizontal restraints were added to the ends, the finite element analysis predicted a lower axial stress than Jiang and Teng's (2007) model at the same hoop strain. In these figures, the axial stress is the average axial stress over a horizontal cross-section, the hoop strain is that obtained on the outer surface of the concrete cylinder at mid-height (i.e. the plane of symmetry), and the axial strain is the axial displacement on the outer surface of the concrete cylinder at a height of 60 mm divided by half of the gauge length, which is equaled to 60 mm in this case.

Based on the information given in Figs 9.1 & 9.2, it is clear that end restraints have a negative effect on the responses of FRP-confined concrete in terms of the compressive strength and the strain capacity. This negative effect arises because end restraints result in non-uniform confinement, which was found to have insignificant effect in increasing the axial stress of FRP-confined concrete. By contrast, end restraints prevent the

FRP-confined cylinder from lateral expansion at the ends and lead to non-uniform straining of the FRP jacket along the height. When the FRP jacket reaches its hoop rupture strain at the mid-height, its hoop strain is still much smaller away from the mid-height and is equaled to zero at the ends. As a result of this non-uniform straining of the jacket, the FRP-confined concrete reaches its ultimate axial stress earlier at a smaller value of axial strain.

An important point to note is that, when an analysis-oriented stress-strain model is used to derive the input parameters for finite element analysis, an assumption is implied that this model represents the local behaviour of a material point of concrete in the finite element model and the effects of end restraints do not exist. However, as mentioned in section 9.2.1, if this analysis-oriented stress-strain model (e.g. Jiang and Teng 2007) has been calibrated using test results of FRP-confined circular concrete cylinders with end restraints, this assumption is not valid (i.e. Jiang and Teng's model is not a local analysis-oriented model). Therefore, when such an analysis-oriented stress-strain model is used to derive the input parameters, the end effects are considered twice if end restraints are added to the finite element model as a boundary condition. This explains why the finite element model reproduces the responses predicted by Jiang and Teng's (2007) model when end restraints are not added, but does not do so when they are (see Fig. 9.2).

9.2.3. Recalibration of Analysis-oriented Stress-strain Model

To address this problem, a local analysis-oriented model is needed. The key

components in the analysis-oriented stress-strain model of Teng et al. (2007) or Jiang and Teng (2007) are the lateral strain equation describing the axial strain-lateral strain relationship of concrete under varying lateral confinement and the expressions defining the compressive strength and corresponding axial strain of actively confined concrete. In order to remove the effects of end restraints, these expressions have to be recalibrated. As it is not realistic to recalibrate the expressions against test data free of the effects of end restraints, the coefficients used in these expressions were adjusted by a trial-and-error process. This process was executed until the finite element model with end restraints could reproduce the predictions of the original analysis-oriented stress-strain model (i.e. the one proposed by Jiang and Teng 2007).

As a result of the recalibration, the lateral strain equation becomes

$$\frac{\varepsilon_c}{\varepsilon_{co}} = 1.05\left\{\left[1 + 0.75\left(\frac{-\varepsilon_l}{\varepsilon_{co}}\right)\right]^{0.7} - \exp\left[-7\left(\frac{-\varepsilon_l}{\varepsilon_{co}}\right)\right]\right\} \times \left(1 + 8\frac{\sigma_l}{f'_{co}}\right) \qquad (9.1)$$

where ε_c and ε_l are the axial strain and lateral strain in the concrete, and ε_{co} is the axial strain at the compressive strength of unconfined concrete. On the other hand, the expressions for the compressive strength and corresponding axial strain of actively confined concrete become

$$f'^{*}_{cc} = f'_{co} + 4\sigma_l \qquad (9.2)$$

This change in the confinement effectiveness coefficient also leads to the following equation for the axial strain of concrete at f'^{*}_{cc}:

$$\frac{\varepsilon^{*}_{cc}}{\varepsilon_{co}} = 1 + 20\left(\frac{\sigma_l}{f'_{co}}\right) \qquad (9.3)$$

where ε_{cc}^{*} is the axial strain at the peak axial stress of concrete under a lateral confining pressure σ_l.

The only difference between the original lateral strain equation proposed by Teng et al. (2007) (also used in Jiang and Teng's model) and Eq. (9.1) is that a coefficient of 0.85 in the former is changed to 1.05 in the latter. Similarly, Eq. (9.2) is slightly different from the original equation proposed by Teng et al. (2007) (also used in Jiang and Teng's model), and it is closer to the equation of Richart et al. (1928) with a confinement effectiveness coefficient of 4.1. The change of Eq. (9.3) from the equations used in Teng et al. (2007) and Jiang and Teng (2007) is a result of the change in the confinement effectiveness coefficient, following the approach of Richart et al. (1929) who used a factor of five times the confinement effectiveness coefficient in the equation for the axial strain at the peak stress. It seems that the assumption of path-independency is still valid as the local analysis-oriented stress-strain model can provide accurate predictions for both actively-confined concrete and FRP-confined concrete. The effect of end restraints is included in Jiang and Teng (2007) model. Therefore, an active-confinement model which slightly underestimates the peak axial stress and the corresponding axial strain is used to remedy the underestimation caused by end restraints. This underestimation is excluded from the local analysis-oriented stress-strain model, which leads to an active-confinement model capable of providing close predictions for actively-confined concrete. In addition, it is worth noting that Eq. (9.2) results in a K value of 0.699 instead of the original value of 0.725 that was

suggested by Yu et al. (2010b).

Eqs. (9.1), (9.2) and (9.3), together with the stress-strain model of Popovics (1973), form a new analysis-oriented stress-strain model which can be considered as a local stress-strain model for confined concrete. Fig. 9.3 shows the performance of the finite element model with the input parameters produced by this new local stress-strain model. It is clear that with end restraints, the finite element model can very closely reproduce the predictions of Jiang and Teng's (2007) analysis-oriented stress-strain model (Fig. 9.3). It is also evident that with end restraints the finite element model predicts the test results reasonably closely. In Figs. 9.4a-b, 9.4c and 9.4d, the concrete cylinders were wrapped with CFRP (Lam et al. 2006), GFRP (Teng et al. 2007), and Aramid FRP (AFRP) (Dai et al. 2011), respectively. Details of the specimens are provided in the figures.

9.3 SIMULATION OF FRP-JACKETED CIRCULAR RC COLUMNS

9.3.1 Test Columns

The tri-axial stress states in FRP-jacketed circular RC columns have been studied by several researchers (e.g. Montoya et al. 2004; Eid and Paultre 2007; Rougier and Luccioni 2007; Karabinis et al. 2008; Doran et al. 2009) using different constitutive models. Among these studies, Montoya et al. (2004) utilized MCFT in a nonlinear finite element analysis; Rougier and Luccioni (2007) used a plastic-damage model to describe the material behaviour of concrete in their finite element models; and Eid and Paultre (2007), Karabinis et al. (2008), Doran et al. (2009) adopted the DP type

plasticity model for confined concrete. These existing studies have achieved partial success in predicting the stress-strain behaviour of FRP- confined RC columns but there is still room for improvement.

To verify the capacity of the plastic-damage model based on the local analysis-oriented stress-strain model in representing the structural behaviour of concrete columns under confinement provided by both FRP jackets and transverse steel, test results from Eid et al. (2009) were chosen for comparison with the numerical results based on the current concrete constitutive model. In the experimental program, a total of 21 large-scale reinforced concrete (RC) columns (303*1,200mm) were tested and stress-strain curves of confined concrete were provided for ten of them. These large-scale RC columns were designed to examine confinement provided by transverse steel, FRP jackets, or both. Moreover, two types of transverse steel, hoops and spirals, were adopted to examine their corresponding confinement effects. Both ends of these specimens were confined by additional thick steel jackets with a length of 300mm for each to ensure that the failure of these specimens would occur in their mid-height region. Most of these specimens (18 out of 21) were tested with load control, and the remaining three specimens (C2MP0C, C2MP2C and C2MP4C) were tested with displacement control. The diameters of all the longitudinal bars are 16mm, and other detailed information of these specimens selected for comparison can be found in Table 9.1.

To obtain stress-strain curves for the confined concrete, the axial forces carried by the longitudinal steel bars were removed from the total load carried by the whole column. For the 10 specimens with the test stress-strain curves predicted, the axial loads carried by the longitudinal bars were calculated based on the steel stress-strain curves obtained from their corresponding tension tests. As the results of these tension tests were not reported by the original authors, the following two steps were adopted in the comparison. First, a specimen labeled A5NP2C was modeled using a 3D finite element model, in which the concrete was modeled using 3D solid elements, both the longitudinal and the transverse steel bars were modeled using 3D truss elements, and the FRP jacket was modeled using 3D membrane elements. As the stress-strain curves of the longitudinal bars of this specimen were unknown, an elastic-perfectly-plastic model was utilized in the finite element analysis to consider their contribution. The effect of the end restraints for such a large-scale specimen was also considered in this step. Then, based on the conclusions obtained from this step, axi-symmetric models with half the steel spacing of the concrete columns were adopted for the specimens to reduce the size of the finite element models, and their stress-strain results for confined concrete were compared with experimental results except for specimen C4NP0C. The results of this specimen were not adopted for comparison due to the following two reasons. First, the axial stress of the specimen C4NP0C is even higher than that of specimen C4NP4C which was strengthened with 4 layers of additional FRP jackets. This abnormally high axial stress indicates a large variation existing in the test results. Secondly, as this specimen was under load control, the

descending branch of its stress-strain curves lacks stability and may not be suitable for comparison with the numerical results. The detailed information of the finite element model used for comparison is given in the following sub-sections.

9.3.2 Finite Element Model

9.3.2.1 Three-dimensional finite element analysis for specimen A5NP2C

In the finite element model, due to symmetry in geometry and loading, only 1/24 of this specimen (top 1/12) was modeled using ABAQUS. The concrete was modeled using 8-noded solid elements; the steel bars (both longitudinal and transverse bars) were modeled using 2-noded truss elements; the FRP jackets were modeled using 4-noded membrane elements. The relative positions of the steel bars, FRP jackets and concrete are shown in Fig. 9.5. The mesh of the concrete is also shown in the same figure.

For the plastic-damage model, the required material parameters f'_{co} and ε_{co} are given in Table 9.1. For steel bars, the elastic modulus of all the transverse steel bars is 200GPa (this value was used for all the steel bars in the present study). The yield strength of the longitudinal steel bars f_{ylh} is 423 MPa and the corresponding value of the transverse steel bars f_{yh} is 602 MPa. For FRP, the elastic modulus E_{frp} of the FRP jacket is 78 GPa. The values of these parameters are also summarized in Table 9.1.

Periodic symmetry conditions were imposed at two planes perpendicular to

the circumferential direction. This boundary condition was achieved by restraining the displacement components along the circumferential direction of these two planes. In addition, the middle horizontal plane (i.e., the plane of symmetry) was restrained in the vertical direction to consider the symmetry condition of this plane. Furthermore, forced displacement boundary conditions were imposed on the top plane to subject the column to a compressive stress state. Similar to the case of FRP-confined circular concrete cylinders, the effects of end restraints on the overall axial force-strain performance of specimen A5NP2C were investigated. The axial force-strain curves obtained from finite element analysis with or without end restraints are given in Fig. 9.6, and these numerical results are compared with the corresponding experimental results in the same figure. In this figure, the axial strain is for a gauge length of 300mm and the hoop strain is for the mid-height of the column, which are the same as the experimental conditions. The curves obtained from finite element analysis using different end restraint conditions are almost identical. The consistency between these two cases suggests that for large-scale columns with a ratio of L/D close to 4, the effects of end restraints on their axial force-strain behaviour are negligible. Fig. 9.6 further indicates that although the finite element results slightly underestimate the axial force, the axial force-strain curves, obtained numerically, closely correlate with the experimental results. The slight underestimation of the axial force may be due to the reason that the finite element analysis neglects the possible strain-hardening part of both the longitudinal and transverse steel bars. In addition, as the end restraints only have negligible effects on the structural behaviour, periodic

conditions of symmetry in the axial direction can also be applied and only half a steel spacing of the concrete column needs to be modeled in finite element analysis.

9.3.2.2 Axi-symmetric finite element analysis of FRP-confined RC columns

Ten specimens were selected to verify the capacity of the finite element model by comparing their experimental stress-strain curves with those obtained in finite element analyses. Among these ten specimens, seven of them were reinforced with steel spirals. In order to apply axi-symmetric conditions to further reduce the size of the finite element model, steel spirals were replaced by equivalent steel hoops with the same steel spacing. Mander et al. (1988) suggested an equation to calculate the equivalent cross-sectional area A_{eq} for steel hoops. The equation is as follows:

$$A_{eq} = K_{sh} A_s \tag{9.4}$$

where A_s is the cross-sectional area of the original steel spirals, and K_{sh} is the conversion factor given by:

$$K_{sh} = \frac{1}{1-\frac{s'}{2d_s}} \tag{9.5}$$

where s' is the clear spacing between two spiral bars and d_s is the diameter of the spiral circle from centre to centre. The detailed definitions of the two parameters are shown in Fig. 9.7.

Eq. (9.4) indicates that when the centre-to-centre diameter and the spacing between steel bars provide the same, steel spirals are more effective

confinement than steel hoops. Fig. 9.8 shows the experimental stress-strain curves for specimens C4NP2C and B4NP2C. The only difference between these two specimens is the type of transverse steel used. The experimental results show the same tendency as predicted by Eq. (9.4). That is, the concrete confined by steel spirals has larger axial stress at a given axial or lateral strain.

Taking into account the symmetric features of the finite element model as discussed above, just as for specimen A5NP2C, an axi-symmetric plane with half a steel spacing of the concrete column was modeled in ABAQUS. The concrete is modeled using 4-noded solid elements; the transverse steel bars and the FRP jacket were both modeled using 2-noded axi-symmetric membrane elements. A typical example of the concrete mesh is shown in Fig. 9.9 for specimens B4NP2C.

What should also be noted is that there is no axi-symmetric truss element in ABAQUS, and thus transverse steel bars were modeled as membrane elements. The geometric height of the steel membrane is considered to be the same as the radius of the centre of the transverse original steel bar R_{ts}, and the thickness of the membrane element $t_{ts,eq}$ is determined based on the principle of equivalent cross-sectional area shown in Eq. (9.6). As this study was focused on examining the confinement effects of transverse steel bars, Eq. (9.6) ensures that an identical lateral load is provided by the equivalent steel membrane.

$$t_{ts,eq} = \frac{A_{ts}}{R_{ts}} \tag{9.6}$$

where A_{ts} is half of the cross-sectional area of the transverse steel bar A_{eq}.

As for specimen A5NP2C, the material properties f'_{co} and ε_{co} of concrete, the yield stress f_{yh} for the transverse steel and the elastic modulus E_{fRP} for the FRP jacket are given in Table 9.1.

For these axi-symmetric models, the bottom surface of the axi-symmetric plane was restrained in the vertical direction to reflect the symmetry condition of this surface and axial displacements were applied on the top surface of the finite element model to exert axial loadings. For FRP-confined RC columns, axial displacements were uniformly imposed on the top surface until the maximum hoop strain in the FRP jacket reached its rupture strain.

Fig. 9.10 compares the stress-strain behaviour between the numerical results obtained using the new plastic-damage model and available test results (Eid et al. 2009). Both axial stress-strain curves and axial stress-lateral strain curves are considered in the comparison. For the numerical results, the axial stress was obtained by dividing the load carried by the concrete by the total cross-sectional area; the axial strain is defined as the average values over the whole height of the finite element model; and the hoop strains was obtained from outer edge of the column where the lateral displacement is the largest. Finite element analysis was terminated when the hoop strain reached the

rupture strain of the FRP jacket that was observed in the experiment. Figs. 9.10a-h show that the overall predicted stress-strain responses are in good agreement with the test results although the axial stresses of some specimens were slightly underestimated. This underestimation is generally smaller than that shown in Fig. 9.4 as the effects of longitudinal bars have been removed and the majority of the underestimation have resulted from neglecting the hardening effects of transverse steel bars. These figures indicate finite element model developed in this study can provide close predictions for FRP-confined RC columns. Moreover, the stress-strain curves of concrete confined only by an FRP jacket are also plotted in these figures to illustrate the rough contribution of steel bars. These curves are marked as "FE w/o steel" in Fig. 9.10. Comparison between these two cases (i.e. with or without the contribution of steel bars) shows that steel bars have significant effects on both the strength and ductility of FRP-confined RC columns. This comparison further verifies the capacity of the finite element model to predict the behaviour of FRP-confined RC columns, although the improved model itself was only recalibrated by FRP-confined concrete cylinders.

9.3.2.3 Finite element analysis and analytical modelling of steel-confined RC columns

For specimen C2MP0C, confinement is only provided by the transverse steel bars. The distribution of confinement in this specimen is much more uneven than that for an FRP-confined RC column. For FRP-confined RC columns, lateral confinement exists all over the whole column due to the

FRP jacket. For a concrete column confined only by transverse steel bars, part of the column is under very weak lateral confinement as steel bars are discontinuous in the axial direction. To model this uneven confinement effect, two different approaches have been utilized by researchers. Besides the finite element model, the "effective confinement" method (e.g. Mander et al. 1988) has also been adopted to estimate the amount of lateral confinement acting on the concrete. The partial confinement effect between the upper transverse steel bar and the lower transverse steel bar is considered through the arching action assumption which is generally assumed to occur in the form of a parabola with an initial slope of 45^{o} starting from the edge of each transverse steel bar (Sheikh and Uzumeri 1980). The smallest cross-sectional area of effectively confined concrete core A_e is thus located at the mid-height of the gap between the two transverse steel bars (Mander et al. 1988). In the studies of Mander et al. (1988) and Saadatmanesh et al. (1994), except the ineffectively confined concrete annulus with a radial thickness of a quarter of the clear spacing of the lateral confinement ($s'/4$), the concrete core within the area A_e is assumed to be uniformly confined (also shown in Fig. 9.7). The area of the effectively confined concrete core (A_e) is given by

$$A_e = \frac{\pi}{4}\left(d_s - \frac{s'}{2}\right)^2 \tag{9.7}$$

Fig. 9.11 compares the axial stress-strain behaviour of specimen C2MP0C obtained from the empirical model, the numerical model and the test results (Eid et al. 2009). In this figure, analytical results using the "effective confinement" approach are referred to as "empirical equation"; numerical

results are referred to as “FE” and the test results are referred to as “test”, respectively. It should be noted that, unlike an FRP-confined specimen, the stress-strain curve for a concrete column without an FRP jacket is just based on the core concrete as the arching action is taken into account using this zone rather than the whole concrete column. Thus, only the concrete core was considered in the finite element analysis. This finite element model is similar to that of the axi-symmetric model developed for FRP-confined RC columns except that the FRP jacket was not considered in the model.

Fig. 9.11 shows that the finite element results give smaller axial stresses compared to both the test results and the empirical results. In the new plastic-damage model used in the finite element model, two parameters, K and α, control the confinement effectiveness of concrete under non-uniform confinement. As mentioned earlier, K is a derived parameter calculated from the strength ratio between the concretes under equal biaxial compression and equal tri-axial compression. Therefore, when Eq. (9.2) is used, changing the value of K leads to changes in the value of the $\frac{f_b'}{f_{co}'}$ ratio, but this ratio has been assigned a fixed value of 1.16 in the yield function of the CDPM model as adopted in the present study (see Eqs. 8.1 and 8.2). This ratio can be obtained from a test range of 1.16 to 1.2. Changing this ratio within this given range results in little difference. Therefore, it is better to keep K as a constant rather than a variable. As the parameter α is a fitted value, it was recalibrated to provide closer predictions of the test results and the obtained stress-strain curves shown in the same figure are referred to as “FE-II”. In

this recalibrated finite element model, the value of α was varied from 0.039 to 0.1, and a closer prediction was achieved. Generally, there are two options for using the new plastic-damage model in the finite element analysis of steel-confined RC columns: (1) if the model is used for making predictions, α should be taken as a constant and the default value 0.039 suggested by Yu et al. (2010b) should be used; (2) if the model is used to explain experimental results, α can be recalibrated to fit the uncertain confinement when the experimental results are not closely reproduced.

Although there are differences between the numerical results (including both "FE" and "FE-II") and the empirical results, the test results fall within the range of these two types of results and have good agreement with both of them. Similar to the finite element models the empirical model can give close predictions of stress-strain curves. However, the empirical model cannot explicitly consider the variations in the axial stress and the confinement pressure over the whole section and over the height. To investigate the confinement mechanism of transverse steel bars, the actual stress distribution obtained from finite element analysis is illustrated in Figs. 9.12-9.14. Fig. 9.12 shows the distribution of the axial stress within the concrete core when the peak axial stress is reached. This figure indicates that within a section close to the transverse steel bars, the concrete stress achieves its largest enhancement near the outer surface, and the effect of this enhancement decreases along the height direction away from the steel bar. This variation of the axial stress is similar to the assumption of the arching action. What is different between the finite element results and the arching

action assumption is that the arching action assumption is focused on the axial stress distribution along the radial direction. With the arching action assumption, the section at the height of the steel bar centre is assumed to be uniformly stressed and is considered to be effectively confined, while the finite element analysis predicts a large stress near the steel bar, a smaller stress enhancement away from the steel bar, and finally a moderate stress near the axis of axi-symmetry. It is a more reasonable distribution as the finite element analysis takes into account the balance of axial forces along the height direction, which is neglected in the arch action assumption. In addition, the numerical results indicate that a non-uniform zone of stress is mainly located near the outer surface of the concrete core, and within a certain radius, there is a zone of uniformly distributed axial stress, which is similar to the results of the elastic analysis conducted by Eid and Dancygier (2006). Zones of uniformly distributed stress can also be observed in the distribution of confining pressure. Fig. 9.13 shows that, for the confining pressure, the largest value appears in the place adjacent to the steel bar on the outer surface of the concrete core and the smallest one also appears on the outer surface of the concrete core but always on the plane of symmetry between the two steel bars. Unlike the confining pressure in the radial direction, the largest confining pressure in the hoop direction appears in the middle zone between the steel bar and the plane of symmetry. The different distributions of the confining pressure result in a complicated axial stress distribution near the outer surface of the concrete core. Figs. 9.13-9.14 indicate that, within a certain radius, there are zones of uniformly distributed confining stresses, which result in the uniformly distributed axial stress

within them. The existence of a uniformly confined concrete zone is an important reason why the empirical approach using the arching shape assumption can achieve good accuracy in predicting the steel bar-confined concrete columns even though it overlooks the balance of axial forces. As long as the radius predicted by the empirical approach is not too far from the actual value of the radius of uniformly confined concrete, the results predicted by the empirical approach can be accurate. To further illustrate the stress distribution, Figs. 9.15-9.17 show the predicted stress distributions along the radial direction at three selected sections/heights. Fig. 9.15 shows the distribution of the axial stress; Fig. 9.16 shows the distribution of the confining stress in the radial direction; and Fig. 9.17 shows the distribution of the confining stress in the hoop direction. The locations of the three selected sections are marked in Fig. 9.12. It is again obvious that a large uniform zone exists away from outer edge. The width of this uniform zone is about 2/3 of the column radius. Within this zone, all the three stress components have insignificant variations. However, near the outer edge, the rate of variation of stress is more significant due to the effect of the arching action. The capability of predicting stress variations over the whole column is one of the advantages of this 3D finite element model over a slice model.

9.4 CONCLUSIONS

Three-dimensional finite element models for FRP-confined circular concrete cylinders and RC columns based on Yu et al.'s (2010b) plastic-damage model have been presented in this chapter. These finite element models are capable of modelling uneven deformation in the axial direction due to

factors such as end restraints and discrete transverse steel bars. Numerical results obtained from the finite element models have revealed that end restraints lead to smaller axial strains at a given hoop strain. This reduction effect necessitates a revised lateral-to-axial strain relationship and then leads to a local analysis-oriented stress-strain model. This local analysis-oriented stress-strain model is proposed for adoption to avoid the double counting of end restraint. Consequently, the finite element model with the input parameters produced by this local analysis-oriented stress-strain model can very closely reproduce the predictions of the original analysis-oriented stress-strain model proposed by Jiang and Teng (2007). Moreover, the finite element model with the input parameters produced by this local analysis-oriented stress-strain model was used to model the behaviour of FRP-confined RC columns and transverse steel bar-confined concrete. Ten large-scale RC columns were simulated using a finite element model with the input parameters produced by this local analysis-oriented stress-strain model. This finite element model is shown to produce accurate predictions of the stress-strain behavior of FRP-confined RC columns and transverse steel bar-confined concrete although the local analysis-oriented stress-strain model was only calibrated using results of FRP-confined circular concrete cylinder. In addition, it has been found that the assumption of path-independency is still valid. Finally, the finite element model has been compared with the empirical model for transverse steel-confined concrete. It has been shown that the finite element analysis can describe the stress distributions of concrete confined by transverse steel. With careful verification, the finite element model is a useful tool for the exploration of

confinement mechanisms in various FRP-confined concrete columns in the development of simple stress-strain models for design purposes.

9.5 REFERENCES

ABAQUS (2004). *ABAQUS Analysis User's Manual*, version 6.5.

American Concrete Institute (ACI) (2008). "Building code requirements for structural concrete (318M-08) and commentary." *ACI 318M-08*, Detroit.

ASTM (2010). *Standard Test Method for Static Modulus of Elasticity and Poisson's Ratio of Concrete in Compression*, Designation: C469/C469M-10, ASTM International, West Conshohocken, US.

Bisby, L. A., and Take, W. A. (2009). "Strain localizations in FRP-confined concrete: new insights." *Proceedings of the Institution of Civil Engineers-Structures and Buildings*, 162(5), 301-309.

Dai, J. G., Bai, Y. L., and Teng, J. G. (2011). "Behaviour and modelling of concrete confined with FRP composites of large deformability." *Journal of Composites for Construction*-ASCE, Accepted.

Doran, B., Koksal, H. O., and Turgay, T. (2009). "Nonlinear finite element modelling of rectangular/square concrete columns confined with FRP." *Materials & Design*, 30(8), 3066-3075.

Eid, R., and Dancygier, A. N. (2006). "Confinement effectiveness in circular concrete columns." *Engineering Structures*, 28(13), 1885-1896.

Eid, R., and Paultre, P. (2007). "Plasticity-based model for circular concrete

columns confined with fibre-composite sheets." *Engineering Structures*, 29(12), 3301-3311.

Eid, R., Roy, N., and Paultre, P. (2009). "Normal- and high-strength concrete circular elements wrapped with FRP composites." *Journal of Composites for Construction*-ASCE, 13(2), 113-124.

Grassl, P., and Jirasek, M. (2006). "Damage-plastic model for concrete failure." *International Journal of Solids and Structures*, 43(22-23), 7166-7196.

Jiang, T., and Teng, J. G. (2007). "Analysis-oriented stress-strain models for FRP-confined concrete." *Engineering Structures*, 29(11), 2968-2986.

Karabinis, A. I., and Rousakis, T. C. (2002). "Concrete confined by FRP material: a plasticity approach." *Engineering Structures*, 24(7), 923-932.

Karabinis, A. I., Rousakis, T. C., and Manolitsi, G. E. (2008). "3D finite-element analysis of substandard RC columns strengthened by fiber-reinforced polymer sheets." *Journal of Composites for Construction*-ASCE, 12(5), 531-540.

Kupfer, H., Hilsdorf, H. K., and Rusch, H. (1969). "Behaviour of concrete under biaxial stresses." *ACI Journal Proceedings*, 66(8), 656-666.

Lam, L., Teng, J. G., Cheung, C. H., and Xiao, Y. (2006). "FRP-confined concrete under axial cyclic compression." *Cement & Concrete Composites*, 28(10), 949-958.

Lan, Y. M. (1998). *Finite Element Study of Concrete Columns with Fiber Composite Jackets*, PhD Dissertation, School of Civil Engineering,

Purdue Universtiy.

Lee, J. H., and Fenves, G. L. (1998). "Plastic-damage model for cyclic loading of concrete structures." *Journal of Engineering Mechanics*-ASCE, 124(8), 892-900.

Lubliner, J., Oliver, J., Oller, S., and Onate, E. (1989). "A Plastic-damage model for concrete." *International Journal of Solids and Structures*, 25(3), 299-326.

Luccioni, B. M., and Rougier, V. C. (2005). "A plastic damage approach for confined concrete." *Computers & Structures*, 83(27), 2238-2256.

Mahfouz, I., Rizk, T. and Sarkani, S. (2001). "An innovative FRP confining system for repairing rectangular columns." *Construction and Materials Issues 2001, Proceedings of the Second Congress,* ASCE *and Construction Institute*, 16-25.

Mander, J. B., Priestley, M. J. N., and Park, R. (1988). "Theoretical stress-strain model for confined concrete." *Journal of Structural Engineering*-ASCE, 114(8), 1804-1826.

Mirmiran, A., Zagers, K., and Yuan, W. Q. (2000). "Nonlinear finite element modelling of concrete confined by fiber composites." *Finite Elements in Analysis and Design*, 35(1), 79-96.

Montoya, E., Vecchio, F. J., and Sheikh, S. A. (2004). "Numerical evaluation of the behaviour of steel- and FRP-confined concrete columns using compression field modelling." *Engineering Structures*, 26(11), 1535-1545.

Oh, B. (2002). *A Plasticity Model for Confined Concrete under Uniaxial*

Loading, PhD Thesis, Lehigh University.

Richart, F. E., Brandtzaeg, A. and Brown, R. L. (1928). “A Study of the Failure of Concrete under Combined Compressive Stresses”, *Bulletin No. 185, Engineering Experiment Station*, University of Illinois, Urbana, U.S.A.

Richart, F. E., Brandtzaeg, A. and Brown, R. L. (1929). “The failure of plain and spirally reinforced concrete in compression.” *Bulletin No. 190, Engineering Experiment Station*, University of Illinois, Urbana, Ill. U.S.A

Popovics, S. (1973). “Numerical approach to the complete stress-strain relation for concrete”, *Cement and Concrete Research*, 3(5), 583–599.

Rougier, V. C., and Luccioni, B. M. (2007). "Numerical assessment of FRP retrofitting systems for reinforced concrete elements." *Engineering Structures*, 29(8), 1664-1675.

Rousakis, T. C., Karabinis, A. I., and Kiousis, P. D. (2007). "FRP-confined concrete members: Axial compression experiments and plasticity modelling." *Engineering Structures*, 29(7), 1343-1353.

Sangha, C. M., and Dhir, R. K. (1972). "Strength and complete stress-strain relationships for concrete tested in uniaxial compression under different test conditions." *Materials and Structures*, 5(6), 361-370.

Saadatmanesh, H., Ehsani, M. R., and Li, M. W. (1994). "Strength and ductility of concrete columns externally reinforced with fiber composite straps." *ACI Structural Journal*, 91(4), 434-447.

Sheikh, S. A., and Uzumeri, S. M. (1980). "Strength and ductility of tied concrete columns." *Journal of the Structural Division*-ASCE, 106(5), 1079-1102.

Teng, J. G., Huang, Y. L., Lam, L., and Ye, L. P. (2007). "Theoretical model for fiber-reinforced polymer-confined concrete." *Journal of Composites for Construction*-ASCE, 11(2), 201-210.

Teng, J. G., and Lam, L. (2004). "Behaviour and modelling of fiber reinforced polymer-confined concrete." *Journal of Structural Engineering*-ASCE, 130(11), 1713-1723.

Teng, J. G., Yu, T., Wong, Y. L., and Dong, S. L. (2007). "Hybrid FRP-concrete-steel tubular columns: Concept and behaviour." *Construction and Building Materials*, 21(4), 846-854.

Xiao, Q. G., Teng, J. G., and Yu, T. (2010a). "Behaviour and Modelling of Confined High-Strength Concrete." *Journal of Composites for Construction*-ASCE, 14(3), 249-259.

Xiao, Q. G., Teng, J. G., Yu, T., and Lam, L. (2010b). "Three-Dimensional Finite Element Model for FRP-Confined Circular Concrete Cylinders under Axial Compression." *Advances in Frp Composites in Civil Engineering*, Ye, L.P., Feng, P., and Yue, Q. R. eds., Springer-Verlag Berlin, Berlin, 654-657.

Yu, T., Teng, J. G., Wong, Y. L., and Dong, S. L. (2010a). "Finite element modelling of confined concrete-I: Drucker-Prager type plasticity model." *Engineering Structures*, 32(3), 665-679.

Yu, T., Teng, J. G., Wong, Y. L., and Dong, S. L. (2010b). "Finite element modelling of confined concrete-II: Plastic-damage model." *Engineering Structures*, 32(3), 680-691.

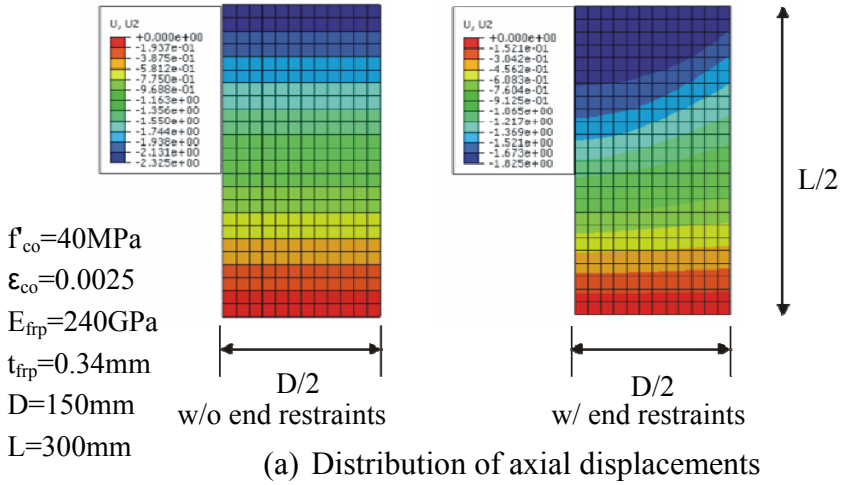

(a) Distribution of axial displacements

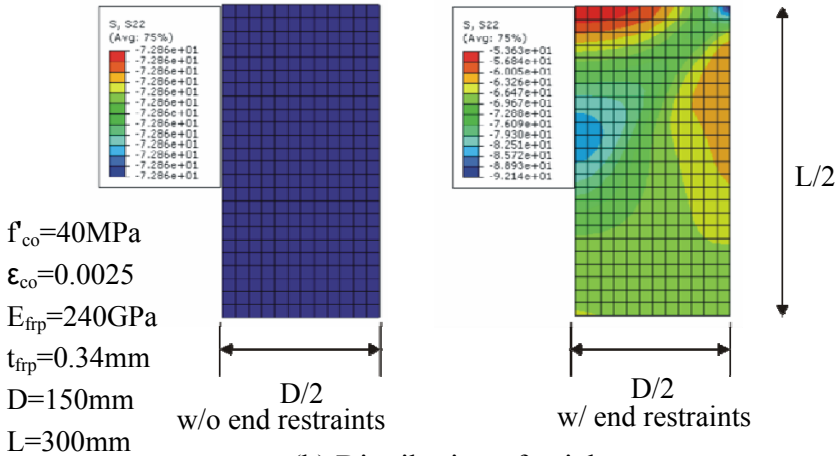

(b) Distribution of axial stresses

Figure 9.1 Distributions of axial displacements and axial stresses in FRP-confined circular concrete cylinders with and without end restraints

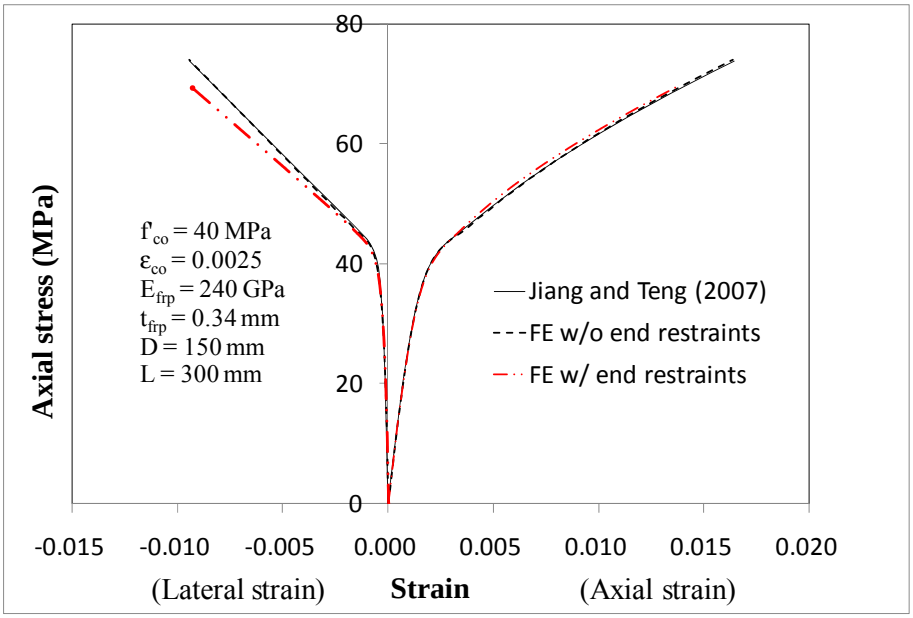

(a) Axial stress-strain curves

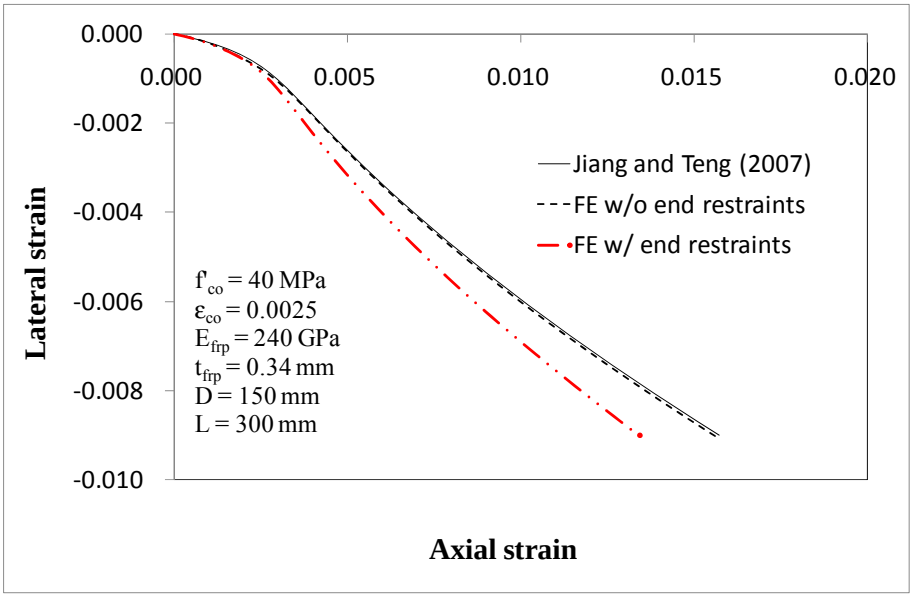

(b) Lateral-to-axial strain curves

Figure 9.2 Comparison between Jiang and Teng's analysis-oriented stress-strain model and finite element simulation with input parameters derived from the same model

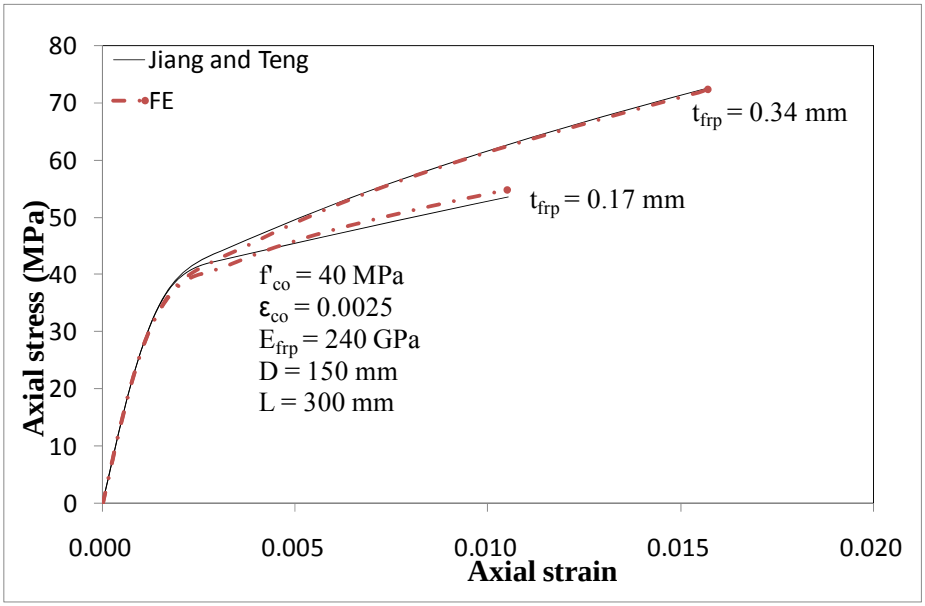

(a) Axial stress-strain curves

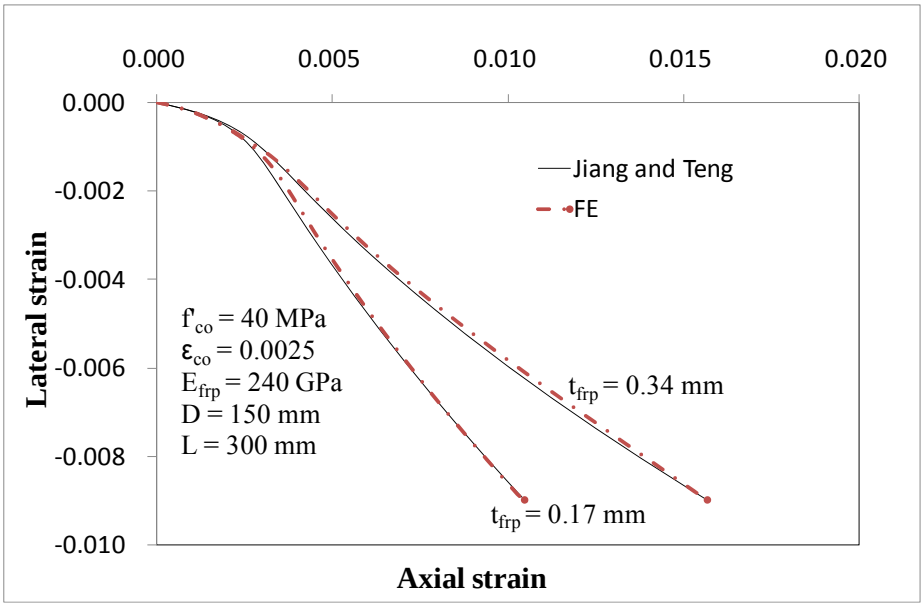

(b) Lateral-to-axial strain curves

Figure 9.3 Recalibration of the analysis-oriented stress-strain model

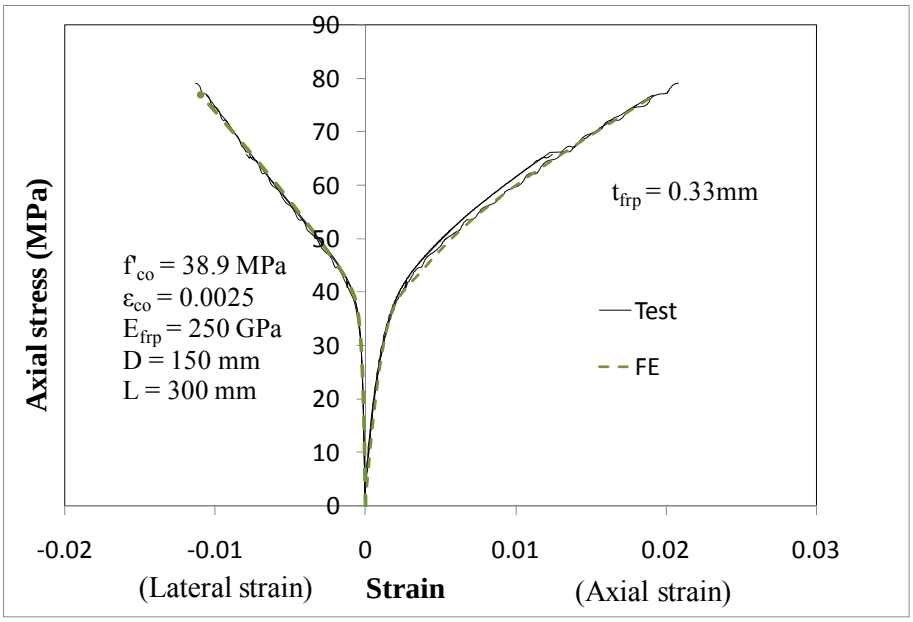

(a) Test data of CFRP-confined concrete from Lam et al. (2006)

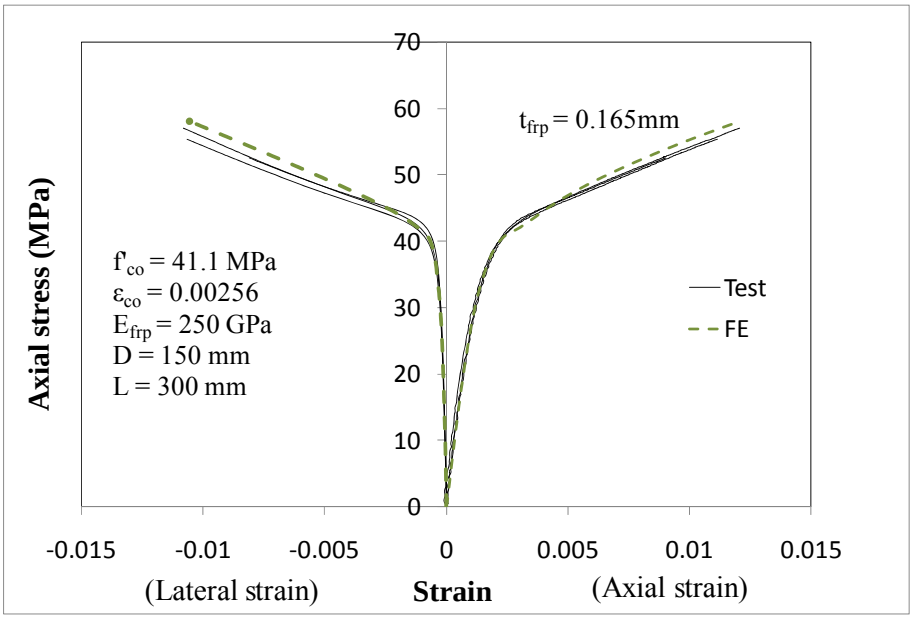

(b) Test data of CFRP-confined concrete from Lam et al. (2006)

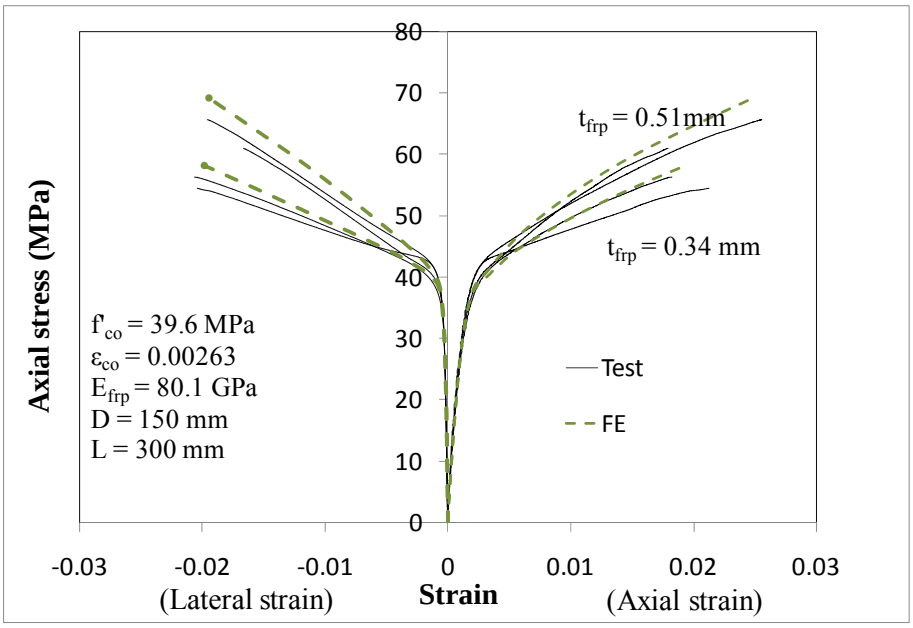

(c) Test data of GFRP-confined concrete from Teng et al. (2007)

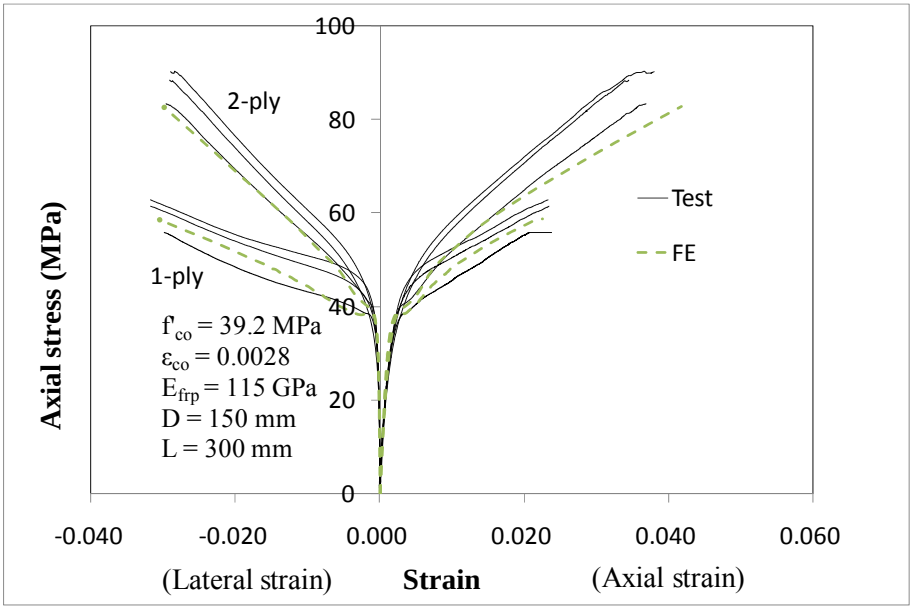

(d) Test data of AFRP-confined concrete from Dai et al. (2011)

Figure 9.4 Comparison between test and finite element for the stress-strain behaviour for FRP-confined concrete cylinders

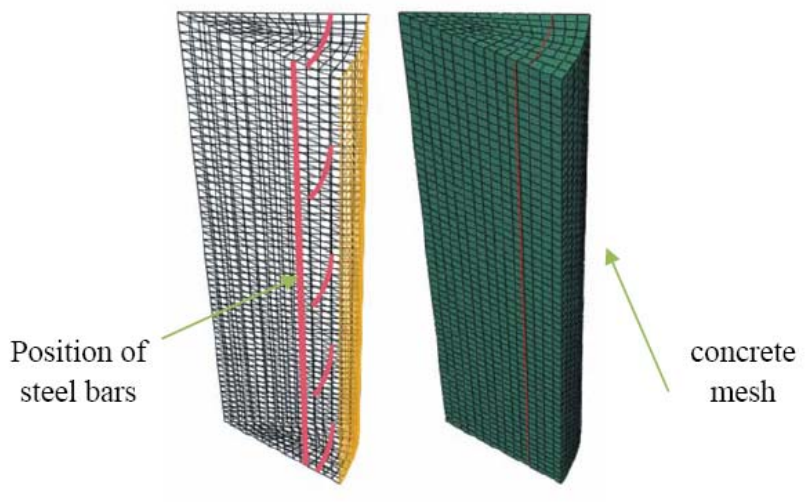

Figure 9.5 Finite element mesh of specimen A5NP2C and positions of steel bars

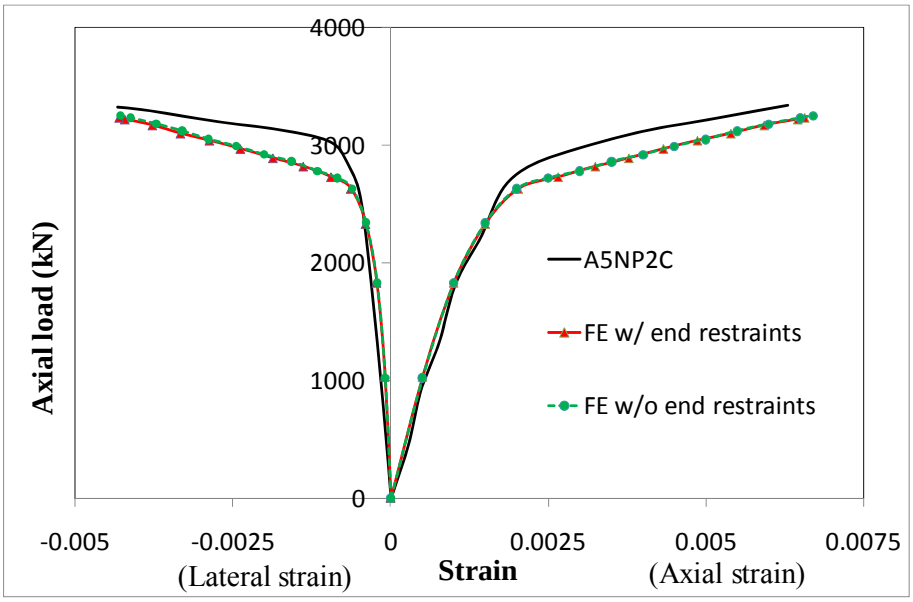

Figure 9.6 Comparison between test and finite element for specimen A5NP2C

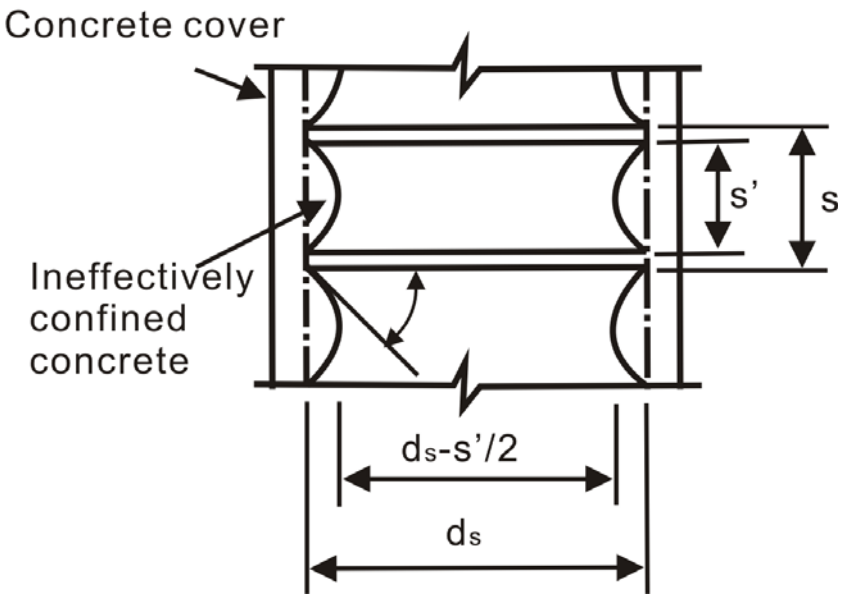

Figure 9.7 Illustration of clear spacing (s') and arch action

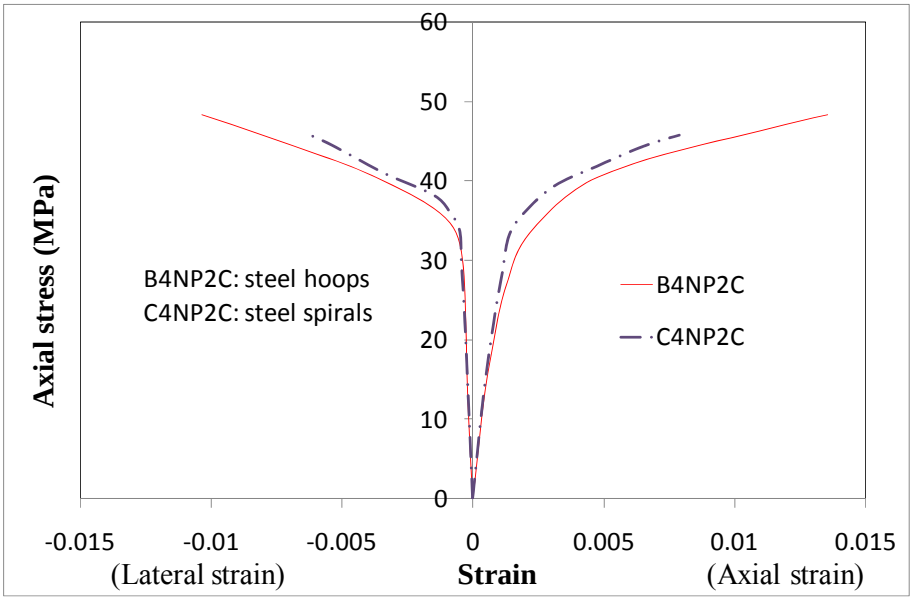

Figure 9.8 Test results showing the effects of different types of transverse steel bars

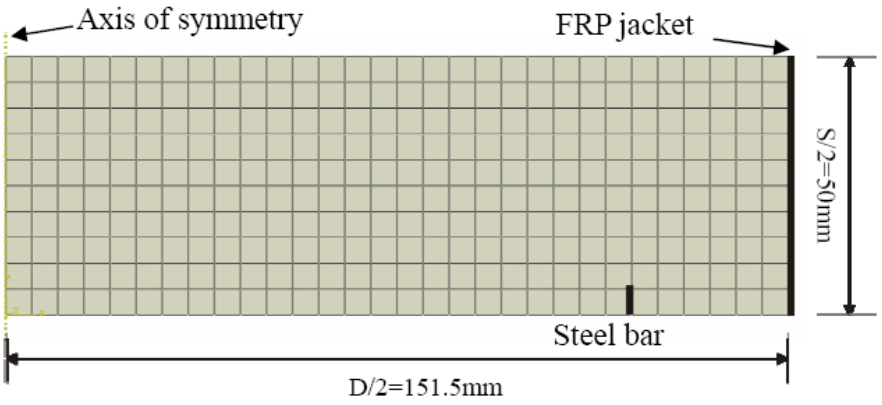

Figure 9.9 Axi-symmetric finite element model for specimen B4NP2C

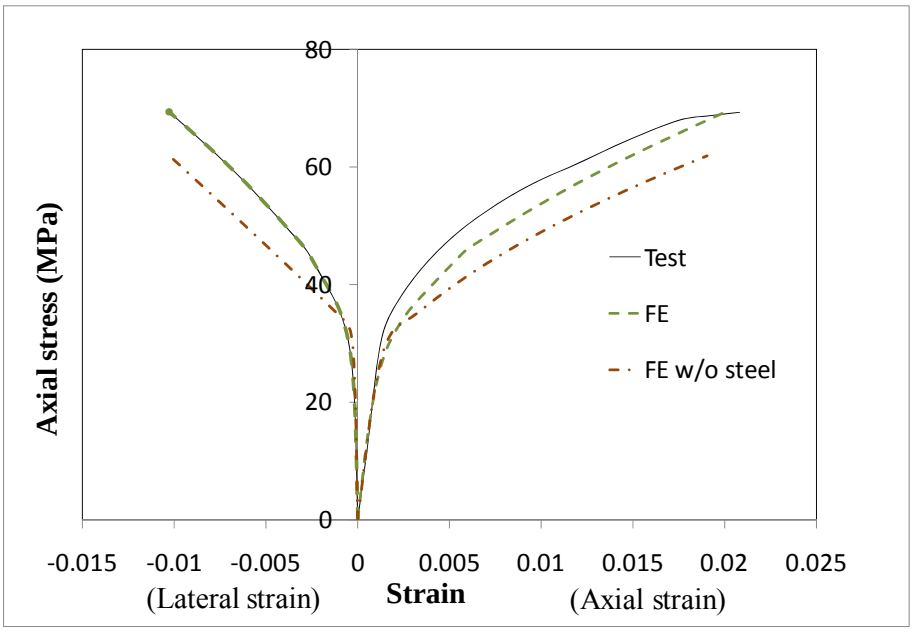

(a) Specimen C4NP4C

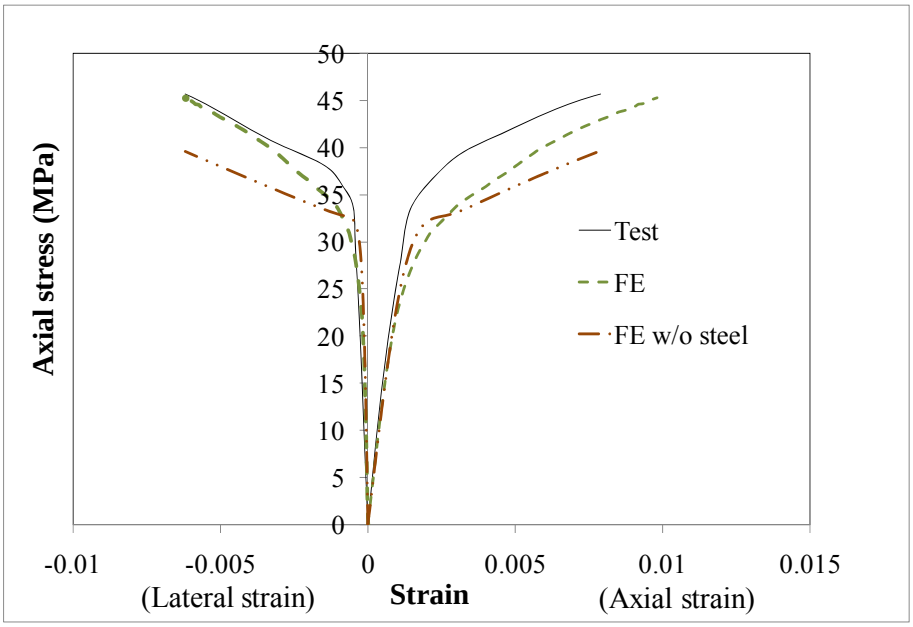

(b) Specimen C4NP2C

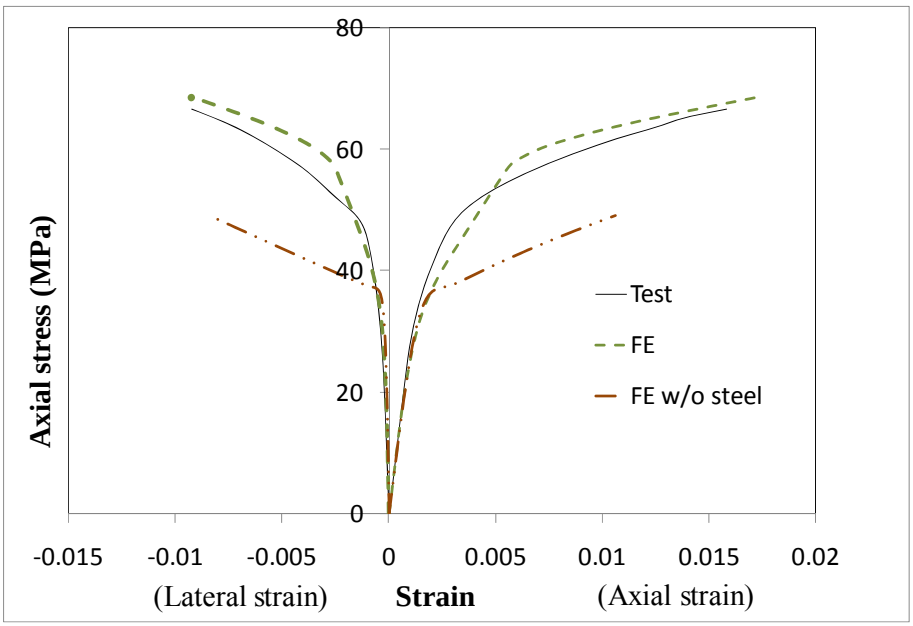

(c) Specimen C2N1P2N

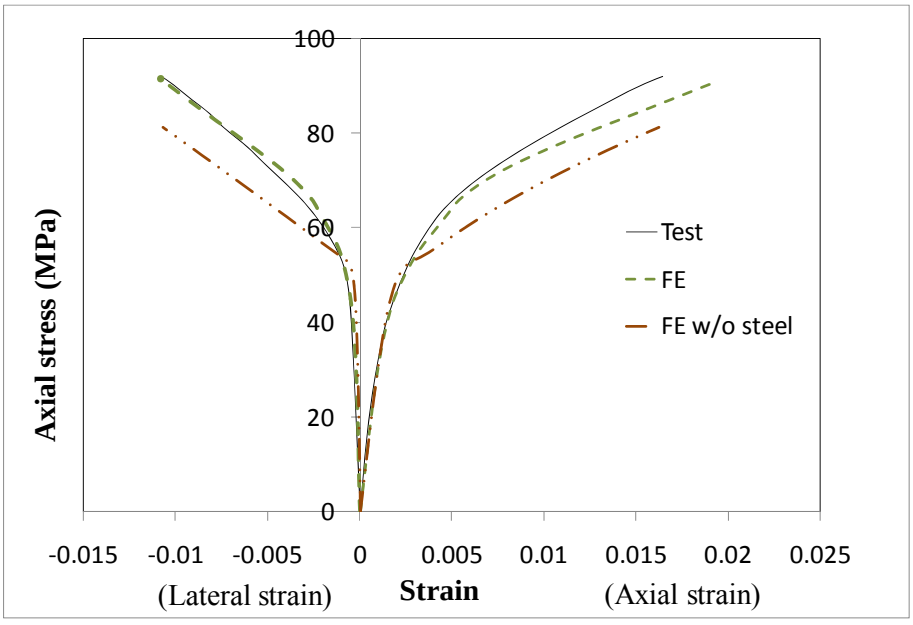

(d) Specimen C2MP4C

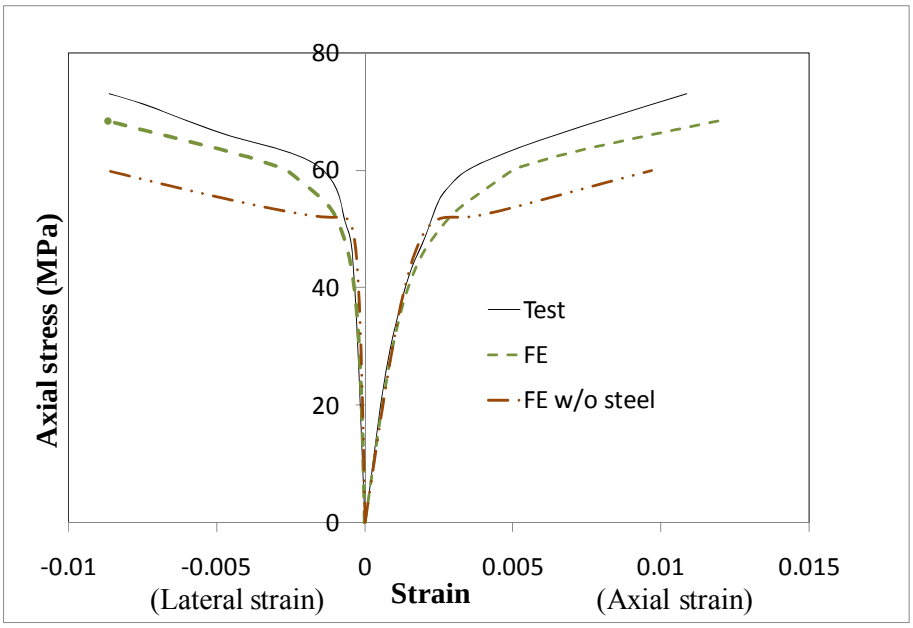

(e) Specimen C2MP2C

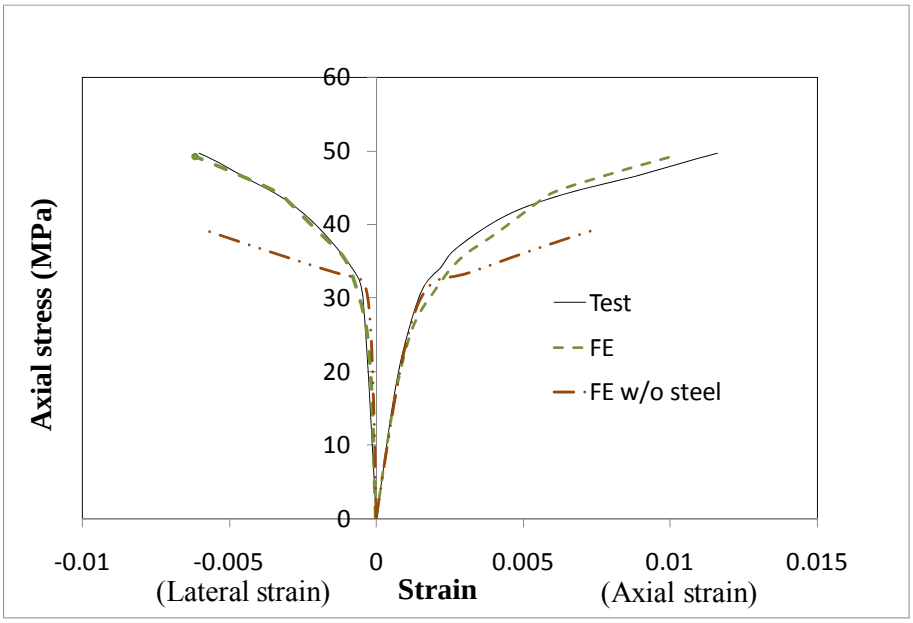

(f) Specimen C2NP2C

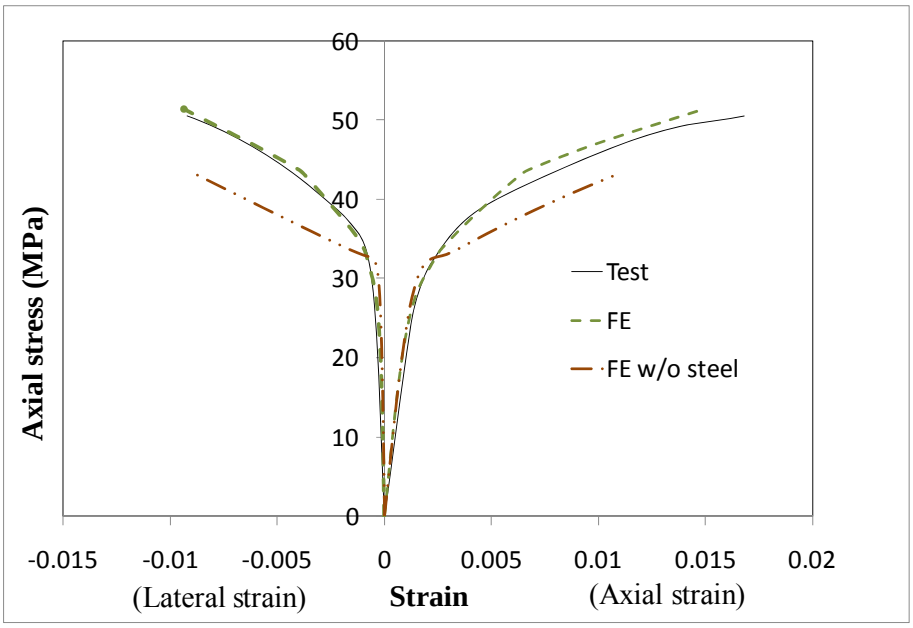

(g) Specimen A3NP2C

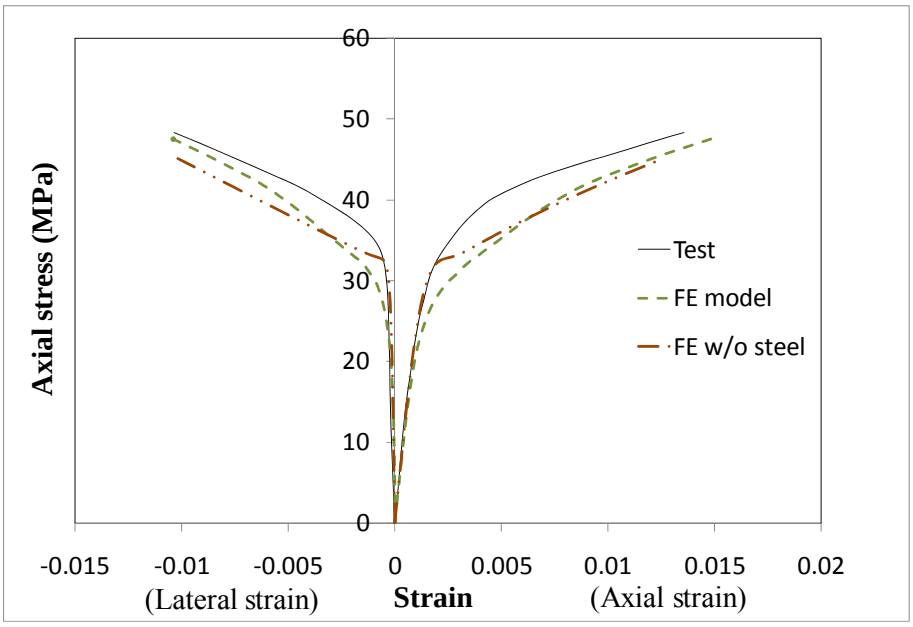

(h) Specimen B4NP2C

Figure 9.10 Comparison of stress-strain behaviour from the finite element results and test results of FRP-confined concrete columns

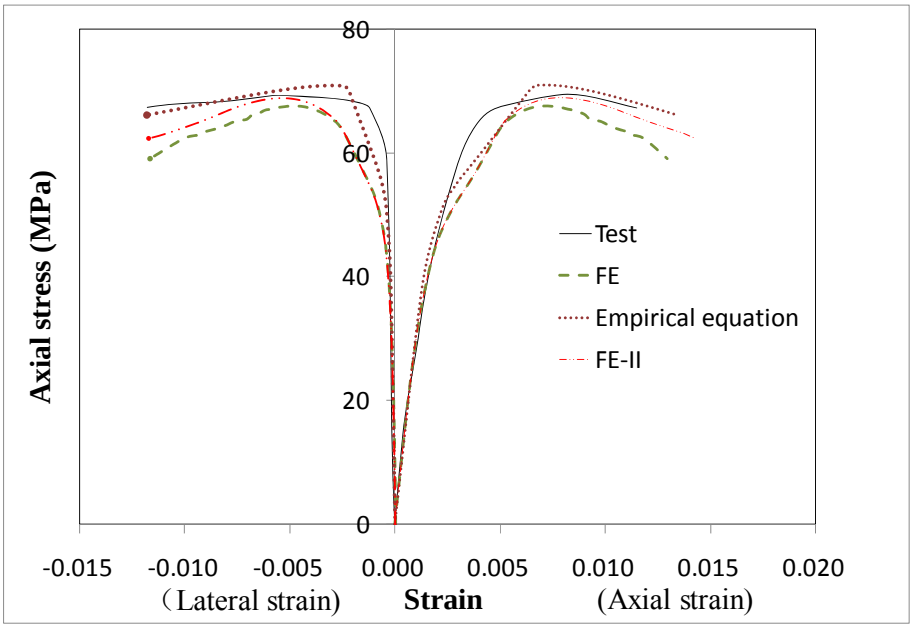

Figure 9.11 Comparison of stress-strain behaviour for the specimen C2MP0C confined by transverse steel bars

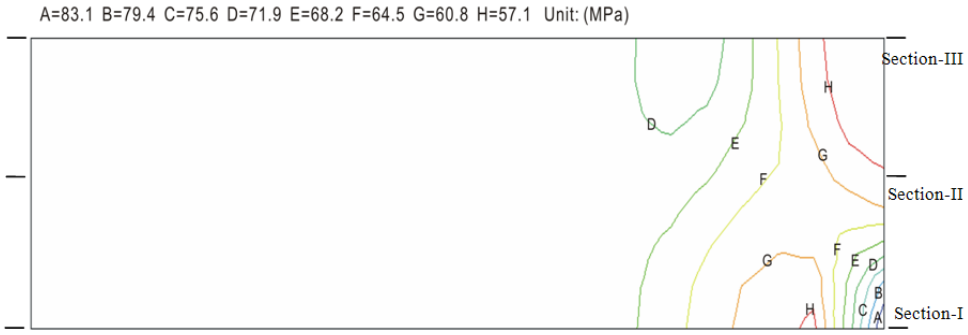

Figure 9.12 Contours of axial stress in the specimen C2MP0C confined by transverse steel bars

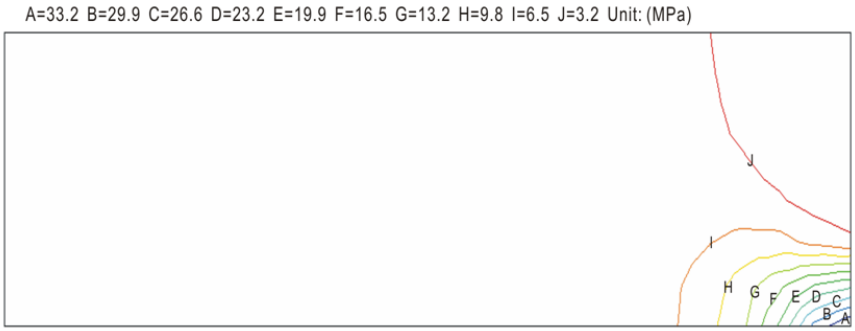

Figure 9.13Contours of radial stress in the specimen C2MP0C confined by transverse steel bars

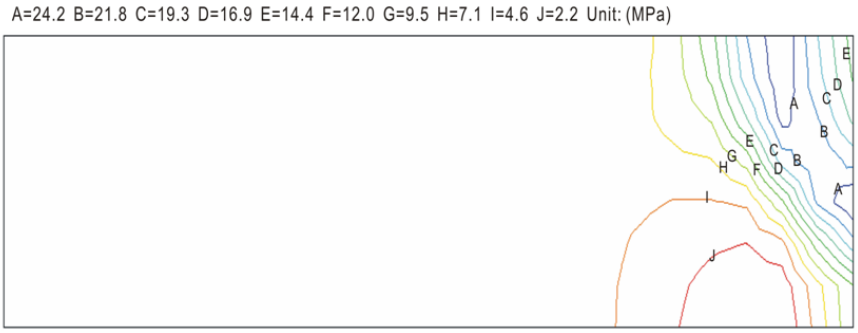

Figure 9.14 Contours of hoop stress in the specimen C2MP0C confined by transverse steel bars

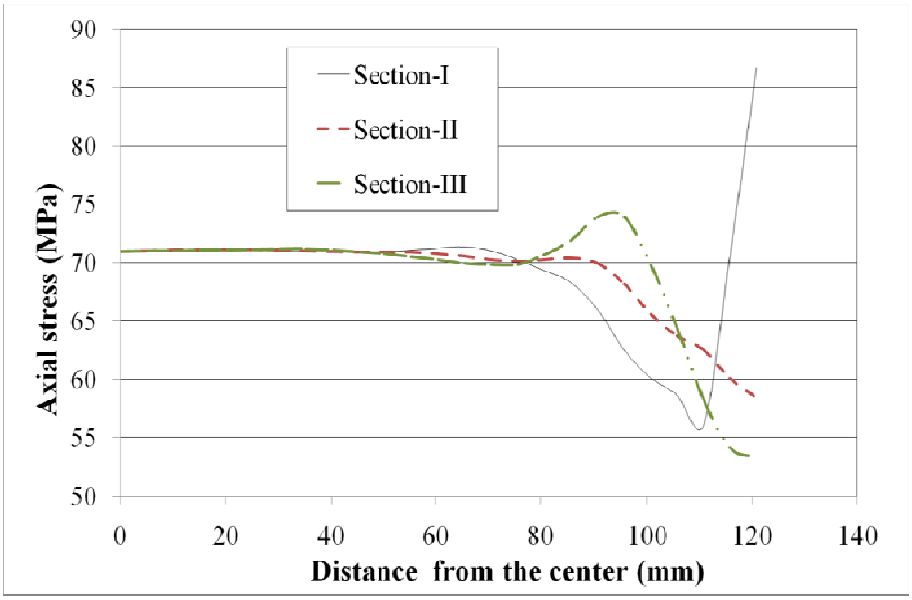

Figure 9.15 Distribution of axial stress in the specimen C2MP0C confined by transverse steel bars

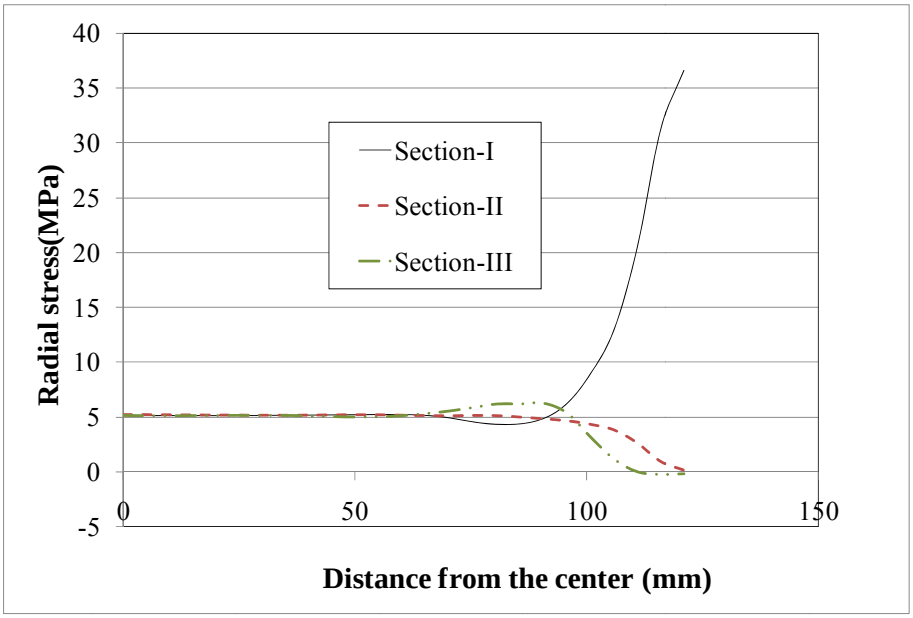

Figure 9.16 Distribution of radial stress in the specimen C2MP0C confined by transverse steel bars

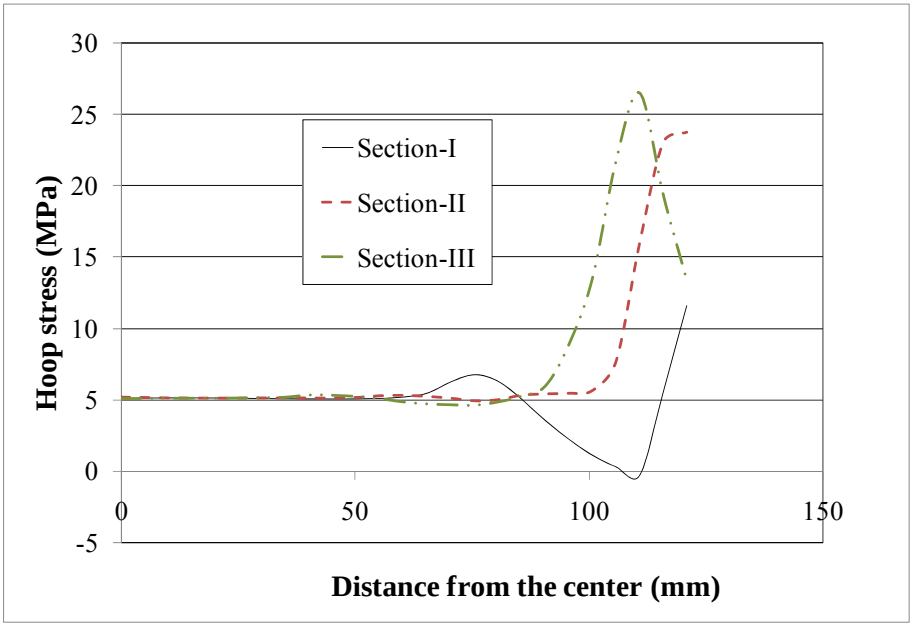

Figure 9.17 Distribution of hoop stress in the specimen C2MP0C confined by transverse steel bars

Table 9.1 Material properties of FRP-confined RC columns

specimen No.	D (mm)	c[a] (mm)	f'_{co} (MPa)	ε_{co}	FRP composite			Transverse steel			
					t (mm)	E_{frp} (Mpa)	$\varepsilon_{h,rup}$	type	f_{yh} (Mpa)	*s* (mm)	ø (mm)
C4NP4C	303	25	31.7	0.002	1.524	78000	0.0119	S	456	100	11.3
C2NP2C	303	25	31.7	0.002	0.762	78000	0.0059	S	456	65	11.3
C4NP2C	303	25	31.7	0.002	0.762	78000	0.0062	S	456	100	11.3
C2N1P2N	253	0	36	0.002	0.762	78000	0.0084	S	456	65	11.3
A3NP2C	303	25	31.7	0.002	0.762	78000	0.0090	H	602	70	9.5
C2MP4C	303	25	50.8	0.0024	1.524	78000	0.0107	S	456	65	11.3
C2MP2C	303	25	50.8	0.0024	0.762	78000	0.0086	S	456	65	11.3
B4NP2C	303	25	31.7	0.002	0.762	78000	0.0104	H	456	100	11.3
A5NP2C	303	25	29.4	0.002	0.762	78000	0.0044	H	456	150	11.3
C2MP0C	303	25	50.8	0.0024	0.0	---	---	S	456	65	11.3

[a] Concrete cover, S: Spiral, H: Hoops,

D is diameter of the specimens, f_{yh} is the yield strength of steel bars, and ø is the diameter of the steel bar.

CHAPTER 10

CONCLUSIONS AND FUTURE WORK

10.1 INTRODUCTION

This thesis has presented a systematic study covering the testing and analysis of FRP-confined concrete columns. In particular, this thesis has focused on the constitutive behaviour of concrete under lateral confinement, aiming to develop generic constitutive models which can accurately predict the behaviour of concrete under non-uniform confinement. The work presented in this thesis has been limited to the compression behaviour of concrete, which is the relevant part directly influencing the confinement mechanism.

A series of axial compression tests on FRP-confined high strength concrete cylinders have been presented in this thesis to complement the existing experimental data and to gain an adequate understanding of the stress-strain behaviour of FRP-confined high strength concrete. Similar to that of normal strength concrete, the FRP jacket has been shown to significantly enhance the performance of high strength concrete. These test results have provided not only a direct insight into the mechanical behaviour of FRP-confined high strength concrete but also a way for assessing theoretical models.

Theoretical modelling of actively-confined and FRP-confined concrete

columns has the main focus of the present thesis. Finite element models using different concrete constitutive models have been employed for simulating the behaviour of confined concrete. These constitutive models were developed based on different theories. The general performance of these constitutive models was assessed. Based on this assessment, two potential constitutive models, i.e. the $M4^+$ model and the revised CDPM model, were utilized for modelling FRP-confined concrete in non-circular sections. Based on the work presented in this thesis, the corresponding conclusions have been drawn in the following section.

10.2 CONCLUSIONS

Chapter 3 presented an experimental study on the behaviour of confined high strength concrete. The behaviour of actively-confined high strength concrete was first examined. A unified active-confinement model was found to be applicable to both high strength concrete and normal strength concrete. After that, an experimental study on FRP-confined high strength concrete was presented. It was found that the analysis-oriented stress-strain model proposed by Jiang and Teng (2007), initially developed for FRP-confined normal strength concrete, can also provide accurate predictions for FRP-confined high strength concrete. Comparing the empirical model for actively-confined concrete with that for FRP-confined concrete indicated that the path independence assumption commonly utilized in an analysis-oriented

stress-strain model is just partially fulfilled for FRP-confined high strength concrete.

Chapters 4 and 5 examined the use of typical plasticity-based concrete models for predicting the behaviour of confined concrete. These concrete models were categorized into two groups based on the techniques employed in the hardening rule. The hardening variables used in these two techniques are the scaled equivalent plastic strain and the plastic volume strain, respectively. Plasticity-based concrete models based on these two techniques were implemented with the ABAQUS software through UMAT; and they were used for predicting the stress-strain response of plain concrete in both uni-axial and equal tri-axial compression once the parameters have been determined through calibration. These two models, with properly calibrated parameters, were found to be capable of predicting both the stress-strain behaviour of unconfined concrete and actively-confined concrete accurately. Further, among these two types of models, Papanikolaou and Kappos's (2007) model, which belongs to the second type, provides the simplest process in calibrating the material parameters. However, both these two models failed to predict the lateral deformation of FRP-confined circular concrete cylinders accurately in a general sense, although they may succeed within a certain confining stiffness range. The failure of these two models in predicting the response of FRP-confined circular concrete cylinders indicated that a modification of the

hardening rule has an insignificant effect on the lateral deformation of confined concrete.

Chapter 6 investigated the application of plastic-damage models in modelling the behaviour of confined concrete. Similar to the plasticity-based concrete models, two types of plastic-damage models were used for predicting the stress-strain response of plain concrete in uni-axial and equal tri-axial compression once the parameters have been calibrated. The techniques used in Chapter 4 to improve their behaviour for confined concrete were also employed in these two models separately. Additionally, isotropic damage variables were utilized in these two models. For the response of confined concrete, similar conclusions, as those given in Chapters 4 and 5, were drawn. These two plastic-damage models were found to be capable of providing accurate predictions for actively-confined concrete but incapable of capturing the varied dilation characteristics of FRP-confined concrete under different levels of confining stiffness. The damage variable was also found to have an insignificant effect on the lateral deformation of confined concrete. This effect is similar to that of the hardening rule.

In the work presented in Chapter 7, the Microplane model M4, proposed by Bazant et al. (2000), was employed in investigating the response of FRP-confined circular concrete cylinders. However, this M4 model was found

to have some drawbacks in the computational aspects and was incapable of accurately capturing the effect of confinement, especially on the ductility of concrete. Proper modifications were thus made to the original M4 model to eliminate its drawbacks in the computational aspects and to enhance its prediction accuracy for confined concrete especially for FRP-confined concrete, which resulted in the so-called $M4^+$ model. Some material parameters such as k_1, c_7, and c_8 in this $M4^+$ model were set to be confinement-dependent variables instead of constant values suggested in the original M4 model. These parameters were chosen for modification here because they had significant effects on the predicted confinement effect. Finally, a comparison between the numerical predictions using the $M4^+$ model and the experimental results were presented. This comparison showed adequate agreement between the numerical predictions and the experimental results. This comparison suggested that in modelling FRP-confined concrete, the parameters controlling the dilation behaviour of the M4 model should be properly addressed.

In the work presented in Chapter 8, two constitutive models, that is, Yu et al.'s (2010b) plastic-damage model and the $M4^+$ model were employed in finite element models for the analysis of the FRP-confined square and elliptical columns subjected to axial compression. Numerical results from the finite element analysis showed favourable agreement with the experimental results. Furthermore, the above numerical results were compared with the results of

two typical empirical models. This comparison focused on the ultimate state of FRP-confined concrete in square columns. From this comparison, the numerical results obtained using the modified CDPM model showed the best performance among these four analytical models. In addition, the numerical results obtained using the $M4^{+}$ model also showed its relatively high accuracy compared with the two empirical models. By virtue of numerical simulation, the thickness of FRP jackets was demonstrated to have an effect on the stress distribution of FRP-confined non-circular columns. This effect exists because concrete is a typical non-linear material and the thickness of the FRP jacket changes the stress state of concrete at failure.

Chapter 9 focused on three-dimensional finite element analysis of FRP-confined circular concrete cylinders and RC columns based on Yu et al.'s (2010b) plastic-damage model. Some fundamental issues associated with the finite element analysis of FRP-confined circular concrete cylinders were addressed. A local analysis-oriented stress-strain model was identified by recalibrating the finite element results to reproduce the results of the original analysis-oriented stress-strain model such as that of Jiang and Teng (2007). A consistent definition of the mean axial strain in both experimental measurement and finite element results was achieved and the reduction effect on the axial strain due to end restraints considered in the finite element model was eliminated by introducing this local analysis-oriented stress-strain model. Based on this local analysis-oriented model, the assumption of

path-independency was found to be valid. The finite element model was also shown to have properly captured the stress-strain behaviour of steel bar-confined concrete and FRP-confined RC columns, although the analysis-oriented stress-strain model was only calibrated by results of FRP-confined concrete. The finite element results were also found to be able to describe the stress distribution in the concrete confined by transverse steel and to reflect the confinement effect of transverse steel bars.

10.3 FUTURE WORK

The following issues need further research.

There is still a need to widen the database of test results for FRP-confined concrete especially FRP-confined concrete in non-circular columns.

More data on the lateral-to-axial relationship is required. The present research has found that the constitutive models which can provide accurate predictions for FRP-confined concrete are sensitive to the lateral behaviour of concrete. Additionally, measurements of hoop strains should be standardized. It has been discussed that the lateral strains reported in the experimental results of FRP-confined circular concrete cylinders are generally limited to the maximum strain that could be measured.

Constitutive models using the scaled equivalent plastic strain or the plastic volume strain as the hardening variable have shown their advantages in predicting the stress-strain behaviour of actively-confined concrete. Among these constitutive models, Papanikolaou and Kappos's (2007) model provides a simple process for calibrating the material parameters. Modifications to this constitutive model can be made in the future for providing accurate predictions for FRP-confined concrete.

In this study, a scaling technique was actually employed in the $M4^{+}$ model to provide accurate predictions for confined concrete. Due to the characteristics of the microplane model, other approaches such as directly modifying the stress boundary may be adopted to achieve similar results as that of the scaling technique.

The modified CDPM model was implemented through the technique of USDFLD (i.e. user subroutine to redefine field variables at a material point), which is an explicit scheme. An implicit algorithm or an explicit algorithm with error control can be developed for this model in the future work.

Another important issue that needs to be clarified is the size effect on the stress-strain behaviour of FRP-confined concrete. In the numerical model, it was assumed that the strength of plain concrete was that given by the

researchers in their reports. In Chapter 8, most of the FRP-confined non-circular concrete columns had sizes close to the standard cylinder. Therefore, no significant size effect of these columns was observed. In Chapter 9, the behaviour of large-scale FRP-confined circular columns was found to be capable of being reasonably predicted by the finite element models. Therefore, size effects are much more significant in non-circular columns.

Finally, the verified constitutive models in the present study can be used to study the behaviour of short or slender FRP-confined RC columns under eccentric loading. Eccentric loading is an important topic and some research has been conducted on this topic (e.g. Binici and Mosalam 2007; Mosalam et al. 2007; Talaat et al. 2008), but much more work, especially three-dimensional finite element analysis, is needed. This topic should be investigated in the future.

10.4 REFERENCES

Binici, B., and Mosalam, K. M. (2007). "Analysis of reinforced concrete columns retrofitted with fiber reinforced polymer lamina." *Composites Part B: Engineering*, 38(2), 265-276.

Mosalam, K. M., Talaat, M., and Binici, B. (2007). "A computational model for reinforced concrete members confined with fiber reinforced polymer laminar: implementation and experimental validation." *Composites Part B: Engineering*, 38(5-6), 265-276.

Talaat, M., and Mosalam, K. M. (2008). *Computational modeling of progressive collapse in reinforced concrete frame structures*, PEER Technical Report 2007/10, May 2008, 310pp.

APPENDIX

COMPUTER PROGRAMME

A matlab programme is developed to calculate the values of A, B, and C for Papanikolaou and Kappos's (2007) model.

```
fco=40;
E=30011;
nu=0.2;
epvp=fco/E*(1-2*nu);
eco=0.0022;
e3p=eco-fco/E;
e3p=-e3p;
e1p=(epvp-e3p)/2;
% e1p,e3p
ft=2.906;
dlamda=1.376;
m=(fco^2-(dlamda*ft)^2)/(fco*dlamda*ft)
Fi1=sqrt(2/3)*abs(e3p-e1p)/((e3p+2*e1p)/sqrt(3));
% x1=fzero('(x-1)^2+3*9.9*0.5198/1.5198*((x-1)/3-(x+2)/3)-1',2);
x1=fzero('(x-0.5)^2+3*9.9*0.52/1.52*((x-0.5)/3-(x+1)/3)-1',2);
% x1=fzero('(x-1)^2+3*9.9*0.52/1.52*((x-1)/3-(x+2)/3)-1',2);
fcc=x1*fco;
ecc=9.5*eco;      %%correspond to ecc=eco*(1+17.5*fl/fco)
% ecc=18*eco;
e3p=ecc-1/E*(fcc-2*nu*fco*0.5);
e3p=-e3p;
e1p=(epvp-e3p)/2;
% e1p,e3p
Fi2=sqrt(2/3)*abs(e3p-e1p)/((e3p+2*e1p)/sqrt(3));
n=3;
no1=sqrt(2/3)*fco;
no2=sqrt(2/3)*(fcc-fco*0.5);
A=(Fi1-Fi2)/n/((no1/fco)^(n-1)-(no2/fco)^(n-1));
B=Fi1-n*A*(no1/fco)^(n-1);
x2=fzero('(x)^2+3*9.9*0.52/1.52*((x)/3*1/0.52-(2*x)/3)-1',1.1);
fbc=x2*fco;
ebc=x2*eco;
e3p=ebc-fbc/E*(1-nu);
e3p=-e3p;
e2p=e3p;
e1p=epvp-2*e3p;
Fi3=sqrt(2/3)*abs(e3p-e1p)/((e3p*2+e1p)/sqrt(3));
no3=sqrt(2/3)*(fbc);
```

```
C=Fi3-n*A*(no3/fco)^(n-1);
A,B,C
```